A Study of Beam-Beam Effects in Hadron Colliders with a Large Number of Bunches

THÈSE N^{O} 4211 (2008)

PRÉSENTÉE LE 4 DÉCEMBRE 2008

À LA FACULTÉ SCIENCES DE BASE
LABORATOIRE DE PHYSIQUE DES HAUTES ÉNERGIES 1
PROGRAMME DOCTORAL EN PHYSIQUE

ÉCOLE POLYTECHNIQUE FÉDÉRALE DE LAUSANNE

POUR L'OBTENTION DU GRADE DE DOCTEUR ÈS SCIENCES

PAR

Tatiana PIELONI

laurea in fisica, Università degli studi di Milano, Italie
et de nationalité italienne

acceptée sur proposition du jury:

Prof. R. Schaller, président du jury
Prof. A. Bay, Prof. L. Rivkin, directeurs de thèse
Dr W. Herr, rapporteur
Dr B. Holzer, rapporteur
Prof. M. Q. Tran, rapporteur

ÉCOLE POLYTECHNIQUE
FÉDÉRALE DE LAUSANNE
Suisse
2008

...memento audere semper...
Gabriele D'Annunzio

Abstract

A particle beam is a collection of a large number of charges and represents an electromagnetic potential for other charges, therefore exerting forces on itself (space charge) and other beams (Beam-Beam Interactions, BBIs). The control of th BBIs in particle colliders is fundamental to preserve beam stability and achieve the optimum collider performance. In the case of the Large Hadron Collider (LHC) at CERN, these forces are experienced as localized periodic distortions when the two beams cross each other in the four experimental areas. The forces are most important for high density beams, i.e. high intensity and small beam sizes. Each LHC beam is composed of 2808 bunches, each containing 10^{11} protons and with a transverse size of 16 μm at the interaction points. These extreme parameters are the key to obtain high "luminosity", i. e. the number of collisions per second needed to study "rare" physics phenomena. The BBI is therefore often the limiting factor for the luminosity of colliders. Within all BB effects, this thesis covers coherent and incoherent beam-beam effects in hadron colliders with particular emphasis on those with a large number of bunches, like the LHC.

Complementary numerical tools have been developed to study the effects of BBIs on the particle beams. The use of new parallel algorithms was fundamental to allow the scale of the calculations. The objectives are a better understanding of these effects and if necessary to propose changes to the LHC beam parameters to keep detrimental effects small.

We have demonstrated the numerical predictibility of bunch to bunch differences and for the first time compared the results to analytical predictions and experimental data from the Relativistic Heavy Ion Collider (RHIC). Beam-beam transfer function measurements had been reproduced and understood in terms of coherent beam-beam modes. An implementation of the measurement devices had been suggested in order to avoid misinterpreted diagnostics.

An emittance growth caused by the BBIs had been observed and characterized with numerical studies and explained with a simple physical picture. A study of the parametrical dependency of this effect defines qualitatively the expected limiting factors to avoid detrimental deterioration of the beams. The variation of the LHC tune spectra for different collision symmetries and in the presence of long range as well as head-on collisions had been presented and explained. This will be of fundamental importance to correctly interprete the observations of single bunch measurements during the operation of the collider and to improve the performances.

Keywords: Hadron colliders, Beam dynamics, Beam-beam effect, Collective effects, Coherent and incoherent effects, Luminosity, High intensity beams.

Resume

Un faisceau de particules chargées induit un champ électromagnétique macroscopique qui, à son tour, induit des forces tant sur les particules de ce même faisceau que sur d'autres faisceaux simultanément présents. Le contrôle des forces qui s'appliquent entre les faisceaux (en anglais "beam-beam interactions", abrégé BBI) est fondamental pour préserver la stabilité et maximiser la luminosité d'un collisionneur. Dans le cas du projet LHC, ces forces s'exercent localement dans les sections proches des expériences, où les deux faisceaux de protons se trouvent dans une chambre à vide commune. Ces forces sont proportionnelles à la densité des faisceaux, ou proportionnelles à leur intensité et inversement proportionnelles à leur dimension. Dans le LHC chaque faisceau est composé de 2808 paquets qui contiennent chacun 10^{11} protons pour un courant total de 0.5 Ampère. Les paquets ont une dimension transversale de 16 micromètres aux points de collisions. Ces valeurs extrêmes sont nécessaires pour obtenir une luminosité qui permettra d'observer des phénomènes physiques rares. L'effet BBI est un facteur limitant pour la performance en luminosité, comme cela a été observé dans plusieurs collisionneurs.

Le sujet principal de ce travail est l'étude des effets dits 'strong-strong', c'est à dire des effets qui s'appliquent de paquets à paquets d'intensité similaire, et en particulier les effets cohérents qui y sont associés. A cet effet, nous avons développé et étendu aux cas de points d'interactions multiples, en présence d'un grand nombre de paquets, trois outils numériques complémentaires. Notre objectif est de mieux comprendre ces effets et d'être en mesure, si nécessaire, de proposer des améliorations pour le collisionneur LHC. Avec les outils développés, nous avons pu prédire des différences de comportement entre paquets de particules qui ont effectivement été observées dans le collisionneur RHIC. Cette approche sera donc utile pour interpréter le comportement des paquets individuels durant l'opération de futurs collisionneurs et d'optimiser leurs performances. Un effet du BBI sur l'émittance a été observé et caractérisé dans les études numériques et peut être expliqué par un argument physique simple. Une analyse paramétrique de cet effet permet de définir qualitativement certaines limitations et de les éviter. Nous proposons une prédiction de la distribution spectrale du nombre d'onde bétatronique pour différentes symétries de collisions frontales et distantes. La prédictibilité numérique a été testée à RHIC, où des mesures de fonctions de transfert ont été reproduites et comprises en termes de mode faisceau-faisceau cohérents. En particulier, le comportement singulier de certains paquets est expliqué quantitativement par le fait qu'ils croisent moins de paquets de l'autre faisceau (effet 'Pacman'). Ceci a permis de proposer une adaptation du système de mesure pour éviter de biaiser certains diagnostics.

Keywords: Collisionneur de hadrons, Dynamique des faisceaux, Effets faisceau-faisceau, Effets collectives, Effets cohérents et incohérents, Luminosité, Faisceaux de haute intensité .

Acknowledgements

These last four years of work had been very important for my professional as well as for my private life. With these few lines I would like to thank all the people who have helped me in one way or an other to overcome the stressful periods and enjoy the more satisfactory ones.

I would like to start expressing my appreciation for Professor A. Wrulich, my initial thesis director, who first supported my PhD thesis and welcomed me to the EPFL. I am very grateful I was given the chance to do this PhD. I then want to thank my official EPFL thesis directors: Professors A. Bay and L. Rivkin who both followed my work with interest during these last three years. Thanks to Aurelio for listening and solving all administrative problems and for suggesting to access the EPFL computing resources. I am very grateful to Lenny for the good advice to step in the accelerator physics "world" and for giving me the opportunity to assist him in the teaching activities. I, more than any undergraduated student, have learned and profited from it. I would like to thank them both for their endless enthusiasm which reflects their love for this field and had always represented for me a motivating guiding force.

It is difficult to overstate my gratitude to my CERN supervisor Dr. W. Herr. This thesis would not have been possible without our 1600 coffees. With his probing questions, his great efforts to explain things clearly and his infinite patience, he transmitted me his true and faithful passion for physics. Throughout my thesis-writing period, he provided encouragement, wise advice and so many corrections. It has been an honor and a lot of fun working together with Werner. I am grateful he shared with me his broadband knowledge in physics, as well as in fishing. I want here to express my gratitude to the late Dr. F. Ruggiero who had welcomed me in the world of collective effects and helped me with my first steps in beam-beam.

I want to thank the Accelerator and Beam Physics group leaders Jean-Pierre Riunaud and Oliver Bruning for admitting me to the group and for their hospitality over the years.

I would like to thank Dr. F. Jones (TRIUMF) for his precious contribution to the code development. I would have been lost in the "parallel" world of computing without him.

A special thank to the colleagues of the Brookhaven National Laboratory for giving me the opportunity to work on an operational collider. Thanks to Dr. W. Fischer who first invited me, to Dr. R. Calaga with whom I have worked with and Dr. T. Roser for sponsoring my visit and welcoming me in his team.

I am indebted to the efficient EPFL-DIT Mizar and BlueGene teams who answered all of my questions and solved all my bugs. A special mention goes to J. Menu, J.C. Leballeur, C.Clemencon and P.Jermini.

I have to thank the friends and colleagues who have made the effort to correct this

thesis: thanks for the English corrections to Giulia, for finding the weak points Wolfram, for pointing out my non-logical structures to Federico, for the RHIC part to Rama and for the French corrections to Jean-Bernard, Malika and Simon.

A special thank to A. Hofmann, Y. Alexahin, G. Rumolo, S. Redaelli, J. Qiang, R. Tomas, G. Bellodi, R. Calaga and W. Fischer for their inspiring discussions.

I wish to thank Dr. W. Scandale for sponsoring my participation to the CARE workshops and for encouraging me to start this PhD.

I would like to express my gratitude to Dr. L. Bottura and Dr. S. Sanfilippo who tought me how to work in research and who first believed I would be able to do a PhD. Thanks to Professor L. Rossi who first introduced me to CERN.

I am glad to thank Dr. M. Meddahi and Dr. K. Elsener for letting me participate in the CNGS commissioning. It was a motivating experience I loved to be part of, no matter the hundreds of Gaussian fits to do.

Thanks to the CERN Accelerator School, in particular to Dr. D. Brandt and his team for the nice moments of study and fun spent together.

I would like to thank some of my old colleauges at CERN of the R&D and LHC Collective effects section (Elias and Frank) and others of the ABP group (Massimo, Gianluigi, F. Schmidt, E. Mcintosh, Jean-Bernard and Helmut).

A special thought to my extraordinary officemates Javier and Peder with whom I have lived exhilarant moments which are fixed in my memories. I will not miss the office but I will miss them both.

Also thanks to the kind and precise work of Erika, Esther and Anh at EPFL, Marlen at PSI, Juliette, Lauriane and Claudine at CERN for all their administrative assistance.

And last but not least, thanks to Madeleine for that precious every morning kindness and cappuccino.

" Everyone hears what you say. Friends listen to what you say. Best friends listen to what you do not say..."

Thanks to the good old friends of these years for the long or short moments spent together but which left in my heart a special and magic memory: Antonio, Bobo, Esther, Fede, Rocio, Mirko, Ester, Irene, Luis, Lulu, Georgina, Albi, Alessandro Masi, Mirco, Giovanni Spiezia, PierPaolo, Marco, Arianne, Elena, Christos, Dall'Occhio, Sere, Valentina, Glen, Sandra, the Fata Morgana sisters, Denise, Stephane, Pascale, Ralph, Rama, Sophie, Ana, Rogelio, Benoit, Christine, Simon, Alex, Pivi, Eva, Ezio, Fabio, Lassen, Delphine, Rossano, Bren, Verena, Andrea Latina, Andrea Franchi, Giuliano, Thibaut, Enrico, Diego, Chiara, Marco, Fede, Matteo, Arturo, Ema, Sterbini, Elena B, Mel, Gia, Carsten, Markus, Isabel, Babi, Rita, StePau, Alex, Cri, Paola, Davide, Davide, Mena, Sud69, Paz, Ubaldo, Nico, Teo, Lucia, Alessandro, Gloria, the Leanza family, Aldo, Mino, the Redaelli's of Brianza and all those I maybe forgot mentioning.
As for Laura, Giovanni, Nathy, Didi, Sissi, Giulia Bellodi, Paoletta, Patty, Dory, Chiarona, Vale and Bianca I don't need to spend more words.
Vorrei qui ringraziare tutta la mia famiglia. In particolare e al di sopra di tutti mia madre Grazia alla quale dedico questa tesi perche' e' solo grazie alla sua forza ed al suo amore che ho saputo e voluto superare le difficolta' e conseguire questo traguardo. Un grazie di cuore alle mie due sorelle Nathascia e Diane, negli anni abbiamo avuto momenti di confronto e

di discussione, a volte abbiamo intrapreso strade diverse che ci hanno allontanate ma non per questo ci siamo divise. E' la sicurezza di poter sempre fare affidamento su di voi che mi ha resa cosi' sfrontata nell'affrontare la vita. Un grazie a mio padre Giuseppe il cui ricordo mi e' sempre caro in ogni momento della mia vita.
C'e' una strada che va dagli occhi al cuore senza passare per l'intelletto, questa e' la strada che mi ha portato a te Stefano. Grazie per il semplice sapermi rendere felice. In questi anni abbiamo intrapreso un'eccitante avventura insieme che spero sia per tutta la vita.

Contents

Chapter 1

Beam-Beam Effects in Colliders

When we study the dynamics of particles in circular accelerators, it is customary to distinguish between longitudinal and transverse dynamics.
In this study we are mainly concerned with transverse beam dynamics and want to make a further division into two separate domains: the behaviour of single particles, the subject of Single Particle Dynamics (SPD), and the behaviour of groups of particles, usually referred to as Collective Effects (CE).
Single particle dynamics is one of the most important subjects in accelerator physics and important for the operation of any machine. It is conceptually simple and the existing theoretical framework is rather complete, in particular from the simulation point of view. The main topic of such studies is the answer to the key question, i.e. whether the motion of the particle is stable. Different ways to treat this question have been developed, analytical as well as numerical, and they give satisfactory and reliable results. In complex machines it is a standard procedure to evaluate the stability by particle tracking, treating all machine elements as functionally independent objects (e.g. magnets) and computing the transport maps for the individual elements. In such a description the behaviour and dynamics are determined as a global property of the ring.
We have a more complicated situation when the beams are made of a large number of particles which interact with the environment, with other particles, and as a collective ensemble. This is the subject of collective effects in particle accelerators. The exact knowledge and description of the machine itself is now not sufficient to answer the questions related to this topic. Not only are the questions more complex than just assessing stability in single particle dynamics, but a complete theory does not exist. However, an impressive number of tools and models are now available to study these effects and their predictive power is improving.
A very particular type of collective particle behaviour is when two beams interact with each other in particle colliders, which are used in particle and nuclear physics. This is referred to as Beam-Beam Interaction (BBI). A very special feature of this problem is that both single particle effects as well as collective effects are present and important. This makes it one of the most interesting and challenging fields in accelerator physics together with the fact that this is often the limiting factor for the performance of particle colliders including the largest and most expensive machines.
To study single particle dynamics including the Beam-Beam Interactions, that will be described later, we can apply the theory and many of the tools developed so far. The ability

to answer the question: "Is a single particle stable under the influence of the beam-beam interaction ?" is by now satisfactorly proven, at least for machines without too much complexity.
However, a complete theory and exact treatment of the collective effects of beam-beam interaction are not available especially for the case of multiple interactions and in the presence of many bunches in the beam. The last 20 years have however seen large improvements in the understanding and evaluation of beam-beam effects in particle colliders. This is true for analytical models and to an even larger extent for the numerical treatment of the problem. However, a correct and successful treatment of beam-beam effects requires an exact definition of the questions one intends to answer and the development of the necessary tools to do that.
We investigate the beam-beam effects for hadron colliders in general but focusing on the CERN Large Hadron Collider (LHC), which in the framework of beam-beam interactions is the most complex machine ever conceived, this is what is been mainly attempted in this work, where the development of the necessary tools represents an important part.

1.1 The beam-beam interaction

A particle beam is a collection of a large number of charges and represents an electromagnetic potential for other charges, therefore exerting forces on itself and other beams. In the case of particle colliders like the Large Hadron Collider (LHC) the beam-beam forces are experienced as localized, periodic distortions where the two beams cross each other in the experimental areas, schematically shown in Fig.1.1 (corresponding to the location of the ALICE, ATLAS, CMS and LHCb detectors).

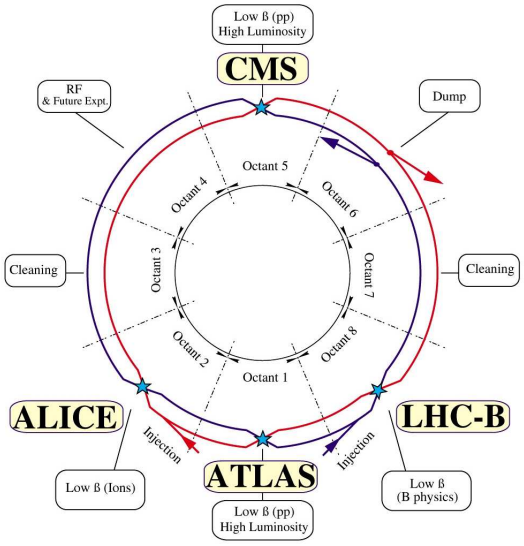

Figure 1.1: LHC schematic layout with in evidence the experimental areas

These forces are most important for high density beams, i.e. high intensity and small beam sizes. The LHC current will be of about 0.5 A per beam, with an energy storage of 720 MJ. The minimum transverse beam size will be of about 17 μm at the interaction point. These extreme parameters are the key to obtain high "luminosity", i. e. the number

of collisions per second needed to study rare physics phenomena. Improving these parameters to obtain higher luminosities results in stronger beam-beam effects. The beam-beam interaction is therefore often the limiting factor for the luminosity of colliders, as already observed at the Tevatron at FERMILAB, at the Relativistic Heavy Ion Collider (RHIC) at the Brookhaven National Laboratory (BNL), at the Cornell Electron Storage Ring (CESR) at Cornell University in Ithaca, at the PEP-II at the Standford Linear Accelerator Center (SLAC), at the Hadron Electron Ring Accelerator (HERA) at the Deutsches Elektronen-Synchrotron (DESY), at the KEKB accelerator at the High Energy Accelerator Research Organisation (KEK) and at the Super $p\bar{p}$ Synchrotron (S$p\bar{p}$S) and Large Electron Positron (LEP) colliders at CERN.
The aim of this introduction is to give the reader an overview of possible beam-beam effects [1] known from past and present experiences in circular lepton and hadron colliders focusing on those which are of interest for the LHC. An explanation of the different physical effects will be given together, where possible, with experimental evidence and confirmation from past and present accelerators. An explanation of the present limits in the understanding of this phenomenon will be given in order to show the need for an extension of the beam-beam studies and modeling to address the LHC case.
The LHC collider represents a new and unknown regime for what concerns beam-beam interactions, and present models do not have the predictive power needed for this accelerator layout. Even if a general, qualitative understanding of the beam-beam interaction is available, a quantitative and detailed study for the case of multiple bunch beams and multiple beam-beam interactions has not been developed so far. Therefore, to improve substantially the accelerator diagnostics and performances for any new high energy physics requirement we need to extend the present knowledge and modeling to the multiple bunch and multiple interactions regime. To address this goal we had to define a consistent modeling strategy which will involve analytical, semi-analytical as well as numerical simulations of the phenomena. For this purpose the use of modern numerical techniques involving parallel computation were of fundamental importance since so far no numerical calculation of this order of magnitude would have been possible.

1.2 Perturbative and self-consistent models

In order to get higher luminosity, present and future colliders rely on a large number of bunches and multiple interaction points. The consequences are parasitic interactions around the IPs which appear as higher order effects due to the large number of interactions and to the coupling of many bunches through strongly non-linear forces [39, 40]. These interactions represent a strong simulation limiting factor, since reproducing a realistic picture of the effect with multiple bunches made of particle samples interacting in several locations in the accelerator is impossible, or at least can require months of computational time with standard techniques and common devices. Hence the need to move to new technology and new techniques to make feasible what was so far impossible.
When talking about analysis techniques one should first understand the regime in which the two beams operate in order to define the appropriate approximations to be applied in the calculations. Not all colliders operate in the same conditions: beam characteristics change from machine to machine and beam-beam interactions are strongly dependent on

the beam characteristics. We basically have to distinguish two cases: where a perturbative treatment is possible and a second case where a fully self-consistent treatment is required. In the problems considered here,the forces and electromagnetic fields are produced by the beams themselves. When the effects of these forces are strong enough, they can change the properties of the beams and hence vary the same forces responsible for the effects. Beam-beam forces are time dependent and two cases can be distinguished:

- An equilibrium of time independent forces is established (after some time).
- Full time dependence.

In both cases it is important to take into account the change in the forces due to the interactions themselves. A self-consistent treatment is required, either analytical or by computer simulations.
In a simpler cases, when the forces are not strong enough to change significantly the properties of the two beams, the beam-beam interaction can be treated as a perturbation, i.e. with constant (time independent) non-linear forces. A word of clarification is needed to explain what we mean by properties: although strong non-linear forces can be responsible for the loss of large amplitude particles and short life time of the beam, the number of particles affected is not sufficient to change the main properties which determine the beam-beam force in the simplest case: i.e. the beam intensity and beam size. In the case of separated beams the distance between the beams is included in the list of vital parameters. It is therefore the first priority to identify which approach is necessary to obtain the correct results for the problems under study. A wrong choice of the techniques will eventually lead to wrong and irrelevant results and conclusions. In the following we shall give some illustration of cases where the two situations are valid and we discuss some of the standard techniques which are used to get reliable results.

1.3 Single particle effects

A perturbative model can apply in a situation where the properties of the beam-beam interaction do not change in time. This means that when the two beams collide the forces produced by these remain constant collision after collision. A typical and often used example are the fields produced by a weak beam which does not affect the strong one while the strong beam electromagnetic force will perturb and change the properties of the weak beam. As a consequence the electromagnetic fields produced by the strong beam, since unperturbed, will remain constant. On the other hand the force produced by the weak beam, strongly modified, does not perturb the opposite beam and therefore can be neglected. An analogue is a static electromagnetic lens.
A perturbative approach applies for example when a strong disparity is present between the two colliding beams (i. e. in intensity). In this specific case only one beam is affected by the beam-beam force (weak beam) while the other remains unperturbed (strong beam). Due to a higher density (higher intensity and/or smaller beam sizes) the beam-beam force produced by the strong beam is larger than the one from the weak one and as a result of the interaction the strong beam will be unperturbed while the weak one changes

significantly its characteristics without however affecting the system. Working in this regime are for example the S$p\bar{p}$S collider at CERN and previously the Tevatron proton-anti-proton collider at Fermilab. The p beam intensity is more than twice the $\bar{p}$ intensity, therefore when interacting at the experiments or along the helical path the strong field produced by the protons will affect the $\bar{p}$ beam while the optical properties of the proton beam remains almost unperturbed. At successive interactions the protons will produce the same field since they were not perturbed. In this frame numerical simulations and calculations become simpler since one of the two beams remains the same and therefore the force calculations can be simplified and standard techniques applied. With this approach one can study effects of beam-beam on dynamic aperture, phase space structure, detuning with amplitude and in general the perturbed dynamics of a single particle.
When the beam-beam forces are not strong enough to change the optical properties of a beam, they can be considered as originating from a static, non-linear lens. The dynamics of the beam is then basically determined by single particle dynamics in non-linear fields and well established tools can be applied although we should allow for new effects which do not exist in single particle dynamics.
The main categories of effects that can be studied by single particle perturbation treatment are:

- Incoherent effects, particle losses and reduction of dynamic aperture.
- Distortion of the transverse phase space. The amount of distortion is an important measure of whether a perturbative treatment is applicable or not.
- Non-linear detuning and excitation of resonances due to the very non-linear nature of the forces.
- Dynamic beta effects.

For a better understanding of the single particle effects we will describe the effects listed above trying to give a physical picture of the mechanisms.

1.3.1 Dynamic aperture effects

Since the beam-beam force is strongly non-linear, the motion of particles can become unstable or chaotic. This often leads to a reduction of the available Dynamic Aperture (DA). The dynamic aperture is the phase space region in which particles of the beam remain stable. Particles outside the dynamic aperture can eventually get lost. The dynamic aperture is usually evaluated by tracking particles of a beam through the machine under the effect of the fields from the machine elements and other effects such as wake fields or beam-beam interactions. Particles are usually considered lost when they have reached large amplitudes for which they touch the mechanical aperture of the machine, defined by the beam screen and or other physical devices, i.e. collimators. In the real machine these effects are noticed by the measurement of particle losses and a reduced beam life time. When one wants to study the effect or behaviour of the losses due to beam-beam interaction one can apply at the location of the IP a beam-beam element using the weak-strong model. A particle with initial coordinates in the phase space (x, p_x, y, p_y) is tracked along

the machine and at the beam-beam element it will receive an angular deflection which is determined by the properties of the opposite beam. As a result the particle trajectory will be changed. The beam-beam element will not see the effect from the single particle and therefore will stay constant in time. This is repeated for samples of particles representative of a beam with a defined particle distribution in amplitude and angle. Long term stability of the LHC beams in the presence of beam-beam effects has been studied using the tracking code SixTrack [4, 91, 3].
Studies of long term stability of particles which experience head-on as well as long range beam-beam interactions can be investigated for different optical configurations and machine imperfections [3]. An example of the effect of beam-beam interactions on the LHC dynamic aperture is shown in Figure 1.2. In Figure 1.2 we show the DA for a particle of defined amplitude but with different initial angle in the $x - y$ space, with and without nominal beam-beam interactions in the LHC. In the picture we also show an intermediate case with reduced beam-beam effects. The definition of minimum or average DA comes from the fact that these studies are performed including also machine non-linear imperfections which are defined statistically through different machine configurations and therefore a statistical evaluation is more appropriate.

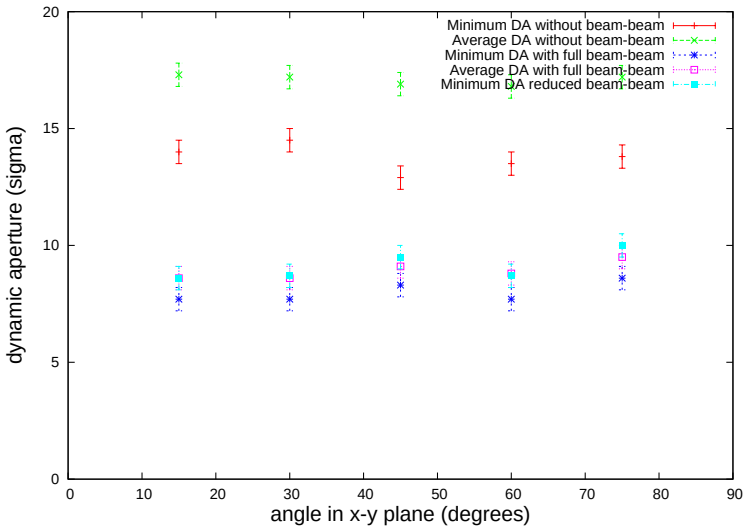

Figure 1.2: Minimum and average dynamic aperture for different x-y angles with and without beam-beam interactions for the LHC case [6].

1.3.2 Detuning with amplitude

Like all non-linearities also the non-linear beam-beam force manifests as an amplitude dependent tune shift and for a beam with many particles this results in a tune spread. Tune shift and spread are usually quantified with beam-beam footprints which show the two-dimensional tune space occupied by the particles. The overall tune spread can extend across resonances and produce a reduction of the dynamic aperture of the machine. Figure 1.3 shows the distribution of particles of one beam undergoing a head-on beam-beam interaction. The interaction is evaluated for round beams for the nominal LHC beam parameters and betatron oscillating frequencies. It is clear that particles at smaller amplitudes are strongly affected by the interactions and therefore move farther away from

the unperturbed tunes. Due to this tune spread particles can cross resonance lines in the tune diagram and therefore can become unstable and are eventually lost. Resonances can be excited either by non-linear errors of the accelerator elements or by the beam-beam force itself.

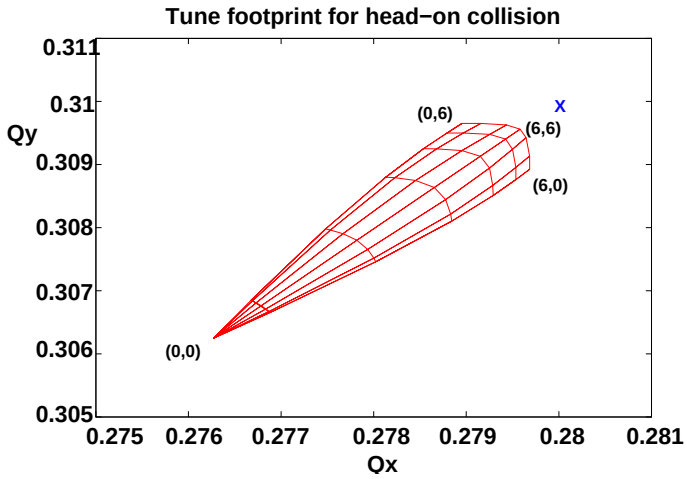

Figure 1.3: Particle distribution in tune diagram in the presence of one head-on collision. Particles at different amplitudes move away from their unperturbed horizontal and vertical fractional tunes, $Q_x = 0.28$ and $Q_y = 0.31$, indicated by the cross due to the beam-beam interaction.

For this study beam-beam elements are modeled with electrostatic lenses located at the interaction points. Samples of particles representative of one beam are tracked trough the accelerator components in the presence of these non-linear lenses and the resulting perturbed betatron frequencies are plotted on a scatter plot defined as the machine tune diagram. In this case a self-consistent treatment is not required. Beam-beam elements are considered as static objects which do not change their properties. Studies of the tune distribution of particles (footprints) are done using the MADX code [5]. Beam-beam elements are added using a MADX module. Detailed studies on this subject can be found for the LHC in [7].

1.3.3 Phase space structure modification

The presence of beam-beam interaction leads to a modification of the phase space structure. Due to the strong non-linear field from beam-beam interaction we have the formation of resonances of higher orders which lead to particle loss, short life time and possibly to an unstable beam. An example of these effects is given in Figure 1.4 where we show the horizontal phase space modification, simulated with the SIMUL code, in the presence of beam-beam interactions. In the two cases of Figure 1.4 we apply a weaker and stronger beam-beam strength which leads to a weak (left picture) and strong (right picture) phase space modification all in the presence of synchrotron motion coupling to the transverse plane. The motion of particles in the phase space is shown for different amplitudes of the particles. In the case of a completely linear machine particles at different amplitudes should stay on a stable trajectory and turn after turn describe a simple circular trajectory in phase space with a frequency equal to the machine tune. This is almost the case shown

in Figure 1.4 left. Particles go back to their initial location with a frequency of exactly $2\pi Q_x$. As soon as a strong beam-beam interaction is included (Figure 1.4, right) the elliptical trajectory of the particles is deformed. The deformation depends on the interaction intensity and influences different particles according to their amplitude. Particles at smaller amplitude are less affected by the non linear beam-beam force while larger amplitude ones are strongly influenced and therefore deviate from their linear motion.

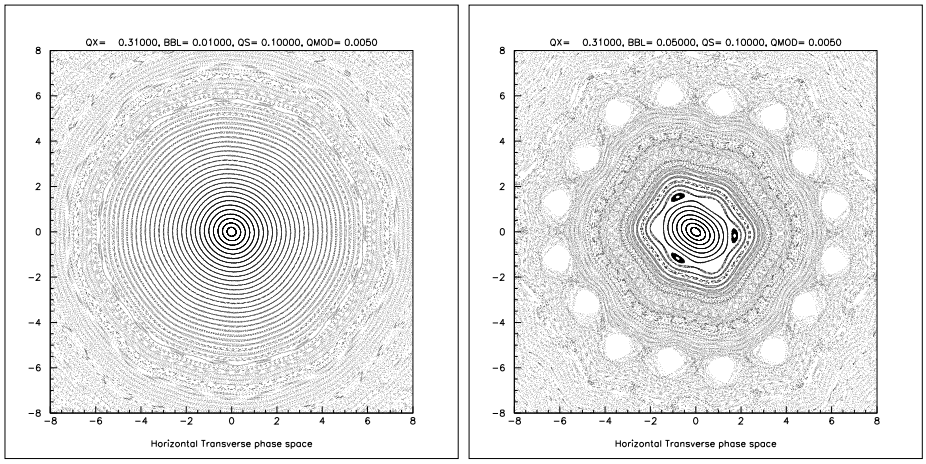

Figure 1.4: Particles' horizontal phase space when undergoing four head-on beam-beam interaction for different beam-beam strengths. Left plot for weaker $\xi = 0.01$. Right plot for a stronger $\xi = 0.05$.

It should be clear from these simple phase space plots in Figure 1.4 how the effects of beam-beam interactions can change the beam dynamics and how one has to choose modeling tools accordingly. Using a perturbative method is a good approximation for the case of Figure 1.4 (left) for which the beam-beam effects are small and particle dynamics is not significantly changed due to the interaction itself. In this case the particles and therefore the beam motion do not deviate much from the unperturbed case. On the other hand in the case where the beam-beam interaction is strong enough, the modifications of the particle motion are significant and able to change the beam characteristics (Figure 1.4, right) and therefore the interaction itself. One has therefore to apply a self consistent treatment of the problem which will evaluate these modifications in a time evolving frame.

1.3.4 Dynamic beta

Since the beam-beam interaction is basically an additional non-linear lens in the machine, it distorts the optical properties of the accelerator. In addition to visible tune shift ΔQ, an amplitude dependent beating of the optical functions appear. In particular it may create a noticeable variation of the β function around the whole machine and at the location of the beam-beam interaction itself. This can be approximated by inserting a quadrupole which produces the same tune shift at the position of the beam-beam interaction. The r.m.s. beam size at the collision point is now proportional to $\sqrt{\beta_p^*}$, where β_p^* is the perturbed β-function which can be significantly different from the unperturbed β-function β^*. This in turn changes the strength of the beam-beam interaction and the parameters have to

be found in a self-consistent form. This is called the dynamic β effect.
A strong dynamic β effect was found in LEP [67] due to its very large tune shift parameters. In the LEP case changes in the optical beta function at the experimental area locations were of the order of several cm in the vertical plane. The β function at the IP could be decreased from the unperturbed values ($\bullet$) by 5 cm down to 2.5 cm for a symmetric beam-beam interaction without imperfections ($\triangle$).

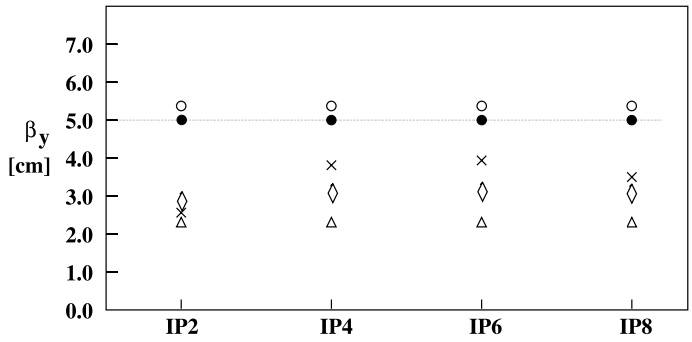

Figure 1.5: Optical beta functions at the interaction points as modified by the beam-beam interactions [67].

Beta beating induced by beam-beam interactions is sensitive to other parameters: the phase advance between IPs, the tune of the machine and the offset at collision. This was experimentally demonstrated in LEP. Figure 1.5 shows the effects of changes in these parameters on the β-function for the LEP collider. The β-function at the IPs are plotted for the unperturbed case ($\bullet$), when a pure phase advance error is introduced ($\circ$), when four beam-beam symmetric interactions are introduced ($\triangle$), when a phase advance error is added ($\times$) and when a small offset is introduced at the beam-beam interaction in IP2 ($\diamond$).
For the LEP case dynamic beta effects coming from the beam-beam interactions were contributing positively to the accelerator performances and therefore deliberately emphasized. A luminosity increase was produced due to the significant β_p^* reduction at the IP locations. Moreover, a decrease of the tune spread as obtained by controlled variations on the accelerator tune. Thanks to the strong damping of leptons it was possible to operate the accelerator with tunes just above the integer resonance without significant losses. Due to the beam-beam tune shift dependency on the tunes this resulted in a significantly reduced frequency spread. The beam foot print was reduced and more space in the tune diagram was available for operation.

A clear example of this effects which directly relates with machine luminosity is shown in Figure 1.6. In this plot the luminosity is shown as a function of the total current for two days of high energy physics run in the CESR e^+e^- collider for two different working points just above the half integer tune. Closer to a half integer betatron frequency, Figure 1.6 at the bottom, the dynamic β effect is visibly stronger, producing a reduction of the β^* at the IPs and therefore a direct increase of the measured luminosity (+ sign in Figure 1.6). The effect is explained as soon as we consider the dynamic β effects coming from beam-beam (black $\triangle$ in Figure 1.6) in the simulations. Without this a reduced luminosity increase is

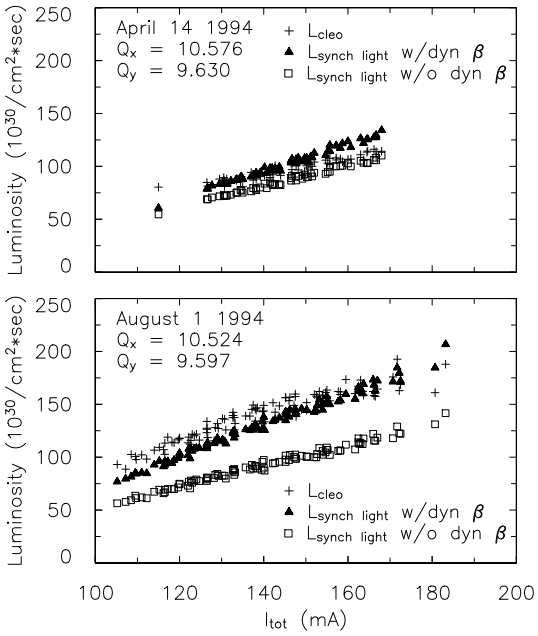

Figure 1.6: Luminosity as a function of total stored current for two days of high energy physic running at the CESR, Cornell,$e^+ - e^-$ storage ring. The two plots are for two different working points just above the half integer value. The plots show the luminosity as measured in one of the experiment CLEO (+) and simulated with (black $\triangle$) and without (squares) dynamic beta effects.

expected (square).
The LHC case is different since the accelerator will operate protons against protons. This will lead to an increase of β^* instead of the decrease typical of opposite charge colliders and therefore to a direct deterioration of the machine luminosity. However in terms of variations in the optical functions we do not expect significant modifications, therefore the β beating due to beam-beam interactions will not represent an issue. For the LHC nominal case we expect an increase in the optical β-function from the nominal value of $\beta^* = 0.550$ m to a perturbed one of $\beta^*_p = 0.557$ m at the main IPs [9]. This translates into a $\Delta\epsilon = 1\%$ emittance variation of the beams at collision. We just have to remember that due to the injector chain, an emittance variation of approximately 10% is expected in the LHC and therefore this particular beam-beam effect stays in the shadow of more important contributions. On the other hand it is not possible to achieve a reduction of the particle tune spread by operating a proton machine close to a half integer tune where the beam-beam tune shift is smaller. Proton beams do not show a significant damping and therefore the half integer tune resonance represents an extremely dangerous working point. The LHC will operate at $Q_x = 0.28$ $Q_y = 0.31$, far enough from the detrimental integer resonance.
For dynamic β studies it is essential to simulate the particle's behaviour in a self consistent manner. Due to the beam-beam interactions the optical functions change and therefore also the interaction itself. Turn after turn the changes should be evaluated and used for the computations in the next revolution. These studies are done using MADX with beam-beam elements where needed. The optical functions are evaluated and recomputed self consistently with all machine elements.

1.4 Collective effects

When we want to study self-consistent beam-beam interactions, we must assume that the source of the field itself can change as a result of the interaction. In this frame the beam-beam force is changing in time due to the new distribution of charges created as a consequence of the previous collision. This is the regime where the beams can show coherent motion: particles develop a collective and organized motion. The most visible effects in an accelerator of this type are the following:

- Coherent modes (dipolar and higher orders).
- Orbit effects.
- Emittance effects.
- Bunch coupling.

Past and recent colliders which worked and will work in this regime are the CESR, the CERN LEP collider, S$p\bar{p}$S and Large Hadron Collider (LHC), the RHIC at BNL and in our days also the Tevatron.

1.4.1 Coherent modes

Beyond single particle dynamics it is interesting to look at the response of the beam as a whole when interacting with the electromagnetic field of other beam. It is known that particles can develop a collective motion due to the coherent interaction with the counter-rotating beam and vice versa. Particles of a bunch organize their motion coherently and the effects of a beam-beam interaction can lead to a new collective motion of the two beams. Due to the beam-beam interaction the two beams will be a strongly coupled system and the dynamics of one will directly influence the second one and vice versa. This was visible and measured in LEP, S$p\bar{p}$S collider, RHIC and will be of strong interest in the LHC.

Figure 1.7 shows betatron frequency spectra of colliding beams in LEP (left) and RHIC (right) colliders. The unperturbed horizontal tunes of the two colliders were at a frequency of $Q_{LEP} = 0.28$ and $Q_{RHIC} = 0.213$, respectively. However, in the plots two peaks are visible: one represents the betatron frequency (the machine unperturbed tune) and the second peak which is the developed coherent mode frequency. In addition to the detuning which creates the tune spread between the two peaks, the second peak shows a new collective motion. The new frequency is shifted to higher frequencies ($Q_{LEP} = 0.34$) in the case of an opposite charge collider and to lower frequencies for equally charged beams ($Q_{RHIC} = 0.209$). The shift in frequency depends on the strength of the interaction. Without any beam-beam interaction the beams will independently oscillate at the Q_0

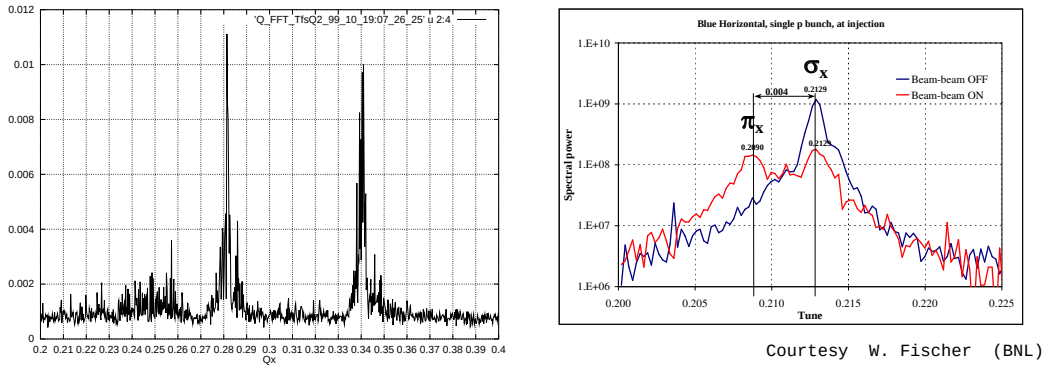

Figure 1.7: Coherent mode frequencies in LEP (left). Coherent mode frequencies in RHIC collider (right) [100].

unperturbed tunes. As soon as the beams are brought into collision, the beam-beam force coherently excites the beams which develop a new collective oscillating mode with frequency Q_p.
The system of two beams colliding at the main IPs can be compared to a system of two coupled harmonic oscillators. Due to the beam-beam force which relates the two beams the coupled system develops a coherent motion which differs from the independent single oscillators behaviour. The coupled oscillator's new motion will then be a linear combination of these two coherent modes developed by the interaction. Appearance of coherent modes is enhanced by symmetric cases when the beam-beam interactions occur between equal size and charged beams and equal betatron oscillating frequencies. To simulate a coupled system like two beams colliding, a self-consistent treatment of the interaction is essential. The two beams and/or bunches will distort each other and turn after turn the interaction has to be reevaluated using the modified beams' properties. In Figure 1.7 only two modes are visible. However, one should expect many more for multiple bunch beams and for asymmetric multiple interactions. Coherent modes in lepton machines are rarely an issue. Synchrotron radiation damps coherent excitations. On the other hand protons can easily organize their motion and coherent effects could be an issue during operation since in this situation one has to realize that anything happening to a single bunch propagates to the whole coupled system. In RHIC, in order to avoid coherent modes and to decouple the two beams, the accelerator is operated with two different betatron tunes for the two beams [15]. In this way the symmetry of the system is broken and for the beams it is more difficult to organize the motion in a collective way. A more detailed discussion of coherent modes will follow later.

1.4.2 Self consistent orbits

The beam-beam interaction between two beams can occur either at almost zero distances which corresponds to the case of the two beams colliding at the IP location, like in RHIC, or at a large distance as is the case of the LEP collider, the Tevatron and the LHC. The first type are called head-on collisions while the second type are known as long range interactions. For the LEP and Tevatron cases the parasitic interactions are due to the

fact that we have one machine with a single beam pipe and two beams which circulate avoiding collisions around the arcs with separated trajectories. Therefore, around the ring they interact at several locations at a long range distance. The LHC case is different since more parasitic long range interactions occur due to the high number of bunches per beam and to the fact that a crossing angle is foreseen, in this case to avoid multiple head-on collisions in the interaction regions (IR) around the IP before the two beams are separated into two different beam pipes (as schematically sketched in Figure 1.1 where the trajectories along the two rings are shown: blue line for the clockwise beam and red for the anti-clock wise one). At IPs 1, 2, 5 and 8 the beams exchange from the outer to the inner ring and vice versa. The crossings at the IPs happen for the LHC case with a small external crossing angle as schematically sketched in Figure 1.8. Therefore, bunches left and right of the IPs suffer from long range interactions. Although less strong than a head-on collision, these long range interactions become important due to the high number. Furthermore, when two beams do not collide exactly head-on, the force has a constant contribution. The bunches receive a coherent kick which changes this closed orbit as schematically illustrated in Figure 1.8.

Moreover, since these long-range interactions occur at different locations around the IP

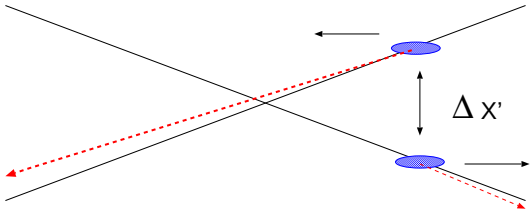

Figure 1.8: Offsets at collision due to beam-beam interactions in the LHC

and at different beam separations, this results in strong bunch to bunch differences in the closed orbit. When the orbit of a beam changes, the separation between the beams at the IP will change as well, which in turn will lead to a slightly different beam-beam effect and so on. The orbit effects must therefore be computed in a self-consistent way [45, 46], in particular when the effects are significant. The closed orbit of an accelerator can usually be corrected, however an additional effect which is present in some form in many colliders, sets a limit to the correction possibilities. When the bunches experience many long range beam-beam interactions, depending on the single bunch collision pattern, then the picture becomes very complex as shown in Figure 1.9. There we show the beam-beam orbit effects on three different bunches(red, blue and green dots) when the LEP collider was operated with bunch trains. The Figure 1.9 is a transverse scan [16] for luminosity optimization done by steering the orbits of the bunches at the IP. One should notice that depending on the position of the bunch in the train the location of the luminosity maximum changes (red, blue and green dots). This is symptomatic of different offsets at the collision points. Therefore, optimizing the luminosity for one bunch could result in a deterioration for the others.

For the LHC case the large number of long range interactions will lead to many different families of bunches (not only three as in the case of the LEP collider). We define a nominal bunch as the one which will see all possible beam-beam interactions, i.e. a bunch in the centre of a train. Bunches at the head and tails of the trains will see

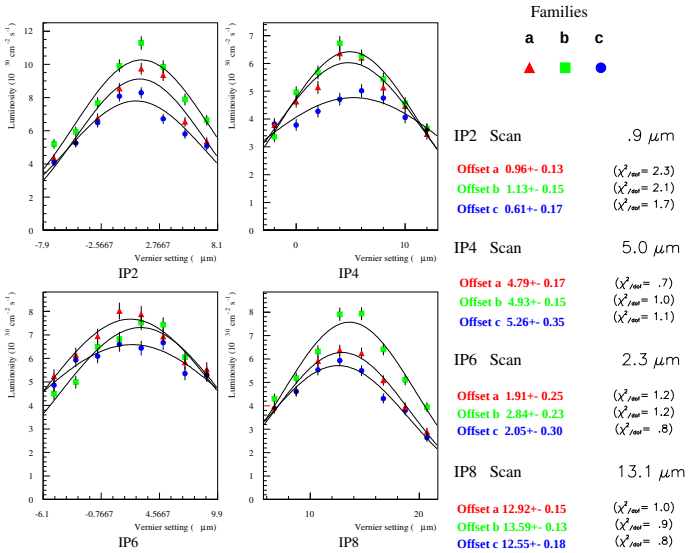

Figure 1.9: Vertical orbit measured at the separation scan at LEP for three different bunches of a train. Offsets at the four collision points due to long range beam-beam interactions are visible at the four experimental areas.

a different number of parasitic encounters. Due to the different collision patterns for different bunches excursions of $1 - 2$ μm are expected at the IP. These effects at the IPs will lead to different peak luminosities and therefore to other beam-beam effects as will be explained in a later chapter. Also, it is not possible to apply a single bunch orbit correction, therefore an average correction over the whole beam should be found in order to maximize the machine luminosity. A fully self consistent treatment of trains of bunches is of fundamental importance to evaluate the train behaviour and to define the representative family to correct for best luminosity.

1.4.3 Effects on beams emittance

A further beam-beam effect which can develop during machine operation is the variation of the beam emittance. The beams exert a force on each other and the effect on the emittance can be a systematic growth. This is a very important effect since it has a direct implication on the machine luminosity, by reducing it. In Figure 1.10 we show as an example the emittance growth ratio (%) versus beam-beam strength for different runs in 2005 and 2006 of the RHIC over four hours in store.

The evolution of the beams' emittance is another effect requiring self consistent treatment. Since the parameters which determine the beam-beam strength are changing as a result of the interaction. Many studies have been done so far using only a perturbative model [17, 18] in comparison with a self consistent approach. Simulations were used to study possible emittance growth effects for the LHC in the presence of external noise. However, recent studies with fully self consistent modeling of the emittance evolution in time for defined machine operational conditions show that further physics effects develop and should be taken into account. In a dedicated chapter a demonstration of the necessity of strong-strong simulations to study the beam emittance evolution in proton-proton colliders will be addressed for the case of the LHC when as a result of long-range beam-beam

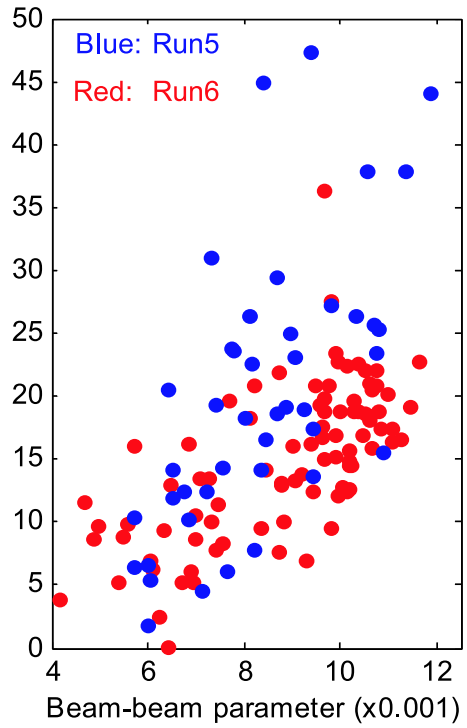

Figure 1.10: Measured beam emittance growth of early 4 hours in store RUN 2005 and RUN 2006 versus the beam-beam strength ξ at the RHIC [8]

interactions, the head-on collisions occur at a static orbit offset.

1.4.4 Bunch coupling

A system of bunches colliding can be compared to a system of harmonic oscillators coupled through the beam-beam interactions. The number of interactions are usually equal to the number of experiments in the storage ring and here the bunches of opposite beams directly interact. Depending on the symmetry of the collisions it is not always the same bunches that undergo collisions therefore we can have a crosstalk of bunches inside the same beam as a consequence of multiple interactions. In bunched beam colliders, the study of rare physical events requires higher and higher luminosity. This is obtained by either increasing the bunch densities (i.e. smaller beam sizes and/or higher intensities per bunch) or increasing the number of bunches in the ring.

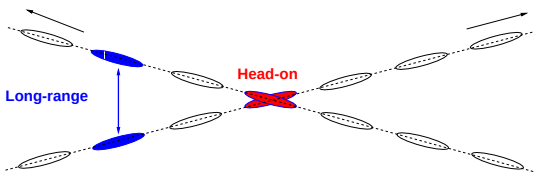

Figure 1.11: Schematic layout of the LHC beams colliding with an external crossing angle

Increasing the number of bunches by a factor N_b will result in a luminosity increased by the same factor. However, filling the machine with too many bunches could also bring

multiple head-on collisions in the experimental areas which must be avoided. Therefore in the case of high number of bunches a small external crossing angle is normally applied as schematically shown in Figure 1.11. This external correction transforms unwanted multiple head-on collisions into weaker long range interactions. However, the crossing and therefore the many long range interactions increase the crosstalk of bunches. This is very important since increasing the interactions between different bunches increases the coupling of our two beam system. In this situation during operation one should always evaluate the coupling effects coming from the crosstalk of bunches before acting on a single bunch. Depending on the interaction scheme, any excitation will be transmitted to other bunches of the same and opposite beam.

1.5 The LHC beam-beam effects

As we have already mentioned in our previous discussion on perturbative and self-consistent treatment, the Large Hadron Collider (LHC) represents an impressive complication in terms of beam-beam studies. To obtain the highest luminosity, the LHC is operated with a large number of bunches which are subject to the strong beam-beam effects of the head-on as well as long-range interactions. There are 4 main experimental areas in total where the two beams collide through four head-on and up to 120 long-range interactions. This represents the major challenge for beam-beam simulations. On top of this, the LHC is also an accelerator where beam-beam effects will be pushed to the limit, and only a self-consistent treatment of the physics behind must be applied. Other storage rings may be studied with simplified approximations while for the LHC only a global and complete description will lead to a correct physical picture. Most of the known major beam-beam effects will be of interest at different stages of the collider operation and one has to reproduce them all self-consistently to be able to provide quantitative correct predictions and when possible propose countermeasures to improve the performance. Improving one effect is never enough since this can imply deterioration of others.
In the table below we have summarized known beam-beam issues for various past, present and future colliders. It is evident that the LHC will be a machine with a full combination of all relevant effects and working in a regime not yet completely understood from the operational point of view. In this frame simulation studies could represent an important tool for understanding diagnostics and predicting machine behaviour.

Beam-beam effect	SPS	LEP	Tevatron	RHIC	LHC
Number of bunches/interactions	*	*	**	*/**	***
Strong-strong regime	N	Y	N/Y	Y	Y
Coherent effects	N	Y	N/Y	Y	Y
Complicated mode spectra	N	N	N	Y	Y
Pacman effects	N	N	N	Y	Y
Flip Flop effect	N	Y	N	N	N
Dynamic beta	N	Y	N	N	N
Long range	Y	Y	Y	Y	Y
Lifetime/DA	Y	N	Y	Y	Y
Crossing angle	N	N	Y	N	Y
Bunch to bunch fluctuations	Y	N	Y	Y	Y
Bunch to bunch orbit effects	N	Y	N	N	Y
Bunch to bunch tune effects	N	Y	N	N	Y
Unequal beam size problematic	Y	N	Y	Y	Y

Table 1.1: Observed and expected beam-beam problems for lepton as well and hadron colliders. The N stays for NO while the Y for YES. The * symbol means low number of bunches/interactions, ** medium level of complexity while *** high number of bunches and BBIs.

In the LHC we have two counter-rotating bunched beams with up to 2808 bunches each, non-uniformly spaced along the rings. The beams travel in two separated beam pipes along the arcs and are brought into one common beam pipe at four interaction regions corresponding to the experimental areas in the CMS, ATLAS, LHCb and ALICE caverns. At the interaction points of these four experimental detectors the beams will collide and experience four head-on beam-beam interactions.

Longitudinal buckets filled with a bunch will be spaced according to the desired operational mode [13, 14]. For a longitudinal bunch spacing of less than 260 ns the beams need to collide with an external crossing angle (i.e. Figure 1.11) in order to avoid simultaneous multiple head-on collisions before and after the interaction point. Operation with an applied external crossing angle avoids multiple head-on collisions but creates long range interactions. For nominal LHC operation [13] one should expect 30 possible locations for long range beam-beam interactions at each experimental region. Depending on the bunch position within a batch (sequence of 72 bunches) bunches can interact up to 120 times. We define these as nominal bunches while bunches at the head or tail of a batch will see less long range interactions and are defined as PACMAN bunches. Depending on the longitudinal position in a batch, bunches will see different collision patterns and therefore will show different properties. The result of this could be:

- Coupling between the bunches.
- Different bunches being affected differently, leading to different parameters such as tunes, orbits and chromaticities.
- All the above effects being amplified by the irregular collision and filling schemes.
- Due to the large number of bunches they will have different initial conditions (e.g. intensities and beam sizes) in the first place.
- The two beams will behave as a strongly coupled system, changes to one beam directly affects the second beam.

The two colliding beams are equally intense and the effects of the interaction will strongly deform both beams at a similar level. Moreover, bunches in a beam will also be organized in a coherent motion, therefore we have to evaluate the behaviour of the entire beam to understand the observables. Under these conditions a single particle, perturbative approach is entirely inappropriate and leads to meaningless results. To qualitatively and quantitatively study beam-beam effects in the LHC a fully self-consistent multiple bunch model is needed. In the past many tools have been developed to address beam-beam strong coupling. For the LHC we take these further allowing any number of bunches as well as collision patterns. This allows to define conditions for the LHC beams, such as bunch pattern and tolerances on parameters relevant for the beam-beam interaction and eventually for the machine luminosity. Operational hadron colliders such as the Tevatron and the RHIC for proton runs define beam-beam effects as the major limiting factor for their performances. All upgrade studies for these machines are based on developing new ideas and/or technologies to compensate for beam-beam interactions (head-on as well as long-range). These two accelerators represent a valuable test bench for studies on the

LHC. The Tevatron collider uses a pretzel collision scheme. Therefore on top of the two head-on collisions at the experiments, along the pretzel the beams experience several long range interactions. Due to these interactions along the arcs of the machine bunch to bunch differences are expected and were observed during the last years of runs.

1.5.1 Need for self consistent treatment

To have a realistic picture of the LHC beam-beam effects it is essential to go for a self-consistent treatment of the beam-beam interaction. Depending on the effects under study, approximations for the charge distributions as well as for the electro-magnetic fields can be valuable. However, only a multi particle description of the beams and therefore a full solution of the Poisson equation for the evolving distributions must be the aim of a deep study of the effects to have a complete and quantitatively correct picture. In this frame we have decided to develop a simulation model which gives the possibility to select different approximations in order to keep computing time under reasonable limits.
The goals of the study are:

- Make a step forward in the understanding of the physics of beam-beam interactions.
- Extend the present knowledge of single-few bunch interaction to the multiple bunch interaction.
- Extend the present knowledge of single-few bunch interaction to the multiple interaction regime.
- Study effects of clustered long range beam-beam effects.
- Provide a tool for a quantitative prediction of the effects for beam diagnostics.
- Where possible, provide countermeasures to improve collider performance.

For these purposes we have developed a set of tools which will represent important instruments for beam diagnostics during accelerator operation as well as a powerful predictive model to define possible upgrade scenarios for new physics requirements.
We have decided to study the phenomena of beam-beam interactions through different but complementary models. We have made the choice of going for 4 different models of the interaction and beams, namely:

- One turn map formalism.
- Rigid bunch Gaussian kick code.
- Multiple particle bunch Gaussian approximation kick code.
- Multiple particle bunch kick code with parallel Poisson solver.

Simplified models are important to understand the qualitative picture and give complementary information about damping mechanisms and in general multi bunch behaviour

due to the interaction itself. However, they are not sufficient when the aim is to reach a good quantitative prediction useful for machine operation. Therefore, the aim of this study, from the very beginning was to build a fully self consistent treatment of beam-beam interactions for beams of the LHC kind. We want to simulate many bunches in particular the nominal LHC case with 2808 bunches per beam with up to 124 interactions per turn. This would not have been possible till our days due to the prohibitive time scale such a simulation would require on a single processor. However, with the development of super computers and parallel algorithms, the situation has improved and multi particle multi bunch beam-beam interactions can be simulated.
The thesis is organized in 5 main parts.
The first part, **Chapter2**, is dedicated to define the mathematical formalism and the physical picture behind beam-beam interactions. We describe all the mathematical tools needed to proceed for a more complex computer modeling of the interaction. Where needed new formalisms for a proper beam-beam modeling are introduced.
Chapter 3 explains the development and implementation of the different models. We want to point out pros and cons of each approximation and the important information one can derive from the results. As a consequence we will demonstrate the importance of the complementary models developed to correctly interpret the results.
From a first interpretation of the results for simplified cases of multiple bunch beams, we will study in **Chapter 4** coherent beam-beam effects. In particular, we will reproduce tune spectra and evaluate possible counter measures to break the collective organization of dipolar motion between the colliding bunches. The break down of organized coherent motion will be studied as a function of the beam and machine parameters such as different working points for the betatron frequencies, fluctuations in the bunch intensities and transverse beam sizes.

Chapter 5 and **Chapter 6** are dedicated to the Large Hadron Collider coherent and incoherent beam-beam effects. We will show expected tune spectra for nominal and PACMAN bunches in different machine configurations. In particular by studying the effects of different phase advances applied through the accelerator arcs. A study of the breaking of this strong coupling will be shown. The emittance behaviour as a function of static offsets in collision is also addressed.
Confident of the interpretation of simulation results, an application to an existing accelerator will be addressed in **Chapter 7**. The study will define the physical picture of coherent and organized bunch motion for the Relativistic Heavy Ion Collider. We will first define the characteristics of the accelerator strong-strong beam-beam effects for proton-proton runs using the different models. In a second step we will reproduce the so called beam transfer function (BTF) measurement performed during physics run. For the first time an interpretation of the measurements feature will be given, focusing on coherent dipolar modes exited by the measurement device. The interpretation of the measurements resulted in a very promising diagnostic tool, and as a result improvements of the diagnostics were proposed.

Chapter 2

Beam-beam Interactions

The Beam-Beam Interaction (BBI) has been the subject of many studies since the first particle collider was built. It has been and will be one of the main limiting factor to the performance of colliding beam facilities. A particle beam is a collection of charges and represents an electromagnetic potential for other charges. A charged beam will therefore exert forces on itself and other charges. In a collider these interactions can be very strong and can occur whenever the two counter rotating beams share a common space. This happens either at the locations corresponding to the experimental points where for the physics one aims to have the beams in collision, or in other parasitic locations defined by the geometry of the collider. The electromagnetic forces from the particle distributions are very non-linear and result in a wide spectrum of effects for the beam dynamics as we have phenomenologically discussed in the introduction. Furthermore, as a result of the interaction itself, the particle distribution changes which has strong implications for the field and forces mainly in circular machines where the beams interact for many hours during the high energy physics runs. Beam-beam interactions lead to several and different consequences and although we have a good qualitative understanding of the underlying physics of the various phenomena, a complete theory does not exist and exact predictions are difficult. Numerical simulations have been used with great success to improve the picture on some aspects of the beam-beam interaction while for other problems the available models are not fully satisfactory in their predictive power.
In this chapter an overview of the most important effects and on the underlying physics of the beam-beam interactions from the analytical formulation to the experimental evidences and understandings of the effects will be given [21, 22, 23, 24]. A brief description of the different existing models to study the phenomena is summarized in order to highlight their limitations and the need for a new quantitatively correct approach for future studies of multiple bunch effects.

2.1 Particle colliders

In particle physics experiments one is interested in the energy available for the study of new effects but also in the number of useful interactions (events produced). This is especially true when rare events with a small production cross section σ_p are studied. The quantity that measures the ability of a particle accelerator to produce the required number

of interactions is called luminosity and represents the proportionality factor between the number of events per time dR/dt and the cross section σ_p:

$$\frac{dR}{dt} = \mathrm{L} \times \sigma_p \tag{2.1}$$

The luminosity is a parameter given by the machine and beam properties. In this specific case of a circular collider a general formula for the luminosity when two Gaussian beams collide is of the form [33]:

$$\mathrm{L} = \frac{N_1 N_2 \mathrm{f} N_b}{4\pi\sigma_x\sigma_y} \cdot \mathrm{S} \tag{2.2}$$

where N_1 and N_2 are the two colliding bunch intensities while σ_x and σ_y are the horizontal and vertical beam sizes, respectively. The factor f is the revolution frequency of the bunches and N_b the number of bunches per beam. The factor S is a factor related to the geometrical overlap of the two particle distributions and can be equal to one in the case of perfectly overlapping beams while it is smaller than one in the case of collisions with a crossing angle and/or offsets and hourglass effect.

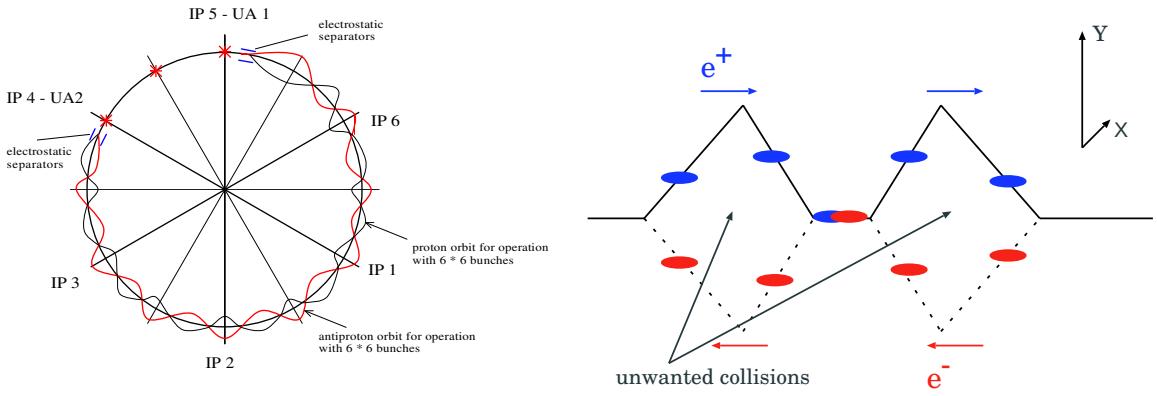

Figure 2.1: Beam separation with a Pretzel scheme in the S$p\bar{p}$S collider (left) and with short bunch trains in LEP interaction region (right).

Colliders can work either with equally charged or with oppositely charged beams. In the first case the machine will have two separate rings with one beam circulating in each one while in the second case a single ring can house both beams. To reach the highest luminosity, one can optimize the parameters of Equation 2.2. Present and past colliders push for the highest beam densities (high intensities and small beam sizes). In our days it is desired to operate a collider with as many bunches as possible since the luminosity is proportional to their number [33]. While going for higher densities make beam-beam interactions stronger, going for a higher number of bunches make the number of interactions higher. Therefore luminosity should be optimized by balancing the pros and cons of all the parameters.

In a single ring collider such as the SPS, Tevatron or LEP, the operation with k bunches leads to $2{\cdot}k$ collision points. When k is a large number, most of the interactions

are unwanted and must be avoided to reduce perturbations due to the beam-beam effects. Various schemes have been used to avoid these unwanted "parasitic" interactions. Two prominent examples are shown in Figure 2.1. The use of Pretzel schemes to operate multi-bunch beams in a collider had been first proposed and used at the CESR [19], then successfully applied to the SPS, Tevatron and the LEP. When the bunches are equidistant, this is the most promising method. When two beams of opposite charge travel in the same beam pipe, they can be moved onto separate orbits using electrostatic separators. In a well-defined configuration the two beams cross when the beams are separated (Figure 2.1, left). To avoid a separation around the whole machine, the bunches can be arranged in so-called trains of bunches following each other closely. In that case a separation with electrostatic separators is only needed around the interaction regions. Such a scheme was used in LEP in the second phase [63] and it is schematically illustrated in Figure 2.1 (right). This was possible for trains made of few bunches and a small number of trains. The RHIC and LHC on the contrary collide particles of the same type which therefore must travel in separate beam pipes. RHIC and LHC have two separate rings for the two counter rotating beams. At the collision points the two beams are brought together and into collision (as schematically shown for the LHC case in Figure 1.1). An arrangement of separation and recombination magnets is used for the purpose to make the beams cross (Figure 2.2).

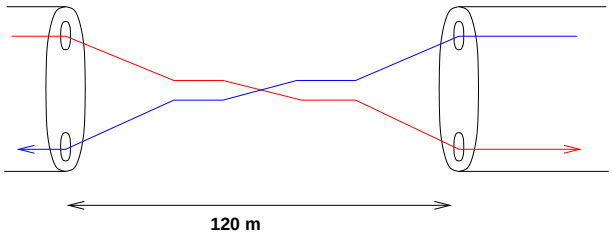

Figure 2.2: Cross over between inner and outer vacuum chamber in the LHC (schematic).

During that process it is unavoidable that the beams travel in a common vacuum chamber. In the RHIC case the bunch spacing is large enough to have the bunches collide already in the separated pipes before another set of bunches enter the experimental area. On the contrary in the LHC the distance between the bunches is only 25 ns at nominal conditions and therefore the bunches will meet in this region since the common part is 120 m long. The bunches will then meet each other not only at the foreseen interaction point but also to the left and right of it before being separated in the two rings. In order to avoid multiple head-on collisions, the bunches collide at a small crossing angle of 285 μrad as illustrated schematically in Figure 2.3.

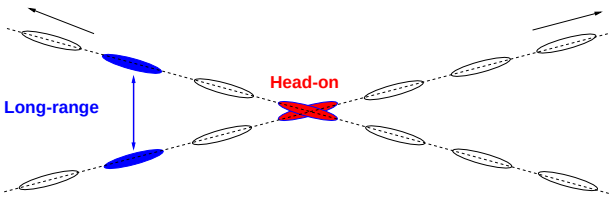

Figure 2.3: Head-on and long-range interactions in a LHC interaction point.

In Figure 2.3 while two bunches collide at a small angle (quasi head-on) at the centre,

the other bunches are kept separated by the crossing angle. However, since they travel in a common beam pipe, the bunches still feel the electromagnetic forces from the bunches of the opposite beam, even though when the separation is large enough, these so-called long-range interactions should be weak. From the bunch spacing and the length of the interaction region one can easily calculate that at each of the four LHC interaction points we must expect 30 of these long-range encounters, i.e. in total 120 interactions. The typical separation between the two beams is between 7 and 10 in units of the beam r.m.s. size of the opposing beam. Therefore, even if long range interactions distort the beams much less than a head-on interaction, their large number and some particular properties require careful studies.
From now on we distinguish between two different regimes of the beam-beam interactions which are present in particle colliders:

- Short range electromagnetic interaction, so called Head-On (HO) BBIs.
- Long range interactions, called Long Range (LR) BBIs.

While the first type is for obvious reasons unavoidable in a collider and correspond to interactions at the experimental points, the second type appears either as distributed parasitic interactions when the collider is designed with a Pretzel scheme (i.e. CECR, Tevatron, S$p\bar{p}$S collider) or as localized interactions around the experimental point (i.e. LHC, LEP II) when an external crossing angle is applied to avoid multiple HO collisions per IP.

2.2 Electromagnetic field of a moving beam

The particle distribution of the beam produces an electromagnetic field. In the rest frame of the beam we have only electrostatic fields and to find the forces on other moving charges, we have to transform the field into the moving frame and calculate the Lorentz forces. The fields are calculated by integrating over the charge distributions.
The beam-beam force is defocusing or focusing depending on the charge of the test particle (opposite beam), which can have the same or opposite sign with respect to the beam producing the field. For the force of the bunch on itself, i.e. the direct space charge, the kinematic factor is $(1 - \beta^2)$. This results in the known $1/\gamma^2$ behaviour of direct space charge effects, which are always defocusing [25]. Moreover, in the case of high energy colliders they are negligible due to this energy scaling. Therefore in this study they will be neglected since they are not relevant for the LHC case.
The distribution of particles producing the fields can follow various possible functions, leading to different fields (forces). It is not always possible to integrate the distribution to arrive at an analytical expression for the forces in which case either an approximation or numerical methods have to be used. This is in particular true for hadron beams, which usually do not experience significant synchrotron radiation and damping. In this case particle distributions can undergo important variations during operation. On the contrary for lepton colliders, i.e. e^- e^+, the distribution functions are most likely Gaussian with truncated tails and usually are the result of an equilibrium of the forces present.
A general and common [20] approach in electromagnetic problems and already applied

to beam-beam interactions [21, 22, 81, 24] is to derive the potential U(x, y, z) from the Poisson equation which relates the potential to the charge density distribution $\rho(x, y, z)$ of the beam.

$$\Delta U = -\frac{1}{\epsilon_0}\rho(x, y, z) \tag{2.3}$$

Then one computes the fields from:

$$\vec{E} \;=\; -\nabla U(x, y, z, \sigma_x, \sigma_y, \sigma_z) \tag{2.4}$$

The Poisson equation can be formally solved using e.g. the Green's function method (e.g. [26]) since the Green's function for this boundary value problem is well known and used in electrostatic problems. The formal solution using a Green's function $G(x, y, z, x_0, y_0, z_0)$ is then given by:

$$U(x, y, z) = \frac{1}{\epsilon_0}\int G(x, y, z, x_0, y_0, z_0) \cdot \rho(x_0, y_0, z_0) dx_0 dy_0 dz_0 \tag{2.5}$$

For the solution of the Poisson equation we get [27]:

$$U(x, y, z, \sigma_x, \sigma_y, \sigma_z) = \frac{1}{4\pi\epsilon_0}\int\int\int \frac{\rho(x_0, y_0, z_0) dx_0 dy_0 dz_0}{\sqrt{(x - x_0)^2 + (y - y_0)^2 + (z - z_0)^2}} \tag{2.6}$$

In the case of a beam with Gaussian beam density distributions, we can factorize the density distribution $\rho(x_0, y_0, z_0) = \rho(x_0) \cdot \rho(y_0) \cdot \rho(z_0)$ with standard deviations of σ_x, σ_y and σ_z along the corresponding axes:

$$\rho(x_0, y_0, z_0) = \frac{Ne}{\sigma_x\sigma_y\sigma_z(2\pi)^{3/2}} e^{\left(-\frac{x_0^2}{2\sigma_x^2} - \frac{y_0^2}{2\sigma_y^2} - \frac{z_0^2}{2\sigma_z^2}\right)} \tag{2.7}$$

Here N is the number of particles in the bunch of positive charge e. We obtain a potential of the form:

$$U(x, y, z, \sigma_x, \sigma_y, \sigma_z) = \frac{1}{4\pi\epsilon_0}\frac{Ne}{\sigma_x\sigma_y\sigma_z\sqrt{2\pi}^3}\int\int\int \frac{e^{\left(-\frac{x_0^2}{2\sigma_x^2} - \frac{y_0^2}{2\sigma_y^2} - \frac{z_0^2}{2\sigma_z^2}\right)} dx_0 dy_0 dz_0}{\sqrt{(x - x_0)^2 + (y - y_0)^2 + (z - z_0)^2}} \tag{2.8}$$

This is difficult to solve and therefore we follow instead the proposal by S. Kheifets [30] and solve the diffusion equation:

$$\Delta V - A^2 \cdot \frac{\delta V}{\delta t} = -\frac{1}{\epsilon_0}\rho(x, y, z) \qquad (\text{for } \; t \geq 0) \tag{2.9}$$

and to obtain the potential U we go to the limit $A \;\rightarrow\; 0$, i.e.

$$U = \lim_{A\to 0} V \tag{2.10}$$

The reason for going through the diffusion equation instead of the Poisson solution is that the Green's function takes a more appropriate form [27]:

$$G(x, y, z, t, x_0, y_0, z_0) = \frac{A^3}{(2\sqrt{\pi t})^3} \cdot e^{-A^2/(4t\cdot((x-x_0)^2+(y-y_0)^2+(z-z_0)^2))} \tag{2.11}$$

and we get for $U(x, y, z, \sigma_x, \sigma_y, \sigma_z)$:

$$\frac{Ne}{\sigma_x\sigma_y\sigma_z\sqrt{2\pi}^3\epsilon_0}\int_0^t d\tau\int\int\int e^{\left(-\frac{x_0^2}{2\sigma_x^2}-\frac{y_0^2}{2\sigma_y^2}-\frac{z_0^2}{2\sigma_z^2}\right)}\frac{A^3\cdot e^{-A^2/(4\tau((x-x_0)^2+(y-y_0)^2+(z-z_0)^2))}}{(2\sqrt{\pi\tau})^3}dx_0dy_0dz_0 \tag{2.12}$$

This allows to avoid the denominator in the integral and to collect the exponential expressions which can then be integrated. Changing the independent variable τ to $q = \frac{4\tau}{A^2}$ and using for the three integrations the formula [27]:

$$\int_{-\infty}^{\infty} e^{-(au^2+2bu+c)}du = \sqrt{\frac{\pi}{a}}e^{(\frac{b^2-ac}{a})} \qquad (for: u = x_0, y_0, z_0) \tag{2.13}$$

we can integrate (2.5) and with (2.10) we get the potential $U(x, y, z, \sigma_x, \sigma_y, \sigma_z)$ [28, 30] produced by our positively charged particle distribution:

$$U(x, y, z, \sigma_x, \sigma_y, \sigma_z) = \frac{1}{4\pi\epsilon_0}\frac{Ne}{\sqrt{\pi}}\int_0^{\infty}\frac{\exp(-\frac{x^2}{2\sigma_x^2+q}-\frac{y^2}{2\sigma_y^2+q}-\frac{z^2}{2\sigma_z^2+q})}{\sqrt{(2\sigma_x^2+q)(2\sigma_y^2+q)(2\sigma_z^2+q)}}dq \tag{2.14}$$

Since we are interested in the transverse fields, in the two-dimensional case of a beam with bi-Gaussian beam density distributions, ρ(x,y) = ρ(x) $\cdot$ ρ(y) in the transverse planes :

$$\rho_u(u) = \frac{1}{\sigma_u\sqrt{2\pi}}\exp\left(-\frac{u^2}{2\sigma_u^2}\right) \text{ where } u = x, y \tag{2.15}$$

we can work with the two-dimensional potential $U(x, y, \sigma_x, \sigma_y)$ as a closed expression:

$$U(x, y, \sigma_x, \sigma_y) = \frac{ne}{4\pi\epsilon_0}\int_0^{\infty}\frac{\exp(-\frac{x^2}{2\sigma_x^2+q}-\frac{y^2}{2\sigma_y^2+q})}{\sqrt{(2\sigma_x^2+q)(2\sigma_y^2+q)}}dq \tag{2.16}$$

where n is the line density of particles in the beam, e is the elementary charge and ϵ_0 the permittivity of free space. From the potential we can derive the transverse fields $\vec{E}$ by taking the gradient $\vec{E} = -\nabla U(x, y, \sigma_x, \sigma_y)$.
For completeness and to demonstrate some of the applications of (2.16) to lepton as well as hadron accelerators it is useful to evaluate (2.16) and consequently the fields $\vec{E}$ for two relevant cases: for elliptical beams with $\sigma_x \neq \sigma_y$ and for round beams with $\sigma_x = \sigma_y$. The first approximation is characteristic of lepton distributions while the second is more appropriate for hadron beams.

2.2.1 Elliptical beams

In the particular case of bi-Gaussian elliptical beam distributions with $\sigma_x \neq \sigma_y$ the fields can be derived as in [29] and for the case of $\sigma_x > \sigma_y$ we have:

$$E_x = \frac{ne}{2\epsilon_0\sqrt{2\pi(\sigma_x^2-\sigma_y^2)}}\text{Im}\left[\text{erf}\left(\frac{x+iy}{\sqrt{2(\sigma_x^2-\sigma_y^2)}}\right)-e^{\left(-\frac{x^2}{2\sigma_x^2}+\frac{y^2}{2\sigma_y^2}\right)}\text{erf}\left(\frac{x\frac{\sigma_y}{\sigma_x}+iy\frac{\sigma_x}{\sigma_y}}{\sqrt{2(\sigma_x^2-\sigma_y^2)}}\right)\right] \tag{2.17}$$

$$E_y = \frac{ne}{2\epsilon_0\sqrt{2\pi(\sigma_x^2-\sigma_y^2)}}\mathrm{Re}\left[\mathrm{erf}\left(\frac{x+iy}{\sqrt{2(\sigma_x^2-\sigma_y^2)}}\right) - e^{\left(-\frac{x^2}{2\sigma_x^2}+\frac{y^2}{2\sigma_y^2}\right)}\mathrm{erf}\left(\frac{x\frac{\sigma_y}{\sigma_x}+iy\frac{\sigma_x}{\sigma_y}}{\sqrt{2(\sigma_x^2-\sigma_y^2)}}\right)\right] \tag{2.18}$$

The function erf(t) is the complex error function

$$\mathrm{erf(t)} \;=\; e^{-t^2}\left[1+\frac{2i}{\sqrt{\pi}}\int_0^t e^{z^2}\,dz\right] \tag{2.19}$$

Fast algorithms exist for the numerical evaluation of the complex error function and the fields E_x and E_y can be computed more efficiently. It is therefore advantageous to express the fields in terms of the complex error function for computational reasons.
The magnetic field $\vec{B} = \vec{\beta}\times\vec{E}/c$ of a bunch moving with speed $\vec{\beta}c$ in the negative z-direction of the laboratory frame follows from the electric field $\vec{E}$. In Cartesian coordinates, the relations between the components of electric and magnetic fields are:

$$B_y \;=\; -\beta_r E_x/c \quad \text{and} \quad B_x \;=\; \beta_r E_y/c \tag{2.20}$$

The Lorentz force acting on a particle with charge q is finally:

$$\vec{F} \;=\; q(\vec{E}+\vec{v}\times\vec{B}) \tag{2.21}$$

We must stress that the force will be either a repulsive or an attracting force depending on the two colliding beams. For equally charged beams with $q=+e$ in Equation 2.21 $\vec{F}$ will have the same sign as the electric field $\vec{E}$. For oppositely charged beams this will not be the case and the force and fields will have opposite sign.

2.2.2 Round beams

In the simplified case of round beams we assume that $\sigma_x = \sigma_y = \sigma$. Due to the symmetry of the problem from (2.16), with $r^2 = x^2 + y^2$ by calculating the gradient of the radial potential we can immediately write the fields in cylindrical coordinates as:

$$E_r = -\frac{ne}{4\pi\epsilon_0}\cdot\frac{\delta}{\delta r}\int_0^\infty \frac{\exp(-\frac{r^2}{(2\sigma^2+q)})}{(2\sigma^2+q)}dq \tag{2.22}$$

and

$$B_\Phi = -\frac{ne\beta c\mu_0}{4\pi}\cdot\frac{\delta}{\delta r}\int_0^\infty \frac{\exp(-\frac{r^2}{(2\sigma^2+q)})}{(2\sigma^2+q)}dq \tag{2.23}$$

The expressions (2.22) and (2.23) can easily be evaluated when the derivative is done first and $\frac{1}{2\sigma^2+q}$ is used as integration variable. We find that the electric field $\vec{E}$ (2.22) and magnetic field $\vec{B}$ (2.23) have only a radial and azimuthal component, respectively.

2.3 Incoherent beam-beam force

It follows from the Lorentz force (2.21) that the force has only a radial component and its action on a test particle with opposite charge $-e$ can be expressed in a closed form

(using $\epsilon_0\mu_0 = c^{-2}$) as follows:

$$F_r(r) = \frac{ne^2(1+\beta^2)}{2\pi\epsilon_0} \cdot \frac{1}{r} \cdot \left[1 - \exp(-\frac{r^2}{2\sigma^2})\right] \tag{2.24}$$

and for the Cartesian components in the two transverse planes we get:

$$F_x(r) = \frac{ne^2(1+\beta^2)}{2\pi\epsilon_0} \cdot \frac{x}{r^2} \cdot \left[1 - \exp(-\frac{r^2}{2\sigma^2})\right] \tag{2.25}$$

and

$$F_y(r) = \frac{ne^2(1+\beta^2)}{2\pi\epsilon_0} \cdot \frac{y}{r^2} \cdot \left[1 - \exp(-\frac{r^2}{2\sigma^2})\right] \tag{2.26}$$

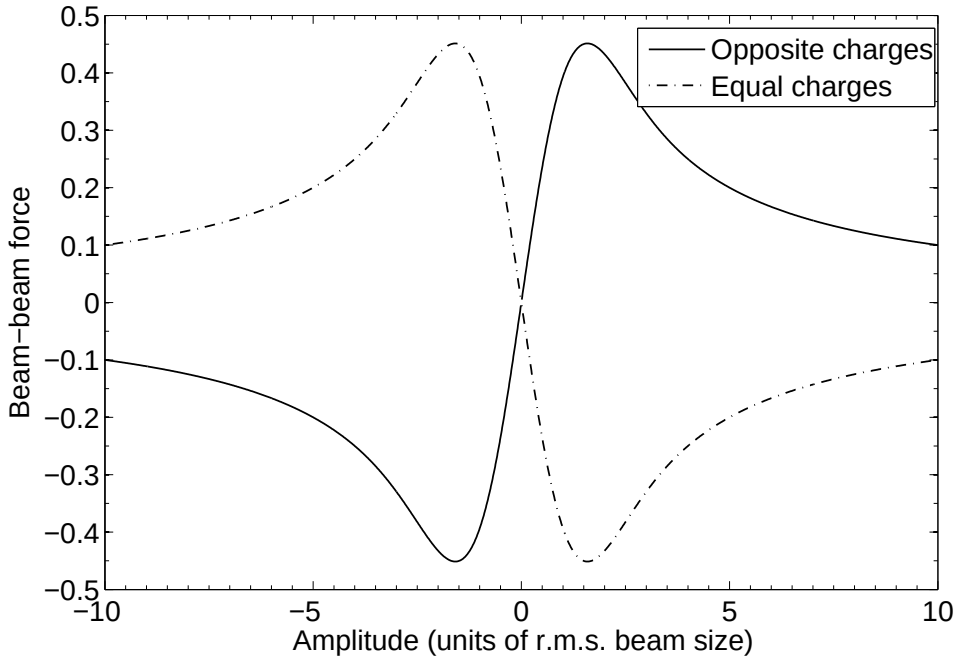

Figure 2.4: Beam-beam force on a single test particle produced by a round beam. For equal charged particles (dashed line) and opposite charged particles (solid line). Force in arbitrary units, amplitude in units of r.m.s. beam size.

The shape of the force as a function of the amplitude is given in Figure 2.4. For very small amplitudes the force is approximately linear and the test particle crossing a beam in this range experiences a linear field like the one encountered in a quadrupole magnet(i.e. a defocusing quadrupole for the solid line in Figure 2.4, while for the case of an oppositely charged test particle it will experience an extra focusing term, shown with the dashed line). At larger amplitudes (i.e. above $\approx 1\ \sigma$) the force deviates strongly from this linear behaviour and, as is also evident from the analytical form of Equation 2.26, we can see that the beam-beam force includes higher order multipoles. One therefore has to expect

that a large number of resonances can be driven by the beam-beam force. A test particle centered with the beam producing the electromagnetic force defined by Equation 2.24 and with very small amplitude of betatron oscillations will feel in first approximation an almost linear force. As we already explained in this simpler case the beam-beam interaction can be linearized and treated as an extra focusing or defocusing lens in the accelerator. We use the force to calculate the kick, i.e. the change of the slope of the trajectory the test particle receives from the opposite beam while traveling through it. Starting from the two-dimensional force of Equation 2.24 and multiplying it with the longitudinal distribution which depends on both, position s and time t with the assumption of a Gaussian shape with a width of σ_s, we get:

$$F_r(r,s,t) = \frac{Ne^2(1+\beta^2)}{\sqrt{(2\pi)^3}\epsilon_0\sigma_s} \cdot \frac{1}{r} \cdot \left[1 - \exp(-\frac{r^2}{2\sigma^2})\right] \cdot \left[\exp(-\frac{(s+vt)^2}{2\sigma_s^2})\right] \tag{2.27}$$

where N is the total number of particles of the beam. We make use of Newton's law and integrate over the collision range to get the radial deflection:

$$\Delta r' = \frac{1}{mc\beta\gamma}\int_{-\infty}^{\infty} F_r(r,s,t)dt \tag{2.28}$$

The radial kick $\Delta r'$ a particle with a radial distance r from the opposing beam centroid receives is then:

$$\Delta r' \quad = \quad \frac{2Nr_0}{\gamma} \cdot \frac{1}{r} \cdot \left[1 - \exp\left(-\frac{r^2}{2\sigma^2}\right)\right] \tag{2.29}$$

where the constants had been re-written using the classical particle radius definition:

$$r_0 = e^2/4\pi\epsilon_0 mc^2 \tag{2.30}$$

where m is the mass of the particle. After the integration along the bunch length, N is the total number of particles. In the two transverse planes the test particle will experience the following kicks:

$$\Delta x' = \frac{2Nr_0}{\gamma} \cdot \frac{x}{r^2} \cdot \left[1 - \exp(-\frac{r^2}{2\sigma^2})\right] \tag{2.31}$$

$$\Delta y' = \frac{2Nr_0}{\gamma} \cdot \frac{y}{r^2} \cdot \left[1 - \exp(-\frac{r^2}{2\sigma^2})\right] \tag{2.32}$$

A kick is defined as the angular deviation a test particle will experience while crossing the other beam. This will result in a change of the test particle coordinates and represents the effect on it in the transverse plane.
For small amplitudes r we can derive the asymptotic limit of Equation 2.29 by expanding the exponential in brackets. The Taylor series is well known and for our case the expression takes the form:

$$\Delta r' \quad = \quad \frac{2Nr_0}{\gamma} \cdot \frac{1}{r} \cdot \left[1 - \left(1 - \left(\frac{r^2}{2\sigma^2}\right) + \ldots\right)\right] \tag{2.33}$$

and after the adequate simplifications:

$$\Delta r'|_{r\to 0} \quad = \quad \frac{Nr_0 r}{\gamma\sigma^2} \quad = \quad +f \cdot r \tag{2.34}$$

Parameter	LEP	LHC
Beam sizes	160μm · 4μm	16.6μm · 16.6μm
Intensity N	$4.0 \cdot 10^{11}$/bunch	$1.15 \cdot 10^{11}$/bunch
Energy	100 GeV	7000 GeV
$\beta_x^* \cdot \beta_y^*$	1.25 m · 0.05 m	0.55 m · 0.55 m
Crossing angle	0.0	0/285 μrad
Beam-beam parameter(ξ)	0.0700	0.0037/0.0034

Table 2.1: Comparison of parameters for a lepton and hadron collider.

This limit is the slope of the force at r = 0 and the force becomes linear in r as for the case of a quadrupole with a focal length as the proportionality factor.
It is well known how the focal length relates to a tune change. Since the focal length in first approximation relates to the first derivative of the force Equation 2.27, we can derive a quantity ξ which is known as the linear beam-beam parameter:

$$\xi = \frac{Nr_0\beta^*}{4\pi\gamma\sigma^2} \tag{2.35}$$

r_0 is the classical particle radius, (e.g.: r_e, r_p) and β^* is the optical amplitude function (β-function) at the interaction point.
For small values of ξ and a tune far enough away from linear resonances this parameter is equal to the linear tune shift ΔQ.
The beam-beam parameter can be generalized for the case of non-round beams and becomes:

$$\xi_{x,y} = \frac{Nr_0\beta^*_{x,y}}{2\pi\gamma\sigma_{x,y}(\sigma_x + \sigma_y)} \tag{2.36}$$

The beam-beam parameter is often used to quantify the strength of the beam-beam interaction, however it does not reflect the non-linear nature. Nevertheless, it can be used for comparison and as a scaling parameter. In Table 2.1 some beam parameters for LEP and the LHC are shown. Some of the differences are striking: while the beams in the LHC are round at the interaction point, they are very flat in LEP. This is due to the excitation of the beam in the horizontal plane by the strong synchrotron radiation. Another observation is the much larger beam-beam parameter in LEP. The reason for this enormous difference will be discussed in a later section.

2.4 Single particle effects

The incoherent force derived in Equation 2.27 is the force of an opposing beam on a single test particle. From Figure 2.4 it is clear that the beam-beam force is a strongly non-linear force. This strong non-linearity present in the accelerator perturbs the motion of each single particle of the counter rotating beam. One can assume that particles cross a beam like they are moving through a complex, static electromagnetic lens. Depending on the complexity of the lens one will have to expect all effects that are known from non-linear beam dynamics. As already seen in the introduction from general particle non-linear

dynamics one should expect as an effect of the beam-beam interaction the following main effects which will deviate the particles from their linear and stable dynamics:

- Non-linear detuning and excitation of resonances.
- Transverse phase space modification.
- Dynamic aperture reduction and particle losses.

All these effects become more and more important for increasing beam-beam strength. However for a very strong beam-beam interaction the beams can reach the so called beam-beam limit which is different for lepton and hadron colliders and that defines also the performance limit of the machines. A detailed description of single particle effects as well as analytical derivations are given together where possible with the definition of the beam-beam limit for both hadron and lepton colliders.

2.4.1 Detuning with amplitude

The non linear beam-beam force manifests itself as an amplitude dependent tune shift and for a beam with many particles this results in a tune spread. The picture depends on the interaction type. We will therefore first look at the case of a test particle centered with the beam producing the electromagnetic force and for this case we will analytically derive the detuning which particles with different betatron oscillation amplitudes will undergo. In a second step we will extend this concept to analyse the case of long range interactions, for which the test particle is not centered with the beam and therefore a static offset should be considered. The resulting effects are different and an intuitive approach to understand the physical picture will be given.

Head-on case

The instantaneous tune shift of a test particle when it crosses the other beam is related to the derivative of the force with respect to the amplitude (see above for the derivation of the **linear** tune shift) $\delta F/\delta x$. For a particle performing an oscillation with a given amplitude the tune shift is calculated by averaging the slopes of the force over the range (i.e. the phases) of the particle's oscillation amplitudes. For the one-dimensional case this is illustrated schematically in Figure 2.5. The derivative of the beam-beam force from Figure 2.4 is plotted for the two cases of oppositely (solid line) and equally (dashed line) charged beams together with the oscillation range of two particles, one with small ($< 0.5\ \sigma$) and another with large amplitudes ($> 3.0\ \sigma$). One could make the following observations:

- The particles with small amplitudes have the largest tune shift.
- Particles with larger amplitudes have a smaller tune shift.
- At very large amplitudes ($r \approx \infty$) the tune shift becomes zero.

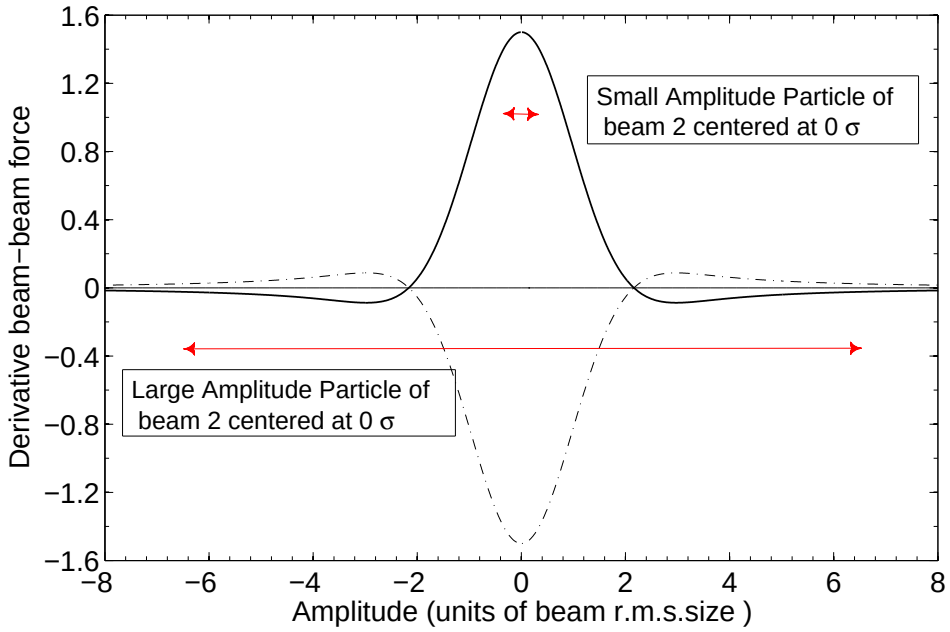

Figure 2.5: Derivative of beam-beam force for round beams. Oscillation range of particles with large and small amplitudes.

In addition if we look at the two cases of oppositely charged (i. e LEP, Tevatron) and equally charged beams (i. e. RHIC and LHC) we can see that the tune shifts have opposite signs. In the first case particles go to higher frequencies while in the second they will go to smaller frequencies.
A calculation can be done using the Hamiltonian formalism [22, 60, 62, 89] developed for non-linear dynamics. However, here we decided to use the Lie formalism as in [31] by Chao. If we consider the 1-D motion of a particle with position x and momentum p_x, in the absence of any beam-beam perturbation, the one-turn map of the accelerator around the interaction point assumed to be at the longitudinal coordinate $s = 0$ can be written in terms of canonical coordinates (x, p_x) as follows:

$$x = x_0 \cos\mu + \beta p_{x_0} \sin\mu \tag{2.37}$$

$$p_x = -\frac{x_0}{\beta} \sin\mu + p_{x_0} \cos\mu \tag{2.38}$$

where β is the unperturbed β-function at $s = 0$, μ is the nominal betatron phase advance per turn, and the parameter α is assumed equal to zero at the observation position $s = 0$. In matrix form, Equation 2.38 represents Courant-Snyder map:

$$\begin{bmatrix} \cos\mu & \beta \sin\mu \\ -\frac{1}{\beta} \sin\mu & \cos\mu \end{bmatrix} \tag{2.39}$$

In Lie algebraic form, the one turn map of an accelerator has the general form $e^{-C:H_{eff}:}$ where C is the accelerator circumference and H_{eff} is the effective Hamiltonian. For the linear case, the effective Hamiltonian is represented by the the Courant-Snyder invariant, while the accelerator circumference can be represented by the one turn phase advance μ.

In this way the Courant-Snyder map of Equation 2.39 acquires the Lie operator form as follows:

$$e^{:f_2:}, \quad where \quad f_2 = -\frac{\mu}{2}\left(\frac{x^2}{\beta} + \beta p_x^2\right) \tag{2.40}$$

i.e.,

$$x = e^{:f_2:}x|_{x=x_0,p_x=p_{x_0}}, \quad and \quad p_x = e^{:f_2:}p|_{x=x_0,p_x=p_{x_0}} \tag{2.41}$$

We now introduce one single beam-beam interaction per turn at the collision point. The beam-beam perturbation is then represented as a δ-function kick at the location $s = 0$,

$$x = x_0 \quad and \quad p_x = p_{x_0} + f(x_0) \tag{2.42}$$

where $f(x)$ is the non linear beam-beam kick. The form of $f(x)$ depends on the particle distribution of the opposing beam at the interaction point. For round Gaussian beams it is given by Equation 2.31:

$$f(x) = \frac{Nr_0}{\gamma}\frac{2}{x}(1 - e^{\frac{-x^2}{2\sigma^2}}) \tag{2.43}$$

The beam-beam map (2.42) can then be written in Lie form as:

$$e^{:F:} \quad and \quad F = \int_0^x f(x')\,dx'. \tag{2.44}$$

The quantity F is just the potential due to the beam-beam force. Observing the particle motion at the exit of the collision point, the one-turn map of the particle motion, in the Lie formulation, reads

$$e^{:f_2:}e^{:F:} = e^{:h:} \tag{2.45}$$

Assuming the beam-beam interaction as a small perturbation to the rest of the accelerator, we can make use of the Baker-Campbell-Hausdorff (BCH) formula [32] in its second form to concatenate the exponential operators to obtain the effective Hamiltonian of the system (from h in Equation 2.45). For the case of multiple interactions one should only add the extra factors in Equation 2.45 making sure that they all respect the initial hypothesis to represent a small perturbation. To proceed with the concatenation by using the BCH rule, we first introduce the more appropriate action-angle variables (ϕ , A) as defined below:

$$x = \sqrt{2A\beta}\sin\phi \quad and \quad p_x = \sqrt{\frac{2A}{\beta}}\cos\phi \tag{2.46}$$

Secondly, we decompose F(x) of Equation 2.44 as a Fourier series in ϕ as

$$F(x) = \sum_{n=-\infty}^{\infty} c_n(A)e^{in\phi} \tag{2.47}$$

With the new action-angle variables the function describing the accelerator f_2 becomes $f_2 = -\mu A$ and by remembering some useful properties of Lie operators we have that

$$: f_2 : g(A) = 0 \quad and \quad : f_2 : e^{in\phi} = in\mu e^{in\phi} \tag{2.48}$$

for any arbitrary function $g(A)$. By summing over f_2, the summation can be done analytically to first order in F to yield

$$h = f_2 + \left(\frac{: f_2 :}{1 - e^{-:f_2:}}\right)F + \mathcal{O}(F^2) \tag{2.49}$$

$$= -\mu A + \sum_n c_n(A) \left(\frac{in\mu}{1 - e^{-in\mu}} \right) e^{in\phi} \tag{2.50}$$

$$= -\mu A + \sum_n c_n(A) \frac{n\mu}{2 \sin \frac{n\mu}{2}} e^{in\phi + i\frac{n\mu}{2}} \tag{2.51}$$

Equation 2.51 is the expression for the beam-beam perturbed invariant, to first order of perturbation, away from resonances. In this approximation one can make a normal form transformation which removes the oscillating terms in Equation 2.51. The only term left will be the zero-th Fourier harmonic term, and the effective Hamiltonian becomes

$$h = -\mu A + c_0(A) = \text{const} \tag{2.52}$$

On resonances, i.e. for the condition:

$$Q = \frac{p}{n} = \frac{\mu}{2\pi} \tag{2.53}$$

and with $c_n \neq 0$ we have that for any integers p and n:

$$\sin(\frac{n\pi p}{n}) = \sin(p\pi) = 0 \tag{2.54}$$

and the invariant h diverges due to the expansion of Equation 2.51.
Away from resonances, the amplitude A dependent tune shift due to beam-beam perturbation is then given by:

$$\Delta\mu(A) = -\frac{1}{2\pi} \frac{dc_0(A)}{dA} \tag{2.55}$$

This represents the detuning with action A due to the beam-beam interaction. If we take the case of the round Gaussian distribution in Equation 2.43, we obtain:

$$F(x) = \frac{Nr_0}{\gamma} \int_0^{A\beta/2\sigma^2} \frac{d\alpha}{\alpha} (1 - e^{-2\alpha \sin^2 \phi}) \tag{2.56}$$

The decomposition coefficients c_n are then calculated by making use of the relation:

$$e^{x \cos y} = \sum_{k=-\infty}^{\infty} I_k(x) e^{iky} \tag{2.57}$$

where $I_k(x)$ is the Bessel function of order k in x. By using Equation 2.56 and the above decomposition we obtain for c_n the following solutions

$$\begin{aligned}
c_n(A) &= \frac{1}{2\pi} \int_0^{2\pi} d\phi e^{-in\phi} F(x) \\
&= \frac{Nr_0}{\gamma} \int_0^{A\beta/2\sigma^2} \frac{d\alpha}{\alpha} \frac{1}{2\pi} \int_0^{2\pi} d\phi e^{-in\phi} (1 - e^{-2\alpha \sin^2 \phi}) \\
&= \frac{Nr_0}{\gamma} \int_0^{A\beta/2\sigma^2} \frac{d\alpha}{\alpha} \frac{1}{2\pi} \int_0^{2\pi} d\phi e^{-in\phi} \left[1 - e^{-\alpha} \sum_k I_k(\alpha) e^{2ik\phi} \right] \\
&= \frac{Nr_0}{\gamma} \int_0^{A\beta/2\sigma^2} \frac{d\alpha}{\alpha} \begin{cases} 1 - e^{-\alpha} I_0(\alpha), & \text{if } n = 0 \\ e^{-\alpha} I_{n/2}(\alpha), & \text{if } n = even \neq 0 \\ 0 & \text{otherwise} \end{cases}
\end{aligned}$$

and the $n = 0$ coefficient is, for round Gaussian distribution, of the form:

$$c_o(A) = \frac{Nr_0}{\gamma} \int_0^{A\beta/2\sigma^2} \frac{d\alpha}{\alpha}(1 - e^{-\alpha} I_0(\alpha)) \tag{2.58}$$

One observes that due to the symmetry of the beam-beam force, only resonances with even n are excited in this approximation. However, as soon as the approximation is not anymore valid the resonances excited change and this simple rule does not apply. It should be clear that this result is a consequence of the assumptions made on the beam-beam interaction which is assumed to be a small perturbation at the particle dynamics and allows to apply the map concatenation of Equation 2.45 using the BCH Equation 2.49. This is correct only in a perturbative regime for the beam-beam interaction. Moreover, the derivation of h is made by assuming that away from resonances one can make use of a normal form transformation which removes the oscillating terms of Equation 2.51 bringing back the motion to a simple rotation in phase space or action-angle space. For a realistic picture where for a strong enough beam-beam interaction one has a significant modification of the particle motion one should go for a different mathematical approach. The BCH formula is not applicable and in this regime the beam-beam interaction can drive resonances of any order. The formula for the non-linear tune shift as a function of the action A of Equation 2.55 assumes the form:

$$\Delta Q(A) = \frac{1}{2\pi} \frac{Nr_0}{\gamma} \frac{d}{dA} \left[\int_0^{A\beta/2\sigma^2} \frac{d\alpha}{\alpha}(1 - e^{-\alpha} I_0(\alpha)) \right] \tag{2.59}$$

$$= \frac{1}{2\pi} \frac{Nr_0}{\gamma A} \left[1 - e^{-A\beta/2\sigma^2} I_0(A\beta/2\sigma^2) \right] \tag{2.60}$$

Going back to the particle amplitude variable x as defined in Equation 2.46 in units of the beam size σ we obtain the expression for the detuning with particle amplitude:

$$\Delta Q(x) = \frac{Nr_0\beta}{4\pi\gamma\sigma^2} \frac{1}{(\frac{x}{2})^2} \left(e^{-(\frac{x}{2})^2} I_0 \left(\frac{x}{2} \right)^2 - 1 \right) \tag{2.61}$$

where the particle amplitude x is expressed in units of the beam r.m.s. size assuming a Gaussian distribution. Plotted in Figure 2.6 (left) we show the tune shift ΔQ normalized with respect to the linear beam-beam parameter ξ as defined in Equation 2.35 for the case of equally (dashed line) and oppositely (solid line) charged beams undergoing one single beam-beam interaction.

For a small betatron amplitude particle, the tune shift is equal to the linear beam-beam parameter ξ, the sign of the shift depends on the relative beams' charges:

$$\lim_{x \to 0} \Delta Q(x) = \pm \frac{Nr_0\beta}{4\pi\gamma\sigma^2} \tag{2.62}$$

If we then think of an entire beam with many particles at different amplitudes, it's clear that the beam-beam tune shift as a function of the particles' amplitudes has also the physical meaning of a beam-beam induced tune spread in the beam. And the maximum tune spread for a single head-on collision is defined by the tune shift of a single particle with small amplitude and therefore it is equal to ξ. Particles at bigger amplitudes on the

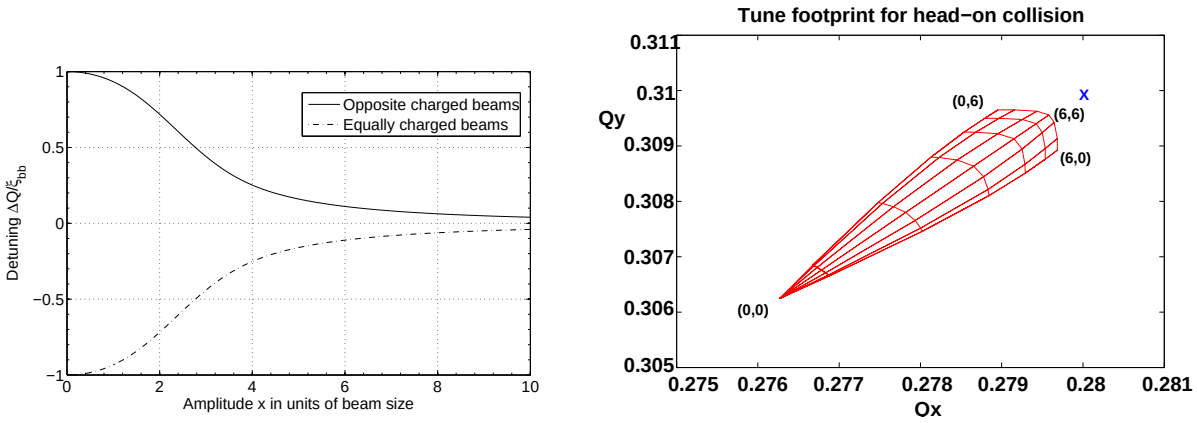

Figure 2.6: Tune shift (non-linear detuning) as a function of the amplitude for equally charged beams (dashed line) and oppositely charged beams (solid line) on left plot. On the right picture we show the detuning with amplitude in both transverse planes (horizontal and vertical) which particles at different amplitudes will undergo for the LHC case with only one single beam-beam interaction also called 2-dimensional tune footprint [24]. The cross indicates the tune without beam-beam interactions.

other hand will experience reduced tune shifts and theoretically no tune shift in the case of an infinitely large amplitude. However, for all amplitudes the sign of the shift will be the same as in the head-on case.

This derivation applies to both horizontal and vertical transverse planes. Another way of representing the effects of the beam-beam tune shift with amplitude are the already mentioned footprints as shown in Figure 2.6 (right). A footprint is a 2-dimensional mapping of the transverse amplitude into the 2-dimensional tune space. Figure 2.6 (right) represents the LHC case with only one head-on interaction. Starting from the initial, fractional unperturbed horizontal and vertical betatron frequencies (0.28 and 0.31 cross in Figure 2.6 right) the detuning with amplitude of the non-linear beam-beam interaction shifts the particles frequencies depending on their amplitude. This results in a spread of frequencies represented by the area enclosed by the red lines in Figure 2.6. Particles at very small amplitudes are moved furthest apart by the interaction, while those at larger amplitudes $(6, 6)$ experience less detuning and remain closer to the unperturbed working point.

Long range detuning with amplitude

Even if the beam-beam force decreases rapidly with amplitude and therefore long range interactions distort the beams much less than a head-on interaction, their large number and some particular properties require careful studies.

The first difference with respect to a head-on collision is the sign of the resulting tune shift. A particle undergoing a long range interaction (i.e. 5 σ distance in Figure 2.5) can show a tune shift with different sign depending on its betatron oscillation amplitude around the closed orbit and the relative distance of the two beams. The change in sign of the tune shift can easily be understood when we come back to the method for calculating the tune spread, explained with the help of Figure 2.5 in a 1-dimensional case.

We average again the oscillation of a small amplitude particle as it samples the force

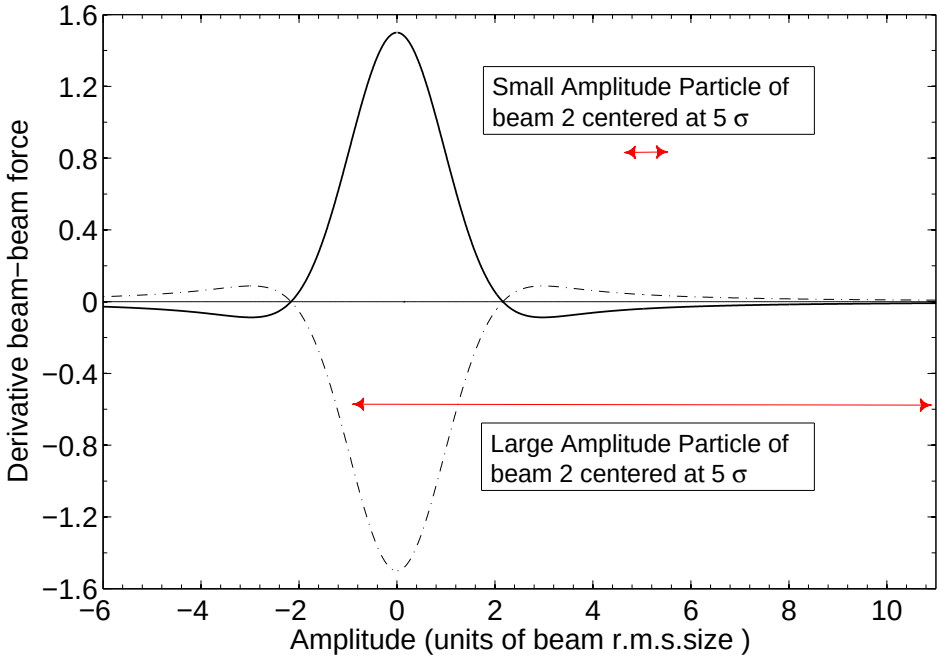

Figure 2.7: Derivative of beam-beam force for round beams. Oscillation range of particles of separated beams. The separation in this case is of 5 σ.

of the beam-beam interaction at 5 σ range. In Figure 2.7 the ranges of oscillation of two particles with small and larger amplitudes for the interaction of 5 σ separated beams are shown. When the separation is larger than $\approx$ 2.0 σ, the slope of the force as a function of the amplitude changes the sign and the resulting tune shift assumes the opposite sign with respect to the head-on case. However, the situation becomes more complicated for the case of a large amplitude particle. In this case the average over the collision range can change the sign of the tune shift since the particle experiences negative as well as positive focusing forces (slopes).

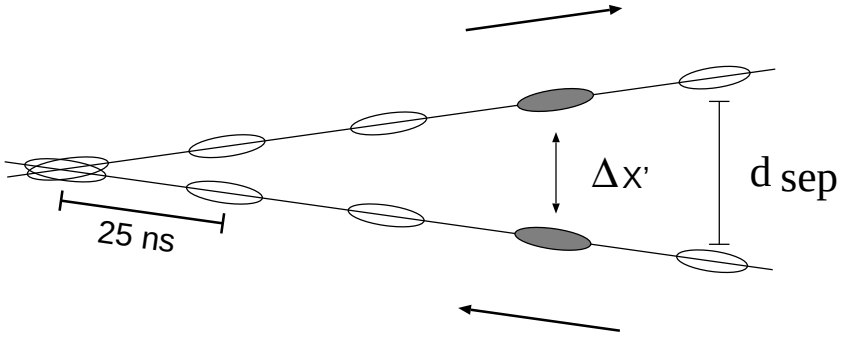

Figure 2.8: Long-range interaction, schematic with horizontal separation.

Using the geometry of a single encounter as in Figure 2.8 one can evaluate the strength of a long-range interaction as a function of the separation d between the bunch producing the force and a particle of a test bunch. Assuming a separation d in the horizontal plane, the potential of Equation 2.16 assumes the form:

$$U(x,y,\sigma_x,\sigma_y) = C\int \frac{1-\exp-\left(\frac{(x-d)^2}{2\sigma_x^2+q}+\frac{y^2}{2\sigma_y^2+q}\right)}{\sqrt{(2\sigma_x^2+q)(2\sigma_y^2+q)}}dq \tag{2.63}$$

In order to calculate the tune, i.e. the focusing force $1/f$, one has to calculate the gradient around the central orbit of the particle, i.e. $x = 0$:

$$\Delta Q_x \propto \frac{1}{f} \propto \frac{\delta^2 U(x,y)}{\delta x^2} = C\frac{\delta}{\delta x}\left((x-d)\int dq \frac{e^{-\left(\frac{(x-d)^2}{2\sigma_x^2+q}+\frac{y^2}{2\sigma_y^2+q}\right)}}{\sqrt{(2\sigma_x^2+q)^{3/2}(2\sigma_y^2+q)^{1/2}}}\right) \tag{2.64}$$

Performing the derivative one obtains that:

$$\Delta Q_x = C\int dq \frac{e^{-\left(\frac{(x-d)^2}{2\sigma_x^2+q}+\frac{y^2}{2\sigma_y^2+q}\right)}}{\sqrt{(2\sigma_x^2+q)^{3/2}(2\sigma_y^2+q)^{1/2}}} - 2C(x-d)^2\frac{e^{-\left(\frac{(x-d)^2}{2\sigma_x^2+q}+\frac{y^2}{2\sigma_y^2+q}\right)}}{\sqrt{(2\sigma_x^2+q)^{5/2}(2\sigma_y^2+q)^{1/2}}} \tag{2.65}$$

Analysing the small amplitude particle behaviour $x \approx 0$ one obtains:

$$\Delta Q_x = C\int dq \frac{e^{-\left(\frac{d^2}{2\sigma_x^2+q}+\frac{y^2}{2\sigma_y^2+q}\right)}}{\sqrt{(2\sigma_x^2+q)^{3/2}(2\sigma_y^2+q)^{1/2}}} - 2Cd^2\frac{e^{-\left(\frac{d^2}{2\sigma_x^2+q}+\frac{y^2}{2\sigma_y^2+q}\right)}}{\sqrt{(2\sigma_x^2+q)^{5/2}(2\sigma_y^2+q)^{1/2}}} \tag{2.66}$$

The first part is the classical linear tune shift which for $d \approx 0$ becomes again the head-on tune shift. For the long-range the tune shift depends on d. The tune shift can change sign due to the contribution of the second term which becomes bigger than the first term beyond a certain separation d. Figure 2.9 shows the horizontal (black dashed line) and vertical (red dashed line) tune shifts in units of the linear beam-beam parameter for an almost zero amplitude test-particle undergoing a beam-beam interaction for different distances d added in the horizontal plane. The horizontal tune shift changes sign when a certain distance d has been reached, while in the other plane no changes in the sign are visible as expected.
In the case of large enough separation, i.e. above $\approx 6\ \sigma$, the tune shift ΔQ_{lr} from long-range interactions alone follows an approximate scaling:

$$\Delta Q_{lr} \propto -\frac{N}{d^2} \tag{2.67}$$

where N is the bunch intensity and d the separation.
In addition to the change of sign compared to head-on interactions where the small amplitude particles are mostly affected, now the large amplitude particles experience a strong non-linear long range beam-beam perturbation as shown in Figure 2.7. This is rather intuitive since the large amplitude particles are the ones which can come closer to the

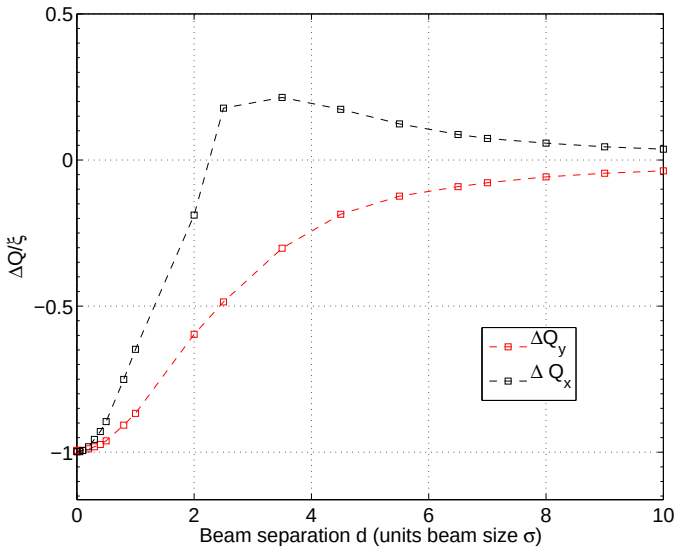

Figure 2.9: Horizontal and Vertical tune shift as a function of horizontal separation for one single long range interaction between two proton beams.

opposite beam as they perform their oscillations. We must therefore expect a different tune footprint.

Such a footprint for only long-range interactions is shown in Figure 2.10. The two beams are separated in the vertical plane while no separation is applied in the other plane. Since the symmetry between the two planes is broken, the resulting footprint shows no symmetry. In fact, the tune shifts have different signs for x and y, as expected. For large amplitudes one observes a "folding" of the footprint. This occurs when large amplitude particles are considered for which the oscillation amplitudes extend across the central maximum in Figure 2.7, i.e. when the oscillation amplitude is close to the separation between the beams. Such large amplitudes are treated in Figure 2.7 to demonstrate this feature. In practice, these amplitudes are usually not important since in most accelerators no particles reach these amplitudes.

2.5 Coherent beam-beam force

Coherent beam-beam effects arise from the forces which an exciting bunch exerts on a whole test bunch during a beam-beam collision. When one considers the coherent motion of bunches, the collective behaviour of all particles in a bunch is studied. A coherent motion requires an organized behaviour of all particles in a bunch. To calculate the coherent force between two Gaussian charged particle distributions one proceeds as for the incoherent calculation. To get the coherent kick, the individual kicks of all test particles have to be integrated over the particle distribution. Starting from the Poisson Equation 2.3 one has now to take into account two Gaussian distributions ρ^* and ρ^{**} which will produce now coherent potentials for the two beams. Due to the symmetry of the beam-beam force the effect of a perfect head-on collisions is zero. Therefore, to evaluate the mutual interaction of the beams we assume their barycentres are offset and

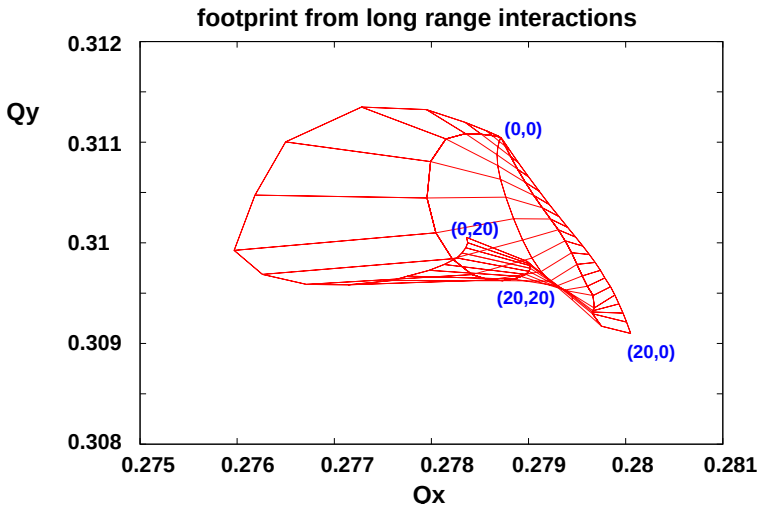

Figure 2.10: Tune footprint for long-range interactions only. Vertical separation and amplitudes between 0 and 20 σ.

we evaluate the potential and force at a general location x. The two density distributions are Gaussian with barycentres and squared transverse beam sizes $(X^*, Y^*, \Sigma_X^*, \Sigma_Y^*)$ and $(X^{**}, Y^{**}, \Sigma_X^{**}, \Sigma_Y^{**})$. The * and ** signs are used to distinguish between the two counter rotating bunches. Assuming that the squared transverse beam sizes are equal for the two beams ($\Sigma_{X,Y}^* = \Sigma_{X,Y}^{**}$) and by following the same analytical derivation as for the incoherent case, one obtains the following expression for the transverse coherent potential:

$$U_C = \frac{ne}{4\pi\epsilon_0}\int_0^\infty \frac{\exp(-\frac{(X^*-X^{**})^2}{4\Sigma_X^2+q} - \frac{(Y^*-Y^{**})^2}{4\Sigma_Y^2+q})}{\sqrt{(4\Sigma_X^2+q)(4\Sigma_Y^2+q)}}dq \tag{2.68}$$

The coherent potential U_C is very similar to the incoherent one of Equation 2.16. What should be noticed is the dependence on the differences of the bunch barycentres (X^*-X^{**}) and (Y^*-Y^{**}) instead of x and y and the factor 4 instead of 2 in front of the Σ's coming from the integration over the test beam distribution. In the case of round Gaussian beams this yields the following expressions for the coherent beam-beam force and for the coherent kick obtained by integrating the force over the collision as done in Equation 2.28:

$$F_{\bar{r}}(\bar{r}) = -\frac{ne^2(1+\beta^2)}{2\pi\epsilon_0\bar{r}}\left[1-\exp(-\frac{\bar{r}^2}{4\Sigma^2})\right] \quad \Delta\bar{r}' = \frac{2Nr_0}{\gamma\bar{r}}\left[1-\exp(-\frac{\bar{r}^2}{4\Sigma^2})\right] \tag{2.69}$$

with $\bar{r}' = \sqrt{(X^*-X^{**})^2+(Y^*-Y^{**})^2}$. In Figure 2.11 a comparison is given of the one dimensional coherent (solid line) and incoherent (dashed line) beam-beam force as a function of the distance between bunch and a test-bunch or bunch and test-particle in units of the beam size. Using the same arguments as in the case of the incoherent beam-beam kicks, one finds for the case of $\bar{r} \ll \sigma$ for round Gaussian beams with $\beta \approx 1$ that the kick approaches the following limit:

$$\Delta\bar{r}'|_{\bar{r}\to 0} \quad = \quad \frac{Nr_0\bar{r}}{2\gamma\sigma^2} \quad = \quad +F \cdot \bar{r} \tag{2.70}$$

Here , $F = f/2$ is the inverse focal length of the quadrupole representing the linear coherent beam-beam kick. This quantity relates to a tune change and as done for the

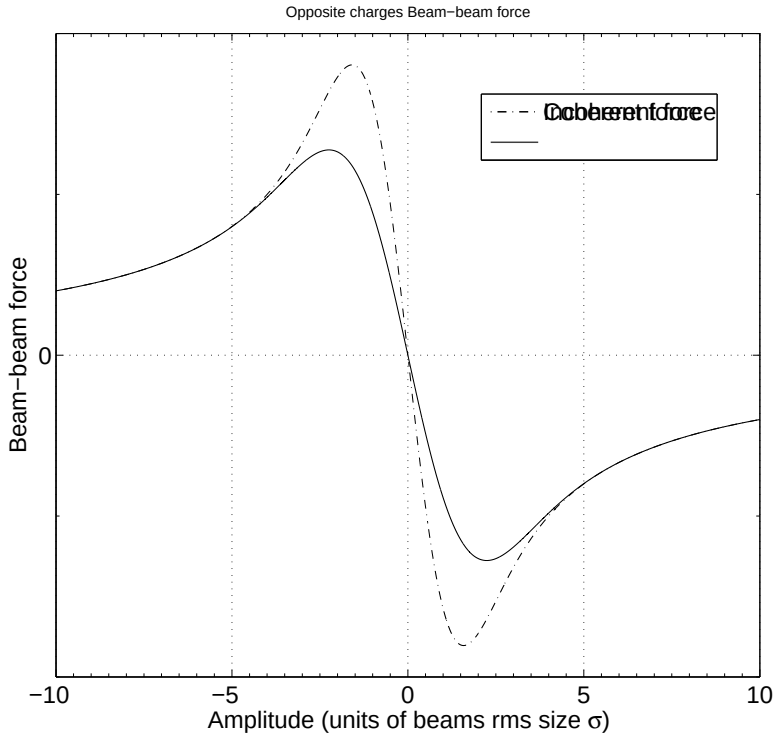

Figure 2.11: Coherent (solid line) and incoherent (dashed line) beam-beam force as a function of amplitude r and $\bar{r}$.

incoherent case one can derive the coherent beam-beam parameter Ξ for $\bar{r} \to 0$ for the case of elliptical Gaussian bunches:

$$\Xi_{X,Y} = \frac{N r_0 \beta_{X,Y}}{4\pi\gamma\sigma_{X,Y}(\sigma_X + \sigma_Y)} \tag{2.71}$$

For round beams ($\sigma_X = \sigma_Y$) it simplifies to:

$$\Xi_{X,Y} = \frac{N r_0 \beta_{X,Y}}{8\pi\gamma\sigma^2} = \frac{1}{2}\xi_{X,Y} \tag{2.72}$$

The overall effect on an entire beam is half the one on a single particle for small amplitudes, i.e. much smaller than the actual beam size σ. This is not true at large amplitudes where the effects of the two become equal. This is clear since at large distance $d \gg \sigma$ the two beams appear as point like charges. The multi particle beams seen at a large distance produce an electromagnetic field as the one produced if the whole charge were concentrated at one point. Therefore the force at large distances can be approximated by the one produced by a point charge.

2.6 Collective effects

So far we have mainly studied how the beam-beam interaction affects the single test particle behaviour. However a beam is a sample of many particles and due to the beam-beam interaction an organized and collective behaviour can occur. The beams will be

coupled through the force and will show not only a perturbed single particle dynamic but also new collective effects. The main collective effects typical of beam-beam interactions are:

- Orbit effects.
- Coherent oscillating modes.
- Multi Bunch coupling.

The beam as a whole is affected by the opposite beam and vice versa.

2.6.1 Orbit effects

The first example of such a situation is the orbit effect where the beams mutually change their closed orbits. Starting from the potential of Equation 2.63 one can evaluate the kick a particle receives:

$$\delta x' = \frac{\delta U}{\delta x}\delta x' = C(x-d)\int \frac{1-e^{-\left(\frac{(x-d)^2}{2\sigma_x^2+q}+\frac{y^2}{2\sigma_y^2+q}\right)}}{\sqrt{(2\sigma_x^2+q)^{3/2}(2\sigma_y^2+q)^{1/2}}}dq \tag{2.73}$$

For zero amplitude particles, with a x coordinate much smaller than the interaction distance d, the contribution coming from oscillation amplitude is negligible therefore the term $(x-d)$ can be replaced by d and the kick expression is reduced to the form:

$$\delta x' = Cd\int \frac{1-\exp-\left(\frac{d^2}{2\sigma_x^2+q}\right)}{\sqrt{(2\sigma_x^2+q)^{3/2}(2\sigma_y^2+q)^{1/2}}}dq \tag{2.74}$$

The dependency on particle amplitude oscillation cancels and this represents a pure dipolar kick, with an effect exactly like an additional bending magnet at the interaction location. This part of the long range beam-beam interaction therefore changes the particle orbit. This approximation is valid for distances d much larger than the particle betatron amplitudes. For very small kicks, the orbit change is negligible, but for sizable kicks the reference system changes and one must subtract the constant part to bring the reference system back. Otherwise it could lead to a wrong interpretation of the particle dynamics. Without the subtraction small amplitude particles would seem to be moving to larger betatron amplitudes while what is changed is only the orbit. A constant contribution, i.e. more precisely an amplitude independent contribution, changes the orbit of the bunch as a whole (Figure 2.12). When the beam-beam effect is strong enough, i.e. for high intensity and/or small separation, the orbit effects are large enough to be observed.
As soon as the orbit of a beam changes, the separation between the beams will change as well, which in turn will lead to a slightly different beam-beam effect and so on. The orbit effects must therefore be computed in a self-consistent way [45], in particular when the effects are sizeable. The closed orbit of an accelerator can usually be corrected, however an additional effect which is present in some form in many colliders, sets a limit to the correction possibilities. A particularly important example is the LHC therefore, an example of the orbit effects feature is shown in Figure 2.13 where the offsets of 432 out

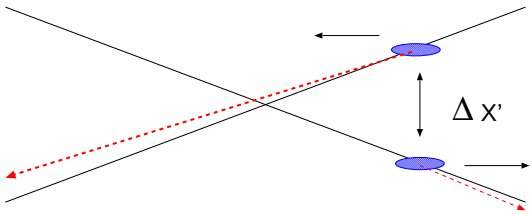

Figure 2.12: Beam-beam deflection leading to orbit changes.

of 2808 bunches of one of the LHC beams are shown. Bunch to bunch differences in the offset amplitudes at the IP1 are due to the different number of long range interaction each bunch undergoes as will be explained in a later section on the multi bunch coupling.

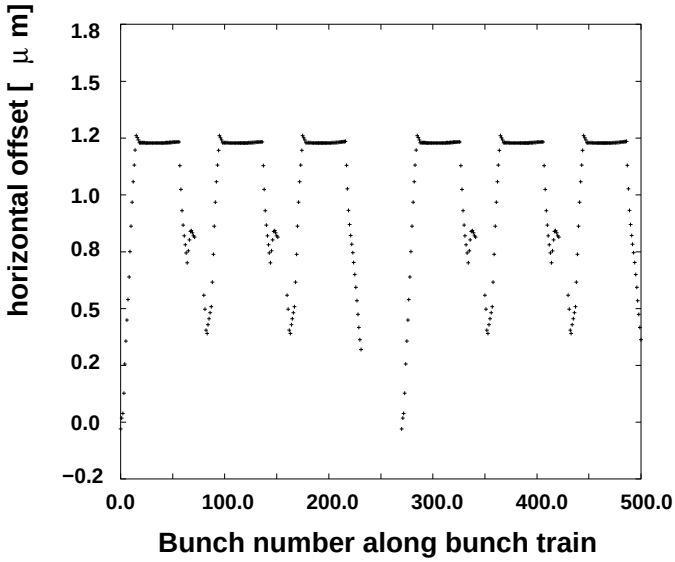

Figure 2.13: Horizontal orbits of the first 432 bunches at the location of ATLAS experiment (IP1).

2.6.2 Coherent beam-beam modes

Bunches in a beam, in addition to the harmonic motion in the storage ring, receive beam-beam kicks when they pass through each other at the interaction points. All bunches (in both beams) are then coupled together through the beam-beam kicks to form a dynamic system in which all bunches oscillate in time. To understand the dynamics of dipole oscillations we first study the simplest case with one bunch in each beam. When the bunches meet turn after turn at the collision point, their oscillation can either be exactly in phase (0 degree phase difference) or out of phase (180 degrees phase difference). Any other oscillation can be constructed from these basic modes. The modes are sketched very schematically in Figure 2.14. The relative positions of the bunches as observed at the interaction point are shown for two consecutive turns n and $n+1$. The first mode is called the 0-mode (or sometimes called σ-mode) and the second the π-mode. In the first mode the distance between the bunches does not change turn by turn and therefore there is no net force driving an oscillation. This mode must oscillate with the unperturbed

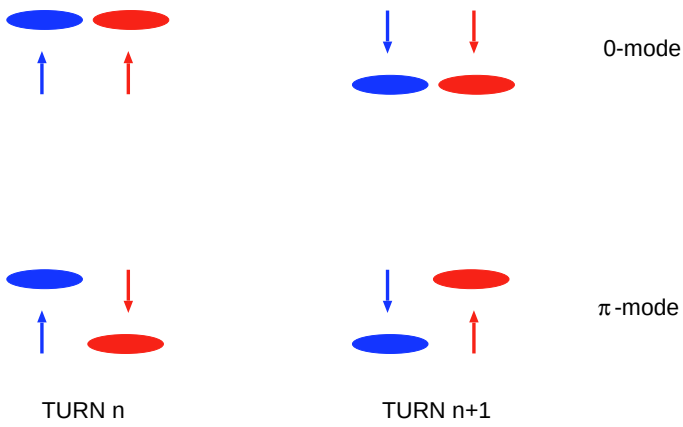

Figure 2.14: Basic dipole modes of two bunches. Relative position of the bunches at the interaction point at two consecutive turns.

frequency (tune) Q_0. For the second mode the net force difference between two turns is a maximum and the tune becomes $Q_0 + \Delta Q_{coh}$. The sign of ΔQ_{coh} depends on whether the two beams have equal charge (defocusing case) or opposite charge (focusing case).

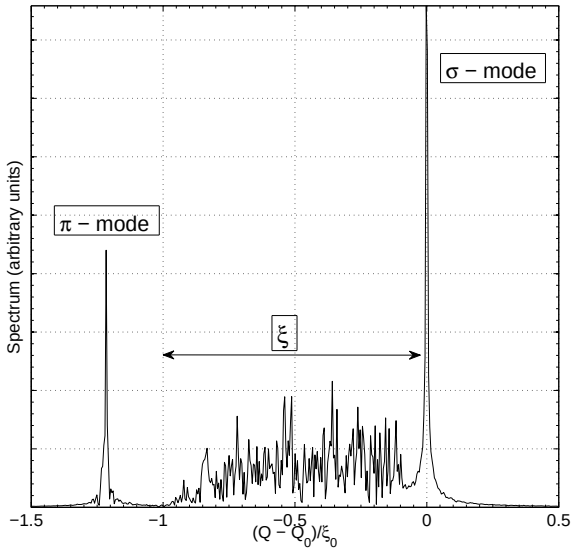

Figure 2.15: Beam-beam coherent modes and incoherent spectra for the case of two bunches colliding head-on. From a fully self-consistent simulation.

The calculation of ΔQ_{coh} is non-trivial: when the bunches are considered as rigid objects, the tune shift can be computed easily using the coherent kick but is underestimated [36]. The correct calculation must allow for changes of the density distribution during the collision and moreover, must allow for a deviation from a Gaussian function. The computation requires solving the Vlasov-equation of two coupled beams [10, 11, 37, 38, 76] or a self-consistent simulation.
The results are shown in Figure 2.15. The σ-mode is found at the unperturbed tune

as expected. The π-mode is shifted by 1.2-1.3 ξ. The precise value depends on the ratio of the horizontal and vertical beam sizes and is called the Yokoya factor [11]. For the LHC beam characteristics, round beams at collision, the Yokoya factor expected is of approximately $1,23$. We have seen before the incoherent tune spread (footprint) the individual particles occupy and we know that it spans the interval [0.0,1.0] ξ, starting at the σ-mode (Figure 2.15).
Here we can make an important observation: under the strong-strong condition the π-mode is a discrete mode outside the incoherent spectrum [38, 10]. This has dramatic consequences for the stability of the beams. A coherent mode that is outside an incoherent frequency spectrum is not stabilized by Landau damping [77]. Under these conditions the coherent beam-beam effect could drive the dipole oscillation to large amplitudes and may result in the loss of the beam.

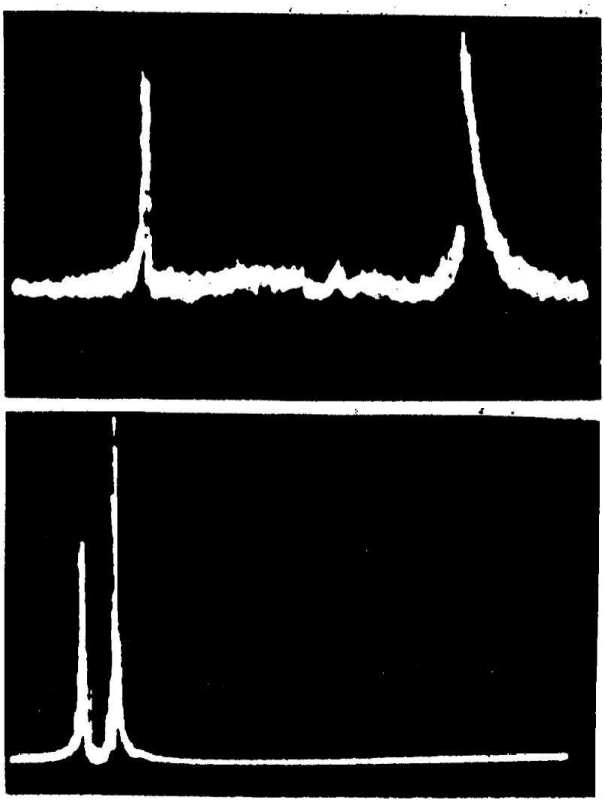

Figure 2.16: Coherent beam-beam modes observed in PETRA[36]. The pictures show the frequency spectra for two cases at PETRA. The top picture is for a head-on collision while the bottom picture is when the two beams are separated by an electrostatic separator.

Figure 2.16 shows observations at PETRA of the coherent beam-beam eigenfrequencies of colliding $e^+ - e^-$ beams in the case of a head-on collision (top picture) and when the two beams are separated by an electrostatic separator (bottom picture) and therefore experience a long range interaction. The head-on spectrum (top plot of Figure 2.16) shows the unperturbed machine tune σ-mode (left peak) and the π-mode frequency shifted to higher frequencies since it is a storage ring with oppositely charged beams. Also the spectrum of separated beams (bottom plot of Figure 2.16) shows the presence of a coherent mode

proper of the long range interaction shifted at smaller frequencies [36]. The coherent beam-beam modes have also been observed at LEP during a special experiment with only one bunch in each beam. The frequency spectrum of two bunches in LEP is shown in Figure 1.7 (left) and clearly demonstrates the two oscillating modes.
Observations in a lepton collider are simplified by the presence of strong damping which reduces the danger of a beam loss. Nevertheless experimental evidence exist for the observation of coherent beam-beam modes in hadron colliders. Beam-beam modes have been observed with high intensity coasting beams in the ISR [73], and more recently one has succeeded to measure the beam-beam modes in a bunched hadron collider at RHIC [100]. In Figure 1.7 (right) the spectra with (red line) and without (blue line) the beam-beam interaction are compared and a significant signal can be observed. Without the beam-beam interaction only the σ-mode is observed and in the presence of the other beam, the π-mode is visible.
Coherent beam-beam modes can be driven by head-on collisions with a small offset or by long-range interactions. In the first case and for small oscillations, the problem can be linearized and the theoretical treatment is simplified. The forces from long-range interactions are very non-linear but the numerical evaluation is feasible. Since the coherent shift must have the opposite sign for long-range interactions, the situation is very different. In particular the π-mode from long-range interactions alone would appear on the opposite side of the σ-mode in the frequency spectrum as visible for PETRA in Figure 2.16 [10, 54]. Both the incoherent and the coherent spectra include both types of interactions.
The loss of Landau damping for coherent beam-beam modes can be a problem for hadron colliders and possible measures against coherent beam-beam modes may have to be considered.
We have argued that the coherent motion requires an 'organized' motion of many particles and this will help us to suppress the coherent modes. In order to maintain this organized motion, a high degree of symmetry between the two beams is required and breaking this symmetry can be used to destroy the collective behaviour. Several possible mechanisms have been proposed:

- Different bunch intensities [10].
- Different tunes in the two beams [79, 80].
- Unequal distribution of interaction points [40].
- Phase differences between interaction points[52].
- Synchrotron motion [83].

This list is not complete but sufficient to demonstrate the principle.

2.6.3 Multi bunch coupling

So far we have treated coherent beam-beam interactions at a single interaction point. In case of two or more interaction points, additional symmetry breaking effects exist. Like in the case with one interaction point but unequal tunes, the symmetry can be broken when

the phase advance between multiple interaction points is not the same [40]. It can be demonstrated [40, 42] that the symmetry and periodicity of the head-on and long-range interaction points play an important role in the excitation of beam-beam resonances.
With many bunches colliding, the frequency spectrum will change. When a bunch collides with more than one other bunch, the bunches will couple and more modes than only the σ-mode and π-mode will be excited [39, 81, 90, 52, 11]. This coupling can be through head-on as well as long range interactions. In the case of the LHC, every nominal bunch couples with 90 other bunches through long-range interactions and eventually all bunches are coupled together. This would result in a large number of possible modes. Their frequencies must all lie between the σ-mode and the π-mode which is the mode with the highest frequency shift. Depending on the symmetry of collision the spectrum can have a very complicated number of frequency peaks. However, the assumption of rigid bunches does not give any information on Landau damping which can be defined only through a multi particle study in a fully self consistent treatment.
In general, symmetry breaking effects and additional degrees of freedom make it more difficult for coherent effects to sustain. For future colliders with many interaction points and head-on as well as multiple long-range collisions, it is very likely that coherent beam-beam oscillations can easily be damped by the lack of symmetry and the help of synchrotron motion. The bunches in the LHC do not form a continuous train of equidistant bunches spaced by 25 ns, but some empty space must be provided to allow for the rise time of kickers. These gaps and the number of bunches per batch are determined by requirements from the LHC injectors (PS, SPS etc.) and the preparation of the LHC beam (bunch splitting). The whole LHC bunch pattern is composed of 39 smaller batches (trains of 72 bunches) separated by gaps of various length followed by a large abort gap for the dump kicker at the end. Figure 2.17 shows the actual LHC filling scheme with the various gaps in the train. In the LHC, only 2808 out of 3564 possible bunches are present with

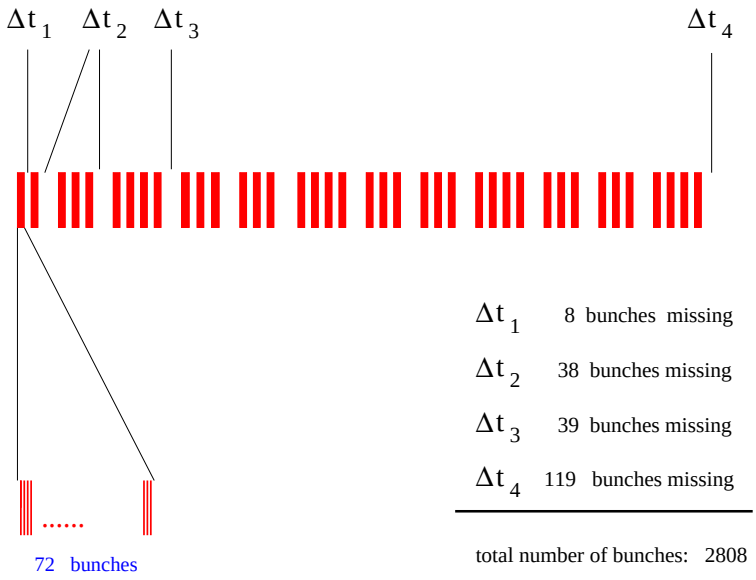

Figure 2.17: Bunch filling scheme in the LHC.

the above filling scheme. Due to symmetry, bunches normally meet other bunches at the

head-on collision point. For the long-range interactions this is no longer the case. This is illustrated in Figure 2.3. Bunches at the beginning and at the end of a small batch will encounter a hole and as a result experience fewer long-range interactions than bunches from the middle of a batch [44]. In the limit, the first bunch of a batch near a large gap encounters no opposite bunch before the central collision and the full number of bunches after, i.e. it sees only half of the long range collisions.
Bunches with fewer long-range interactions have a very different integrated beam-beam effect and a different dynamics must be expected. In particular they will have a different tune and occupy a different area in the working diagram, therefore may be susceptible to resonances which can be avoided for nominal bunches. The overall space needed in the working diagram is therefore largely increased [44, 71].
Another consequence of reduced long-range interactions is the different effect on the closed orbit of the bunches. We have to expect a slightly different orbit from bunch to bunch. This effect is demonstrated in Figure 2.13 where the horizontal position at one head-on collision point for 432 bunches (out of 2808) is shown. The bunches in the middle of a batch have all interactions and therefore the same orbit while the bunches at the beginning and end of a batch show a structure which exhibits the decreasing number of long-range interactions. The orbit spread is approximately 10 - 15% of the beam size. Since the orbits of the two beams are not the same, it is impossible to make all bunches collide exactly head-on. A significant fraction will collide with an offset. Although the immediate effect on the luminosity is small [33], collisions at an offset can potentially affect the dynamics and are undesirable. The LHC design should try to minimize these offsets [44, 71].

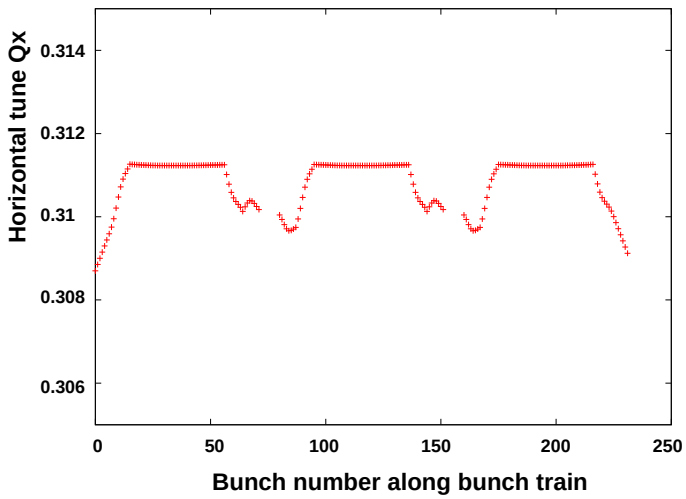

Figure 2.18: Tune variation along the LHC bunch pattern.

A second effect, the different tunes of the bunches, is shown in Figure 2.18. For three batches it shows a sizeable spread from bunch to bunch and without compensation effects [71] it may be too large for a safe operation. In this context it can be essential to study and predict bunch to bunch differences and dynamic behaviour in order to first provide a significant contribution to the diagnostics of the accelerator and second to propose strategies to optimize the machine luminosity and performances taking into account these strong bunch to bunch variations.

2.7 Beam-beam modeling

A particle circulating in an accelerator will see a finite sequence of elements defined at different longitudinal locations. At a beam-beam interaction a beam-beam element can be defined. This element define a deterministic change in the particles trajectory moving from one longitudinal location to the next one. Elements represent a map that can be described by using different mathematical models. All elements of an accelerator such as magnets, radio-frequency accelerating cavities, beam instrumentation and beam-beam elements are described mathematically by a defined model and then concatenated to represent the whole machine. A map defines the local properties of the element and in accelerator physics the most common mathematical descriptions are:

- Linear maps with matrix formalism.
- Higher order maps for non linear elements.
- Simplectic or canonical integration algorithms.
- Local Hamiltonian.
- Lie transformations for linear and non-linear elements.

A beam-beam element can then be described as a linear matrix or by a Lie transformation depending on the approximation required in the calculation and on the study to be performed. Independent of the choice of the mathematical model, this treatment remains a non self-consistent method and applies only to single particle dynamics studies. Going through an element a particle modifies its trajectory and turn after turn it is possible to see how it behaves. This will depend on the particle initial conditions and on the accelerator description. Therefore this method is used to evaluate the accelerator's optical functions and global parameters. A beam-beam interaction can then act as an extra focusing or defocusing element in linear approximation or as a higher order map when expanded to higher precision. However, in all different cases it is not a mutual interaction between two beams. It is possible to apply changes in the beam-beam strength as a function of time but not as a consequence of the interaction with the opposite beam since this is represented by a single particle. Tracking studies are then performed for particles with different initial conditions (amplitudes, energies, etc.) to see how the dynamics correlates with these parameters.
For this purpose several simulation codes were developed and successfully used for different purposes (dynamic aperture studies, beam losses and beam dynamics in general). However, with these models not all beam-beam effect can be reproduced. This can only be done with a self-consistent treatment.

2.7.1 Self-consistent beam-beam models

To evaluate self-consistently beam-beam effects different models are used and different strategies were developed in order to optimize the calculations. It is therefore important to define the problem and consequently make the proper choice for the modeling. The

problem we have to face is that we want self-consistent solutions of a system of charge distributions with densities ψ^a and ψ^b which have the following properties:

- ψ^a and ψ^b are mutually changed by interaction
- Interaction depends on beam distributions
  - Beam 1 ψ^a solution depends on beam 2 ψ^b
  - Beam 2 ψ^b solution depends on beam 1 ψ^a

In general, a self-consistent treatment of the beam-beam interaction starts from the Vlasov equation of the system. To describe the system of two or more bunches interacting electromagnetically we have to first establish the equation of motion of the system and therefore the Vlasov equation. The formalism that allows the solution of this equation is known and used in many other collective effects i.e. wake fields and impedances and has been applied also to beam-beam interactions [10, 11]. While for the case of two colliding bunches one can easily derive the solution of the system, for the case of many bunches interacting many times, solutions are difficult and not always converging. Therefore one has to decide to go for simplified models for the beam distribution as well as for the field calculations to quantitatively predict the beam dynamics in the presence of many beam-beam interactions.
In principle, a system of two or more bunches colliding can be modeled by using the Vlasov formalism. The solution of the system equation gives a self-consistent result for the beams evolution in time. For the specific case of two bunches (a and b) colliding, the Vlasov equation for very flat beams reduces to a one-dimensional problem and becomes of the type:

$$\frac{\partial \psi^a}{\partial t} = -q_x p_x \frac{\partial \psi^a}{\partial x} + (\frac{\partial p_x}{\partial t}) \frac{\partial \psi^a}{\partial p_x} \tag{2.75}$$

The variables q_x and p_x are the accelerator betatron frequency and momentum in the horizontal plane, respectively while ψ^a represents beam a distribution density which depends on q_x, p_x and t. Solving the Vlasov equation means finding the beam distributions and their evolution in time. The coupling to beam b comes from the term $\frac{\partial p_x}{\partial t}$ which represents the change in momentum coming from the opposite beam b since $\rho^b(x;t) = \int_{-\infty}^{\infty} \psi^b(x, p_x; t) dp_x$ represents the beam charge distribution in the (x, p_x) normalized phase plane.

The Vlasov equation then takes the form:

$$\frac{\partial \psi^a}{\partial t} = -q_x p_x \frac{\partial \psi^a}{\partial x} + \left(q_x x + \delta_p(t) 4\pi\xi_x \text{p.v.} \int_{-\infty}^{+\infty} \frac{\rho^b(x';t)}{x - x'} dx' \right) \frac{\partial \psi^a}{\partial p_x} \tag{2.76}$$

Normally it is not easy to find exact solutions for this equation since it represents a coupled differential equation for the unknown beam distributions ψ^a and ψ^b. The purpose

of solving Equation 2.76 is to evaluate the stability of solutions, calculate the frequency spectra of coherent oscillations and identify discrete spectral lines of oscillations. This can be done by solving the equation either analytically or through numerical integration. Analytical solutions have been found for simplified Gaussian distributions of particles and with either a linearized approximation of the equation or through perturbative methods [10, 11]. However, analytical solutions are possible only for simplified cases and for a system of very few bunches and a single interaction. The Equation 2.76 still represents a formidable task for mathematical analysis.
What is more feasible is a numerical integration of Equation 2.76 which provides the momentum deviation beam a will receive from the interaction with the distribution b. The main concept is to replace the derivative by finite differences. Therefore, the continuous function $\psi^{x,t}$ has to be discretized on a three-dimensional grid. After the proper evaluation one proceeds with a one-direction integration. However, numerical solution of the momentum kick are possible for simplified distributions $\rho^b(x';t)$; for more complex cases solutions diverge easily specially for the case of multiple interactions.
Analytically, Equation 2.76 is no more manageable than the complete set of particle orbits. What is commonly done is the discretization of the mathematical model. The first step from the mathematical to the simulation model is to approximate the Equation 2.76 by the algebraic equations required for numerical computations. An easy and common alternative way to proceed for self-consistent beam-beam studies is to replace Equation 2.76 by its characteristic equations. If we replace the search of the time dependency of $\psi^{x,t}$ and directly derive the electric potential U(x, y, z) from the Poisson equation which relates the potential to the charge density distribution $\rho(x, y, z)$:

$$\Delta U = -\frac{1}{\epsilon_0}\rho(x, y, z) \tag{2.77}$$

one can then compute the electric field from:

$$\vec{E} \;=\; -\nabla U(x, y, z). \tag{2.78}$$

The Poisson equation can be formally solved using e.g. the Green's function method (e.g. [26]) since the Green's function for this boundary value problem is well known and used in electrostatic problems. The formal solution using a Green's function will be analytically derived in the next chapter for the cases of Gaussian and elliptical charge distributions. In general the point is to evaluate the integral:

$$U(x, y, z) = \frac{1}{4\pi\epsilon_0}\int\int\int G(x - x_0, y - y_0, z - z_0)\rho(x_0, y_0, z_0)dx_0dy_0dz_0 \tag{2.79}$$

which represents the electric potential a test particle located at (x, y, z) will feel from a distribution of charges described by $\rho(x_0, y_0, z_0)$. The Green's function for this open boundary is of the type:

$$G(x - x_0, y - y_0, z - z_0) = -\frac{1}{4\pi\sqrt{(x - x_0)^2 + (y - y_0)^2 + (z - z_0)^2}} \tag{2.80}$$

To solve the integral and therefore evaluate the electric potential seen by an opposing particle one can decide between different methods which depend on the assumptions made

on the charge distribution $\rho(x_0, y_0, z_0)$.
The possible simulation techniques used for field (force) calculation depend mainly on the approximation used for the charge distribution ρ, which can be defined from a simple point-like distribution to a number N of macro particles representing the particle beam. Depending on the choice of the beam description we can then choose between the following techniques for the field calculation:

- Rigid Gaussian approximation(RG): assumes a Gaussian $\rho(x, y)$ with fixed width but varying centroid. The field is analytically derived at every interaction with new centroid position(x, y).
- Soft Gaussian approximation (SG): assumes a Gaussian ρ with varying centre and width. The field is analytically derived at every interaction with new distribution parameters $(x, \sigma_x, y, \sigma_y)$.
- Particle-Particle methods (PP): accumulate the forces by finding the force $F(i, j)$ between particle i and particle j.
- Particle-Mesh methods (PM): approximate the force as a field quantity on a mesh. Differential operators are replaced by finite difference approximations.
- Hybrid Fast Multiple Methods (HFMM): derived from particle-particle methods it relies on composing multi pole expansions.

A very important issue in the self-consistent beam-beam treatment, apart from the accuracy, is the computational time. This strongly depends on the field calculation. Depending on the method applied the timing issue changes significantly, especially passing from a rigid beam description to a multi particle one, which ensures a correct treatment of the non-linear force. In general, for beam-beam coherent effects we need samples of $N_p > 10^4$ particles while for incoherent effects the number of particles increases to $N_p > 10^6$. For the different methods defined above we summarize here the predictive power and the computational cost required from each technique per interaction:

- RG: fast calculation but very limited quantitative predictive power.
- SG: calculation cost high. Time goes with N_p^2 and the assumption of Gaussian bunches leads to quantitative discrepancies.
- PP: timing goes like N^2, depending on the distribution. Description gives correct results.
- PM: computational cost is $N_g \ln N_g$ depends on the number of grid nodes N_g. It is not ideal when the mesh is largely empty (i.e. long range interactions).
- HFMM: computing time goes between N_p and $N_p \cdot \ln N_p$ numerically correct and ideal for long range interactions.

For multiple interactions, the timing cost scales roughly with the number of interactions. Therefore, for simple machines, i.e. with few bunches all with the same collision pattern, PP simulations are possible and have been used to study coherent modes and

emittance effects. However, this is not possible for the LHC due to the large number of interactions and bunches. The LHC will have at nominal operation 2808 bunches per beam and, due to the external crossing angles to avoid unwanted multiple head-on collisions at the IR, up to 30 BBIs per crossing. This results in 124 interactions per turn which also strongly affect the calculation time. Because of these features one must expect the bunches to behave differently and this requires a large scale simulation with many bunches. The lumping of interactions leads to doubtful results where it cannot be justified.
This issue represents the limiting factor for self-consistent beam-beam simulations for multiple interactions and multiple bunch beams. Simulating the nominal LHC configuration would have been impossible without the development of new computer hardware facilities such as supercomuters which also allow an important reduction of computing time by the use of new parallel algorithm techniques. However, we would also like to stress in this thesis the absolute importance of simplified models for many studies of the qualitative behaviour of bunches, and especially for the understanding of more complex results coming from multi particle calculations which otherwise may be incomprehensible.

Chapter 3

Self-consistent beam-beam models

The spectra of the barycentric motion and the mode frequencies of coherent beam-beam modes are well known and understood for the case of few bunches colliding head-on [10, 11, 36]. In order to get higher luminosity, the LHC relies on a large number of bunches and multiple interaction points. Moreover with multiple bunch beam the picture is complicated by the necessity of colliding the beams at the IP with a crossing angle to avoid unwanted multiple head-on interaction per crossing. The consequences are parasitic long range interactions and a much richer spectrum of modes because many bunches couple through this non linear beam-beam force [39, 40]. This is in particular true when the collision points are not symmetrically distributed. Additional effects due to non symmetric collision schemes [41, 42] or asymmetric machine optics [90] must be expected. The case is further complicated due to Pacman and Superpacman effects [44], beam parameter variations (e.g. emittance and/or intensity fluctuations) as well as synchrotron motion [10]. It must be expected that these effects will lead to different coherent modes and in particular to different Landau damping behavior for different bunches.
In the LHC 2808 bunches in each beam will collide in four experimental regions and experience four head-on collisions as well as many long range beam-beam interactions. Moreover, the accelerator layout presents several characteristics which break the symmetry between the collision points:

- Asymmetric configuration of the collision points.
- Presence of a large number of parasitic long range interactions.
- Unavoidable Pacman and Superpacman bunch effects [43, 44].
- It is impossible to make the bunches collide exactly head-on [45, 46].

In the case of multiple head-on collisions these coherent modes can be analyzed with a linearized model for the beam-beam force searching for the eigenmodes of the full single turn map [21, 36]. However, when the non linear long range interactions are included, the linearized treatment is not adequate. One therefore might expect a fairly large number of modes which may obscure tune measurements and/or feedback systems. The presence of a large number of modes due to the effect of local, parasitic interactions was already studied in [50, 51] with Pacman effects and for a simplified LHC collision scheme.

We have developed three different models to study coherent and incoherent beam-beam effects in the case of multiple bunch beams and multiple head-on and/or parasitic beam-beam interactions. The code developed is the COherent Multi-Bunch Interactions program (COMBI) which allows to simulate a large number of bunches for any arbitrary collision or filling scheme as described in [52, 53]. The bunches can be simulated using three different models depending on the beam-beam effects of interest such as:

- Mode frequencies.
- Mode oscillating pattern.
- Damping properties.
- Emittance behavior.

The first model developed in COMBI is obtained by finding the numerical solutions of a one turn matrix map of many bunches coupled by the beam-beam force. This method is an extension to the multiple bunch regime of what already done in [21, 36] for fewer bunches. In addition, for the first time, we analyzed the eigenmodes which give the bunch oscillating patterns. The fields used for this model are the one analytically derived for the case of Gaussian bunches in a coherent linear approximation for the head-on as well as for the long range interactions.

A second modeling for fast results was done using point-like bunches [52]. The bunches are rigid objects with a Gaussian particle distribution and variable centroid position but with fixed beam sizes for the field calculation. The beam-beam kick is computed by using the analytical solutions for Gaussian beams of Equations 2.69. However, this simplified approximation cannot reproduce important effects such as Landau damping which is due to the natural spread in frequencies of the particles in a bunch.

For this reason a third model implemented in COMBI is a multi-particle model to represent the bunches. Bunches are made by a sample N_{tot} of simulation particles (macro-particles). For these macro-particles the charge to mass ratio is the same as the real particles in the bunch. This treatment allows to reproduce damping mechanisms and to qualitatively understand the beam-beam interactions. In this multi-particle modeling we also have the possibility of choosing between two different field solvers. The first one, called 'Soft Gaussian' approximation, is faster in terms of computing time and assumes the particle distribution to be Gaussian with variable centroid position and transverse size. At the interaction location, each single particle receives the incoherent kick of Equation 2.31 which is calculated using the analytical solution of the field in case of Gaussian distributions for the beams. Another option which aims to give quantitative correct results is to apply a HFMM [54] modeling for the field calculations. This model can evaluate the field produced by any arbitrary particle distribution.

The particle distribution model and number and much more the field calculation used in the program are very important since they determine the speed of the simulations. Simulating thousand of bunches with 10^6 macro-particles, each interacting in several points along an accelerator for at least 2^{16} turns can take several days of running time. For this we have developed parallel algorithms for the multi-particle version of the code to speed

up calculations which would not be possible with scalar calculations.
To understand multi-bunch beam-beam coupling we use in parallel the three complementary models that depending on the different cases help understanding the coherent multi-bunch interaction effects. In this chapter we will describe the details of the models and their applications. The different models will be used for reproducing tune spectra of multi-bunch beams coupled by the beam-beam force. Results will be compared and advantages and limitations will be explained.

3.1 Different models for the beam-beam simulation

Beam-beam effects can be reproduced using different approaches for the field calculations and bunch description. We decided to address the multi-bunch multiple interaction regime of the LHC with three models: an analytical linear method and two numerical approaches. The different models are called Analytical Linear Model (ALM), the Rigid Bunch Model (RBM) and the Multi-Particle Model (MPM). All three models give useful and complementary information about the beam-beam coupling of multiple bunches. Depending on the studies of interest it is possible to choose the best model. These models have intrinsic advantages and disadvantages and used together they can provide a deeper insight into the underlying physics. In Table 3.1 we schematically show for a defined property which

Parameters	ALM	RBM	MPM
Calculation speed	++	0	- -
Non linear effects	-	+	++
Landau damping	-	-	++
Higher order modes	-	-	++
Incoherent effects	-	-	++
Correct field calculation	-	-	+(+)
Flexibility(collision and bunch schemes)	++	++	++

Table 3.1: Schematic summary on the different models performances and result goodness with respect to a given parameter one is interested in. ALM stays for Analytical Linear Model, RBM for Rigid Bunch Model and MPM for Multi-Particle Model.

model is appropriate. For example if we need to simulate thousands of bunches colliding as in the LHC the MPM is time consuming providing quantitative correct results while the RBM and the ALM can give a fast qualitative evaluation of the effects. On the other hand the matrix model assumes a linear approximation of the beam-beam force and this will not give information about the non linearities of the system. Damping mechanism as well as higher order modes can be reproduced and studied only by using the multi-particle treatment. For this reason a parallel processing mode was foreseen from the design stage to overcome the speed limitations of the MPM. In the following we describe the three models in more detail.

3.2 Analytical Linear Model

The ALM model is based on the concept of a map and represents an extension of what was already done for few bunches by [36, 90]. In general, maps are used in accelerator physics to describe local properties of a machine element (i.e. a quadrupole or dipole magnet) or a local interaction (i.e. beam-beam interaction, electron cloud). The map transforms defined properties (coordinates, optical function etc.) through an element. In a two dimensional problem a bunch or a single particle can be described by a system of four coordinates $\vec{z}(s) = (x, x' = \frac{\delta x}{\delta s}, y, y' = \frac{\delta y}{\delta s})$. A map $\mathcal{M}$ simply transforms the coordinates $\vec{z}_1(s_1)$ at position s_1 to new coordinates $\vec{z}_2(s_2)$ at position s_2 through a ring or a beam line.

$$\vec{z}_2(s_2) = \begin{pmatrix} x \\ x' \\ y \\ y' \end{pmatrix}_{s_2} = \mathcal{M} \cdot \begin{pmatrix} x \\ x' \\ y \\ y' \end{pmatrix}_{s_1} = \mathcal{M} \cdot \vec{z}_1(s_1) \tag{3.1}$$

The map $\mathcal{M}$ describes local properties of a machine element and can be:

- A simple linear matrix or transformation,
- A Lie transform,
- High order integration algorithm,
- Derived from local Hamiltonian,
- A computer program, subroutine,
- Any description to go from s_1 to s_2.

In a circular accelerator, starting from a position s_0 by concatenating in sequence around the ring all the N element maps we obtain the so called one turn map, which is a description of the accelerator as the particles or bunches will see traveling along it.

$$\begin{pmatrix} x \\ x' \\ y \\ y' \end{pmatrix}_{s_0+C} = \mathcal{M}_1 \cdot \mathcal{M}_2 \cdot \ldots \mathcal{M}_n \cdot \begin{pmatrix} x \\ x' \\ y \\ y' \end{pmatrix}_{s_0} = \mathcal{M}_{ring}(s_0) \cdot \begin{pmatrix} x \\ x' \\ y \\ y' \end{pmatrix}_{s_0} \tag{3.2}$$

If we assume only linear elements then all our maps are matrices. Therefore the one turn map $\mathcal{M}_{ring}$ is a matrix, the one turn matrix. Beam-beam coherent modes from head-on collisions can be analyzed by searching the eigenstates of a full one turn map where also a beam-beam element has been added. This method has already been used in [36, 90] for few number of bunches per beam and for few head-on beam-beam interactions only. In this approach the beam-beam force was approximated by its linear term and the beam-beam element is represented by a map located at the longitudinal location s_{bb} where an interaction is foreseen. The maps in this linear approximation are matrices and can be easily evaluated. In the arcs a rotation in the transverse phase space is applied. In [36, 90] this method has been used to study the coherent modes of two bunches and the

stability of few bunches (up to three per beam) colliding head-on only. Here we extend the method to multiple bunches undergoing multiple head-on as well as long range beam-beam interactions. The two colliding beams are represented by a vector of length equal to the total number of bunches in the accelerator times four, the number of variables (X, X', Y, Y') for a 2-D description of the bunches. The two counter rotating beams are described by a vector where we have the horizontal and vertical positions and angles of all bunches of beam $1(b_1)$ followed by all bunches of beam $2(b_2)$:

$$\left(X_{1^{b_1}}, X'_{1^{b_1}}, Y_{1^{b_1}}, Y'_{1^{b_1}}, X_{2^{b_1}}, X'_{2^{b_1}}, Y_{2^{b_1}}, Y'_{2^{b_1}}, \ldots, X_{1^{b_2}}, X'_{1^{b_2}}, Y_{1^{b_2}}, Y'_{1^{b_2}}, \ldots \right)_s \tag{3.3}$$

Bunches are assumed rigid point like objects with defined positions (X,Y) and angles (X',Y') in the transverse plane. For small oscillations the beam-beam force is approximately linear in this case. The one turn map is obtained by multiplying the transport matrices from one point of a ring to the next. A standard linear transfer map for all bunches of the two beams is given by the following expression that describes how the horizontal bunch centroid positions($X_{1^{b_1}}$ and $X_{1^{b_2}}$) and angles($X'_{1^{b_1}}$ and $X'_{1^{b_2}}$) of the bunches of the two beams are transformed from the position s_0 to a position s_1:

$$\mathcal{M}_{arc} = \begin{pmatrix} \cos(\Delta\mu_x^{b_1}) & \sin(\Delta\mu_x^{b_1}) & \ldots & 0 & 0 & \ldots \\ -\sin(\Delta\mu_x^{b_1}) & \cos(\Delta\mu_x^{b_1}) & \ldots & 0 & 0 & \ldots \\ \ldots & \ldots & \ldots & \ldots & \ldots & \ldots \\ 0 & 0 & \ldots & \cos(\Delta\mu_x^{b_2}) & \sin(\Delta\mu_x^{b_2}) & \ldots \\ 0 & 0 & \ldots & -\sin(\Delta\mu_x^{b_2}) & \cos(\Delta\mu_x^{b_2}) & \ldots \\ \ldots & \ldots & \ldots & \ldots & \ldots & \ldots \end{pmatrix} \tag{3.4}$$

In the matrix above we show only the case for the first coordinates $X_{1^{b_1}}$ and $X'_{1^{b_1}}$ which represent the horizontal position and angle of bunch number one of beam one and below the same variables for beam two. The $\Delta\mu_x$ is the horizontal phase advances of the beams going through the element. In this case since it represents an arc of the ring, it is the phase advance between two locations s_0 and s along the circular accelerator and it is calculated by other optical programs (for the LHC with MADX [5]). In the vertical plane we have the same matrix but with a different phase advance $\Delta\mu_y$. The phase advance $\Delta\mu_x$ and $\Delta\mu_y$ can be different for the two beams. In this case they are defined with $\Delta\mu_x^{b_1}$ or $\Delta\mu_x^{b_2}$ for beam 1 or beam 2, respectively. This case occurs when the two beams are operated at two different working points in the tune diagram. A linear transfer matrix then looks like a diagonal matrix with the rotational terms of the two beams and for the two planes. The other elements of the matrix are by default set to zero. Linear coupling between the horizontal and vertical plane can easily be added and will result in non zero terms in the matrix of Equation 3.4 for the off-diagonal elements.

Between the rotation in phase space in the arcs we define the beam-beam matrix for head-on and/or long range interactions. For the head-on beam-beam kick we use a linear approximation for the beam-beam force. The matrix in the case of a head-on collision between bunch 1 of beam 1 and bunch 1 of beam 2 for the horizontal coordinates will be as follow:

$$\begin{pmatrix} X_{1,b_1} \\ X'_{1,b_1} \\ \dots \\ X_{1,b_2} \\ X'_{1,b_2} \\ \dots \end{pmatrix}_{s_2} = \begin{pmatrix} 1 & 0 & \dots & 0 & 0 & \dots \\ -k_{HO} & 1 & \dots & k_{HO} & 0 & \dots \\ \dots & \dots & \dots & \dots & \dots & \dots \\ 0 & 0 & \dots & 1 & 0 & \dots \\ k_{HO} & 0 & \dots & -k_{HO} & 1 & \dots \\ \dots & \dots & \dots & \dots & \dots & \dots \end{pmatrix} \begin{pmatrix} X_{1,b_1} \\ X'_{1,b_1} \\ \dots \\ X_{1,b_2} \\ X'_{1,b_2} \\ \dots \end{pmatrix}_{s_1} \tag{3.5}$$

In this example k_{HO} is defined as the head-on beam-beam kick and is:

$$k_{HO} = \frac{2\pi\Xi_{HO}}{\beta^*} \tag{3.6}$$

where Ξ_{HO} is the known coherent linear beam-beam parameter of Equation 2.72 [21, 23, 24]. In the case of round beams we have:

$$\Xi_{HO} = \frac{Nr_0\beta^*}{8\pi\gamma\sigma^2} = \frac{1}{2}\xi_{HO} \tag{3.7}$$

r_0 is the classical particle (e.g.: electron, proton) radius and β^* is the optical amplitude function (β-function) at the interaction point. The term ξ_{HO} is the linear beam-beam parameter as defined in Equation 2.35. The linear coherent beam-beam kick in momentum is then given by the following expression:

$$\Delta X'_{1,b_1} = (X_{1,b_1} - X_{1,b_2}) \cdot k_{HO} \tag{3.8}$$

For the vertical plane one has the equivalent expression.

In the case of a long-range beam-beam interaction the ξ_{LR} is calculated using a linear approximation as for the head-on case. We derived the slope of the beam-beam force at a location $r \gg \sigma$. For our scope and studies the bunch will always be at a distance r larger than 7 σ. This represents a first approximation for oscillations of the bunch barycentres much smaller than the actual separation at the parasitic encounter. As an example, we assume a long range interaction between bunch 5 of beam 1 and bunch 2 of beam 2 with separation in the horizontal plane. The beam-beam kick matrix in the case of a long-range interaction between bunch 5 of beam 1 and bunch 23 of beam 2 would transform the bunch coordinates from s_1 to s_2 as follows:

$$\begin{pmatrix} \dots \\ X_{5,b_1} \\ X'_{5,b_1} \\ \dots \\ X_{23,b_2} \\ X'_{23,b_2} \\ \dots \end{pmatrix}_{s_2} = \begin{pmatrix} \dots & \dots & \dots & \dots & \dots & \dots \\ 1 & 0 & \dots & 0 & 0 & \dots \\ -k_{LR} & 1 & \dots & k_{LR} & 0 & \dots \\ \dots & \dots & \dots & \dots & \dots & \dots \\ 0 & 0 & \dots & 1 & 0 & \dots \\ k_{LR} & 0 & \dots & -k_{LR} & 1 & \dots \\ \dots & \dots & \dots & \dots & \dots & \dots \end{pmatrix} \begin{pmatrix} \dots \\ X_{5,b_1} \\ X'_{5,b_1} \\ \dots \\ X_{23,b_2} \\ X'_{23,b_2} \\ \dots \end{pmatrix}_{s_1} \tag{3.9}$$

In this example k_{LR} is the long-range kick term which links the changes of the slopes to the positions of the two bunches which are interacting at a parasitic encounter. We have 4 kick terms for all the pairs of bunches which interacts at the same time:

$$k_{LR} = \frac{2\pi\xi_{LR}}{\beta} \tag{3.10}$$

where ξ_{LR} is the long-range beam-beam strength defined as the slope of the beam-beam force at distance between the bunches. For the LHC case to be conservative a $r \approx 7\ \sigma$ could be assumed. This is calculated by using the analytical solution of the beam-beam kick for a defined distance of the interaction.

The linear beam-beam kick in momentum is then given by the following expression where the beams are assumed round ($\sigma_x = \sigma_y$):

$$\Delta X'_{1,b_1} = (X_{1,b_1} - X_{1,b_2}) \cdot k_{LR} \tag{3.11}$$

$$\Delta X'_{1,b_1} = \frac{2 r_p N_p^{1,b_2}}{\gamma} \frac{\beta_x}{\sigma_{1,b_2}^2} \cdot F_x(X_{1,b_1} - X_{1,b_2}, Y_{1,b_1} - Y_{1,b_2}, \sigma_{1,b_2}) \tag{3.12}$$

By reading the beam filling scheme and collision pattern the code creates the matrices for the linear transfer $\mathcal{T}_n$ and for the beam-beam interactions $\mathcal{B}_n$ where defined by the inputs. The one turn map $\mathcal{M}_C$ is then calculated by multiplying the matrices in their order along the machine circumference C:

$$\mathcal{M}_C = \mathcal{T}_1 \cdot \mathcal{B}_1 \cdot \ldots \cdot \mathcal{T}_n \cdot \mathcal{B}_n \tag{3.13}$$

Then we calculate the eigenvalues λ_i and eigenvectors v_i of the system by solving the eigenvalue problem:

$$\mathcal{M}_C \cdot v_i = \lambda_i \cdot v_i \tag{3.14}$$

The eigenvalues give the system eigenfrequencies, i.e. the tunes of the machine by:

$$det(\mathcal{M}_C - \lambda \mathcal{I}) = 0 \tag{3.15}$$

The one turn map allows to calculate numerically the eigenvalues and eigenfrequencies of the system of coupled oscillators and we obtain the complete set of oscillation frequencies of the system. The calculation is fast and gives the full solution. However, the linear approximation of the beam-beam interaction leads to a qualitative picture of the beam-beam effects which will complement the other models and helps the understanding of modes in the case of head-on collisions as well as for the long range interactions. This method has the advantage that it is possible to identify and associate the corresponding eigenmodes and eigenfrequencies.

3.3 Rigid Bunch Model

The rigid bunch approximation described in details in [52] is a first COMBI version that defines particle bunches as rigid objects where the particle distribution is assumed Gaussian with fixed RMS defined as a constant for all bunches and all times. To describe the motion of a rigid bunch the following parameters are used:

- Horizontal position and angle of barycenter: X and X'.
- Vertical position and angle of barycenter: Y and Y'.

- Longitudinal phase (or position) and energy deviation: ϕ (or s) and δ.
- Bunch intensity to determine the beam-beam kick, can vary from bunch to bunch.
- Bunch emittance to determine the beam-beam kick, can vary from bunch to bunch.
- Tune shift ΔQ_x and ΔQ_y with respect to a nominal bunch.

The bunches are assumed to be Gaussian in the two planes with fixed squared transverse sizes. In this approximation one can express the coherent beam-beam force analytically as done in Chapter 2. The model is a kick based code where at each BBI the bunches receive a transverse kick from the opposite bunch and change coordinates. The horizontal and vertical coherent beam-beam kicks a bunch with barycentres at (X^*, Y^*) and fixed squared transverse sizes Σ^*_{xx} and Σ^*_{yy} can induce to an opposite bunch at the interaction point are then given by:

$$\Delta X' = \frac{2r_p N_p^*}{\gamma}\frac{\beta_x}{\sigma^2}F_x(X - X^*, Y - Y^*, \Sigma^*_{xx}, \Sigma^*_{yy}) \tag{3.16}$$

$$\Delta Y' = \frac{2r_p N_p^*}{\gamma}\frac{\beta_y}{\sigma_Y^2}F_y(X - X^*, Y - Y^*, \Sigma^*_{xx}, \Sigma^*_{yy}) \tag{3.17}$$

with r_p the classical proton radius, N_p^* the bunch population, γ is the relativistic Lorentz factor, β_x and β_y the horizontal and vertical betatron functions at the IP. The * denotes parameters of the opposing beam, σ_X and σ_Y are the horizontal and vertical RMS size of the observed bunch which for this models are constants. F_x and F_y are the beam-beam force of the opposite bunch on the bunch. In the round beams approximation where $\Sigma_{xx} \approx \Sigma_{yy}$ the force is given by

$$F_{\{x,y\}}(X - X^*, Y - Y^*, \Sigma^*_{xx}, \Sigma^*_{yy}) = \frac{\{X, Y\}}{(X^2 + Y^2)}\left[1 - \exp\left(-\frac{X^2 + Y^2}{\Sigma^*_{xx} + \Sigma^*_{yy}}\right)\right] \tag{3.18}$$

Between the BBIs the phase advance through the accelerator arcs is applied with a simple rotation in phase space.
The rigid model is useful to study coupling of multi-bunch beams and especially to study effects of collision scheme symmetries as well as of the beam filling structure. The processing time is short and gives the possibility to obtain sufficient amount of data on the mode frequencies for different and complicated interaction patterns. However, the model can only give qualitative results without taking into account damping effects. Many of the oscillating modes resulting from this model are expected to be damped when a multi-particle model is used. Moreover, the beam-beam effect is underestimated due to the approximation used for the particle distribution. A quantitative and correct approach requires multi-particle, multi-bunch tracking even if the computing time will strongly increase. However, this approximation will be used as comparison to better understand coupling and damping mechanisms in between bunches undergoing BBIs.

3.4 Multi-Particle Model

If one wants to study in a fully self-consistent way BBIs then the study of coherent motion as well as the presence of Landau damping should be considered. With a multi-particle approach one introduces a natural spread in frequency in the particle sample and the effects coming from damping can be observed and studied. In addition the coherent motion differs from what was found so far with the RBM and ALM. When moving to a multi-particle system with multiple bunches the interpretation of the results still represents the most difficult part in understanding the physical properties of BBI. Therefore one should always step to more complicated problems by going through known approximations. In this frame we decided to first go for a Gaussian approximation for the particle distribution and only after with the proper improvements in the computational structure of the code we decided to go for arbitrary particle distributions which can evolve freely in the computation.

3.4.1 Gaussian distribution

The present version of the multi-particle program assumes Gaussian bunches and a 'soft' Gaussian approximation for the field calculation. With this approximation we can study qualitatively the BBIs. A bunch is assumed to be populated by a Gaussian distribution of particles with an initial barycentre and transverse size. At each interaction each particle of the bunch involved receives a kick that depends on the particle distribution of the opposing bunch. At any time the particle distribution is assumed Gaussian but with recalculated barycentre and transverse size. This approximation gives a qualitatively correct treatment of beam-beam interactions. The understanding of coupling and damping mechanism in between multi-bunch beams as in the LHC case is already a quite important issue to achieve. However, this program is not limited to this approximation and to get a correct quantitative evaluation of beam-beam effects in between the nominal LHC beams (2808 bunches per beam) we implemented the HFMM (Hybrid Fast Multiple Method)[92] for the field calculations. In that stage a parallel processing will be essential in order to keep the computing time within reasonable limits.
Like the rigid model, it is flexible and parameters such as tunes, number of bunches, filling scheme, collision scheme and crossing planes at the interaction points can be easily changed. The possibility to change the phase advance between collision points is very important and different phase advances are possible for the two counter rotating beams. Bunch intensities and emittance fluctuations can be simulated. The possibility to have different filling schemes for the two beams allows to study effects arising from beam asymmetries as well as demonstrating the so called Pacman and Superpacman effects which could play an important role in complex hadron colliders as for example the LHC [44]. In order to get all correct modes of the bunches coupled by head-on and long range interactions, all individual interactions are simulated in full without lumping several interactions.

To describe the motion of particles in a Gaussian bunch the following parameters are used:

- Horizontal position and angle of single particles: x and x',

- Vertical position and angle of single particles: y and y',
- Bunch intensity may vary from bunch to bunch (to determine beam-beam kick),
- Bunch emittance may vary from bunch to bunch (to determine beam-beam kick),
- Longitudinal phase (or position) and energy deviation: ϕ (or s) and δ,
- Tune shift ΔQ_X and ΔQ_Y with respect to a nominal bunch.

The head-on incoherent beam-beam kick on a particle crossing an opposite beam is calculated by assuming a Gaussian bunch particle distribution in the two planes with barycentres at (X^*, Y^*) and squared transverse sizes $\Sigma^*_{xx} =< (x-X)^2 >^*$ and $\Sigma^*_{yy} =< (y-Y)^2 >^*$. The * denotes parameters of the opposing beam. In this approximation one can express the beam-beam force analytically. In the soft Gaussian model the bunch barycentres and the bunch transverse sizes are calculated at each interaction for a self-consistent field calculation.

The horizontal and vertical incoherent beam-beam kicks at the interaction point for a given particle are then given by:

$$\Delta x' = \frac{2r_p N_p^*}{\gamma}\frac{\beta_x}{\sigma_x^2}F_x(x-X^*, y-Y^*, \Sigma^*_{xx}, \Sigma^*_{yy}) \tag{3.19}$$

$$\Delta y' = \frac{2r_p N_p^*}{\gamma}\frac{\beta_y}{\sigma_y^2}F_y(x-X^*, y-Y^*, \Sigma^*_{xx}, \Sigma^*_{yy}) \tag{3.20}$$

with r_p the classical proton radius, N_p^* the bunch population, γ is the relativistic Lorentz factor, β_x and β_y the horizontal and vertical betatron functions at the IP, σ_x and σ_y the horizontal and vertical RMS size of the observed bunch and F_x and F_y the beam-beam force of the opposite bunch on the single particle. In the round beams approximation where $\Sigma_{xx} \approx \Sigma_{yy}$ the force is given by

$$F_{\{x,y\}}(x-X^*, y-Y^*, \Sigma^*_{xx}, \Sigma^*_{yy}) = \frac{\{x,y\}}{(x^2+y^2)}\left[1-\exp\left(-\frac{x^2+y^2}{\Sigma^*_{xx}+\Sigma^*_{yy}}\right)\right] \tag{3.21}$$

Each particle of the bunch involved in the interaction receives a transverse kick from the opposite beam that depends on the single particle position and the opposing bunch's population, size and barycenter position. In the linear limit (for small distances) the incoherent beam-beam kick is twice the coherent one. More details on the beam-beam kick as a function of the particle distribution approximation can be found in [101].
For the calculation of the long range incoherent beam-beam kick we use the same expression as in the rigid bunch model because the two models are equal for big distances. By a Fourier analysis of the barycenter of the bunches, as calculated turn by turn, we obtain the tune spectra of the dipole modes. For only one bunch per beam the two spectra of the

two bunches are equivalent. For more than one bunch per beam the spectra of bunches with the same collision scheme are also equivalent. Analyzing the sum $(X^{(1)} + X^{(2)})$ or the difference $(X^{(1)} - X^{(2)})$ of the barycentres of the two colliding bunches of the two beams (denoted by (1) and (2)) shows the spectra of the σ and π-modes separately. This is useful to analyze the details of the modes frequencies. A tune spectrum is reproduced for each bunch in the two beams.

3.4.2 Arbitrary particle distributions

To increase the accuracy of the simulations and overcome the limiting 'Soft Gaussian' approximation, we have introduced a field solver for an arbitrary distribution of charges in space. The choice of the solver is constrained by the problems under investigation:

- Large number of particles in simulation (from 10^4 to more than 10^6).
- Separated beams (separation between zero and 10 times the beam size or more).

A direct integration of forces (particle-particle methods) is ruled out since the necessary time grows with the square of the number of particles ($\mathrm{O}(N_p^2)$). For the number of particles used in our simulation this is impossible. Other possible solvers employ so-called particle-mesh methods and have been shown to give good results [102]. Their advantage is speed since the number of computations is smaller and depends on the number of grid points N_g: $(\mathcal{O}(N_g ln N_g))$. A strong disadvantage is that particle-mesh methods have problems handling non-uniform distributions. For the case of separated beams (as in our case with the important effect of long-range collisions) most of the space is basically empty. Moving or adaptive grids may be used for that purpose, but may lead to a rather complicated structure. A recent simulation program relies on a Green function approach [104, 105, 106] and is adapted well to the problems of separated beams.

Another possibility is to use Fast Multipole Methods (FMM). In this algorithm the potential or force acting on a particle are divided into two components. The component of close particles is computed directly and between distant particles the potential is computed by multipole expansion [107, 108]. This method is therefore well adapted to handle problems like separated beams. Problems with FMM may be close encounters and "charge-overloading", i.e. for the LHC bunches 10^{11} particles are represented by up to $2{\cdot}10^6$ macro-particles to avoid these problems.

3.4.3 The Hybrid Fast Multipole Method

For our problem we studied a modified version of FMM, a Hybrid FMM (HFMM) [54, 92, 110]. It resembles a particle mesh method for the handling of charges and super-particles. However, the forces on the super-particles are evaluated using the FMM. Smoothing can help to avoid charge-overloading. The HFMM is a robust implementation of a Fast-Multipole Method (FMM) field solver, which is designed to solve the field for an arbitrary collection of discrete charges. It divides the solution domain into a grid and a halo area. The grid area is subdivided into a hierarchical tree of square regions. In the first step of the calculation, the macro-particles inside the grid are assigned to grid points. All

macro-particles outside the grid are treated as discrete, independent super-particles and form the halo. The charge assignment can be done with a 'nearest-grid-point' method, i.e. the charge is assigned to the nearest grid point. This is the simplest method, however the field values are not continuous and the results are more noisy. Alternatively one can use the cloud-in-cell (CIC) charge assignment where the charge is shared between the neighboring grids points. This method gives continuous field values but requires more book-keeping.

Finally, multipole expansions of the field are computed for every point, i.e. for each grid point as well as for every halo particle, and the program derives the resulting forces on the particles of the counter-rotating beam. In the case of a CIC charge assignment, appropriate interpolation between the fields calculated for the grid points have to be applied. The grid size and shape does not have to follow any special geometry and can be chosen freely to achieve the desired speed and precision, depending on the problems under investigation. Unlike other Poisson solvers, the grid points with no charges assigned are left out of the computation and the number of computations scales roughly with the number of particles. More details of the HFMM method are found in [92].

In this work we have implemented the HFMM in our beam-beam simulation program to evaluate the force on a test particle generated by an arbitrary charge distribution. This was applied to study the strong-strong collision of two bunches colliding at one or more interaction points (IP) [92, 54, 110]. We have studied the coherent modes that are excited in the collision of two equal round bunches similar to those of LHC, when colliding head-on or separated by a constant offset at one interaction point (long-range interactions). This allowed to obtain the correct Yokoya factor by multi-particle tracking [59] and in a later stage to study in detail the modes excited by long-range interactions.

Although it was not its original purpose, it allows us to study the possible emittance growth of collisions of partially overlapping bunches [45] in a completely self-consistent way and with exact calculation of the field.

Tracking with HFMM

We simulate the collision of two strong proton beams. Our variables are: horizontal position x, vertical position y, horizontal angle $v_x = x'$, and vertical angle $v_y = y'$. The prime denotes the derivative with respect to longitudinal position s, *e.g.* x' is the slope of the horizontal trajectory.

Each of the beams has one bunch that is represented by a set of N_p macro-particles. Their trajectories are followed over n turns, assuming linear betatron motion without coupling and a beam-beam collision at one interaction point (IP). At the IP every particle in the bunch experiences a deflection by the field of the counter-rotating beam that depends on its position.

The deflection applied to a single particle in one of the beams is calculated using the HFMM.

The map from one IP to the next is

$$\begin{pmatrix} x(n+1) \\ v_x(n+1) \end{pmatrix} =$$

$$\begin{pmatrix} \cos(2\pi Q_x) & \sin(2\pi Q_x) \\ -\sin(2\pi Q_x) & \cos(2\pi Q_x) \end{pmatrix} \begin{pmatrix} x(n) \\ v_x(n) + \Delta v_x(n) \end{pmatrix} \tag{3.22}$$

An equivalent map is applied in the vertical plane, (y, v_y).

The horizontal deflection experienced at the interaction point is:

$$\Delta v_x(n) = \frac{r_p N^*}{\gamma} E_x(x, y) \tag{3.23}$$

where $E_x(x, y)$ is the horizontal force evaluated with the HFMM technique at the particle position (x, y). The number of particles in the opposing beam is N^*.

For the simulation of parasitic (long-range) collisions, the same model is employed. The two beams collide with a horizontal separation L_x (in units of σ_x). For a low β insertion we have about 90° phase advance between the IP and the long-range collision region. Since in the LHC the betatron phase advance between long-range collisions on one side of the interaction region is very small, we can lump all n_{par} parasitic collisions into a single one, to reduce the computing time. This overestimates the effect slightly because the bunches oscillate with different phases with respect to each other. This lumping is acceptable when we are not interested in coherent modes or bunch to bunch differences.

Because a static dipole kick would change the closed orbit of the bunch, the static kick from the long-range collision must be subtracted [51, 92]. The beam-beam long-range kick used in our simulation code is then

$$\Delta v_x(n) = n_{par} \frac{2 r_p N_p^*}{\gamma} (E_x(x + L_x\sigma_x, y) - D_x(L_x\sigma_x, 0)) \tag{3.24}$$

where $D_x(L_x\sigma_x, 0)) = -1/L_x\sigma_x(1.0 - \exp(-\frac{L_x^2}{2.0}))$ is the (constant) dipole kick generated by a Gaussian distribution at a distance $x = L_x\sigma_x$. This assumes that a closed orbit exists [45] and the bunches oscillate coherently around this orbit. At the LHC, there are about $n_{par} = 16$ parasitic encounters on each side of an IP, with a minimum transverse separation of $L_x = 7.5$ (in units of σ_x).

3.5 The code structure: input and output

A desired design feature of the code was to be very flexible to changes in the collision pattern, in the filling scheme and beam models applied. All this to optimize the study of beam-beam interactions for different scenarios and to apply it to any collider. In this section we define the input and output structure of the COMBI code. Extra information required by the model applied for the beam-beam interaction and/or on the bunch description will be pointed out in the relevant sections. At the start of the program, a parameter file is read to define the basic input data. The name of this file is taken as a command line argument of the program. From this file the program takes the collision scheme and the beam filling as described in [52]. The new options introduced at this stage are the possibilities to have two different filling schemes for the two counter rotating beams and to analyze the beam-beam effects on a specified bunch and/or range of bunches. The possibility to have two independent filling scheme is very important to study effects coming from beam asymmetries and/or from special operational modes like

an interleaved injection. Analyzing properties averaged over several bunches are useful to evaluate differences and establish requirements for beam measurements. Other new features are the possibility to excite defined bunches mainly to reproduce instrumentation effects on single or few bunches or excitation of defined bunch oscillating pattern. Below we show an example of an input file:

```
collision:  coll_ref.in           // input collision scheme
filling beam 1: fill_ref1.in      // input filling scheme beam1
filling beam 2: fill_ref2.in      // input filling scheme beam2
use bunch: 1 beam:1               // define bunch 1 beam1 for analysis
average over bunches: 1005,1011   // average output over bunches
number of turns: 14               // number of turns: 2**14
bunches to kick: 2001,2013,2076   // bunches kicked by measurement device
beam-beam parameter: 0.0025       // linear beam-beam parameter
```

3.5.1 Bunches in the ring and beam filling schemes

Each beam is defined by its own filling scheme file which is read in the code as an input file. The description of the filling scheme is given in *groups* . Each group has two parameters: the first specifies the number of slots n and the second whether the n slots are occupied by a bunch (1) or whether the slots are empty (0). The total number of slots must be equal to the machine circumference divided by the bunch spacing. It is therefore very important that all empty slots are defined as well as all filled ones. The number of groups per line is specified at the beginning of the description file. The description used maximizes the readability, although other formats as possible. The example below describes the two counter rotating beams with different number of bunches and differently distributed in the ring. Beam one consists of four equidistant bunches spread out in 160 slots (possible bunch positions) while beam 2 has 8 bunches not equally spaced in 160 slots. The number of slots in the two beams must be the same (for our example 160).

```
# bunch filling beam 1 #        # bunch filling beam 2 #
# Number of groups #            # Number of groups #
2                               2
 1 1 39 0                       2 1 38 0
 1 1 39 0                       1 1 39 0
 1 1 39 0                       4 1 36 0
 1 1 39 0                       1 1 39 0
```

The scheme below represents the nominal LHC bunch filling scheme organized in 72 bunches per batch as defined in [13, 93].

```
# LHC nominal bunch filling scheme
# Number of groups #
8
72 0  8 0  72 1  8 0  72 1  8 0  30 0   0 0
```

```
72 1   8 0   72 1   8 0   72 1   8 0   30 0    0 0
72 1   8 0   72 1   8 0   72 1   8 0   72 1   39 0
72 1   8 0   72 1   8 0   72 1   8 0   30 0    0 0
72 1   8 0   72 1   8 0   72 1   8 0   30 0    0 0
72 1   8 0   72 1   8 0   72 1   8 0   72 1   39 0
72 1   8 0   72 1   8 0   72 1   8 0   30 0    0 0
72 1   8 0   72 1   8 0   72 1   8 0   30 0    0 0
72 1   8 0   72 1   8 0   72 1   8 0   72 1   39 0
72 1   8 0   72 1   8 0   72 1   8 0   30 0    0 0
72 1   8 0   72 1   8 0   72 1   8 0   30 0    0 0
72 1   8 0   72 1   8 0   72 1   8 0   72 1   39 0
```

The number of slots represented in this case is 3564 which is one tenth of the LHC harmonic number. Every tenth bucket can be filled with a bunch. This results in the nominal bunch spacing of 25 ns. Empty slots are imposed by the injectors chain (PS and SPS) extraction kicker rise times while a long abort gap is foreseen for the LHC beam dumping system and are:

- SPS injection: 8 missing bunches, 0.225 μs.
- LHC injection: 38/39 missing bunches, 0.975 μs.
- Abort gap: 119 missing bunches, 3 μs.

Thanks to the flexibility of the COMBI input structure the code is also used to easily evaluate possible filling schemes optimizing the collision rates as required. With this purpose for the LHC an alternative scheme has been investigated and proposed [56] for the case of problems in the injector chains. The scheme provides equal beams of total 2592 bunches clustered in batches of 48 each. Below we show the implementation in the input file.

```
# Alternative LHC bunch filling scheme
# Number of groups #
10
48 0   9 0   48 0   9 0   48 1   9 0   48 1    9 0   31 0    0 0
48 1   9 0   48 1   9 0   48 1   9 0   48 1    9 0   48 1   40 0
48 1   9 0   48 1   9 0   48 1   9 0   48 1    9 0   48 1   40 0
48 1   9 0   48 1   9 0   48 1   9 0   48 1    9 0   31 0    0 0
48 1   9 0   48 1   9 0   48 1   9 0   48 1    9 0   48 1   40 0
48 1   9 0   48 1   9 0   48 1   9 0   48 1    9 0   48 1   40 0
48 1   9 0   48 1   9 0   48 1   9 0   48 1    9 0   31 0    0 0
48 1   9 0   48 1   9 0   48 1   9 0   48 1    9 0   48 1   40 0
48 1   9 0   48 1   9 0   48 1   9 0   48 1    9 0   48 1   40 0
48 1   9 0   48 1   9 0   48 1   9 0   48 1    9 0   31 0    0 0
48 1   9 0   48 1   9 0   48 1   9 0   48 1    9 0   48 1   40 0
48 1   9 0   48 1   9 0   48 1   9 0   48 1    9 0   48 1   40 0
```

Also for this case the total slots number is the same as for the nominal one (3564) while

gaps in between the bunch trains are more relaxed, i.e. larger. However the reduced number of bunches leads to a decrease of 8% in luminosity.
Other studies using COMBI to propose new filling schemes had been carried with the aim to satisfy the experiment requirements when possible. An example is the alternative 50 ns filling scheme proposed to increase the LHCb experiment luminosity decreasing it in Alice detector and is described in [14].

3.5.2 Rotation of bunches in both rings

For N slots defined for beam 1 and N slots defined for beam 2, one has 2N positions where an action can occur. In the description the numbering of the positions goes from 1 to 2N in the direction of the clock-wise beam. The bunches in beam 1 travel in the direction of increasing slot positions while for beam 2 bunch the position instead decreases in the ring. At each step, every bunch is advanced by one slot position, i.e. half a bunch spacing. One complete turn of the machine therefore requires 2·N steps. At each step a bunch may or may not undergo an interaction as will be described in the next section. However, calculations for all bunches of a beam are independent and this was envisaged to make use of parallel processing, in particular when bunches consist of many macro-particles. In the case of the LHC we assume that the available buckets to allocate bunches are 3564 per beam (one tenth of the real LHC capability). This corresponds to a bunch to bunch spacing of 25 ns. The machine is therefore described by 7128 positions in which the counter rotating beams travels stepping from on slot to the next resulting in steps of 12.5 ns.

3.5.3 Beam collision patterns

At any position from 1 to 2·N, an action can be requested for a bunch when it is in that place, can be 0, 1, 2 which restricts the type of action possible. The different actions are specified by a code number as summarized below. The code can be followed by attributes of the action, as will be explained in detail later. The most important codes are:

- Head-on and long range beam-beam interactions at IP (code 2 or -2),
- Long range beam-beam collisions at IP (code 4 or -4),
- Single separated long-range beam-beam collision for pretzel schemes(code 5 or -5),
- Linear transfer map of a bunch (code 3),
- Beam position monitor (code 6),
- Random white noise (code 7),
- Excitation of selected bunches with a kicker (code 8),
- AC excitation of the beam (code 9),
- Synchrotron motion in longitudinal plane (code 1),
- No action (default).

Further user defined actions can be easily added, e.g. wake fields, non-linear elements, correction as well as measurement devices. To describe the LHC nominal collision scheme the collision file looks like the one below:

```
   1  -2   -15  +15  2
 447   3    8.046   6.940   8.046   6.940
 892  -2   -15  +15  2
2229   3   23.015  21.821  23.015  21.821
3565   2   -15  +15  7
4902   3   23.533  20.689  23.533  20.689
6235   2   -15  +15  7
6432   9    0   0
6684   3    7.716   7.870   7.716   7.870
6756   1    0.001
6800   8    0   0
```

One finds 7128 positions corresponding to twice the number of slots defined by the beam filling scheme. The two beams operate at the same working point in the tune diagram. The IPs follow an eight-fold symmetry except for IP 8, corresponding to the LHCb experiment, which breaks the symmetry since it is longitudinaly shifted by 11.25 m [52, 53].

Head-on and long range beam-beam interactions

The action code +2 or -2 defines a head-on beam-beam interaction at the slot where it is defined. The sign of the action code defines the plane on which the two beams are separated by the crossing angle. The negative sign indicates a vertical crossing while the positive a horizontal one. The first two numbers that follow in the collision pattern description define the number of parasitic encounters left (with the negative sign) and right (positive sign) of the IP, respectively. In the case of the LHC we have four head-on collisions:

```
   1  -2   -15  +15  2
 892  -2   -15  +15  2
3565   2   -15  +15  7
6235   2   -15  +15  7
```

At location 1 we have the ATLAS experiment, the bunches will be separated vertically and experience up to 15 long range interactions per side and one head-on at the centre. The 15 long range interactions are all separated by one slot. At locations 892 and 6235 we find the ALICE and LHCb experiments. In this two locations 15 long range encounters are expected with separation in the vertical and horizontal plane. At the CMS location, slot 3565, a horizontal crossing is foreseen. The third number in the description is the bunch separations in units of the beam size σ at the location of the parasitic encounter. The separation can be defined differently depending on the plane of crossing at the IP. In the example above at location 1 we have a vertical separation of the beams which results in up to 15 long range beam-beam interactions at a separation of 2 σ while a horizontal crossing they will interact at a separation of 7 σ. In reality the separation at the different

long range interactions changes from one encounter to the other and is in the range of [7 σ,12 σ] as shown in Figure 3.1. In the picture we show the relative beam separation at the different parasitic encounters, left and right of IP1 for different external crossing angles (the operational LHC scenario is the one at 300 μrad total external crossing angle). The bunch separations are calculated by using the optics code MADX [5].

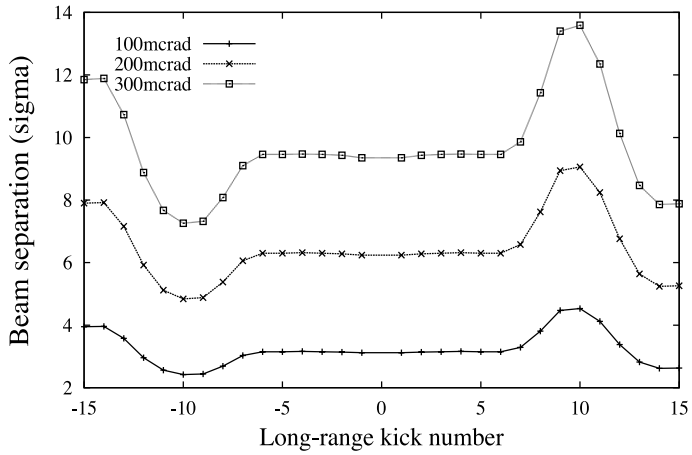

Figure 3.1: Separation in units of the rms beam size σ for different external crossing angles at the different long range parasitic encounters left and right of IP1 at the LHC.

Phase advance through the arcs

The action code 3 represents a linear phase advance, i.e. a rotation in phase space. The linear transfer is controlled by four parameters: $\Delta\mu_x^{b_1}$, $\Delta\mu_y^{b_1}$, $\Delta\mu_x^{b_2}$ and $\Delta\mu_y^{b_2}$. In our example the two LHC beams work at the same working point in the tune diagram and the same phase advance in the arcs.

```
2229   3   23.015  21.821  23.015  21.821
```

After defining the location of the phase advance (slot number 2229) and the action code for the phase advance (number 3), one has the horizontal and vertical phase advance for beam 1 (23.015 and 21.821) and for beam 2 (23.015 and 21.821). This allows to easily simulate and evaluate effects of different working points in the tune space for the two counter-rotating beams. Moreover, in a two ring machine like the LHC, differences in the phase advance between two points for the forward and backward beams are present and possible effects can be evaluated. The phase advance per sector used to describe the accelerator arcs are easily evaluated using the MADX optics code for the machine lattice.

Synchrotron motion in the longitudinal phase space

At a defined location the action code 1 represents the accelerating cavities which will provide a change of the longitudinal coordinates δE and $\delta\phi$ of each particle of the bunch passing through.

```
6756   1    0.001
```

The last parameter represents the synchrotron tune Q_s. In analogy with the transverse plane, the tune represents the number of oscillations in the longitudinal phase space particles undergo in one complete turn of the machine. Particles at the location of the radio-frequency cavity, change their longitudinal coordinates δE and $\delta\phi$ which are the relative deviation of the particle energy and phase with respect to the nominal particle following an oscillating motion with phase advance equal to $2\pi Q_s$. A nominal particle is the one with energy and phase equal to the synchronous particle.

Long range interactions

Code -4 or +4 refers to long range interaction around the position where it is defined. The positive or negative sign before the action code defines the plane in which the two beams are separated through the crossing angle. The negative sign represents a vertical separation while the positive a horizontal one. For example, to evaluate effects coming from the long range interactions only, one can make use of the code 4 at the location of the ATLAS experiment and the description will look like:

```
1  -4   -15  +15  2
```

The beams are separated in the vertical plane and will experience up to 15 long range beam-beam interactions. The code is followed by the number of parasitic encounters left (with the negative sign) and right (positive sign) of the IP and the separation in units of the beam sizes, in the example 2 σ. With this description the interactions will all occur at the same distance following a crossing scheme configuration for the two beams.

For different geometries, like in the case of a pretzel scheme optics (i.e. in the Tevatron) the action code -5 and +5 describes a single beam-beam interaction at a defined separation. As for the action code 4, the minus and plus signs define the beams separation plane, vertical and horizontal, respectively. If instead of a head-on collision at the location of the CMS experiment (3565), we want a beam-beam interaction at a given distance then we define the IP as follow:

```
3565   5   0  0  5
```

In this case the head-on collision at location 3565 is replaced by a long-range beam-beam interaction at 5 σ separation in the horizontal plane. This action is very useful to study effects of off-centered collisions, as will be described in Chapter 6. Depending on the IR optics layout it is possible to address the different beam-beam interactions at the nominal separations and with the relative phase advance from the IP as MADX can provide.

External excitations and monitoring

The action codes 7, 8 and 9 define in general an external excitation force which acts on the beams. The main purpose of introducing these features is to study the effects coming from instrumentation and/or feedback systems always present during normal accelerator operation. With code 7 the two beams are excited with a random noise (white noise), defined by a parameter as shown in the example below. The amplitude of the kick is expressed in units of the beam size σ, in the example it is given by 0.5 σ. The excitation can be applied to a single bunch, to a selected number or to the entire beam.

```
3542   7   +0.5  0
```

The code 8 is a special code to study the possibility of damping defined coherent modes by acting against the associated oscillating modes of the bunches. The oscillating pattern of the bunches, as explained in a later section, is evaluated by searching for the system eigenmodes. The excitation will depend on the bunch contribution to the mode. As for code 7 an extra parameter will define the excitation amplitude applied to the first bunch then the bunch to bunch relative amplitudes are obtained from the eigenvectors.

```
3542   8   1.5  0
```

The action code 9 defines a frequency dependent excitation of the beams. This was implemented mainly to reproduce effects of transverse beam transfer function measurements [57, 58], which measure the amplitude and phase response of a beam to a frequency dependent excitation applied. These results in the presence of beam-beam give a clear picture of the tune distribution during operation. In detail, the beams are excited with a frequency dependent kick with variable frequency obtained by sweeping the kicker frequency across the tune spectrum in steps of 1×10^{-4} tune units. The amplitude of the kick is defined by the first parameter after the action code. The range in frequency as well as the stepping can be also defined depending on the resolution needed. The beam amplitude and phase response are recorded by a beam position monitor located in another position of the ring and defined by action code 6. The Beam Position Monitor action is mainly used to decide the location of the data storing in the ring. This helps to have straight forward comparisons between simulation results and measurement output during accelerator operation.

```
6432   9    0.7   0
6800   6    0   0
```

3.6 Parallel processing

In developing the parallel COMBI code one of the intentions is to be able to accommodate collision models at varying levels of detail, from rigid-bunch and soft-Gaussian treatments to self-consistent field-solve/kick algorithms. For this initial development we chose the intermediate level of the soft-Gaussian model, coupled with linear matrix transport, which can provide qualitatively correct results in coherent oscillation spectra and yet remains accessible to small-scale multi-bunch computations on a single processor, thus allowing a meaningful assessment of parallel efficiency. The structure of the computational core, first developed in a single-processor setting is based on nested stepping over turns, bunches, and ring locations. Zero, one, or two bunches (one from each beam) may occupy a ring location ("slot") and to any location there may be assigned an *action code* that specifies a computation to be done. In the non-parallel code these actions are performed in sequence for each ring location, whereas in the parallel code the computations are distributed to a set of processes which do the computations locally and with local data.

3.6.1 Parallel Algorithm

The parallel scheme sketched in Figure 3.2 comprises 1 supervisor process and a set of worker processes, with tasks as follows:

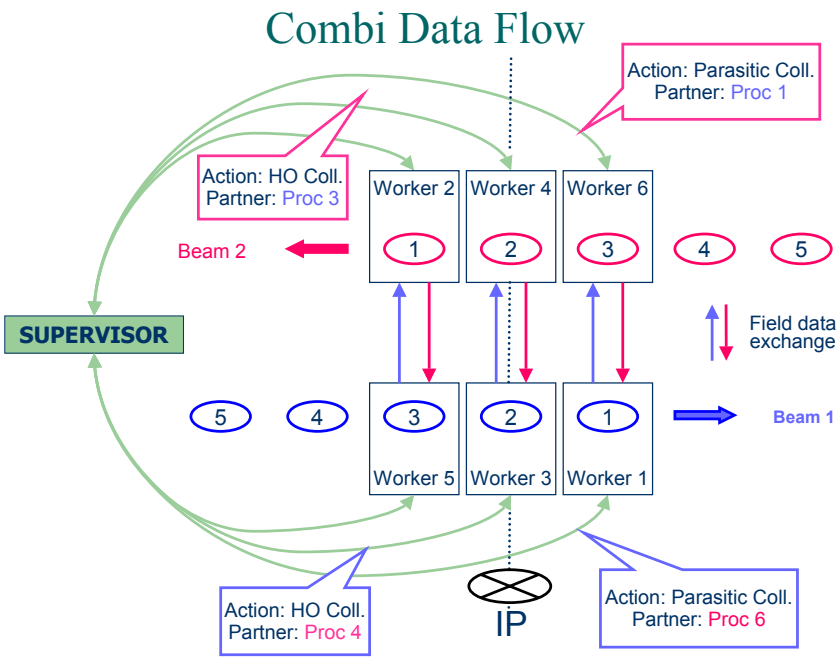

Figure 3.2: Schematic of the parallel architecture and of the data flow through the processors.

Supervisor

The supervisor initiates all computations performed by the worker processes: essentially it is an executive "shell" which performs no computations except for minimal book-keeping of bunch positions, and hence is free to rapidly send task instructions to a large number of workers and keep them maximally occupied. The supervisor activities comprise the following:

1. Reads the input files (run parameters, fill patterns, collision and transport patterns).
2. Initialises the worker processes.
3. Performs stepping of bunches around the rings
4. At each step sends coordinated task messages to the workers for all active bunch pairs.
5. Receives completion messages from workers and ensures proper task synchronization and data integrity.
6. Sends shutdown messages to all workers when the run is complete.

Worker

Each worker process is associated with a particular bunch and stores and calculates all data (coordinates and statistics) for that bunch locally. Depending on available resources and the number of parasitic collisions to be modeled at each IP, in the implementation

each worker process may actually be responsible for several bunches, but for clarity of exposition we retain the processor-bunch duality. Workers perform single-actions (e.g. transport to the next interaction point) or pair-actions (e.g. a head-on or parasitic collision with another bunch).

After initialization, each worker goes into "listen" mode where it waits for an instruction from the supervisor, acts on it, and sends a completion message back to the supervisor. This continues until a shutdown message is received, upon which the process exits. Each instruction message contains the relevant information to perform the task, such as betatron phase advances, and identity of partner bunches. The actions can be itemized as follows:

1. Initialization. Generate initial particle coordinates sampled from the bunch distribution, using the random seed sent by the supervisor. On completion return the random seed to the supervisor.

2. Transport. Advance the particles according to the betatron phases sent by the supervisor. Then send a completion message to the supervisor.

3. Collision. The type of collision (head-on, parasitic) and identity (process id) of the partner (opposing bunch) are sent by the supervisor. Compute the electric field of the local bunch and send the field data to the partner. Receive a message from the partner containing its field data, and perform the resulting kicks on the local bunch coordinates. Send a completion message to the supervisor.

4. Other actions. Additional single- or dual-bunch actions or variants identified by action code and partner bunch number.

5. Output. Workers are responsible for all output involving the local bunch data, and open independent output streams for these. Output can include bunch statistics, centroid coordinates for frequency analysis, and particle coordinates for tracking analysis.

6. Shutdown. Worker process exits.

3.6.2 Performances

We performance-tested the parallel COMBI code on a commodity cluster of Opteron 250 [47](2.4GHz, 1024KB cache) processors in a dual-cpu MYRINET configuration, employing the Portland Group compilers together with the MYRINET GM implementation of MPI. We also performed some preliminary timing on an IBM Blue Gene supercomputer [48](8192 CPUs and 2TB memory). We include the latter architecture since it provides a reference point for possible very-large-scale simulations in which the number of simulated bunches may approach the number of real bunches circulating in the LHC.

As seen in Figure 3.3 the parallel code performs effectively in the MPI setting and scales to large numbers of bunches on the commodity cluster with a modest, and linear, communications overhead, reflecting the predominantly one-to-one messaging scheme, with no all-to-all messages required and minimal one-to-all and all-to-one messaging for task

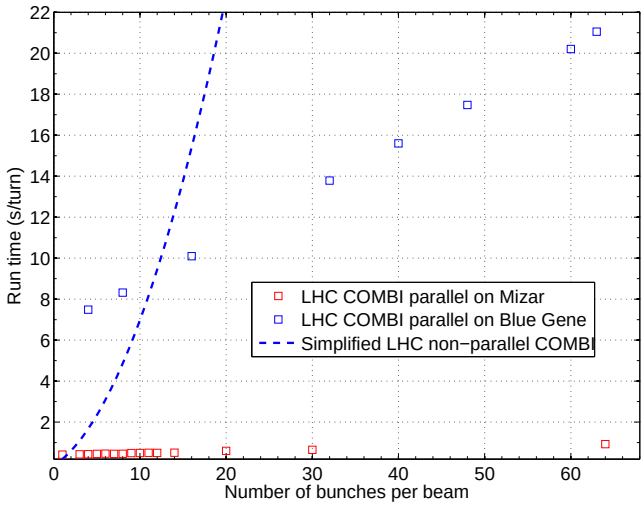

Figure 3.3: Timing of original (single processor) and parallel codes with varying numbers of bunches

assignments and synchronization. The timing trend for the non-parallel code is as expected and indicates that by ∼8 bunches the parallel speed-up is approximately equal to the number of processors.

The initial results for Blue Gene reflect its lower cpu clock speed and also suggest a non-optimal communications overhead, so further testing and development will be required to establish its applicability to large-scale problems.

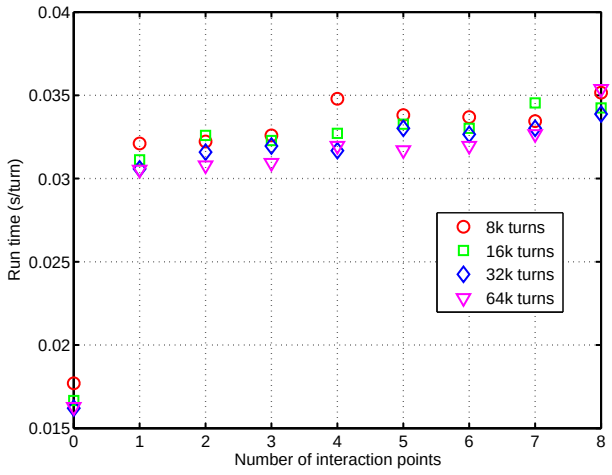

Figure 3.4: Timing of parallel code with varying numbers of interaction points

On the commodity cluster another series of timing were performed for a fixed number of circulating bunches and increasing numbers of IP's, until all bunches were colliding at every step. Figure 3.4 shows again that increasing numbers of collisions can be accommodated with low overhead and good scaling properties.

The code COMBI has expanded the scope of multi-bunch and multi-IP beam-beam simulations and can be used effectively on commodity clusters. This has enabled new studies of coherent beam-beam effects in the LHC, ranging over the variety of collision patterns that will be present and in the RHIC collider exploiting experimental evidences of bunch to bunch difference [114]. The structure of the code allows further refinements such as the recent addition of chromaticity, radio frequency accelerating cavities and measurements devices (transverse beam transfer functions [114]).

Chapter 4

Multiple beam-beam interactions: coherent effects

To validate and demonstrate the program features, we have tried to reproduce properties and well known effects of beam-beam interactions. We start here by analyzing the physics of coherent beam-beam effects. As already explained in Chapter 1 for coherent effects we study how the bunches as a whole develop a coherent motion due to the beam-beam interaction. As first step we analyze single and multiple head-on interactions between bunches, the dependence on the collision scheme symmetries and the damping of modes. The same analysis will be extended to the case of long range interactions. Finally the two regimes are put together in preparation of a complete LHC collision scheme. This stepping from simple cases to complex collision patterns will help understanding the bunch behaviors during collision and testing the program. The results we present focus on a strict comparison between all the models developed in order to demonstrate the advantages and potential of each method and the information they produce. For the simulations we assumed a collider with an eightfold symmetric structure as for the LHC case. The possible collision points are then numbered from 1 to 8, and for the LHC only four are genuine interaction points but for the purpose of this study we assume that at all the eight IP locations the two beams can collide. The Figure 4.1 represents a schematic layout of the eightfold symmetric collider. Also for the long range interactions the locations will be defined as for the nominal LHC case: left and right of an interaction point.

To look at coherent modes we will mainly focus on the bunch frequency spectra and on the mode oscillating pattern for the case of multiple bunches and multiple interactions. Since we will focus here on coherent motion due to symmetry breaking we assume identical parameters for all the bunches. For this studies we assume the nominal LHC bunch parameters listed in Table 4.1. For the MPM model we use 10^4 macro particles per bunch tracked for at least 2^{16} turns. This choice is supported by a dedicated simulation campaign of the frequency resolution and stability of the results as a function of the number of macro particles processed and of the number of turns. Nevertheless, both parameters can easily be changed.

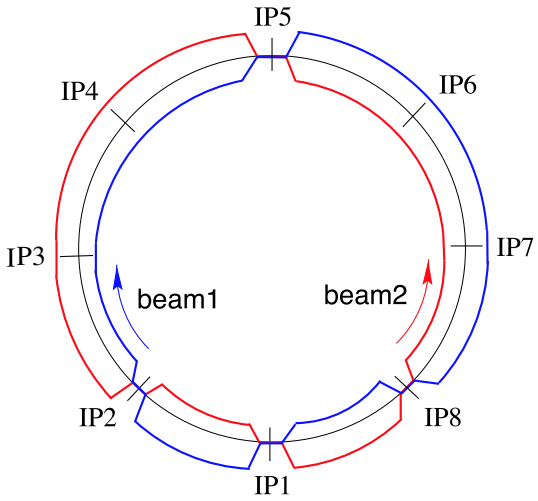

Figure 4.1: Schematic eight fold symmetry straight section geometrical layout, with all Interaction Points (IPs)

Parameters	Values
Bunch Intensity	$1.15 \cdot 10^{11}$
Bunch horizontal RMS	16 μm
Bunch vertical RMS	16 μm
Bunch x' RMS	16E-6/β^*
Bunch y' RMS	16E-6/β^*
Number of macro-particles	10^4
Number of turns	65000
Linear beam-beam parameter ξ	$\approx$0.0035
IPs β^*	0.55 m
Machine horizontal tune Q_x	63.31
Machine vertical tune Q_y	58.32

Table 4.1: Summary table of LHC beams' parameters used for simulations

4.1 Multiple head-on interactions

For the study of multiple head on collisions we simulate simple cases to see the appearance and degeneracy of coherent modes due to the number of interactions and on the symmetry of the collision points in the eightfold symmetric picture of our accelerator. To define the beam configuration we use a convention for the beam description. In the case of equally spaced bunches in the collider we can define the two beams as a set of two numbers N_1/N_2 which means that N_1 bunches are in beam 1 (anti-clockwise beam)and N_2 in beam 2 (clockwise beam). The bunches when defined with this simple ratio are assumed always equally spaced longitudinally in the ring. Where this is not applicable we use the standard input file as defined in the previous chapter. Through the arcs the beams experience a simple rotation in the transverse phase space, as defined in [111]. For the horizontal and vertical tunes we use the LHC nominal values of Q_x =63.31 and Q_y =58.32, respectively. Through each arc of the eight-fold symmetry machine the bunches will rotate of 1/8 of the overall tunes, $Q_{x_{1/8}}$ =7.91375 and $Q_{y_{1/8}}$ = 7.29). For all our cases we'll make use of

this simplified structure for the machine arcs. The phase advance through the arcs will then be of the form:

```
# Collision scheme #
 2   3    7.91375  7.29   7.91375  7.29
 4   3    7.91375  7.29   7.91375  7.29
 6   3    7.91375  7.29   7.91375  7.29
 8   3    7.91375  7.29   7.91375  7.29
10   3    7.91375  7.29   7.91375  7.29
12   3    7.91375  7.29   7.91375  7.29
14   3    7.91375  7.29   7.91375  7.29
16   3    7.91375  7.29   7.91375  7.29
```

In this configuration we assume that the eight Interaction Points are all possible collision points and for convention number them from 1 to 8. Then the possible collision points are located as explained in Table 4.2 where also the real LHC experiments are located.

IP name	Location (step)	LHC Experiments
IP1	1	ATLAS
IP2	3	Alice
IP3	5	none
IP4	7	none
IP5	9	CMS
IP6	11	none
IP7	13	none
IP8	15	LHCb

Table 4.2: Schematic of the interaction points in the simplified LHC model

The bunch frequency spectra for the two planes are obtained as explained in detail in Chapter 3. For the ALM we show the system of eigenfrequencies while for the RBM and the MPM the FFT analysis of the barycenter motion of the bunch is of interest. For convention the tune is expressed as relative tune shift normalized with respect to the linear beam-beam parameter ξ. In all the following cases we assume the nominal LHC beam parameters as specified in Table 4.1. In the ALM and RBM a beam-beam linear parameter $\xi \approx 0.0035$ is assumed in all the IPs where a head-on collision occurs.
In the case of a single bunch beam undergoing a linear transfer without beam-beam interactions (as described in the collision configuration above) the two counter-rotating bunches will oscillate coherently at the unperturbed betatron frequencies in both planes. The frequency spectra show a single peak per plane at the machine unperturbed horizontal and vertical tunes. A simple mechanical model to describe the motion of the two beams is the pendulum. In this simple case the two bunches are like two independent pendula which oscillate at their eigenfrequencies (equal to $2\pi Q_{x,y}$).

4.1.1 1/1 colliding beams

We start from the simplest case of single bunch beams colliding in one IP. The beam description, assumed an eightfold symmetric machine of 16 steps is of the form:

```
# bunch filling beam 1 #          # bunch filling beam 2 #
# Number of groups #              # Number of groups #
2                                 2
 1 1 7 0                           1 1 7 0
```

We are in the 1/1 case with a collision scheme with a single head-on interaction at IP1 and described by:

```
# Collision scheme #
 1   2    0        0      0        0
 9   3    63.31   58.32   63.31   58.32
```

The single head-on beam-beam interaction at IP1 couples the bunches and they start oscillating coherently. The collective motion which develops brings the bunches oscillating at two different frequencies, the σ and π frequencies. The first represents the betatron frequency imposed by the accelerator while the second is a signature of the collective motion of the bunches organized by the beam-beam force.

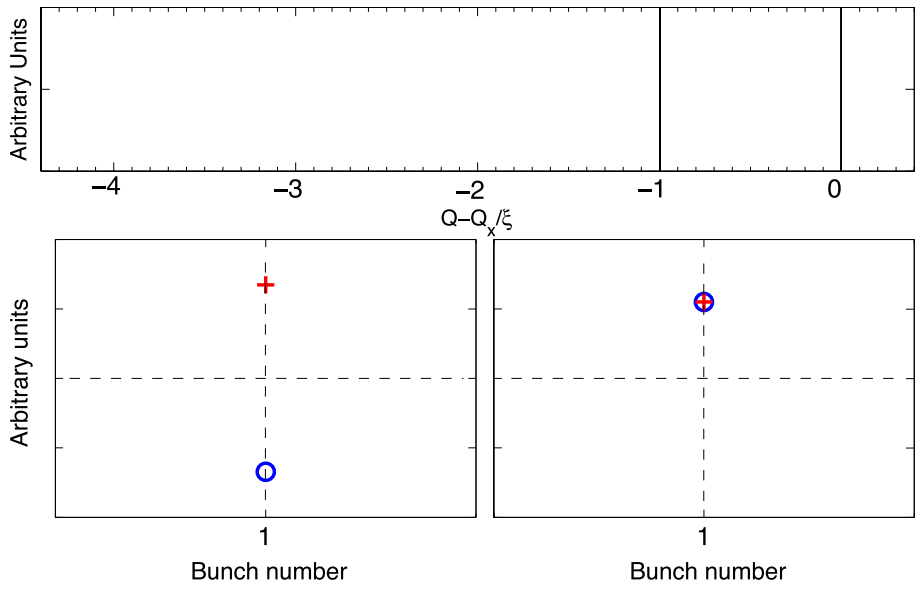

Figure 4.2: Eigenfrequencies (top) and eigenvectors (bottom) of the system of 1/1 bunches colliding head-on in IP1 obtained with ALM. The spectral lines are defined in units of the beam-beam parameter ξ. In bottom + defines beam 1 bunch 1 and ∘ beam 2 bunch 1 eigenvectors.

The system of two bunches colliding head-on develops a coherent motion like for the case of two harmonic oscillators coupled through a force. The resulting motion is a linear combination of the two possible eigenstates which are plotted in Figure 4.2. The ALM spectrum shows the two eigenmodes frequencies, Figure 4.2 top and relative phase amplitude for the two cases Figure 4.2 bottom. In Figure 4.2 top the σ mode and the π spectral line shifted by $-\xi$ are plotted in units of the beam-beam parameter. While the eigenmodes give information about the relative phases of the bunches (∘ beam 1 and +

beam 2). When the two bunches are in phase ∘ and + overlap as shown in Figure 4.2 bottom right while when they oscillate with opposite phase ∘ and + are opposite respect to the zero line (bottom left). The in-phase case corresponds to the bunches oscillating at σ frequency while the opposite phase case is proper of the π frequency.
The RBM results compared to the MPM (Figure 4.3) shows the existence of the same two frequencies. Differences in the absolute value of the tune shifts between RBM results (Figure 4.3 left) and the MPM (Figure 4.3 right) spectra are well known and understood [11]. In RBM result (Figure 4.3 left) the π frequency is shifted by $-\xi$ from the unperturbed σ mode while with the MPM (Figure 4.3 right) the π mode is shifted by $Y \cdot \xi$, where Y is the Yokoya factor for round Gaussian beams and is equal to approximately 1.21 as calculated in [11]. The rigid bunch model tune shift is underestimated due to the approximated bunch description used in this model. A correct calculation must allow changes in the density distribution as a result of the interaction as well as deviations from the Gaussian shape. Moreover, for the multi particle spectrum we find between the two coherent modes a continuum incoherent spectrum that goes from the σ mode down to $-\xi$. The incoherent spectrum in produced by the detuning with amplitude of the beam particles. Particles at small amplitudes are pushed to lower frequencies while the one at larger amplitudes to frequencies closer to the unperturbed as defined in Equation 2.55. Due to the non linear beam-beam interaction the natural spread in amplitude of the particles in a beam results in a spread in frequencies and therefore in a continuum incoherent spectrum as visible in Figure 4.3 right.

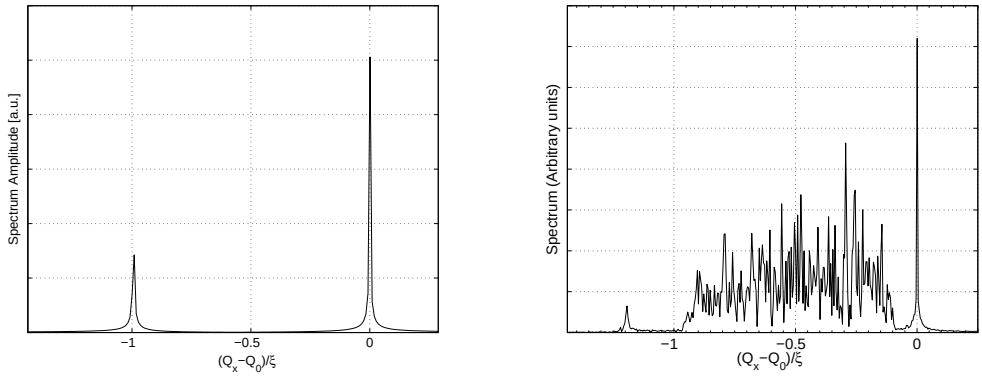

Figure 4.3: Tune spectra of the system of 1/1 bunches colliding head-on in IP1: results from RBM (left) and with MPM (right).

By adding a second head-on collision at IP5, the tune spectra do not change significantly. The two interactions are opposite in azimuthal and represent a symmetric case. The coupling between bunches does not change. It is always a one to one bunch coupling which occurs twice per turn and therefore results are exactly the same as for the single head-on collision case. We can look at this case as a single head-on collision with a double intensity per bunch. The horizontal and vertical spectra show two frequency peaks: the known σ and π modes frequencies. The tune shift between the two eigenfrequency in the tune spectra resulting from ALM is now equal to -2ξ . Due to the symmetric configuration the coherent effects of two head-on interactions simply add up. For the RBM we can conclude the same observations.

4.1.2 4/4 colliding beams

The beam-beam coupling has a strong dependency on the symmetries of the collision points and bunch distribution. Therefore when studying the effects of the interactions one must distinguish and take into account how the bunches couple between them and therefore, for a given bunch fill pattern, the symmetry of the collision schedule. Depending on how the bunches couple the picture changes significantly. The main effect is the appearance of many intermediate oscillating frequencies between the two extreme σ and π modes.
To explain the coupling through head-on collisions we analyze the case of 4/4 bunches colliding in different IPs. In the case of a single head-on the tune spectrum will be the same for all 8 bunches and will be like the one of Figure 2.4. The coupling between the bunches is a one to one coupling as schematically sketched in Table 4.3. One bunch of each beam interacts with only one of the opposite beam, independently from all the others. Therefore, no intermediate modes are expected even if the number of bunches has increased. If we move to more than one interaction then the picture will change significantly depending on the symmetry of the collision points.

	1^{b_2}	2^{b_2}	3^{b_2}	4^{b_2}
1^{b_1}	○			
2^{b_1}		○		
3^{b_1}			○	
4^{b_1}				○

Table 4.3: Schematic of the coupling between bunches due to one head-on beam-beam interaction in IP1 as well as for the case of two head-on collisions in IP1 and IP5. Each bunch couples with one of the opposite beam.

Head-on collisions in IP1 and IP5

If we move to the case of two head-on collisions in IP1 and IP5 which are opposite in azimuth (for the LHC case CMS and ATLAS experiments) we obtain a situation very similar to the single head-on case. The coupling in between the bunches does not change. Also in this case it is a one to one coupling in between the same bunches. To summarize the coupling we can refer to the one collisions case of Table 4.3.
In this case the bunches of beam 1 will just collide twice with the corresponding bunches of beam 2. In the coupling nothing changes with respect to the case of one single collision in IP1 except that the overall effect will be doubled. The tune spectra will be the same for all 8 bunches and look like Figure 4.4. Two peaks are visible in the spectrum, the unperturbed σ mode at a frequency equal to the machine tune (for the x-plane 63.31 and 58.32 for the y-plane) and the π mode frequencies. The shift between the two modes is equal to 2ξ for the ALM and RBM while equal to $2 \cdot Y \cdot \xi$ for the MPM. The tune shift coming from the two head-on collision simply adds up.
In this case just the number of bunches is increased while the collision pattern is kept as in the previous case. The resulting tune spectra do not change. The two possible modes are again the σ and π for which each pair of coupled bunches can collide either in phase

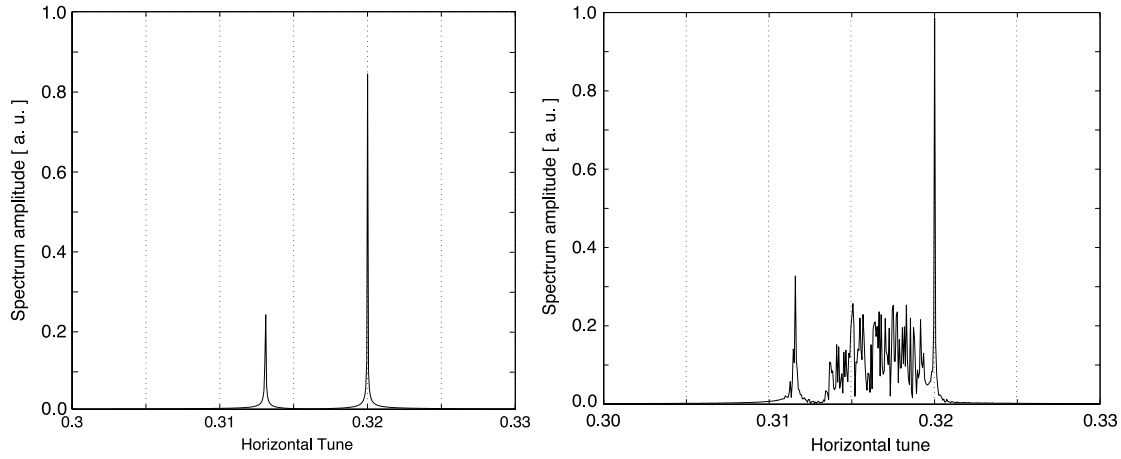

Figure 4.4: Tune spectra of a single bunch for the system of 4/4 bunches colliding head-on in IP1 and IP5. Left picture shows results from RBM while right picture results from the MPM.

or with opposite phase turn after turn. No matter how many bunches one adds to the machine the picture will not change as long as the symmetries are kept unchanged.

Head-on collisions in IP1 and IP3

If we now change the collision pattern and collide the 4/4 beams in IP1 and IP3 the coupling through the beam-beam force involves more and different bunches. Each single bunch of one beam couples with more than one of the opposite beam. This is visible in Table 4.4 where we schematically show how the bunches are coupled. In detail bunch 1^{b_1} collides head-on with the 1^{b_2} and 3^{b_2} while 3^{b_1} collides head-on with the 1^{b_2} and 3^{b_2} and so on for the others. As a result of this, bunches 1^{b_1}, 3^{b_1}, 1^{b_2} and 3^{b_2} organize themselves in a coherent motion independently of the other bunches in the ring. The same applies to bunches 2^{b_1}, 4^{b_1}, 2^{b_2} and 4^{b_2}. We have two identical but independent systems made of 4 bunches coupled through the two head-on collisions in IP1 and IP3.

	1^{b_2}	2^{b_2}	3^{b_2}	4^{b_2}
1^{b_1}	○		○	
2^{b_1}		○		○
3^{b_1}	○		○	
4^{b_1}		○		○

Table 4.4: Schematic of the coupling between bunches due to two head-on beam-beam interaction in IP1 and IP3. Each bunch of one beam couples with 2 of the opposite.

The coherent motion that each family of bunches develops results in three possible modes. The σ and π modes plus a new intermediate one. The appearance of intermediate modes due to the new coupling between sets of four bunches is due to the new collision asymmetry. Associated with the new mode we obtain a new intermediate eigenfrequency as visible in Figure 4.5 (top) as well as associated oscillating patterns for the bunch system as shown in Figure 4.5 (bottom second and third line plots). The new frequency appears at $-\xi$ exactly in between the σ-frequency at zero and the π-frequency at -2ξ as visible

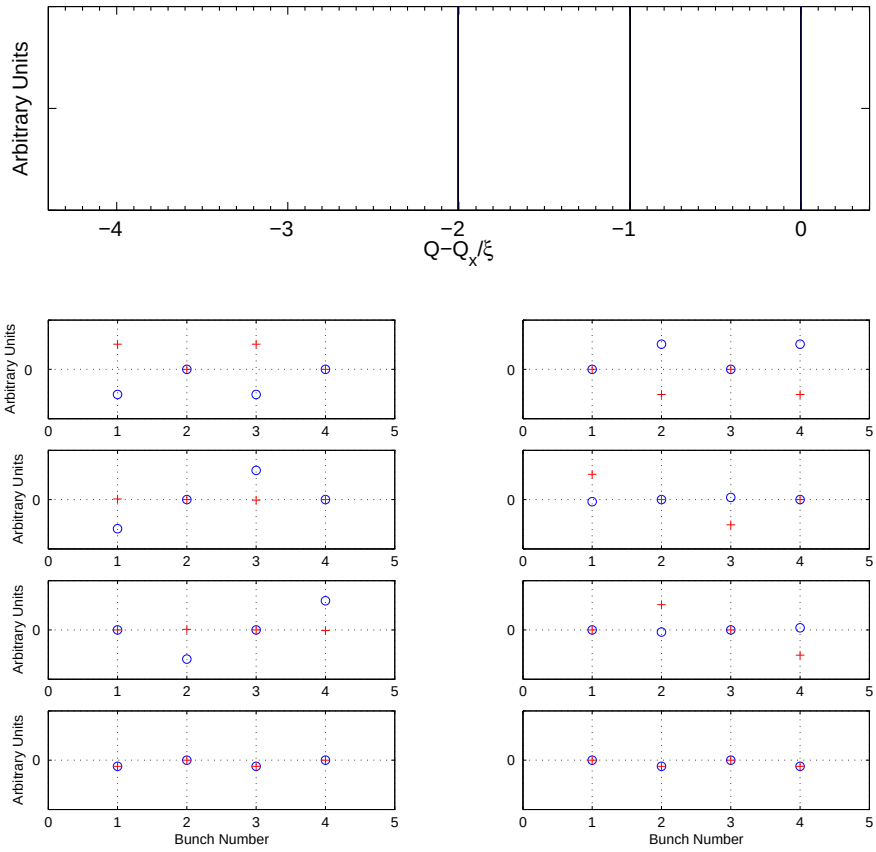

Figure 4.5: Eigenfrequencies and eigenvectors obtained with ALM for the system of 4/4 beams colliding head-on in IP1 and IP3. Top picture shows the spectral lines while bottom the corresponding eigenvectors.

from the ALM spectrum (Figure 4.5 top). In Figure 4.5, bottom, all oscillating patterns associated with the spectral lines are shown. Each subplot represents the eigenvector corresponding to each frequency of the spectrum. Subplots of first line plot of Figure 4.5 bottom represent bunches, 2 by 2, colliding out of phase (when $\circ$ and $+$ have opposite sign amplitudes) proper of the π-mode. Subplots of fourth line show the in-phase collisions of the two independent systems of bunches. Intermediate oscillating patters (second and third line plots of Figure 4.5) are associated to the intermediate spectral line at $1{\cdot}\xi$ of the top plot. For this case the possible bunch to bunch relative phases due to the non symmetric IP3 are two and appear as an intermediate case of the two extreme out or in phase cases.

Results from the RBM and MPM are shown for this case in Figure 4.6. The intermediate mode is visible also in the results from RBM (Figure 4.6, left): a new frequency peak appears in the tune spectra of the bunches. The oscillating frequency is located at $-\xi$ from the unperturbed 0-mode as for the ALM. All bunches are coupled in the same way therefore no bunch to bunch differences are found in the tune spectra.
If we now look at the tune spectrum from the MPM model (Figure 4.6, right) we do not see any intermediate frequency because it is inside the incoherent spectrum and therefore

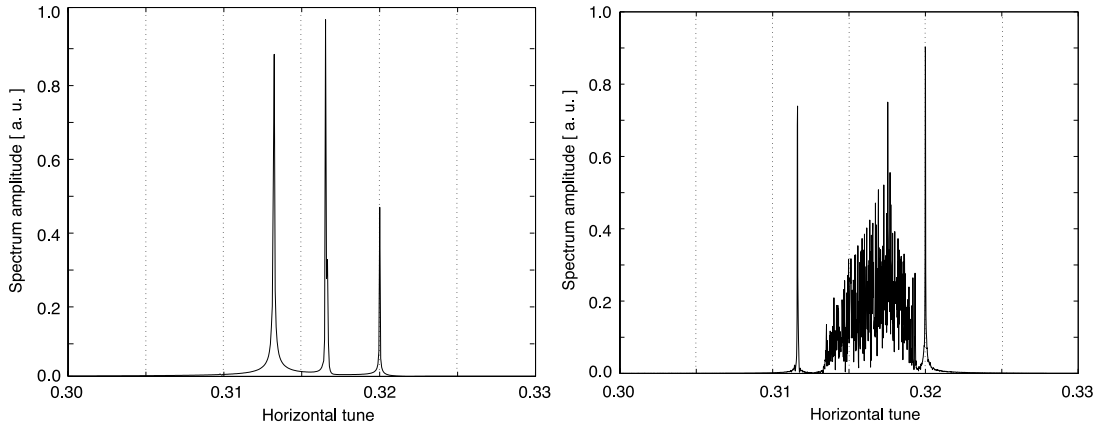

Figure 4.6: Tune spectra of a single bunch for the system of 4/4 bunches colliding head-on in IP1 and IP3. Left picture shows results from RBM while right picture results from the MPM.

is damped due to Landau damping mechanisms. The incoherent spectrum goes from the unperturbed tune (0-frequency in Figure 4.6, right) down to -2ξ. This continuum in frequency is due to the natural spread in amplitude that particles of a bunch have and the relative detuning with amplitude coming from the beam-beam interaction and expressed in Equation 2.60. All bunches undergo the same number of collisions therefore the tune spectrum is identical for all the 8 bunches showing two peaks in the spectrum: the 0-frequency and the π-frequency at $-2Y\xi$.

Two head-on collisions in IP1 and IP2

If we keep the same beam description as for the previous case and we move the head-on collision from IP3 to IP2 we have a different collision pattern and therefore a different coupling of the eight bunches. Each bunch collides twice since we have two IPs, however each bunch is also indirectly coupled to all the others as shown schematically in Table 4.5. Bunch 1^{b_1} collides head-on with bunches 1^{b_2} and 4^{b_2} which undergo collisions with 2^{b_1} and 4^{b_1} which again collides with 2^{b_2} and 3^{b_2} and so on. All bunches are coupled either in a direct interaction or indirectly. The 4/4 beams are now a fully coupled system.

	1^{b_2}	2^{b_2}	3^{b_2}	4^{b_2}
1^{b_1}	○			○
2^{b_1}	○	○		
3^{b_1}		○	○	
4^{b_1}			○	○

Table 4.5: Schematic of the coupling between bunches due to two head-on beam-beam interaction in IP1 and IP2.

Due to the non symmetric collisions schedule and to the higher coupling between bunches the tune spectra for this case present more frequency peaks as shown in Figure 4.7. The left picture shows the tune spectrum obtained with the RBM while the right picture is obtained with the MPM. One should notice the appearance of two extra intermediate modes with respect to those found in the case of collisions at IP1 and IP3 of Figure 4.6. The Landau damping plays an important role in the suppression of many of the intermediate

modes but as shown for those with frequencies out of the continuum the damping is not anymore active. Therefore, it is important to evaluate those which cannot be suppressed by Landau damping since they can drive instabilities.

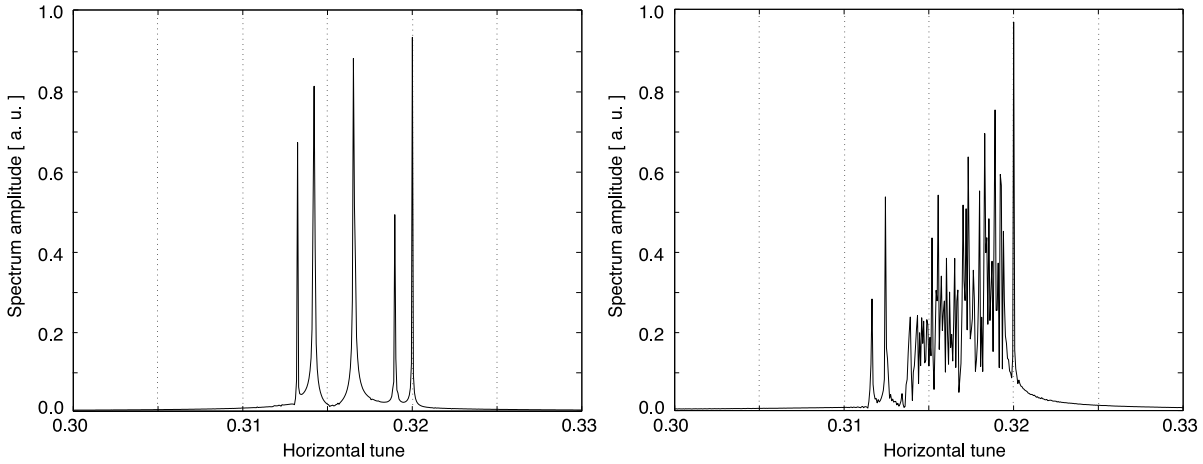

Figure 4.7: Tune spectra of a single bunch for the system of 4/4 bunches colliding head-on in IP1 and IP2. Left picture shows results from the RBM while the right picture represents results from the MPM.

By comparing the tune spectra obtained with RBM and MPM to the ALM eigenfrequencies of Figure 4.8 top one can define the system behaviour. The whole system develops a coherent motion which can be decomposed in different modes. The number of possible modes for this case is five and they are visible in the frequency spectrum obtained with the ALM model (Figure 4.8, top). In addition to the extreme and well known σ and π modes three new intermediate modes appear at $-0.3\ \xi$, $-\xi$ and $-1.7\ \xi$. The coherent motion of the system is given by a linear combination of these possible modes.

Each mode corresponds to a well defined oscillation pattern of the bunches and is associated to one of the system frequencies as shown in Figure 4.8, bottom. Each subplot of Figure 4.8 (bottom) represents the oscillating pattern bunches follow associated to a defined frequency. The first and last subplot correspond to the π and σ spectral lines and represents the out (crosses and circles opposite respect to the axis zero) and in phase (crosses and circles overlapping at the same amplitude) oscillating case. The intermediate eigenvectors are associated to the intermediate eigenfrequencies. Those closer to the π mode show eigenvectors more similar to the one associated with it. Those closer to the zero mode have eigenvectors that reminds the in-phase case of the unperturbed case (last bottom right sub-plot of Figure 4.8). The central intermediate ones are a mixture of the two extreme states.

4.2 Multiple Long range interactions

Depending on the collision symmetries a frequency spectrum can be very complex. If the bunches colliding are fully coupled their eigenmodes become strongly related, i.e. all

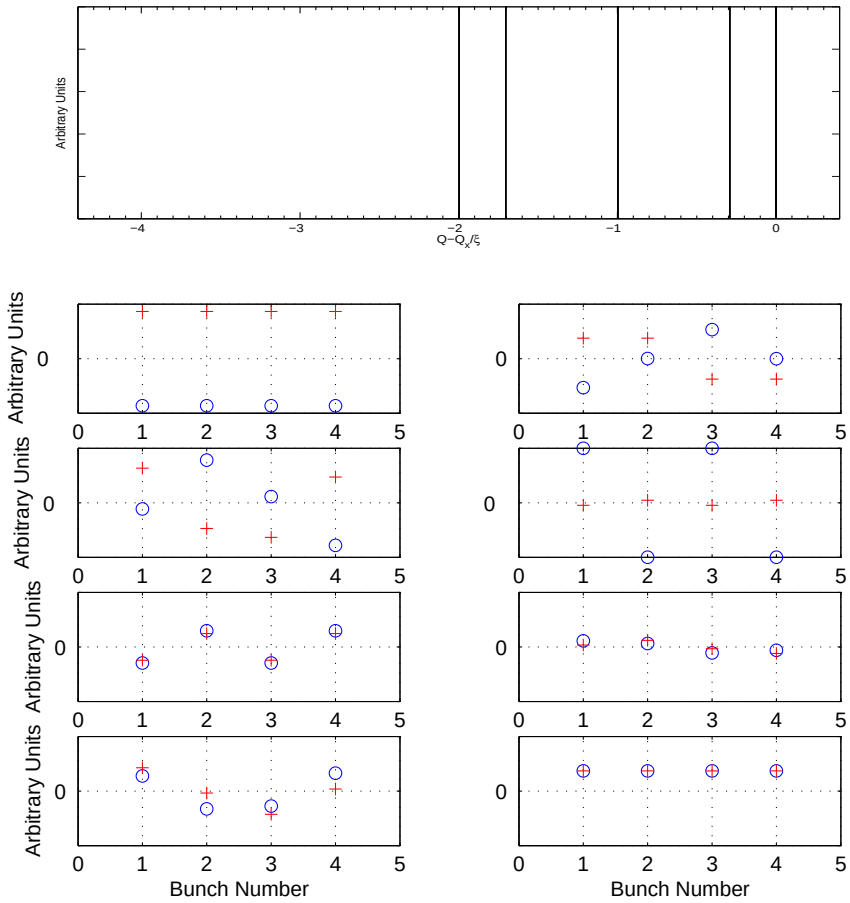

Figure 4.8: Eigenfrequencies (top plot) in units of the beam-beam ξ and eigenvectors (bottom eight subplots) of the system of 4 bunches colliding head-on in IP1 and IP2 obtained with the ALM. The eigenvectors are shown from high shift (top left) to σ mode (right bottom).

eigenmodes are present in each single bunch spectrum. However, the contribution of each bunch to a single eigenmode can be rather different.

4.2.1 Frequency spectra versus eigenmodes

To demonstrate this effect one has to couple the bunches. We show here an example for the case of two trains of 5 bunches and described as:

```
# bunch filling beam 1 #
# Number of groups #
2
 5 1 35 0
```

```
# bunch filling beam 2 #
# Number of groups #
2
  5 1 35 0
```

To couple the bunches together one has to create interactions between different bunches of beam 1 with different bunches of beam 2. This happens in colliders if the collisions are strongly asymmetric. Since head-on collisions are more symmetrically distributed we now introduce the long range interactions as for the LHC case which are on the contrary

assembled around an IP at very short distance (the bunch longitudinal spacing). We start with only 2 interactions on one side of IP1 as the collision scheme below describes:

```
# Collision scheme #
  1  -4    0        +2      0        0
 36   3    63.32    58.31   63.32    58.31
```

In this configuration the bunches of a train can either collide with two or one or none of the bunches of the opposite beam. In Table 4.6 we define the precise coupling of the bunches. We see that all bunches except 2 are all coupled either directly or indirectly. We define a direct coupling when for example bunch 1^{b_1} interacts with 3^{b_2}, they do collide. An indirect coupling is that between bunch 1^{b_1} and for example 2^{b_1} and consequently 4^{b_2} through the collision with 3^{b_2}. In this case we can notice that bunches 1^{b_1}, 2^{b_1}, 3^{b_1}, 4^{b_1},2^{b_2}, 3^{b_2},4^{b_2} and 5^{b_2} are all either directly or indirectly coupled, they cross talk to each other through the two long range interactions.

	1^{b_2}	2^{b_2}	3^{b_2}	4^{b_2}	5^{b_2}
1^{b_1}		○	○		
2^{b_1}			○	○	
3^{b_1}				○	○
4^{b_1}					○
5^{b_1}					

Table 4.6: Schematic of the coupling between bunches due to two long range beam-beam interaction right of IP1. Each bunch couples directly with two or one of the opposite ones.

If we now evaluate the tune spectrum of each bunch of one beam we find that coherent frequencies are the same for 4 of the 5 bunches while for 5^{b_1} and 1^{b_2} the only frequency is the unperturbed since they are not involved at all in the interactions. For the interacting bunches we have the spectra as visible in Figure 4.9 plotted for all 4 bunches (1^{b_1}, 2^{b_1}, 3^{b_1} and 4^{b_1}) from the top to the bottom. Due to the asymmetric collision pattern many coherent modes appear and the bunches show all the same frequencies since these are the result of the direct and indirect coupling of the 8 bunches.

Even if the tune spectra define the same coherent frequencies small bunch to bunch differences are present. The differences are in the amplitude of the peaks. Each peak represents an eigenmode with a defined frequency and pattern of the oscillation. In Figure 4.10 we show the eigenfrequencies (top) and associated eigenvectors (bottom) for this case with two long range interactions and trains of 5 bunches as calculated with the ALM. From the frequency spectrum obtained with the ALM it is not possible to identify bunch to bunch differences. In fact with the ALM all possible eigenfrequencies of the coupled system are evaluated. At each eigenfrequency different bunches contribute differently depending on their collision schedule. This can be seen comparing the eigenvectors of Figure 4.10 bottom with the peaks of Figure 4.9 for a defined frequency.

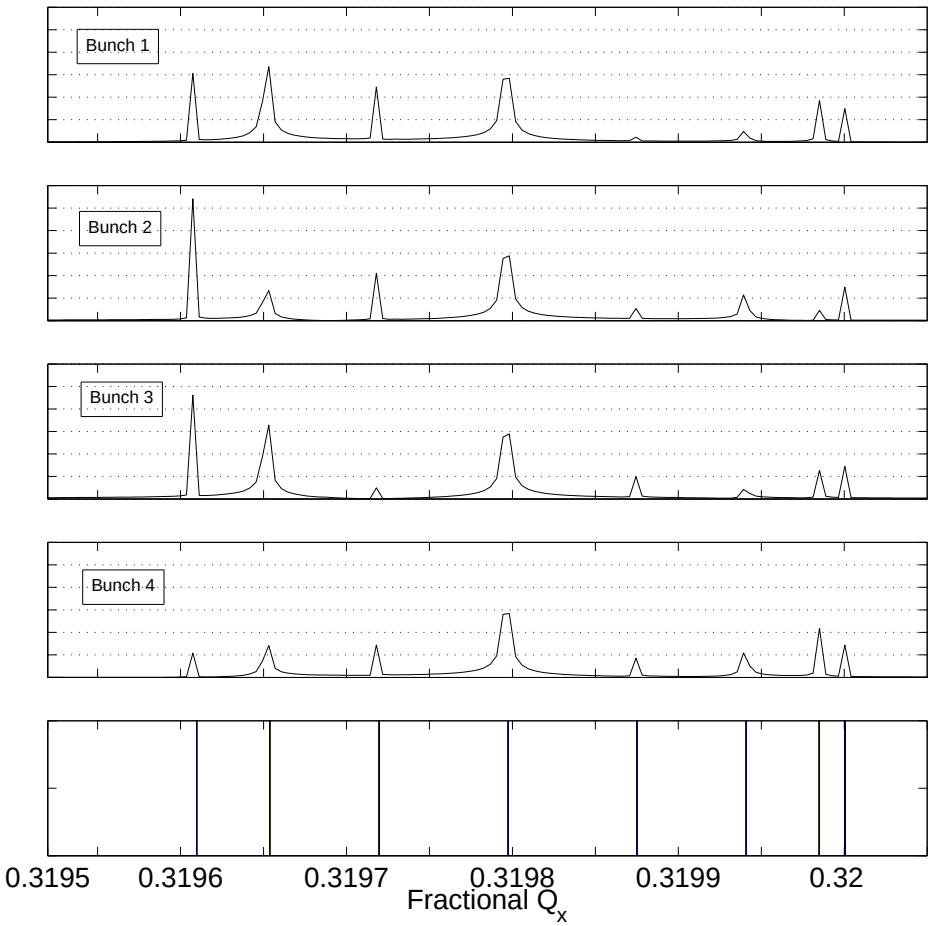

Figure 4.9: Tune spectra for 4 bunches of a train of 5 colliding long range at a distance of 7 σ on the right side of IP1.Results are obtained with the RBM (from top 4 plots). The bottom shows results for the same case with the ALM.

For a defined coherent mode the frequency peak amplitudes of the bunch tune spectra of Figure 4.9 are proportional to the bunch relative phase differences as plotted in Figure 4.10. This occurs for all frequencies. As an example we look at the π-mode at frequency Q_7 in Figure 4.10 and the amplitude of the peaks at frequency Q_7 in Figure 4.9. Bunch 5^{b_1} (bunch 5 blue circle) is not colliding and therefore does not contributes to the mode and is located on the zero axis. Bunch 2^{b_1}(bunch 2 blue circle) is the one most affected and in the tune spectra second plot from the top of Figure 4.9 has the highest peaks amplitude. Relative differences in the peak amplitudes can be predicted from the analysis of the bunch relative phase differences.

We can state that with the ALM eigenvectors associated to the beam-beam coupled system one can predict bunch to bunch differences in the tune spectra produced with the RBM. It is proved for the first time how one can precisely define the bunch to bunch relative contribution to a defined frequency peak by looking at the oscillating pattern proper of

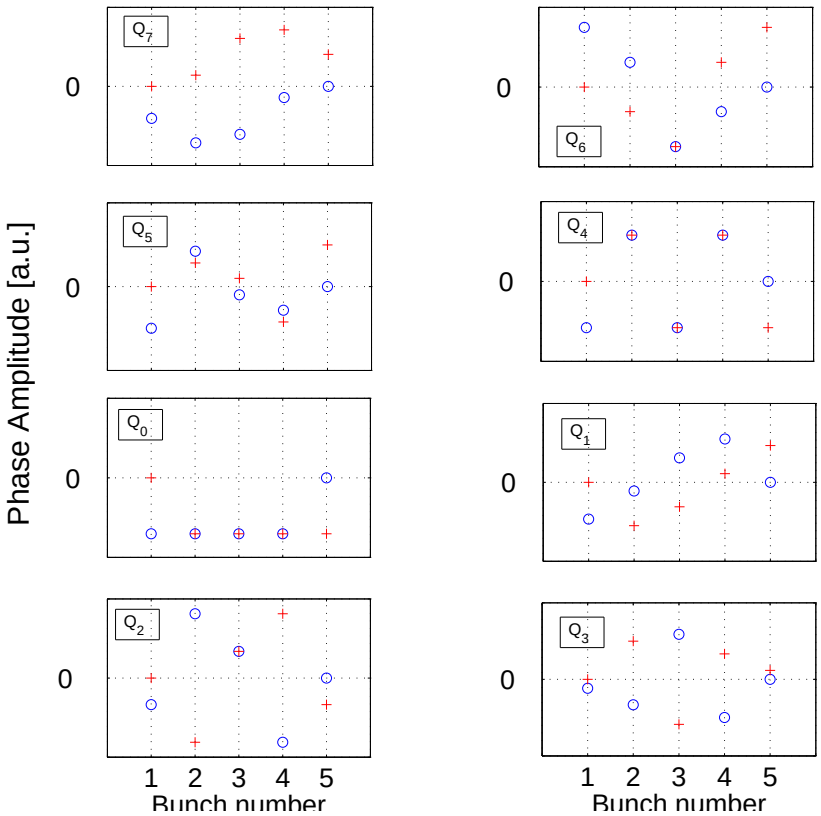

Figure 4.10: Eigenvectors of the system of 2 trains of 5 bunches each colliding at a distance (7 σ) on the right side of IP1. These results are obtained with the ALM and each subplot represents the eigenvector associated to the corresponding eigenfrequency of Figure 4.9.

that frequency. This in principle is what normally bunch to bunch feedback systems do by measuring the bunch different response to an excitation and then applying the correction taking care of the relative variation. This now, can be quantified by comparing the analytical derivation of the eigenvectors with the Monte Carlo approach used in the RBM. In a further section it will be shown that this applies also to the MPM. One can then also think of modulating the feedback to the bunch oscillating pattern found with this method in order to properly weight the effect of the correction to the actual bunch contribution to the effect. As will be demonstrated in the last chapter an external excitation can excite coherent oscillations in origin damped by Landau damping mechanism. One can here think of going in the opposite direction by damping coherent oscillations by acting against the coherent oscillating patter the bunches follow for each frequency, specially those outside the incoherent spectrum. However, further studies should be done on this subject to prove the feasibility of the principle.

4.2.2 Mode degeneracy due to symmetry

In this section we want to highlight the importance of symmetric collision schemes on the appearance of intermediate modes. For the head-on collisions we have shown how by breaking the symmetry between the collision points more coherent frequencies develop.

Here we will proceed the other way by moving from a strongly non symmetric case to a restored symmetry for the case of long range interaction for the LHC.
We assume trains made of 10 bunches each as described below:

```
# bunch filling beam 1 #        # bunch filling beam 2 #
# Number of groups #            # Number of groups #
2                               2
 10 1 30 0                         10 1 30 0
```

The bunches interact only through long range collisions before and after IP1. The number of parasitic encounters N is changed while the plane of separation is the horizontal one. The collision scheme is then given by:

```
# Collision scheme #
  1   4    -N        +N      0        0
 40   3    63.32    58.31   63.32    58.31
```

We have performed calculations using the RBM and the MPM varying the number of long range interactions, N from 1 to 10. In Figure 4.11 we show the tune spectra obtained for three bunches of beam 1 train. Precisely we have the head of the train (bunch 1, blue lines), a central one (bunch 5, green lines) and the tail of the train (bunch 10, red lines). The different plots refer to a different number of long range interaction N for the specific case as indicated (N=1, 3, 6 and 9).
From the plots of Figure 4.11 we should notice that different bunches show different tune spectra due to the different number of interactions (for $N = 1$ bunch 10, red line, have less peaks). Increasing the number of interactions we increase the coupling between the bunches since more bunches interact at multiple locations and the tune shift increases with the maximum number of collisions (for $N = 3$ $\Delta Q_{max} = 6 \cdot \xi_{LR}$). If one keeps increasing the number of collisions many modes degenerate since the head and tail bunches of the train start having similar collision schedules. Central bunches are those which interact more often compared to the head and tail of the train. However, the many interactions (direct and indirect coupling) couples them to all the others. Due to this we see that all bunches have the same maximum tune shift (for $N = 3$ $\Delta Q_{max} = 9 \cdot \xi_{LR}$). However, the central one (bunch 5, green line) spectrum have a more pronounced peak with respect to the head (bunch 1, blue line) and tail (bunch 10, red line). By increasing again the number of interactions, $N = 9$ almost all bunches will see all bunches of the opposite beams therefore a symmetric situations is reestablished and the number of peaks are visibly reduced (for $N = 9$ only four peaks are visible and bunches show similar spectra).

The same case had been studied with the MPM (Figure 4.12) and results are comparable with those from the RBM of Figure 4.11. The same considerations apply for the multi particle case. However, one should notice that modes due to long range are not always damped due to the Landau mechanisms. In Figure 4.12 almost all coherent modes foreseen with the RBM are present.

4.2.3 Landau damping and long range interactions

In Figure 4.12 we should also notice another important aspect of coherent modes produced by long range beam-beam interactions. For the head-on collisions Landau damping

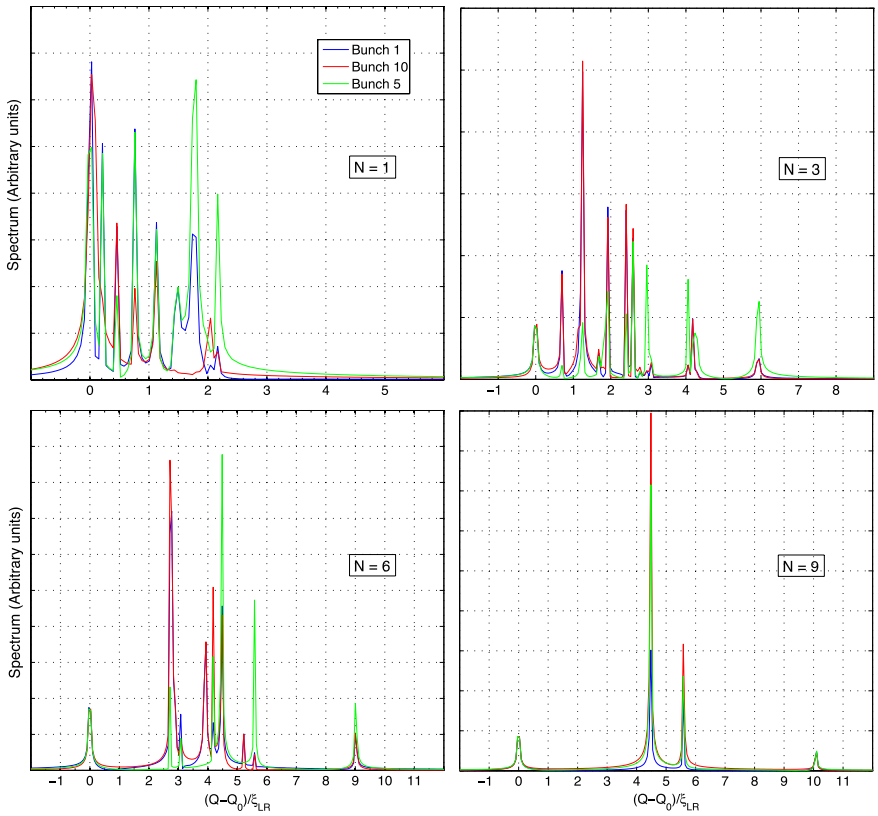

Figure 4.11: Tune spectra of the $1'$ (blue lines), $5'$ (green lines) and $10'$ (red lines) bunch of the train of 10 of beam 1 (clock wise beam) obtained with the RBM for different number of long range interactions as indicated in the plots by the number N.

represents an important mechanism which suppresses most of the collective oscillations. This is not the case for the long range interactions. As visible comparing Figure 4.11 and Figure 4.12 coherent modes from long range interactions are not damped. This effect can be understood thinking to the physical picture behind the coherent oscillations for the two different cases of short and large distances collisions in fact as known different part of the bunches participate in the two coherent oscillation. For the head-on coherent oscillations it is the core of the bunches which collectively organizes their motion while for the long range are the tails who contribute [49].
We know that Landau damping occurs when around a coherent mode there are a sufficient large number of oscillators (single particles) with frequencies close to the coherent one. This happens for the head-on collisions where the core of the bunches collide and due to the detuning with amplitude of the particles with the non-linear beam-beam force our single particle oscillators have oscillating frequencies which go from the unperturbed betatron frequency down to the $N \cdot \xi$ maximum frequency shift, where N is the number of head-on interactions. All the particles of the core of the bunch are shifted to smaller tunes and therefore intermediate modes do have a relevant number of single oscillators around their proper frequency which therefore is damped. Each single oscillator subtracts energy from the collective motion at that frequency and therefore the coherent mode does not appear. This is not the case with long range interactions to which only the tail particles participate. The tail population of particles is very small and therefore there are

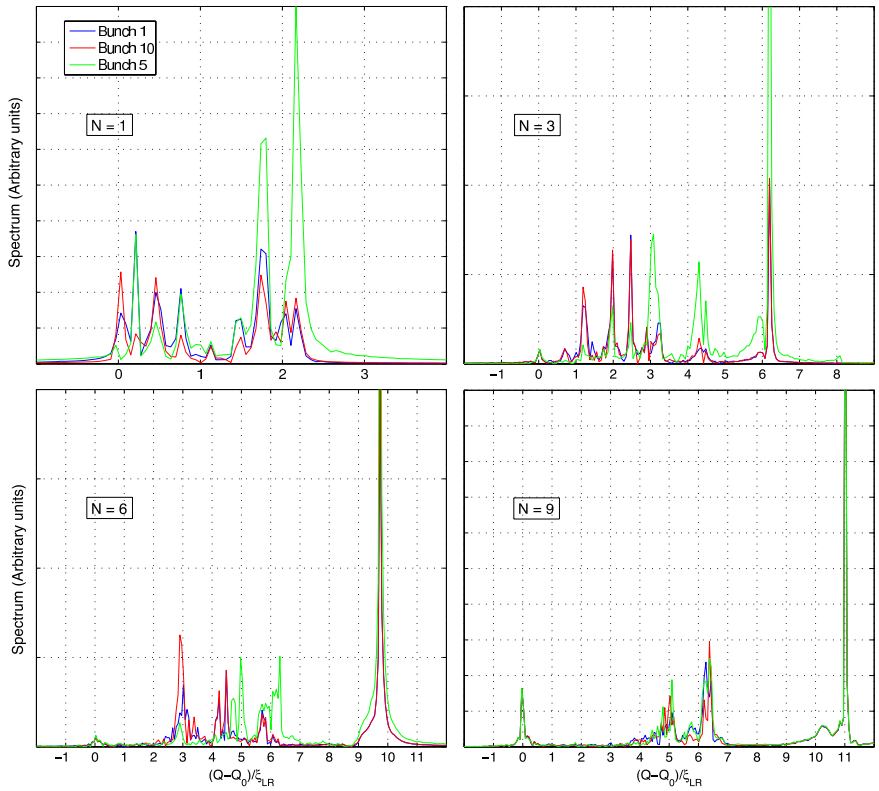

Figure 4.12: Tune spectra of the $1'$ (blue lines), $5'$ (green lines) and $10'$ (red lines) bunch of the train of 10 of beam 1 (clock wise beam) obtained with the MPM for different number of long range interactions as indicated in the plots by the number N.

not enough single oscillators which can extract energy from the coherent mode and no Landau mechanism occurs. This is visible in Figure 4.12 where we can see that also with a multi particle model the coherent modes due to long range interactions are not damped (multi peaks in the various subplots). The spectra are not different from those obtained with the RBM shown in Figure 4.11.

4.3 Head-on and long range multiple interactions

The main goal of these studies is a better understanding of the bunch to bunch differences expected during the accelerator operation. Depending on the coupling, i.e. collisions, bunches of a train show different spectra. Some modes present for one bunch are suppressed or less pronounced for others as demonstrated in the previous sections for the head-on and long range interactions separately. Here, we want to put all together the interactions to get closer to a realistic operational scenario.

To have important bunch to bunch differences we have to create the so called Pacman bunches and this is possible by constructing the beam in such a way to have bunches colliding differently. We assume for this case filling schemes as the followings:

```
# bunch filling beam 1 #          # bunch filling beam 2 #
```

```
# Number of groups #
2
 5 1 35 0
```

```
# Number of groups #
2
  5 1 35 0
```

While the bunches interact head-on at IP1 and long range on the right side of the IP with a horizontal crossing plane as follows:

```
# Collision scheme #
  1   2    0        +1      0        0
 40   3    63.32    58.31   63.32    58.31
```

For this setting of the beams and collision scheme we observe single bunch spectra obtained with the MPM. The Figures 4.13 and 4.14 show the tune spectra obtained with the MPM "observing" only the first and third bunches of a train of five.

Due to the long-range interactions all bunches are coupled and as a result the σ and π modes are split into sidebands. This coupling leads to a breaking of symmetries. Therefore no mode degeneracies are visible, i.e. each eigenmode is defined by one frequency and the corresponding oscillating pattern.

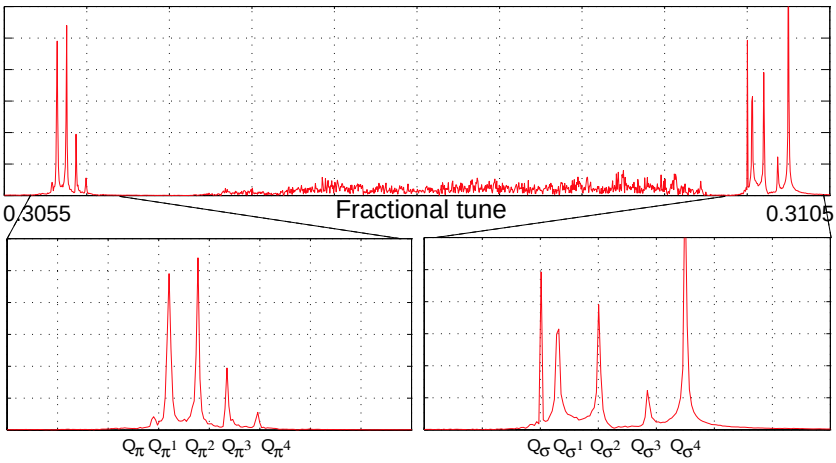

Figure 4.13: Top: MPM tune spectrum of the first bunch of a train of five undergoing head-on and long-range collision. Bottom: zoom of the sidebands around the π and σ-modes.

The spectrum of the first bunch in the train (Figure 4.13) shows ten frequencies as obtained with the ALM (Figure 4.15 top). Bunch number three shows only seven (Figure 4.14). Bunches contribute differently to the different modes.
Looking at the eigenvectors in Figure 4.15, the ones corresponding to the missing and/or smaller amplitude frequencies of Figure 4.14, (Q_{π^1}, Q_{π^3},Q_{σ^1} and Q_{σ^3}), show that bunch three remains at zero level and is not contributing to the related coherent mode. The oscillating pattern of mode Q_{π^4} shows that bunch one of the train is less contributing with respect to bunch three therefore the differences in amplitude in Figures 4.13 and 4.14.

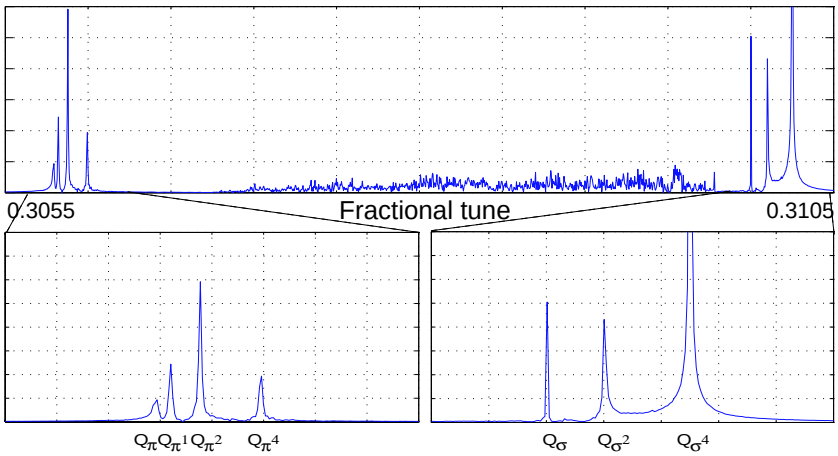

Figure 4.14: Top: MPM tune spectrum of the third bunch of a train of five undergoing head-on and long-range collision. Bottom: zoom of the sidebands around the π and σ-modes.

The analysis of the eigenfrequencies and especially of the eigenmodes obtained from this model allows to understand the oscillation pattern of multi bunch modes for different eigenfrequencies. Moreover, using this model it is possible to predict the different responses of individual bunches to measurements. This enables us to correctly interpret the observations from single bunch measurements. For any beam filling scheme and collision pattern it is possible to identify all the eigenfrequencies associated with the coherent beam-beam modes. The corresponding eigenvectors allow to associate oscillating patterns to eigenfrequency. The ALM is consistent and complements results from RBM and MPM. The eigenvector analysis is a further step in explaining bunch to bunch differences due to coherent BBIs and can be used to correctly interpret measurements from single bunch diagnostics.

4.4 Breaking of coherent motion

Due to the beam-beam interaction particles of the beams organize their motion and coherent oscillations take place during collision. This coherent behaviour of the bunches in a beam can lead to limitations to the machine performances since the system of bunches colliding is a coupled system and actions of one bunch are transmitted to all the rest. The coherent motion moreover is not always damped by Landau mechanisms mainly when the frequencies of the collective oscillations are outside the continuum incoherent spectrum. Therefore, one should always try to avoid or suppress collective motion by breaking the organized dynamics of particles. Since coherent behaviours develop mainly when a high degree of symmetry is present between the two beams (same betatron frequencies, same intensities, same sizes) one can reduce these effects by breaking this symmetry.

As already listened in the previous chapters coherent motion can be destroyed by reducing the symmetry between the beams. The usual methods proposed by [10, 40, 79, 83] are:

- Different bunch intensities.
- Different tunes in the two beams.

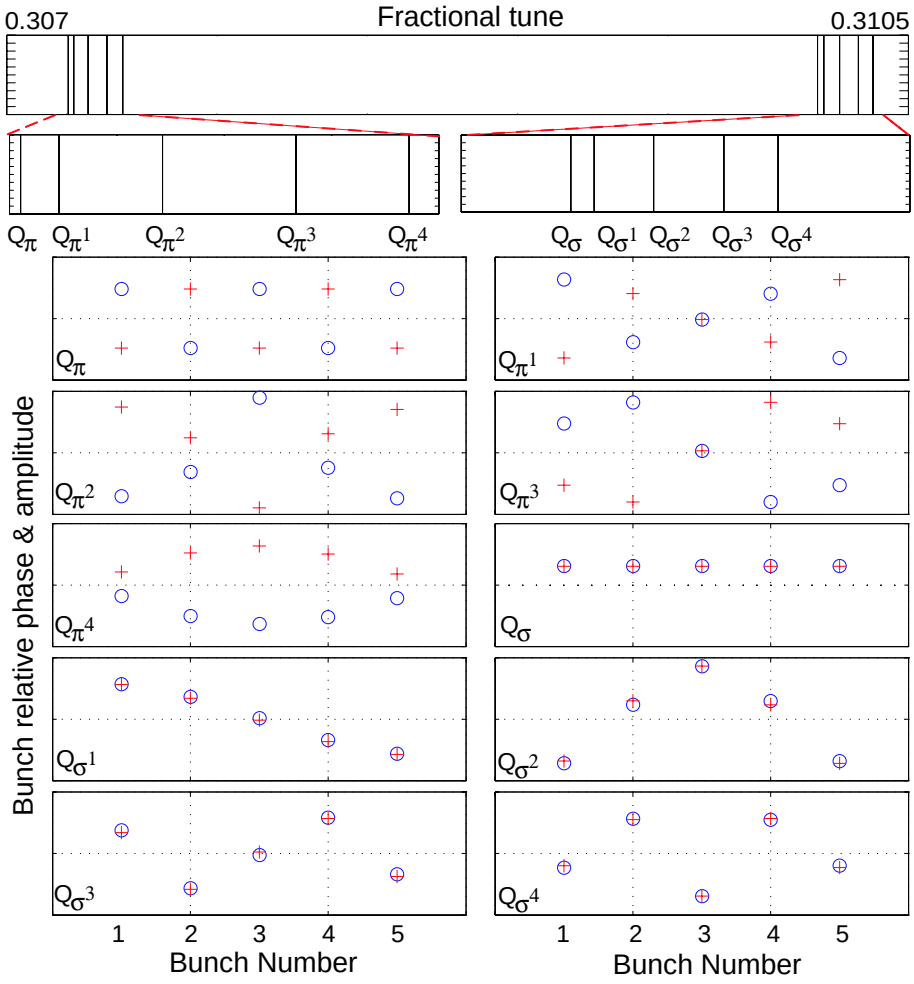

Figure 4.15: Eigenfrequencies and eigenvectors of bunch trains undergoing head-on and parasitic collision.

- Unequal distribution of interaction points.
- Phase differences between interaction points.
- Synchrotron motion.

In this section we will highlight the effects of different bunch betatron frequencies and intensities. The effects of unequal distribution of the interaction points had been discussed in the first part of this chapter while the differences in phase advance between the IPs will be over viewed in detail in the next chapter for the LHC particular case. The effects of the longitudinal synchrotron motion on the coherent modes is a particular feature of hadron colliders that can be very efficient to damp coherent beam-beam modes as suggested in [10, 38]. In hadron colliders it is a coincidence, that the absolute value of the beam-beam parameter and the magnitude of the synchrotron tune are of the same order of magnitude (LHC: $\xi = 0.0033$, $Q_s = 0.0021$). When the transverse and longitudinal motions are coupled, this leads to so-called synchro-betatron coupling, and the appearance of incoherent synchrotron sidebands, separated by $m \cdot Q_s$ from the tune Q_0. This can lead

to a situation where an incoherent **synchrotron** sideband overlaps with the position of the coherent π-mode. The result of this overlap is Landau damping. This effect was clearly demonstrated by multi-particle simulation in [83].

4.4.1 Unequal tunes

The first way to break the symmetry between the two beams is to operate them with different betatron frequencies, *i.e.* different tunes [79]. When the tune difference is large enough, the two beams are decoupled and cannot perform a coherent oscillation [79, 80]. This is visible in Figure 4.16 where the tune spectra for the case of two bunches colliding head-on is shown in the case of equal tunes for the two beams (top spectrum), and when a difference of tune of 0.3, 1 and 2.85 ξ is applied. It is visible how coherent modes disappear as soon as the difference in tune become larger.

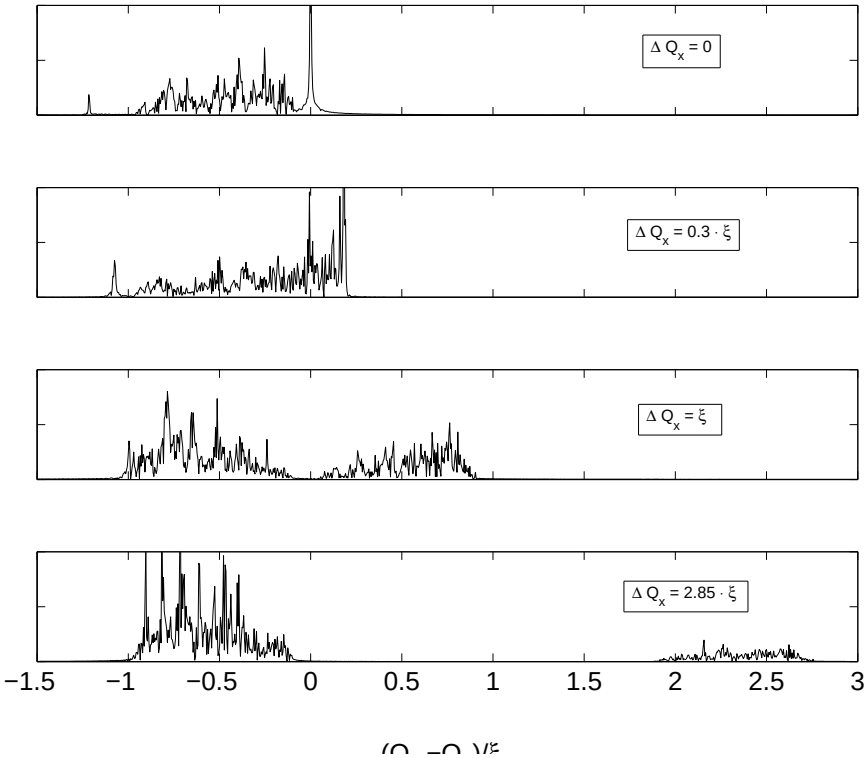

Figure 4.16: Tune spectra in units of ξ due to one head-on interaction when the two beams have different tunes. The different lines are the spectra for different unperturbed tune differences ΔQ. The plots are obtained with the MPM.

The same cases had been reproduced with the RBM and results are shown in Figure 4.17 where the tune spectra are plotted for the case of equal betatron frequencies for the two beams (black line and $\Delta Q = 0$) and for the case where the betatron frequency for the two beams are different (red line is for a difference $\Delta Q = \xi$ while blue and magenta are for larger differences). Results from the RBM and MPM agree in within their approxi-

mations.

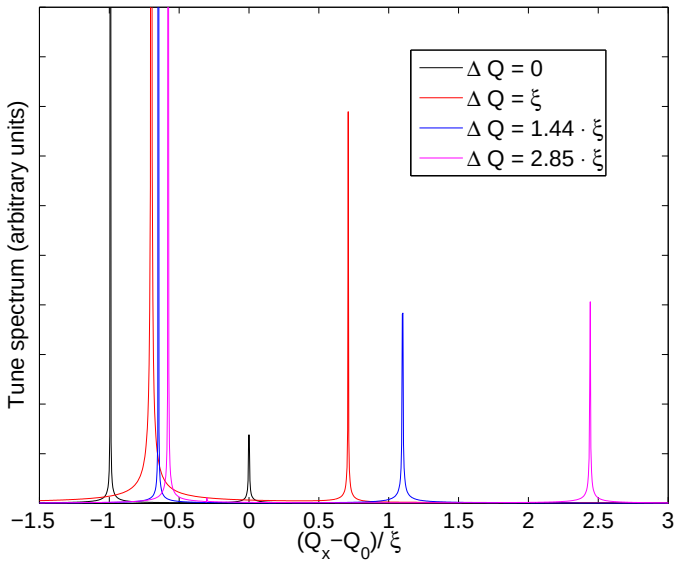

Figure 4.17: Tune spectra in units of ξ due to one head-on interaction when the two beams have different tunes. The different lines are the spectra for different unperturbed tune differences ΔQ. The plots are obtained with the RBM.

Both MPM and RBM calculations reproduce the case of one beam with constant fractional horizontal betatron frequency of 0.31 while the fractional tune of the other beam is slowly changed. The spectrum of the first beam is then determined from its motion and shown in Figure 4.16. In Figure 4.16 (top) the tunes are equal for both beams and therefore coherent modes develop as known (σ and π modes are visible at 0 and $-Y \cdot \xi$). When a difference is introduced between the two beams a suppression of coherent motion starts acting and the effectiveness is proportional to the ΔQ introduced for the two beam tunes. When $\Delta Q = 0.3 \cdot \xi$ the π-mode is still visible as shown in Figure 4.16 (second plot from top). When the tune difference ΔQ between the two beams is increased to ξ (Figure 4.16, second from top), the coherent modes are suppressed and only the two separate incoherent spectra of the two beams are left as predicted in [54, 79]. The same happens increasing further the differences between the tune as confirmed in Figure 4.16 (bottom) where $\Delta Q = 2.8 \cdot \xi$.
We have compared results of RBM and MPM with the analytical findings of [95]. We considered two beams with one bunch each colliding head on in one interaction point. Both bunches have the same distribution with the same RMS dimensions and beam-beam force at the interaction point but with possibly different unperturbed tunes Q_1 and Q_2. As carried out in detail in [79], if the unperturbed tunes are not equal one finds two frequencies corresponding to modes with tunes Q_a and Q_b. The analytical solutions are given for rigid bunches in Figure 4.18, black lines, where we also show the results obtained with RBM (blue dots), as well as for the MPM (red dots). The analytical solutions were extracted, in our case, by solving the equation of motion keeping the tune of beam 1 Q_1 constant while changing Q_2 for beam 2. The analytical solutions give $Q_a \to Q_\sigma$ and $Q_b \to Q_\pi$ with a spacing $Q_a - Q_b$ equal to ξ for $Q_1 - Q_2 \to 0$. As the tune difference

increases the two tunes Q_a and Q_b of the two modes get associated with the two beams respectively and reach the values $Q_a = Q_1 + \xi/2$ and $Q_b = Q_2 + \xi/2$. Qualitatively this means that for large differences in the two unperturbed tunes the beams are decoupled and only the one for which the exciting frequency is close to its tune oscillates significantly. The other beam hardly moves but represents a focusing element for the first one resulting in a tune change of about $\xi/2$.

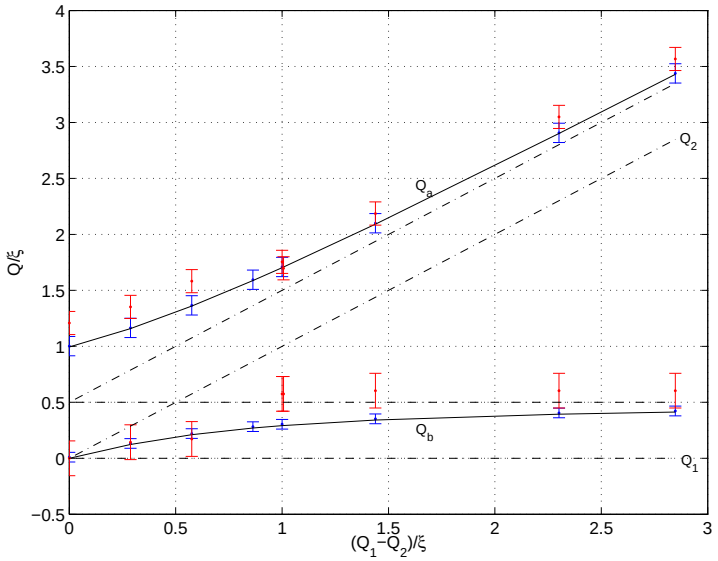

Figure 4.18: Beam-beam coherent mode frequencies versus the tune separation $Q_1 - Q_2$ obtained with Rigid Bunch Model (blue dots) and with the Multi Particle Model (red dots) compared to analytical solutions from [79] (black line).

4.4.2 Different intensities

A quantitative prediction was made in [10, 38] when the strong-strong condition is fulfilled. To lock the two beams into a common motion, the mutual forces on each other (and therefore the tune shift) should be as equal as possible. Different bunch intensities break this condition and it was found in [10, 38] that the intensity ratio between the weaker and the stronger beam must not be less than 0.60.

In Figure 4.19 we show tune spectra obtained with the MPM for the cases of two bunches colliding head-on at one IP when the intensity of one of the bunches is changed. Each line in Figure 4.19 represents the tune spectrum for a defined difference in the intensity of the second bunch as summarized in the legend. For a ratio of 0.65 the π-mode is visible as a peak, however the shift away from the 0-mode is smaller than for equal intensities. As predicted by [10, 38], with a decreasing ratio the frequency of the π-mode moves closer and closer towards the incoherent spectrum until it merges exactly at the predicted ratio. In this case Landau damping is restored and the π-mode has disappeared and only the 0-mode and the incoherent spectrum are visible. Intensity fluctuations cannot

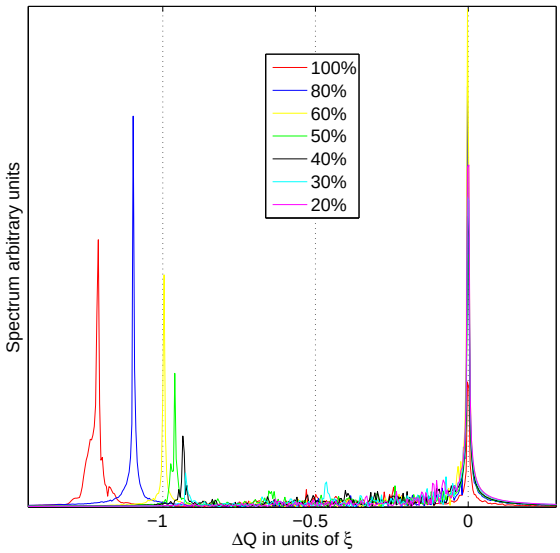

Figure 4.19: Horizontal tune spectra of two bunches colliding for different intensities of one of the two bunches. The intensity is reduced 100% to 20% to show the suppression of the coherent motion.

be avoided in a normal collider. In the LHC bunch to bunch fluctuations in intensity of the order of 10% are expected due to the injector chain. These bunch to bunch intensity differences makes difficult the collective organization of particle motion and consequently the development of coherent modes. As a result modes outside the incoherent continuum can be brought closer to the Landau damping region and eventually be suppressed.

Chapter 5

The Large Hadron Collider tune spectra

The LHC is a proton-proton collider with an unprecedented number of bunches per beam. The large number is a consequence for the need of a large luminosity. This very large number of bunches has strong implications for the machine, i.e. the beam dynamics, as well as for the operation of the experiments.

With the available simulation program, several effects can be studied and the dependence of the results on the optical and collision configuration can be evaluated. In this chapter we treated principally the following aspects:

- Multiple head-on collisions versus modes damping and/or suppression.
- Multiple head-on collisions for different LHC collision layout symmetries.
- Multiple head-on collisions and long range interactions for different LHC collision layout symmetries.
- Multiple head-on collisions and long range interactions for different crossing planes at collision.
- Evidences of Pacman and Super-pacman bunches.

The beam parameters used for this study are those of a nominal LHC beam and are summarized in Table 5.1

For the collision scheme head-on collisions are allowed at the four experimental points IP1, IP2, IP5 and IP8 at equal intensity. The long range interactions are placed left and right of each IP. The number of parasitic encounters varies depending on the configuration. The typical separation between the two beams is between 7 and 10 in units of the beam size of the opposing beam as shown for the case of an external crossing angle of approximately 300 μrad in Figure [**?**]. However, for a better understanding of the tune spectral lines we will enhance the effects of beam-beam allowing separations at 4 σ. To have a clear picture of which parameters are changed in the collision scheme for the simulations we propose Figure 5.1 which shows the LHC layout.

Parameters	Values
Bunch Intensity	$1.15 \cdot 10^{11}$
Bunch horizontal RMS	16 μm
Bunch vertical RMS	16 μm
Bunch x' RMS	30 μrad
Bunch y' RMS	30 μrad
Number of macro-particles	10^4
Number of turns	65000
Linear beam-beam parameter ξ	$\approx$0.0035
IPs β^*	0.55 m
Machine horizontal tune Q_x	63.31
Machine vertical tune Q_y	58.32

Table 5.1: Summary table of LHC parameters used for simulations

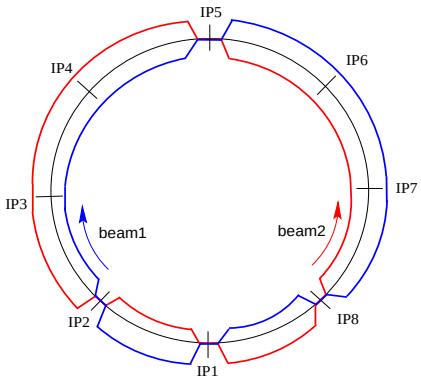

Figure 5.1: Schematic layout of the LHC collision points and beams.

5.1 Multiple head-on interactions versus collision symmetries

In the case of multiple head-on collisions in a machine, the symmetry and periodicity properties of the layout are very important for the spectra. A high degree of symmetry can lead to the degeneracy of modes, i.e. identical frequencies, and their suppression in the spectra while asymmetric collisions lead to multi peak spectra. This is demonstrated in [52] for rigid bunches and is here reproduced using the multi particle COMBI. Now the main goal is to understand qualitatively how this multi-peak spectra change due to Landau damping. One expects a suppression of intermediate modes which lay inside the incoherent continuum. However, extra modes can be suppressed by choosing higher degrees of symmetries in the collision scheme.
In Figure 5.2 we show the horizontal coherent tune spectra obtained with the rigid bunch model (red lines) and with the multi particle (blue lines) for four bunches per beam undergoing four head-on collisions with two different IP schemes. The abscissa shows the tune shift normalized to the linear beam beam parameter ξ. For the RBM results the tune shift is also normalized with respect to the π mode shift obtained from the multi particle simulations that is bigger in amplitude as known from [11]. The left picture of Figure 5.2 shows the tune spectrum when the collisions are asymmetric in IPs 1, 2, 3 and

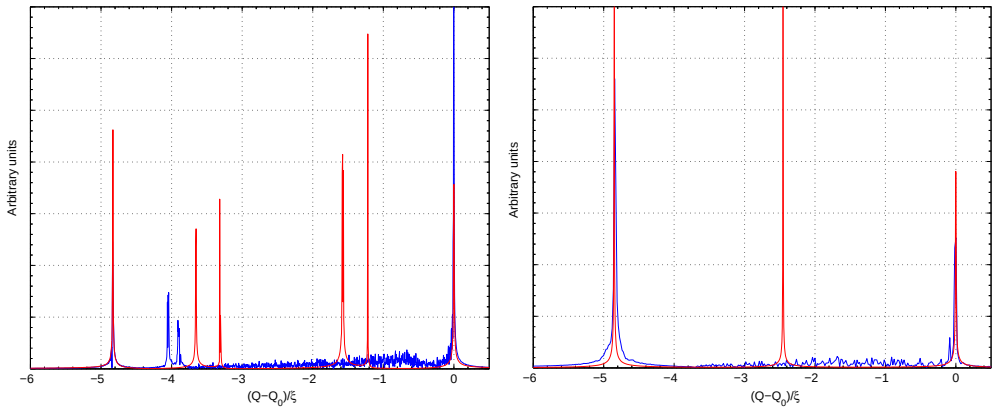

Figure 5.2: Tune spectra of 4 bunch beams undergoing 4 head on collisions in different IPs. Four non symmetric collisions in IP1, IP2, IP3 and IP7 (left). Symmetric head on collisions in IP1, IP3, IP5 and IP7 (right). Red lines refer to the RBM results while blue lines to the MPM results.

7 while the right picture is for symmetric collision in IPs 1, 3, 5 and 7. We see from the spectra that Landau damping suppresses several coherent modes (red lines in between 0 and about -4ξ) that lay inside the incoherent continuum (blue line in between 0 and about -4ξ). In the left picture of Figure 5.2 almost three modes are damped while in the right only one. However, also from the multi particle results one can say that a higher degree of symmetry leads to cleaner spectra. The symmetric collision scheme (right picture in Figure 5.2) results in a spectrum with only two coherent modes one at the unperturbed tune and the π mode at approximately $-4Y\xi$. The non symmetric collision scheme gives more coherent modes which lay outside the incoherent spectrum and so are still present; we then find the unperturbed tune and two modes one at almost $-4Y\xi$ and another one in the range $[-4Y\xi, -4\xi]$. This confirms earlier findings for rigid bunches [41, 42, 50, 51] and the importance of symmetries for coherent modes.

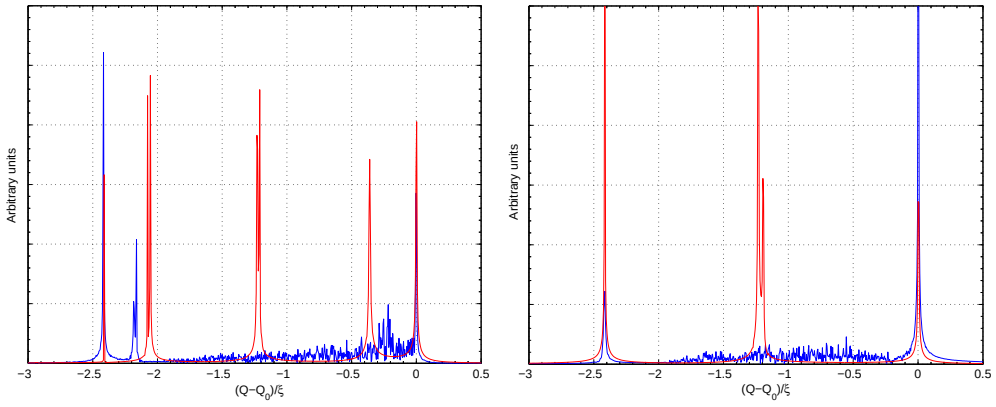

Figure 5.3: Tune spectra of four bunch beam undergoing 2 head on collisions in different IPs. Collisions in IPs 1 and 2 (left) and IP1 and IP3 (right). Red lines refer to the RBM results while blue lines to the MPM results.

In Figure 5.3 two configurations with two head-on collisions at different degrees of symmetry are explored. Also in Figure 5.3 the abscissa shows the tune shift normalized

to the linear beam-beam parameter ξ and the rigid model (red lines) tune shift is also normalized with respect to the π mode shift obtained from the multi particle simulations. The left picture of Figure 5.3 shows the tune spectrum when the collisions are asymmetric in IP1 and IP2 while the right picture is for symmetric collision in IP1 and IP3 (red lines refer to the RBM results while blue lines to the MPM). We see from the spectra that Landau damping suppress several the intermediate coherent modes (red lines in between 0 and about -2ξ) because they lay inside the incoherent continuum (blue line in between 0 and about -2ξ). In the left picture of Figure 5.3 two modes are damped while in the right only one. The symmetric collision scheme (right picture) results in a spectra with only two coherent modes one at the unperturbed tune and the π mode at approximately $-2Y\xi$. The non symmetric collision scheme leads to an extra peak in the range $[-2Y\xi, -2\xi]$.

5.2 Multiple BBIs with the LHC interaction region layout

The collision scheme of the LHC with its four interaction regions was illustrated as an example already. Although the geometry has an eightfold symmetry, the phase advances between the interaction points break this symmetry and we expect a richer spectrum of modes.

5.2.1 LHC interaction region layout with standard phase advance

For the tracking studies we simplified the standard LHC collision scheme as for [52]: the arcs are compressed since no action can happen except a single linear transfer, the number of bunches is reduced to 9 per train. No long range interactions are simulated but only the four head collisions at IP1, IP2, IP5 and IP8. The nominal collision definition scheme used in the simulation is then:

```
  1   2   -0  +0
 41   3    8.046   6.940   8.046   6.940
 81  -2   -0  +0
202   3   23.015  21.821  23.015  21.821
321  -2   -0  +0
441   3   23.533  20.689  23.533  20.689
561   2   -0  +0
601   3    7.716   7.870   7.716   7.870
```

together with a filling scheme equal for both beams :

```
# bunch filling beam 1 #          # bunch filling beam 1 #
# Number of groups #              # Number of groups #
2                                 2
 9 1 71 0                         9 1 71 0
 9 1 71 0                         9 1 71 0
 9 1 71 0                         9 1 71 0
 9 1 71 0                         9 1 71 0
```

In Figure 5.4 one sees the simulation results from the rigid bunch model (red lines) as

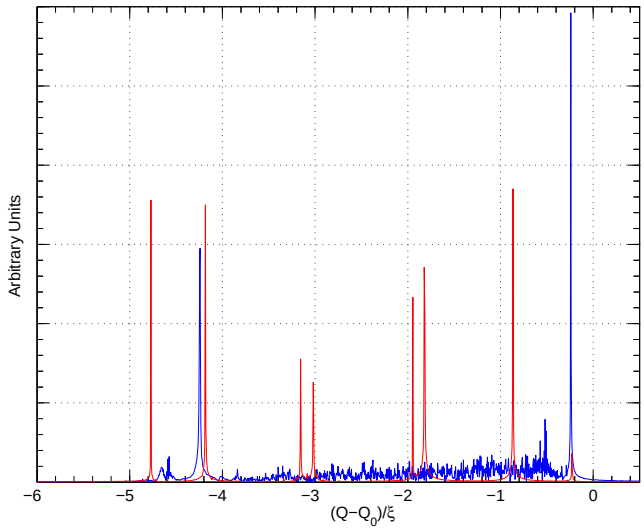

Figure 5.4: Head-on collisions in IP1, IP2, IP5 and IP8 with nominal LHC phase advance between interaction points. Red lines refer to the RBM results while blue lines are results from the MPM.

well as from the multi particle model (blue line). The tune spectra presents several modes in between 0 and -5ξ in the rigid bunch approximation while these modes are completely suppressed by the Landau damping in the multi particle results. All modes inside the incoherent continuum are damped and only two modes are clearly visible.

5.2.2 Phase advance symmetry between IP1 and IP5

The phase advance between the IPs is not symmetric, resulting in a more complex spectrum than in Figure 5.3. To study and to qualitatively understand the effects of symmetries on the spectra we started from the scheme above and by restoring the symmetries in specific sectors of the machine. The first step was to partially symmetrize the original LHC scheme to fulfill:

$$\Delta Q_x^{1\to 5} \quad = \quad \Delta Q_x^{5\to 1} \quad = \quad Q_x/2 \tag{5.1}$$

and we use:

```
  1  -2   -0  +0
 41   3   8.046   6.940   8.046   6.940
 81  -2   -0   +0
201   3  23.109  21.720  23.109  21.720
321   2   -0  +0
441   3  23.439  20.790  23.439  20.790
561   2   -0   +0
601   3   7.716   7.870   7.716   7.870
```

The spectra for such a scheme are shown in Figure 5.5 for the RBM (red line) and

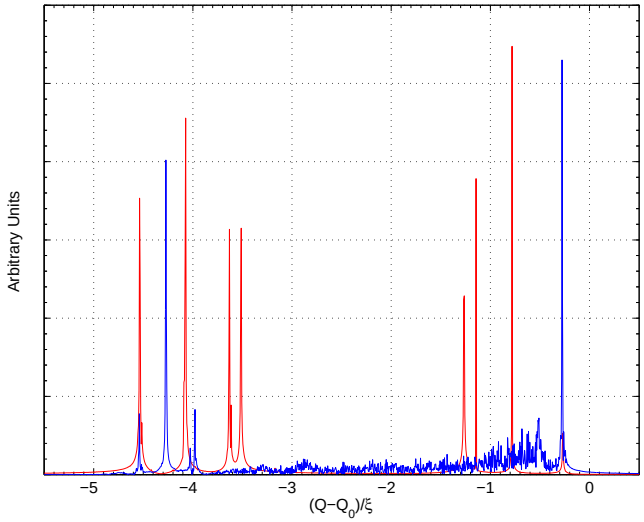

Figure 5.5: Head-on collisions in IP1, IP2, IP5 and IP8. Phase advance symmetry is restored between IP1 and IP5. Red lines refer to the RBM results while blue lines are results from the MPM.

the MPM (blue line). The comparison between Figure 5.4 and Figure 5.5 shows the effect of the symmetry between interaction points 1 and 5. The number of modes is not really changed but the intermediate modes move a part closer to the extreme σ and π modes. As expected for modes in the vicinity of the unperturbed betatron tune (corresponding to the zero in the abscissa) Landau damping is effective and allows cleaner spectra and therefore simplifies the tune measurements. For modes approaching the π-mode the damping mechanism does not apply since they excite the range of incoherent frequencies. As a result, three coherent modes develop at frequencies below $-4 \cdot \xi$.

Till here we have analyzed the effects of the phase advance symmetry on the tune spectra of the LHC beams undergoing only head-on collisions. In this section we will show the effects coming from few long range interactions located left and right of each IP. For the long range interactions we will use the LHC defined plane of separation at the different IPs. In all the simulations the long range interactions are defined for a distance of 4 σ to enhance the effects. On top of the richer spectrum of modes due to the symmetry

breaking of the phase advances into the accelerator arcs side bands are expected around the main head-on spectral lines. Moreover, we will also be able to show pacman effects as well as Superpacman bunch spectra. We again assume the nominal collision definition scheme defined above at which we add two long range beam-beam interactions on each side of the four interaction points. The beam filling schemes are as in the case of only head-on interactions.

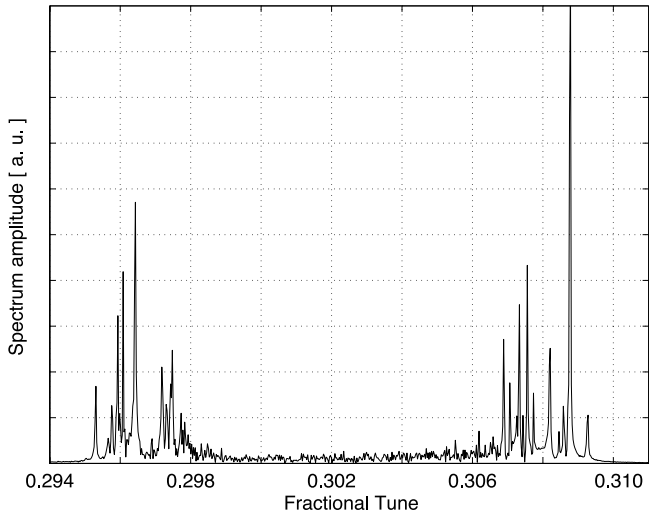

Figure 5.6: Horizontal tune spectrum of bunch number 1 of beam 1 undergoing head-on collisions in IP1, IP2, IP5 and IP8 and 2 long range interactions left and right of each IP. Phase advance symmetry is restored between IP1 and IP5. Results are obtained with the MPM.

Figure 5.6 shows the horizontal tune spectrum obtained with the MPM for the first bunch of the train of 9. Due to the parasitic encounters the tune spectrum becomes even more complicated than the case with only head-on collisions. Comparing Figure 5.5 (blue line) and Figure 5.6 we notice that the number of modes increases and they appear as side bands to the main head-on coherent frequencies. Landau damping suppresses all intermediate modes inside the incoherent tune spread. However, does not cure those modes in the π-mode region outside the continuum, as already seen in many other cases. An interesting finding is that coherent modes coming from long range interactions in the neighborhood of the σ-mode are not completely Landau damped. A lack of damping in this region allows collective oscillations to develop.
In Figure 5.7 we show the horizontal tune spectrum for a bunch in the center of the train. This bunch undergoes all 4 long range interactions around the IPs while the bunch at the head of the bunch train (Figure 5.6) only two on one side of each IP. The amplitude of the additional long range modes change with respect to those of the bunch at the head of the train. However, the coupling between many bunches shows them all, and due to the non symmetric phase advance the degeneracy of modes is difficult. It is important to notice the lack of Landau damping of coherent modes close to the σ-mode which is more evident for this bunch.

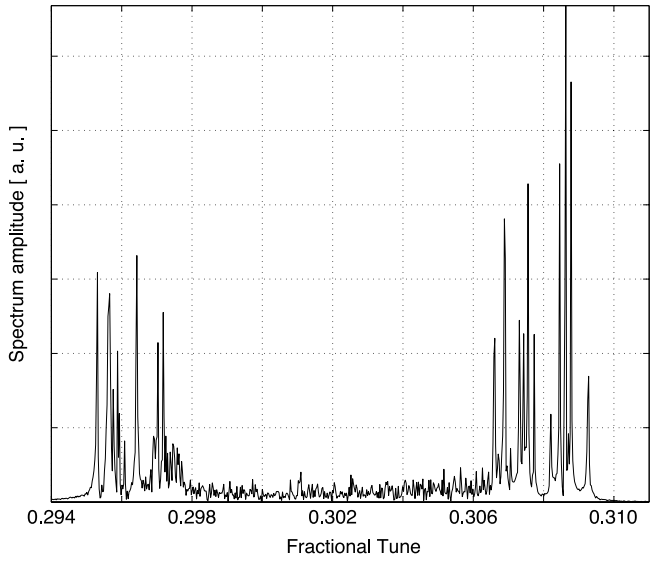

Figure 5.7: Horizontal tune spectrum of bunch number 3 of beam 1 undergoing head-on collisions in IP1, IP2, IP5 and IP8 and 2 long range interactions left and right of each IP. Phase advance symmetry is restored between IP1 and IP5. Results are obtained with the MPM.

5.2.3 Tuned phase advance between IP2 and IP8

A further improvement is done by adjusting the phase advance between interaction points 2 and 8 as shown below.

```
  1  -2   -0 +0
 41   3   8.046    6.940    8.046    6.940
 81  -2   -0  +0
201   3  23.109   21.720   23.109   21.720
321   2   -0 +0
441   3  23.6235  21.270   23.6235  21.270
561   2   -0  +0
601   3   7.5315   7.390    7.5315   7.390
```

The spectra for such a scheme are shown in Figure 5.8 for the RBM (red line) and the MPM (blue line). Comparing the RBM results (red lines) in Figure 5.5 and Figure 5.8 we notice that due to the improved symmetry in the phase advance between IP2 and IP8 many modes degenerate and a fewer number of spectral lines are present with the tuned configuration. In addition, the intermediate modes move inside the incoherent continuum and most of them are therefore damped (blue line in Figure 5.8). Only two modes are outside the range of the incoherent tune spread. The π-mode at approximately -5ξ and a mode at -4ξ. This mode is on the limit of the incoherent continuum therefore we expect that small variations on the beam intensities and/or beam sizes will push the spectral line inside the damping region.

In the presence of long range interactions the tune spectrum become as in Figure 5.9 and Figure 5.10 where we show the horizontal tune spectra for the first and central bunch of a train of 9, respectively. In this configuration where the eightfold symmetry is almost

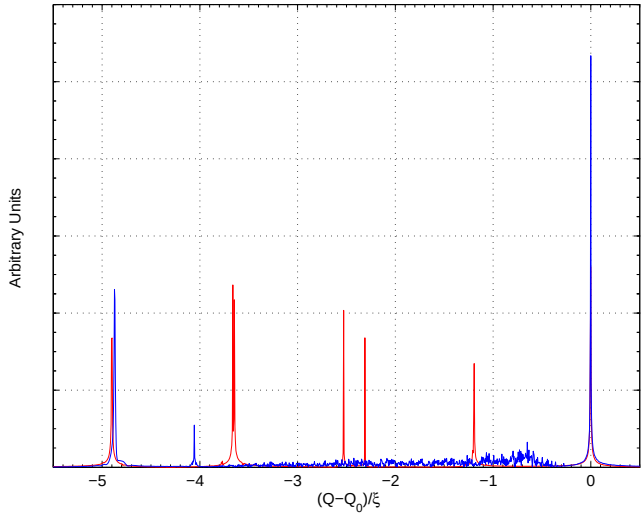

Figure 5.8: Head-on collisions in IP1, IP2, IP5 and IP8. Phase advance symmetry is restored between IP1 and IP5 and adjusted between IP2 and IP8. Red lines refer to the RBM results while blue lines are results from the MPM.

restored most of the intermediate modes are suppressed by Landau damping. The parasitic encounters creates sidebands at the main head-on modes. For peaks around the π-mode this is positive since it pushes the modes at frequencies which are Landau damped while for those closer to the σ-mode a lack of damping allow the development of coherent oscillations. This is demonstrated in Figure 5.9 and Figure 5.10 where modes around $Q_x = 0.307$ are not damped.

5.2.4 LHC interaction region layout with eightfold symmetry

The last case we want to analyze is the one when a full eightfold symmetry of the phase advance is applied. In this configuration the LHC description becomes as follows:

```
  1  -2   -0  +0
 41   3   7.78875  7.165    7.78875   7.165
 81  -2   -0   +0
201   3  23.36625 21.495   23.36625  21.495
321   2   -0  +0
441   3  23.36625 21.495   23.36625  21.495
561   2   -0   +0
601   3   7.78875  7.165    7.78875   7.165
```

In Figure 5.11 we show the RBM (red line) and MPM (blue line) tune spectra for the above collision scheme. The spectra for the fully symmetric machine are very similar to those obtained with the "tuned" collision scheme shown in Figure 5.8. However, it is significant to notice how the fully symmetric configuration of the phase advances in the arcs allow the degeneracy of the two intermediate modes of Figure 5.8 and result in the minimum number of coherent modes. Modes inside the incoherent continuum are damped as demonstrated by comparing the RBM (red line) and the MPM (blue line) results in

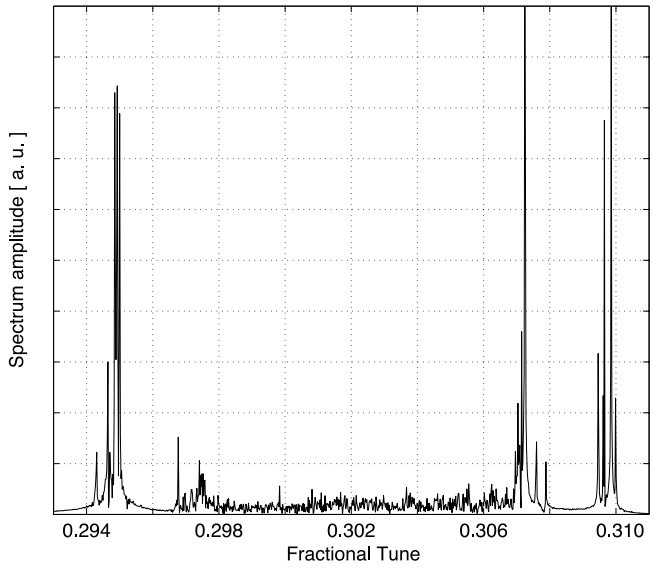

Figure 5.9: Horizontal tune spectrum of bunch number 1 of beam 1 undergoing head-on collisions in IP1, IP2, IP5 and IP8 and 2 long range interactions left and right of each IP. Phase advance symmetry restored between IP1 and IP5 and tuned for IP2 and IP8. Results are obtained with the MPM.

Figure 5.11. Only two modes are not Landau damped and are located at frequencies of $-5\ \xi$ and -4ξ. While the first one (the π-mode) is well outside the damping area the second is at the limit and therefore can be easily damped with an additional symmetry breaking mechanisms such as bunch to bunch intensity and/or transverse size fluctuations.

After adding the long range interactions the tune spectrum appears as in Figure 5.12. The overall picture does not change respect to the "tuned" collision scheme shown in Figure 5.10. The number of sidebands are reduced and the modes at the limit of the Landau damping region are suppressed.

5.2.5 Effect of an abort gap in a full eightfold symmetry

Till here we had always looked at equal beams, the next step is to understand how the tune spectra change when the breaking of symmetries comes from the beam itself. This can occur due to three main causes:

- The presence of an abort gap,
- Asymmetric beam filling schemes,
- Asymmetric collision schemes.

When filling an accelerator with beams one has always to leave a minimum number of empty buckets for the dump system. The empty buckets represent the abort gap. The main function of this empty buckets is to ensure the kicker magnet to extract the beam from the accelerator any time it is required either after a physics run to move to a new store or in case of any non stable and unsafe operational scenario. The kicker magnets which will deflect the beam from its trajectory onto the dump system needs a minimum

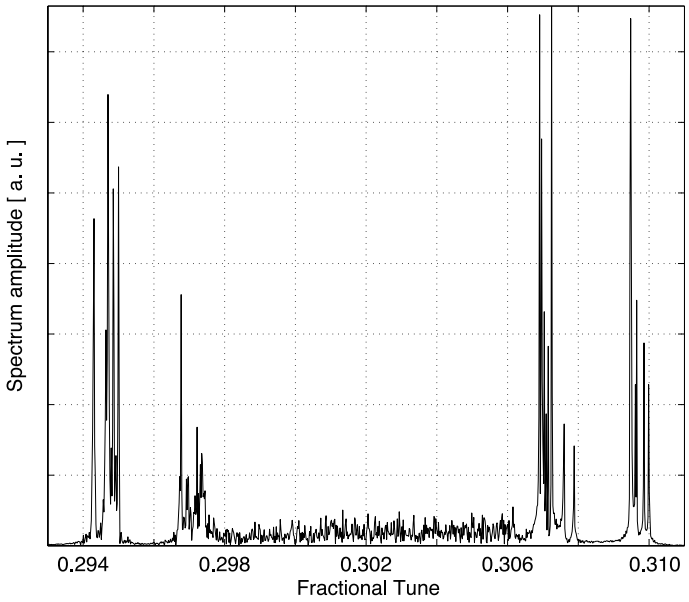

Figure 5.10: Horizontal tune spectrum of bunch number 3 of beam 1 undergoing head-on collisions in IP1, IP2, IP5 and IP8 and 2 long range interactions left and right of each IP. Phase advance symmetry restored between IP1 and IP5 and tuned for IP2 and IP8. Results obtained with MPM.

ΔT to reach the required magnetic field. The abort gap matches this time requirement so that when the beam enters the magnetic field all bunches will see the same bending force and therefore be equally deviated on the new trajectory going out of the accelerator. The length of the abort gap depends on the rise time of the kicker magnet which for the LHC operation results in an abort gap of minimum 3 μs. The abort gap together with the collision scheme and multiple long-range interactions results in the creation of different families of bunches. The bunch to bunch differences come from the different number of head-on collisions and long range interactions each of them will undergo in one turn. Nominal LHC bunches will see 4 head-on and 120 long range interactions. Other bunches will have either less head-on collisions (three instead of four) due to the abort gap and to the longitudinal displacement of the LHCb experiment or less long range interactions due to the opposite beam distribution and their location in the bunch train configuration.

To reproduce the effect of an empty bucket we modify the beam filling schemes as follows:

```
# bunch filling beam 1 #
# Number of groups #
2
 9 1 71 0
 9 1 71 0
 9 1 71 0
 9 1 71 0
```

```
# bunch filling beam 1 #
# Number of groups #
2
9 1 71 0
9 1 71 0
9 1 71 0
7 1 73 0
```

The bunches of the two beams will undergo different collision patterns and will consequently show different tune spectra. Nominal bunches undergo the same collision scheme

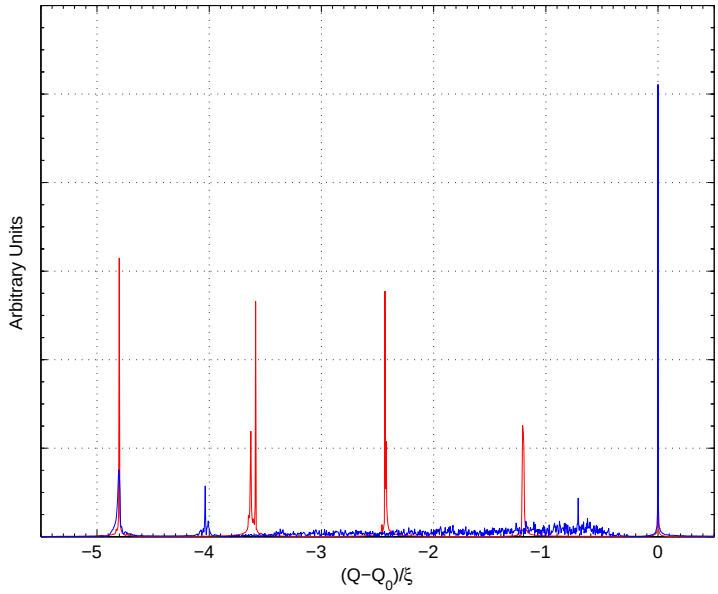

Figure 5.11: Head-on collisions in IP1, IP2, IP5 and IP8 with full eightfold symmetry of the phase advance. Red lines refer to the RBM results while blue lines are results from the MPM.

as for the cases shown in the previous subsections and will therefore exhibit a tune spectrum similar to the one of Figure 5.12. Superpacman bunches, those missing a head-on collision, will show a different spectrum with respect the the one of Figure 5.12. In Figure 5.13 we show results of the MPM on the horizontal tune spectrum of a nominal (top picture) and superpacman bunch (bottom picture), respectively.

5.3 Summary

With this study we have demonstrated with the MPM results that for the case of multiple head-on collisions coherent modes with frequencies inside the incoherent continuum are damped while those outside are not. The effects of the different symmetries in the phase advances between the accelerator arcs on the number as well as on the location of the spectral lines are shown. For asymmetric configurations it is demonstrated that the number of possible oscillating modes increases (more peaks in the tune spectrum) and the oscillating frequencies move in amplitude compared to the symmetric case. The asymmetric case creates coherent modes get close to the extreme π-mode as shown with the RBM results of Figure 5.5 red line. These specific modes have frequencies well outside the incoherent continuum as visible in the MPM results of Figure 5.5 blue line and therefore are not suppressed by Landau damping. As a results of this, one should avoid asymmetric phase advances in the LHC arcs.
In the case of symmetric configurations as for Figure 5.8 and Figure 5.11 the number of peaks in the spectra are considerably reduced and those outside the Landau damping region are only two. However, one of the coherent modes lays at the limit of the incoherent continuum therefore it can be easily damped by any fluctuation in the beam intensities and/or transverse sizes or additional tune spread from the octupole magnets and other non-linearities may help.

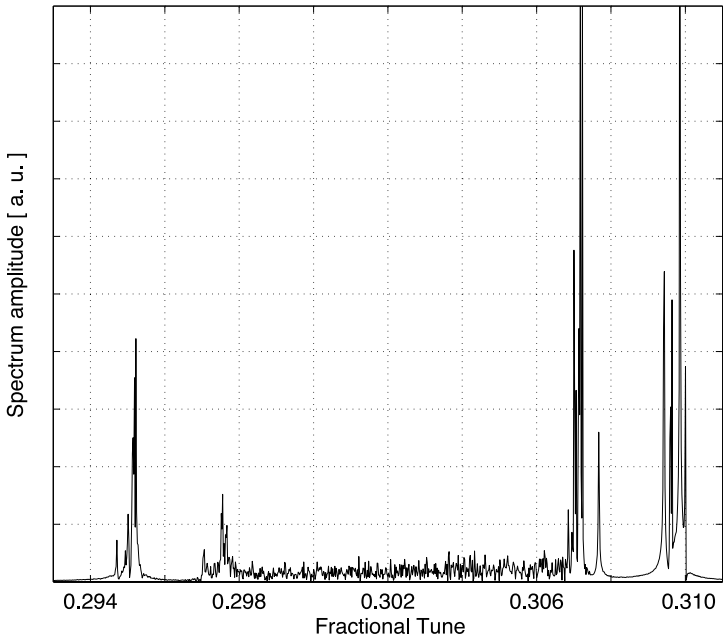

Figure 5.12: Horizontal tune spectrum of bunch number 3 of beam 1 undergoing head-on collisions in IP1, IP2, IP5 and IP8 and 2 long range interactions left and right of each IP. Full eightfold symmetry restored. Results are obtained with the MPM.

In the presence of long range interactions the number of spectral lines increase significantly. However, the peaks due to these parasitic encounters appear as sidebands of the main head-on coherent modes. Depending on the bunch to bunch collision patterns we observe different tune spectra for bunches at the head and in the center of a train. The many interactions couple the bunches strongly therefore no differences are present in the number of the sidebands. Nevertheless, for the case we have analyzed the number of long range interaction was not the LHC nominal. In the case of the LHC the large number of interaction will create relevant differences also in the number of sidebands.

A relevant finding is the lack of Landau damping of modes in the neighborhood of the unperturbed betatron tune. One should expect coherent modes due to long range interactions close to the σ-mode which will not be Landau damped. Significant differences are found for the tune spectrum of bunches missing a head-on collision as shown in Figure 5.13 (bottom picture). Moreover, due to non-symmetric bunch distributions in the two beams in the presence of Superpacman bunches, a break of coherent motion is found in the nominal bunch tune spectra. It becomes more difficult for coherent modes to develop as is shown in the tune spectrum of a nominal bunch in Figure 5.13 (top picture).
Non-symmetric configurations of the bunch distributions in the beams lead to evident bunch to bunch differences. Therefore, single bunch measurements and consequently correction to the beam dynamics should account for these variations. However, the bunch to bunch variation is proved to cure, to some extend, the development of coherent modes where these are not Landau damped.

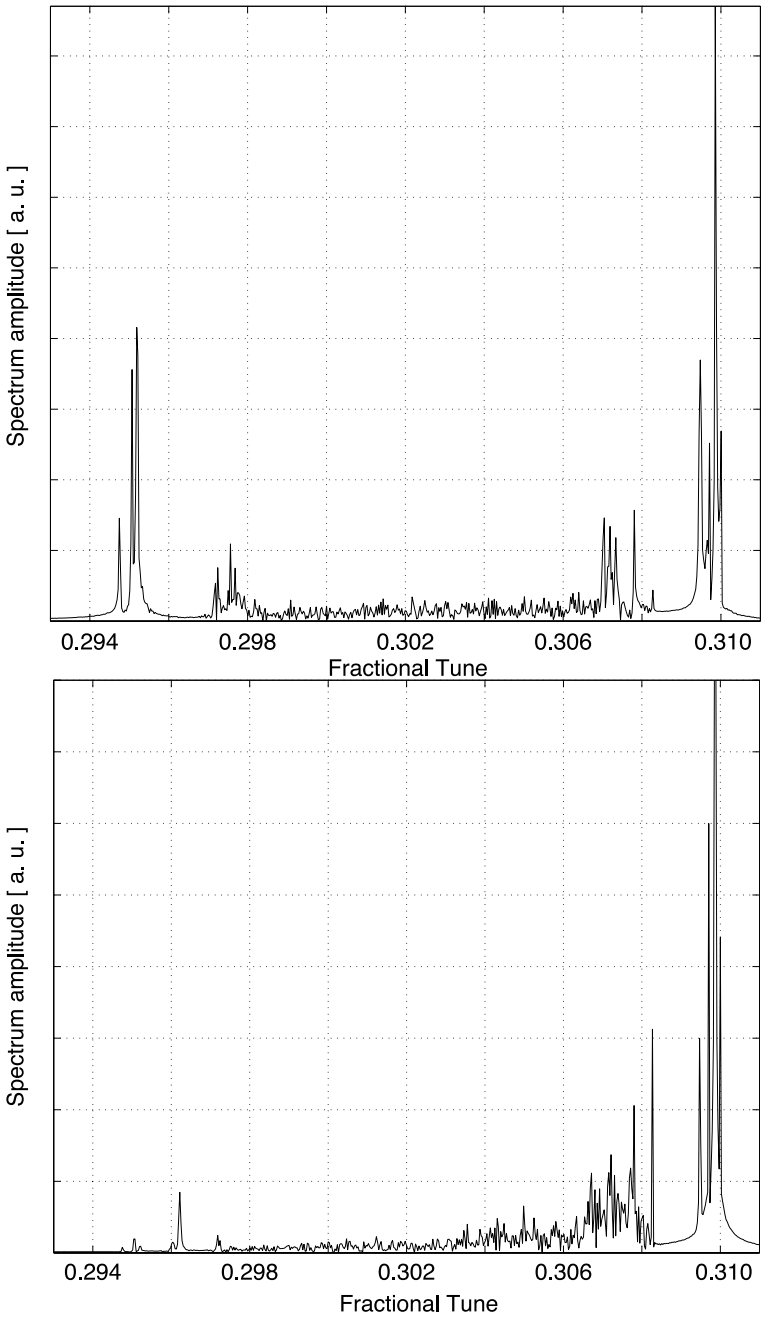

Figure 5.13: Horizontal tune spectrum of bunch number 3 (top) and number 24 (bottom) of beam 1. Head-on collisions in IP1, IP2, IP5 and IP8 and 2 long range interactions left and right of each IP. Full eightfold symmetry restored. Results obtained with the MPM.

Chapter 6

Beam-Beam emittance effects in the LHC

The layout of the LHC features four experimental areas where the two counter-rotating beams collide [96]. The beams collide at finite crossing angles [71, 97, 98, 99]. Any growth of the transverse beam emittance in a proton-proton collider is highly undesirable since it reduces the luminosity and increases the background.
The sources for a growth of the emittance can be:

- Insufficient dynamic aperture,
- Noise,
- Decoherence of coherent oscillations,
- Moving the beam,
- Static offsets,
- Time dependent offsets.

While some of these effects can be minimized or suppressed, the last two are features of the LHC design and cannot be avoided [45, 46, 109].

6.1 Origin of offsets in collision

Coherent oscillations as already explained can be excited and amplified by the beam-beam interaction and these effects have been studied in detail [10, 11, 40, 52, 37, 38, 78, 100] and in the previous chapters. The decoherence of a finite oscillation in the non-linear fields of colliding beams can lead to emittance growth. For this reason a damping of the oscillations should be foreseen, either with an active feedback system or through the Landau damping mechanism.
Under nominal operational conditions, the LHC bunches experience small unavoidable offsets at the collision points, caused by long range beam-beam interactions [43, 44, 45,

46, 71]. Using the TRAIN [45] program it is possible to calculate in a self-consistent way the orbit effects produced at the location of the interaction point IP1 by the long range beam-beam interactions and to have an estimate for each single bunch of the LHC beams.

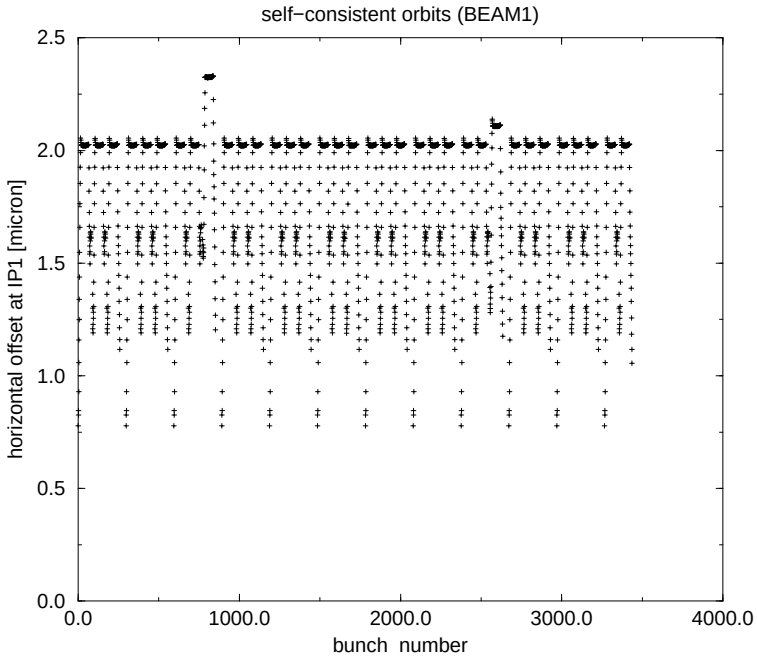

Figure 6.1: Horizontal offset at IP1 for all bunches of beam 1. The offsets are caused exclusively by long range beam-beam interactions [45, 46]. The r.m.s. beam transverse size at the IP1 is equal to 16 μm.

In Figure 6.1 and Figure 6.2 the collision offsets at IP1 are shown for each bunch of beam 1 and beam 2, respectively. The Figure 6.1 shows the offsets at the IP for each single bunch of beam 1 will experience at collision for the LHC case with nominal beam parameters and operational scenario. Figure 6.2 shows the same results for beam 2. As should be clear from the picture due to beam-beam we will have a general orbit effect on both beams which in operation can be corrected with a global orbit correction to maximize the luminosity. On top of a global orbit effect strong bunch to bunch differences are visible and expected. These offsets at the IPs can become substantial due to the different collision patterns and long range interactions seen by the different bunches and are not negligible since they could reach amplitudes up to 0.3 σ. For this spread over the bunches orbit no control is possible and therefore a full understanding of the causes and effects will be of fundamental help in the optimization of the accelerator performance during operation.

Although the geometric loss of luminosity is small, one may have to consider an increase of the transverse emittance, leading to a deterioration of the experimental conditions. It is therefore important to evaluate and understand the dynamics of beam-beam interactions

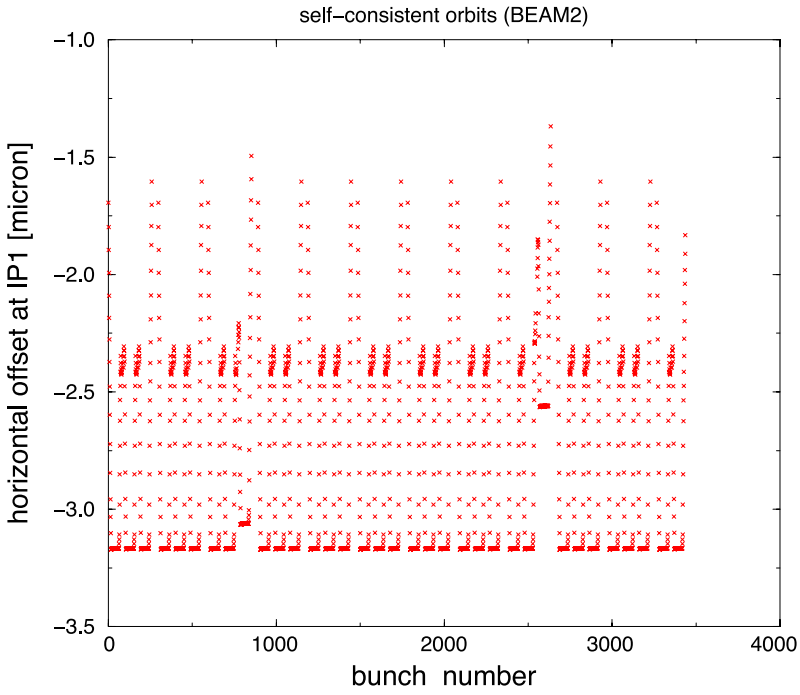

Figure 6.2: Horizontal offset at IP1 for all bunches of beam 2. The offsets are caused exclusively by long range beam-beam interactions [45, 46]. The r.m.s. beam transverse size at the IP1 is equal to 16 μm.

with static offsets and if necessary to implement countermeasures. Due to the parasitic encounters, for the LHC case of Figure 6.1 and Figure 6.2 one should roughly expect offsets in collision of amplitudes between 0.12 and 0.35 σ, where σ is the r.m.s. beam size equal to 16 μm for this case.
However, the offset at the collision point need not to be static, but could depend on time, either as a random or systematic (modulated) movement [109]. Typical random offsets can come from noise sources and have been studied previously [118]. While a source of modulated, time dependent offset is a deliberate movement of the entire beam in the interaction regions, either as a consequence of orbit corrections or a controlled change of position, e.g. during the luminosity optimization process [109].

6.2 Emittance study with the MPM and the HFMM

In a self-consistent model of the beam-beam interaction, the distributions of both beams evolve as a consequence of the mutual interaction. In the case of two strong beams, both beams are equally affected. Such self-consistent simulations have been used extensively to study coherent beam-beam effects [78, 102].
A further application of a self-consistent treatment of the BBIs is the evaluation of the beam emittance evolution in time. It is an intrinsic feature of such an effect that the parameters which determine the beam-beam effect are changing as a result of the interaction. Self-consistent simulation were done in the past for the case of e^+e^- colliders [65, 66]. Here we want to study the emittance behaviour in the presence of static offsets which are a property of the LHC configuration. For this purpose we will use the $COMBI$ code MPM

and HFMM to simulate the beams transverse emittance evolution in time while colliding with a static offset. The basic feature of self-consistent strong-strong simulations is a recalculation of the electromagnetic fields and forces of the two beams every time they collide. A number of studies have been done for the LHC using the so-called 'Soft Gaussian Model' [109]. This model assumes the force experienced by a particle when traversing the counter rotating beam as originating from a Gaussian beam distribution with variable barycenters and rms beam sizes. This allows the use of an analytical expression for the forces and represents one of the possible options in the code $COMBI$, especially developed to handle a very large number of bunches and many interactions. This Gaussian model cannot take into account the non-Gaussian deformations of the distribution and as a result underestimates the force and yields a Yokoya factor that is slightly smaller ($Y = 1.1$ in our case). This symptom has also been discussed by Yokoya [101]. In the worst case this simplification can inhibit the appearance of coherent effects. Nonetheless the use of the analytical expression of the force generated by a Gaussian beam allows simulations in a reasonable computing time and it is therefore more convenient for studies with multiple bunches. Furthermore, in the study of emittance growth it should give qualitatively reliable results giving the possibility to extend the study of those effects to the multiple interaction regime.

6.2.1 Initial condition

For this study we make use of the Multi Particle Model and the HFMM field solvers of $COMBI$ as described in Chapter 3. As output we store at every turn the normalized horizontal and vertical beam emittances for beam 1 and beam 2. The beam emittances are normalized with respect to the initial emittance values and plotted as a function of the number of turns to have a picture of the evolution in time.
For the beam parameters we have assumed the LHC beams characteristics as summarized in Table 5.1. However, the parameters have been changed and scanned in order to evaluate the dependency of the effects on these. The beams are made of a single bunch.

```
#beam filling scheme#
1  1  1  0
```

For the collision scheme and beam filling we have tested two different options. The first with a single interaction at the location of IP1 with a defined separation applied in the vertical crossing plane. In this configuration the beam and accelerator description look as:

```
#beam collision scheme#
#CASE 1#
1  -2  0  0  0  0
2   3  63.31  58.32  63.31  58.32
```

In the second case we apply 2 interactions at IP1 and IP5. In IP1 a vertical separation is always applied while for IP5 the cases of a vertical as well as an horizontal separation

have been tested in order to evaluate the effect of the crossing.

```
#beam collision scheme#
#CASE 2#
1  -2  0  0  0  0
2   3  31.655  29.16  31.655  29.16
3   2  0  0  0  0
4   3  31.655  29.16  31.655  29.16
```

At the location of IP1 a static offset d is applied in the vertical plane. While for the case of two interactions the offset had been tested on both planes in IP5. For this studies we have applied offsets with an amplitude in the range from 0.01 σ up to maximum 2 σ.

6.3 Dependence on simulation parameters

Using the two different field models for the beam-beam interaction several tests have been done in order to evaluate the effectiveness of any emittance increase as a function of time. The tests performed are meant to distinguish the emittance increase due to two possible factors:

- Numerical noise,
- Effect, if any, really coming from beam-beam interactions.

When studying the effects of numerical noise, we always fix the offset at values of about 0.3-0.4 σ since this is the order of magnitude expected for offsets in collision due to the long range parasitic encounters.

For the study of numerical noise coming from the calculation we have evaluated the effects on the emittance growth for a specific case which we have assumed to be a beam-beam interaction with an applied static offset of 0.4 σ in the vertical plane with a collision scheme as the one of case 1 defined in the previous section. The parameters relevant for this study are the number of macro-particles defined to describe the beams colliding. A scan of the number of macro-particles used had been carried out. For the HFMM the effects of the grid size were also taken into account from previous studies performed on the algorithm. These studies have been performed with both the HFMM and the MPM. The results coming from the HFMM will be shown compared where relevant to those obtained with the MPM.

6.3.1 Grid size effect

For the HFMM method the size and spacing of the grid for the field calculation can influence the results. Furthermore, the charge assignment can be done with different techniques, in particular the so-called Nearest-Grid-Point (NGP) assignment and the

Cloud-in-Cell (CIC) charge assignment. The impact has been discussed in some detail in [54, 92]. The grid size for the simulation is a compromise between precision and computing speed. Since in this report we discuss head-on collisions with small offsets between the two beams, it is sufficient to cover the range of 10 σ. A grid spacing of 0.3 σ or below gives good results with the CIC charge assignment, while for the NGP assignment small discontinuities are visible. For most simulations we have therefore chosen such a spacing and the Cloud-in-Cell (CIC) charge assignment.

6.3.2 Macro-particles effect

Using the HFMM option for the field calculation, we simulate the collision of two beams as described in the filling scheme above and with a collision schedule as the one defined as CASE 1. At the interaction we apply a static offset in the vertical plane with an amplitude of 0.4 σ, where the initial rms beam size (σ) is assumed to be 16 μm. For a defined number of macro-particles $N_{\text{particles}}$ when we apply the static offset an emittance increase as a function of time is observed as shown in Figure 6.3 for different values of the parameter $N_{\text{particles}}$. In Figure 6.3 one can notice how the increase varies with the number of macro-particles.

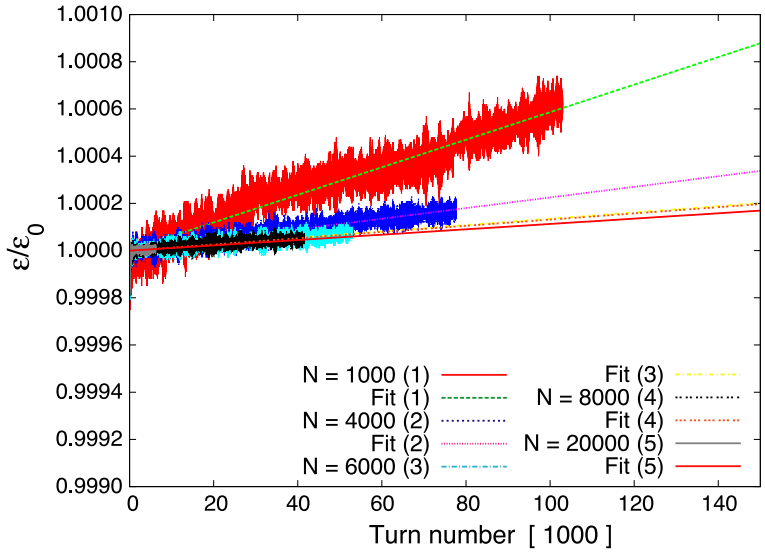

Figure 6.3: Emittance as function of the number of turn in the LHC for different number of macro-particles in the HFMM. The offset applied is equal to 0.4 σ.

The effect of particle parameter $N_{\text{particles}}$ on the emittance evolution however, decreases when going to higher values reaching a saturated value for $N_{\text{particles}} > 10^6$. This is summarized in Figure 6.4 where we have plotted the relative emittance increase resulted from the simulation with HFMM as a function of the number of macro-particles used in the calculation. The number of macro-particles is varied from 10^5 up to $3 \cdot 10^6$ per bunch and the emittance increase is evaluated assuming a linear increase in time.

From Figure 6.4 one can deduce that for studies of beam emittance evolution a sample of at least 10^6 macro-particles must be used to distinguish the physical effect from the

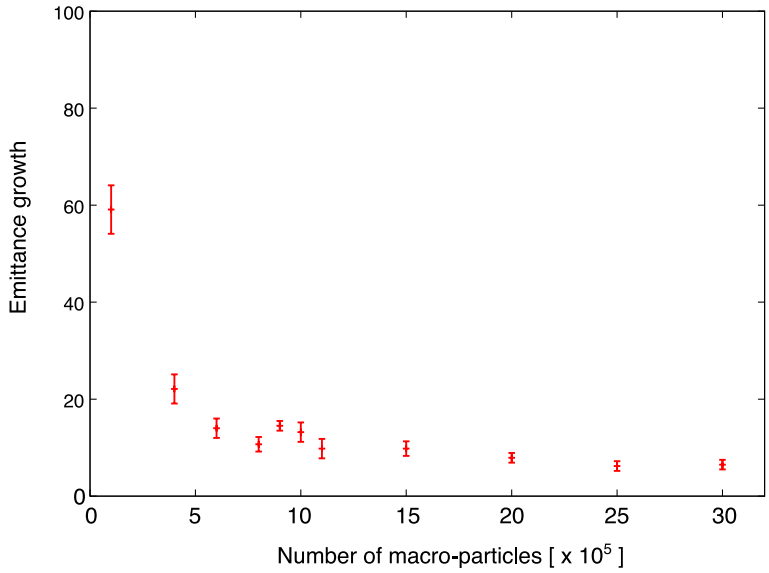

Figure 6.4: Emittance growth for different number of macro-particles. For 0.4 σ offset using the HFMM.

numerical noise of a smaller number of particles.
Similar results are found using the MPM for the field calculations. As a result of the above considerations to study the evolution of beam emittances only samples of 10^6 macro-particles are used for the calculations for both the HFMM and MPM models.

6.3.3 Number of turns effect

In both models, HFMM and MPM, samples of 10^6 macro-particles represent an important challenge. One should expect days of processing for each case. In addition another parameter important for the calculation is the number of turns N_{turn}. The number of turns were pushed to the maximum reasonable in order to study saturation effects of the emittance growth due to the growth itself and to avoid, if any, transient effects. The number of turns used is always of the order of 10^5. However, depending on the model used it was possible to increase N_{turn} by a factor of 5. For the HFMM particles were tracked for a maximum of $1.4{\cdot}10^5$ turns. This means from the computational point of view almost 1 week processing time on a single 3 GHz processor due to the very large computing time needed to process 10^6 macro-particles through the algorithm. For the MPM, since faster, it was possible to simulate up to $5{\cdot}10^5$ turns.

For the MPM, the possibility of tracking particles for up to $5{\cdot}10^5$ turns resulted in a very important issue since for the MPM cases due to the model approximation one has to ignore the first turns in the analysis. In this case other effects appear up to the first 10^5 turns. Since the model assumes always a Gaussian distribution of particles when a beam-beam interaction occurs the beam emittance show decoherence and filamentation effects before finding an equilibrium in collision mode. This is visible in Figure 6.5 for the first $5{\cdot}10^6$ turns. This effect is important when evaluating the effective emittance

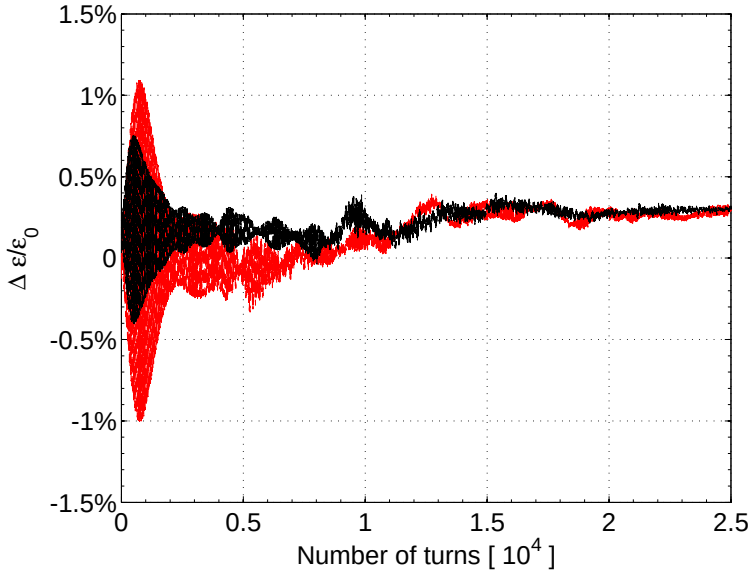

Figure 6.5: Horizontal emittance as a function of time for two bunches of beam 1 (black) and beam 2 (red) for two beam-beam interactions with a vertical offset of 0.3 σ.

growth since one should always use the equilibrium state as a starting point for any consideration. Therefore, for the MPM model where this equilibrium takes longer to develop, it is important to track the emittance evolution for a longer time to be sure to stay away from this non-equilibrium state for any calculation on the emittance increase.

6.4 Dependence on beam parameters

Our second point is now to demonstrate that the emittance increase observed is really due to the beam-beam interaction. The beam-beam force as defined in Equation 2.24 shows that the force depends on three variables:

- Beam intensities $N_{1,2}$.
- Beam emittances (transverse sizes) $\sigma_{x,y}$.
- Beam separation d.

A study of the effects of these parameters on the emittance evolution represents the first step to be addressed before going to a more complex situation. To study independently the effects of the beam intensities and emittances on the emittance growth in the presence of a static offset, the offset itself is fixed in the vertical plane at an amplitude of 0.3 σ.

6.4.1 Effect of the beam intensity

We applied the offset in the vertical crossing of IP1 and have studied how changes in the beams intensities influence the emittances increase. A scan of the intensities from $I = 10^{10}$

protons per beam up to $1.2{\cdot}10^{11}$ was performed. Figure 6.6 shows the evolution in time of the vertical beam emittances for 4 different beam intensities. For this study we have used $1.5{\cdot}10^{6}$ macro-particles and tracked the particles for $4{\cdot}10^{4}$ turns. As expected if the effect is coming from beam-beam interaction a correlation exists and becomes even more visible when the increase of the relative emittances is plotted as function of the intensity itself as done in Figure 6.7.

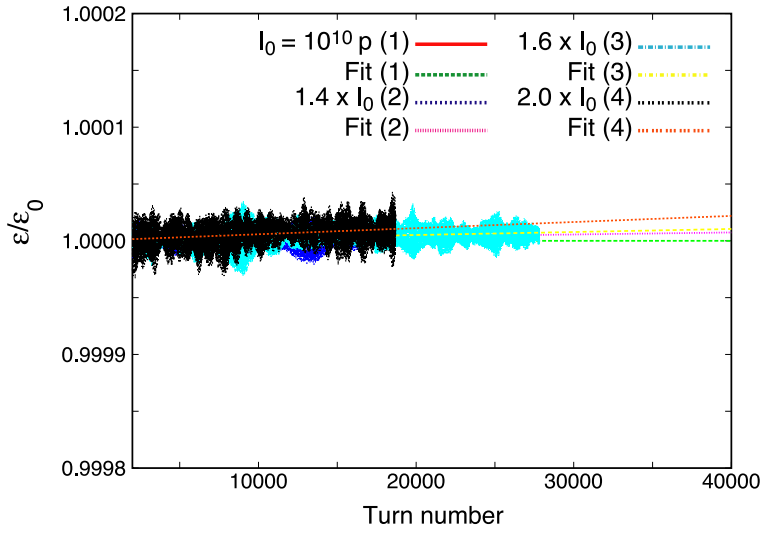

Figure 6.6: Beam emittance normalized to initial value as function of the number of turns in the collider. Different colored lines refer to four different bunch intensity and equal initial emittances. A vertical static offset of 0.3 σ had been applied at IP1.

For the LHC nominal case with bunch intensity of $1.15{\cdot}10^{11}$ protons per bunch and transverse emittances 128 μmμrad and a revolution frequency of 11 kHz we have to expect an increase of the order of 10^{-4} per second of operation. This absolute value is not very large however a doubling time of the emittance occurs in the most pessimistic case at 30 hour in operation which goes well beyond the most optimistic scenario. However, the strong sensitivity of this growth on the bunch intensities, emittances and as will be proved later of the machine tunes can translate in a much faster increase if it is not kept under control.

Moreover, one should expect that the emittance increase saturates after a certain time. Larger emittances imply a decrease in the beam-beam strength. Figure 6.8 shows how for a smaller bunch intensity the effect is almost canceled and not sensitive to the separation applied. These results have been obtained with two beam-beam interactions at IP1 and IP5 with a vertical offset for both IPs. However, one should try, when possible, to reduce the effect to avoid background increase at the experimental regions.

6.4.2 Effect of beam initial transverse sizes

Another beam parameter which has a direct impact on the beam-beam force are the beams emittances themselves. If we remember Equation 2.24 we see that smaller emittances means stronger beam-beam force. Therefore if the emittance increase is a physical effect of the interaction itself we should be able to see a dependency on the initial emittances of the

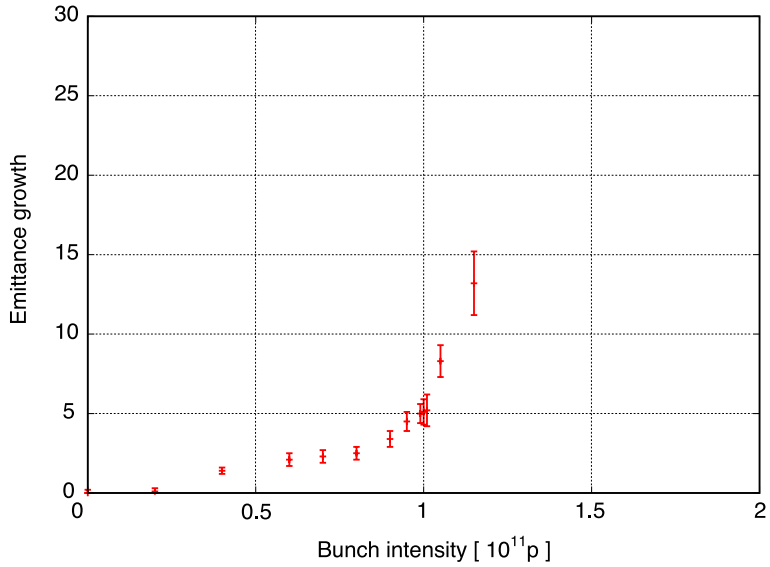

Figure 6.7: Emittance growth for different bunch intensities in units of 10^{11} protons per bunch and equal initial emittances for a vertical static offset of 0.3 σ.

beams. We now assume equal beam intensities of $1.15{\cdot}10^{11}$ which represents the nominal LHC beams intensities and we evaluate the emittance behaviours when changing the initial emittances. As a consequence a decrease of the effect is expected as demonstrated in Figure 6.9 where the beam vertical emittance is plotted as a function of time for different initial emittances. For smaller initial emittance (red line in Figure 6.9 corresponding to initial beam size 10 μm) the effect on the increase is stronger. While for initial larger transverse beams the effect reduces significantly (black line in Figure 6.9 corresponding to initial beam size 41.5 μm). This is even more clear when the relative increase in emittance is plotted as a function of the initial values as in Figure 6.10. Since the emittance contribution to the force goes in first approximation as $1/\sigma^2$ for small offsets the trend of Figure 6.10 confirms this statement.

The same qualitative results is found using the MPM for calculations for the case of multiple interaction (2 offset collisions per turn instead of one) as described in collision scheme named CASE 2. Two beam-beam interaction at IP1 and IP5 and on both a vertical separation of 0.3 σ have been simulated. In Figure 6.11 one can see the emittance evolution in time for this case for two different initial emittances 16 μm and 25 μm. The effect increases significantly when a reduced emittance is used.

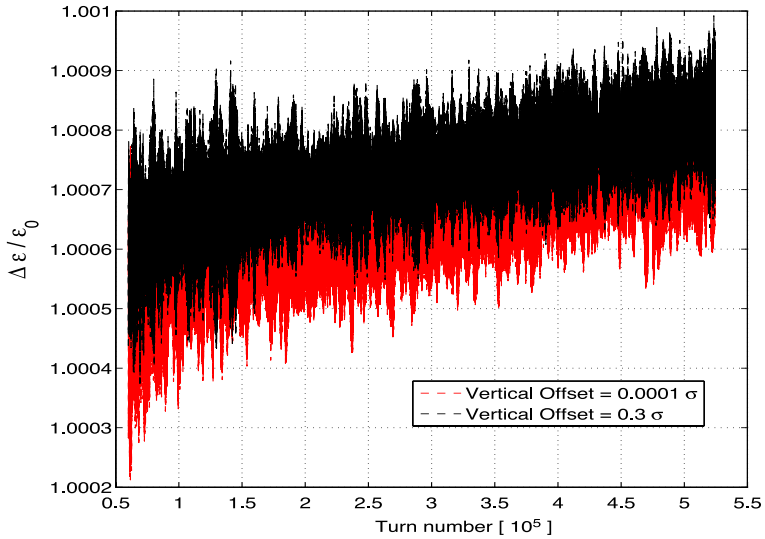

Figure 6.8: Vertical normalized emittance for a bunch intensity of $0.62{\cdot}10^{11}$ protons per bunch and equal initial emittances of 16μm for two vertical offsets of 0.001 and 0.3 σ.

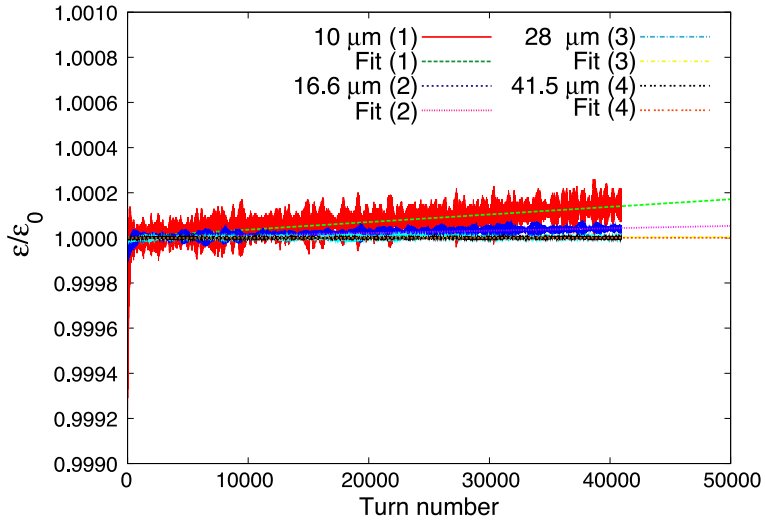

Figure 6.9: Normalized emittance for different initial transverse emittances and equal intensities for a vertical static offset of 0.3 σ. The evolution of the normalized emittance as a function of the number of turns in the collider is shown for the cases of beams with initial beam sizes of 10 μm (red line), 16.6 μm (nominal LHC beams, blue dashed line), 28 μm (light blue dashed line) and 41.5 μm (black line).

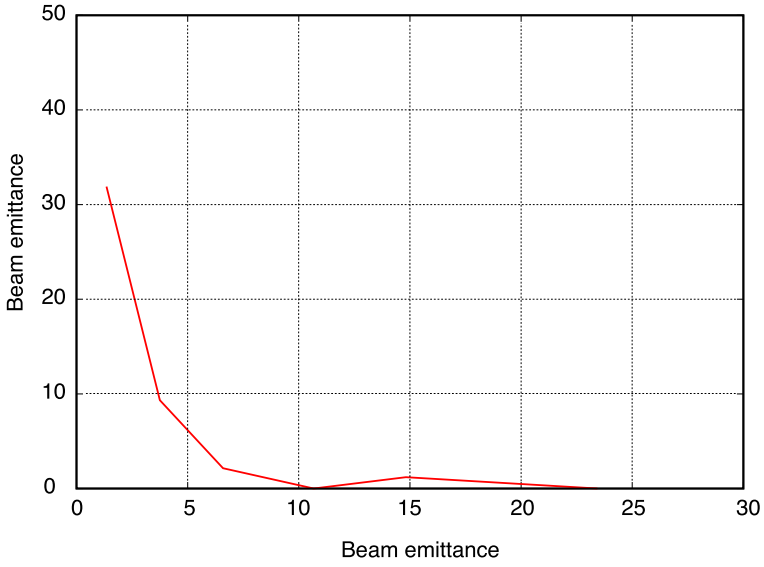

Figure 6.10: Emittance growth for different r.m.s. beam size expressed in μm and equal intensities for a vertical static offset of 0.3 σ.

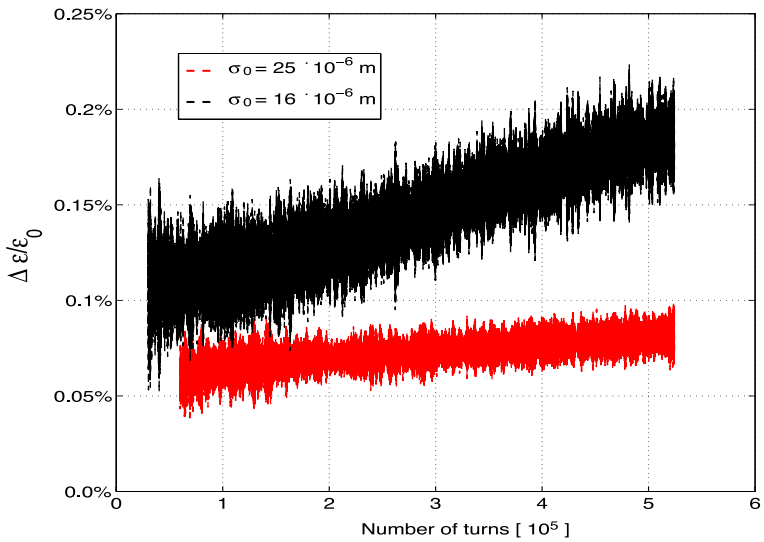

Figure 6.11: Emittance growth for initial emittances of 16μm and 25μm, for equal intensities and for a fixed vertical static offset of 0.3 σ. Results are obtained with the MPM.

6.4.3 Effect of the collision offset

The other important variable which will significantly change the effects is the collision offset. An initial beam size of 16 μm in both planes and a bunch intensity of $N_{1,2} = 1.15{\cdot}10^{11}$ for both beams are assumed. For both MPM and HFMM calculations a sample of 10^6 macro-particles per bunch were used. First using the HFMM with a single interaction as CASE 1 and with a static offset of amplitude d in the vertical plane one obtains that for different values of d from 0.001 σ up to 2 σ the increase of the emittance changes. In Figure 6.12 we show the normalized emittance evolution as a function of time for different offset amplitudes. The change in the emittance growth rate follows a clear trend which

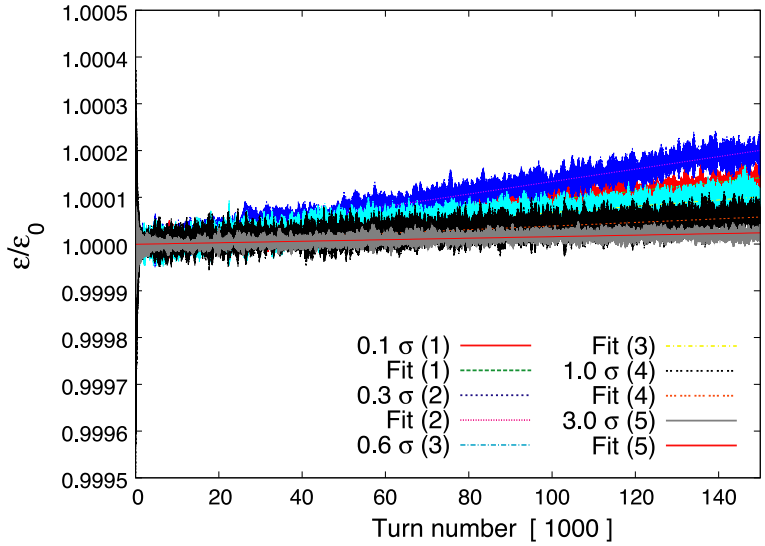

Figure 6.12: Normalized emittance as function of time (turn number) for different vertical offsets in collision at IP1. Calculations done with HFMM.

has been confirmed by the two independent studies. Assumed a linear increase of the emittance in time if one plots the growth rate as a function of the offsets two maxima are observed in Figure 6.13. The increase is maximum for separations around 0.3-0.4 σ. Then one has a decrease and another increase for offsets of approximately 1.5 σ. For offsets above 2 σ the increase becomes zero. In Figure 6.13 the increase as function of the offset is plotted for both vertical (red line) and horizontal (green line) emittance normalized growth rate per turn.
The same study was performed with the MPM but for 2 interactions with variable vertical offsets. A good qualitative agreement was found with results from HFMM. In Figure 6.14 the vertical growth rates as a function of the offsets are plotted. The similar behavior in Figure 6.13 and Figure 6.14 is visible. For offsets in the range of 0.2-0.3 σ a maximum increase in the emittance is found. This is repeated in the neighborhood of 1.5-2 σ distance although with a smaller absolute value.

The particular trend found for the emittance growth rate as a function of the offset amplitude d of Figure 6.14 was unexpected. We tried to explain the observations with simple consideration of non-linear dynamics since the beam-beam force is a strongly non-linear element. We do not attempt to derive a complete model of the dynamics, but rather try to

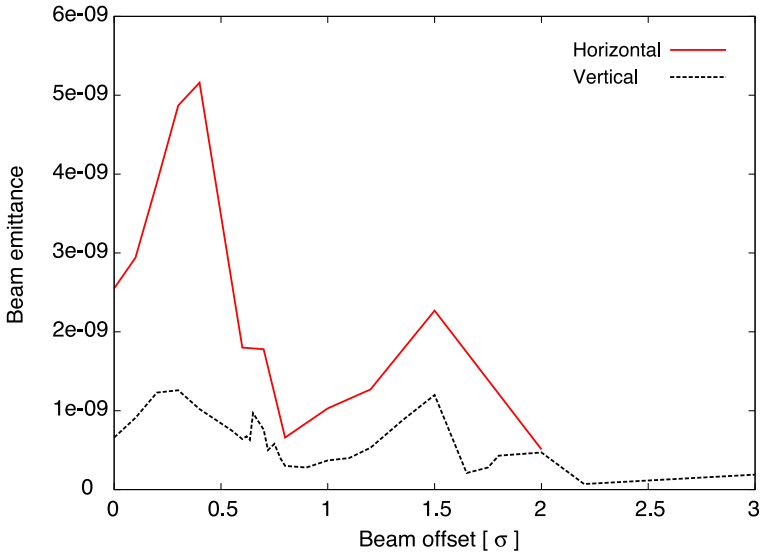

Figure 6.13: Emittance growth rate for different beam separations. Results are obtained with the HFMM.

qualitatively understand the observations in a physical picture. To produce an emittance growth due to an offset applied at collision one has to expect it could be a result of the non-linear beam-beam force produced by a beam located at a distance d weighted over the opposite beam particle distribution in amplitude. For the Gaussian density distribution used to generate the particle beams, the distributions in the amplitudes x and y are Rayleigh distributions given by:

$$R(x) = (x/\sigma_x^2) \cdot e^{\frac{-x^2}{2\sigma_x^2}} \quad R(y) = (y/\sigma_y^2) \cdot e^{\frac{-y^2}{2\sigma_y^2}} \tag{6.1}$$

Reducing the problem to the one-dimensional space x one defines the particle amplitude distribution of beam 1 centered at $x = 0$ defined as in Equation 6.1. As an estimate of the non-linearities of the interaction we take then the second derivative F$''(x - d)$ of the beam-beam force produced by beam 2 at an offset d $= \sigma$.

By evaluating the convolution $R(x) * F''(x - d)$ of the two functions one obtains what can be defined as the strength of the non-linearities of beam 2 on the particles of beam 1 weighted with their distribution. The convolution operator as defined assumes the integration of the effect over the collision area and one then obtains the overall effect of the non-linear terms of beam 2 distant d from beam 1 on the particle amplitude distribution. The convolution integral results in a function of the offset d as by the definition:

$$C(d) = \int_0^\infty R(x) \cdot F''(x - d)\ dx \tag{6.2}$$

In Figure 6.15 the resulting convolution C is plotted as a function of the offset d. In the range between 0 and 5 σ two maxima are found like for the results of the simulations. Also the location of the two peaks are very similar to those found through multi particle simulation and correspond to offsets of 0.3 and 2.0 σ.

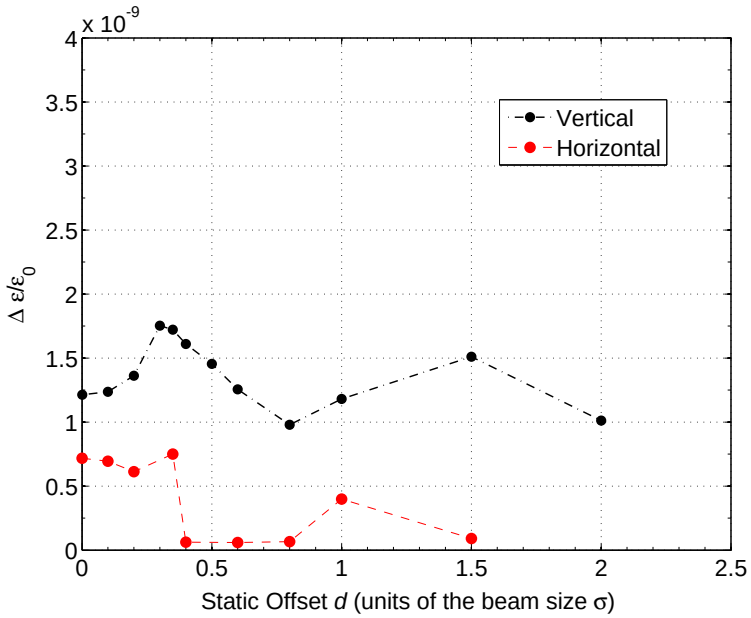

Figure 6.14: Vertical (black dots) and horizontal (red dots) normalized emittance growths per turn for different beam separations.

However, these values correspond to the case were the amplitude distribution of beam 1 is peaked at the same value of beam 2. This means that the Rayleigh function is peaked at 1 σ where the beam size is defined equal for the two beams. Going for a small change of 10% in the amplitude distribution for beam 1 respect to beam 2 then the $R\ (x/0.9 \cdot \sigma_x^2)$ function shows a maximum density at a $x = 0.9 \cdot \sigma_x^2$ and as a consequence the maxima of C (d) move to smaller offsets. On the other side going for larger values of the beam 1 sizes the convolution bumps go to larger offsets.
Therefore, smaller variations of the maximum locations of Figure 6.14 with respect to Figure 6.15 could be due to the fact that for the physics consideration the amplitude and position variable had been all normalized to the beam σ assumed equal for the two beams. This for the simulation is not completely true since the particle distributions are generated through a random statistical process. In conclusion, we can say that the structure of Figure 6.13 and Figure 6.14 can qualitatively be explained by a simple physical picture.

6.5 Effects of the accelerator betatron tune

An important parameter that was not yet treated is the accelerator betatron frequency. The tunes assumed for the previous studies were the nominal LHC fractional tunes. As already shown the betatron frequencies have an important role in beam-beam interactions and in general in non-linear dynamics. Even if a complete study on the emittance growth dependency on the tunes was not addressed, few examples can already highlight the expectations.
In all previous studies only the effects on the vertical emittance had been investigated.

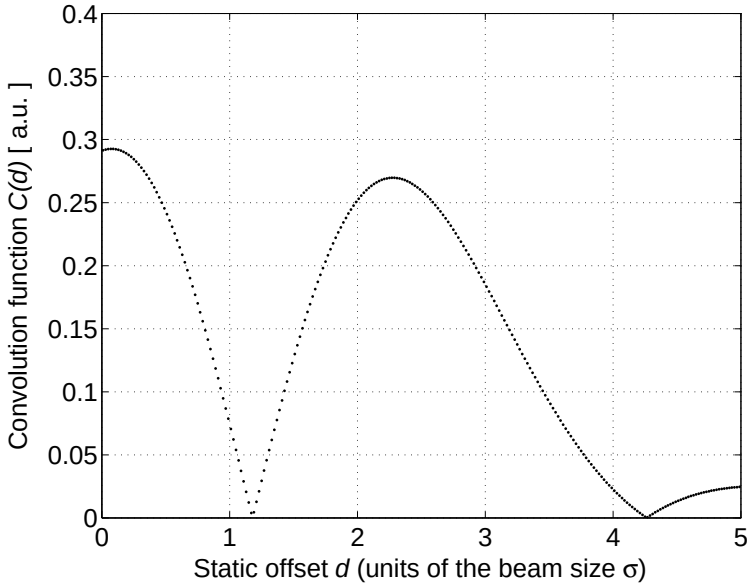

Figure 6.15: Convolution function C as a function of the offset in collision d between beam 1 centered at d=0 and beam 2 centered at an offset d. The picture shows the C function when the amplitude distribution of beam 1 is peaked at 1 σ.

Mainly since the offsets at collision were applied only in the vertical plane while in the horizontal plane the collision was a head-on interaction. The effects on the horizontal emittance are shown however in Figure 6.14 as the red line. The effect on the horizontal plane is much smaller than in the vertical. While at first one might think it is mainly due to the fact that the offsets are added only in the vertical plane, a more careful analysis revealed that the main parameter which determines the emittance growth is the vertical tune value Q_y.
To prove that this effect is mainly coming from the vertical tune value which is much closer to a third order resonance value 1/3 some significant tests were performed. We have reproduced a symmetric case where the effect of the horizontal and vertical tunes on the emittance could be evaluated. We defined the LHC as in CASE 2 collision scheme (2 collision at IP1 and IP5 per turn) with the nominal $Q_x = 0.31$ and $Q_y = 0.32$ for the tunes. Offsets of 0.2 σ were applied in the plane of separation at the two IPs. The planes of separation themselves had been changed in order to evaluate the differences. The configurations used were the following:

- V-V crossing: offsets in the vertical plane for IP1 and IP5.
- V-H crossing: offsets in vertical plane in IP1 and horizontal in IP5.
- H-H crossing: offsets in the horizontal plane for IP1 and IP5.
- V-H crossing: offsets in vertical plane in IP1 and horizontal in IP5 and inverted tunes.

In Figure 6.14 for the case of a V-V crossing with two offsets applied at the IPs one sees

that the effect on vertical and horizontal emittances are significantly different. The effects of the offsets in collision on the vertical emittance (black dots) with respect to the horizontal (red dots) is always about one order of magnitude different. The vertical relative emittance growth is always in the 10^{-9} range per turn while the horizontal corresponding value is in the range $10^{-10} - 10^{-11}$. If one now changes the plane of separation and try to emphasize the effect in the horizontal it is surprising that the difference is not relevant.
In Table 6.1 we summarize the vertical and emittance growths per turn for different planes for the separation at the two IPs. It is evident that for a V-V crossing the vertical growth is maximum while the horizontal is minimum. If one then replaces a vertical offset with a horizontal, one still finds a vertical growth larger than the horizontal for the case but the vertical value is reduced respect to the previous case while the horizontal growth increases. In the case of a H-H crossing the horizontal effect on the corresponding emittance is increased and the vertical growth is reduced but still the vertical growth is larger than the horizontal. Therefore one should conclude that the emittance effect is dependent on the offset applied but there should be an underlying reason that the vertical effect is always enhanced.

Table 6.1: $\Delta\epsilon/\epsilon$ per turn for a 0.2 σ offset in different planes at IP1 and IP5.

Crossing planes	Q_x	Q_y	$\Delta\epsilon_V/turn \cdot 10^{-9}$	$\Delta\epsilon_H/turn \cdot 10^{-9}$
V-V crossing	63.31	59.32	1.27	0.612
V-H crossing	63.31	59.32	1.2	0.665
H-H crossing	63.31	59.32	1.12	0.742
V-H crossing	63.32	59.31	0.586	1.22

The reason appears obvious as soon as one tests the fourth case of Table 6.1. Swapping the horizontal and vertical fractional tunes one obtains an inversion in the effects to the horizontal and vertical emittances. The more pronounced growth of the vertical emittance ϵ_V now disappears and one can see it on the horizontal emittance ϵ_H. In Figure 6.16 and Figure 6.17 one can see this swap in the effect due to the inversion of the tunes when a H-V crossing is applied.

In Figure 6.16 we show the normalized vertical emittance growth per turn in the accelerator for nominal LHC tunes (black dashed line) and for swapped tunes (red dashed line). One can notice how for the nominal tunes the emittance increase is bigger than that produced when the tunes are swapped.
On the other hand, Figure 6.17 shows the normalized horizontal emittance growth per turn in the accelerator for nominal LHC tunes (black dashed line) and swapped tunes (red dashed line). The effect on the horizontal ϵ_H is exactly the opposite the one on ϵ_V.
Further studies are needed to assess the effect of the machine tunes on the emittance behavior. However, with the studies addressed here one can state that on top of the general trend for the emittance growth as a function of the offset amplitude what defines the amplitude of the effect is the betatron frequency of the accelerator. For fixed offsets in collision the effect of the tunes on the emittance behaviour is the most crucial and for our specific case this is strongly related to the value of Q_V. The vertical tune really defines

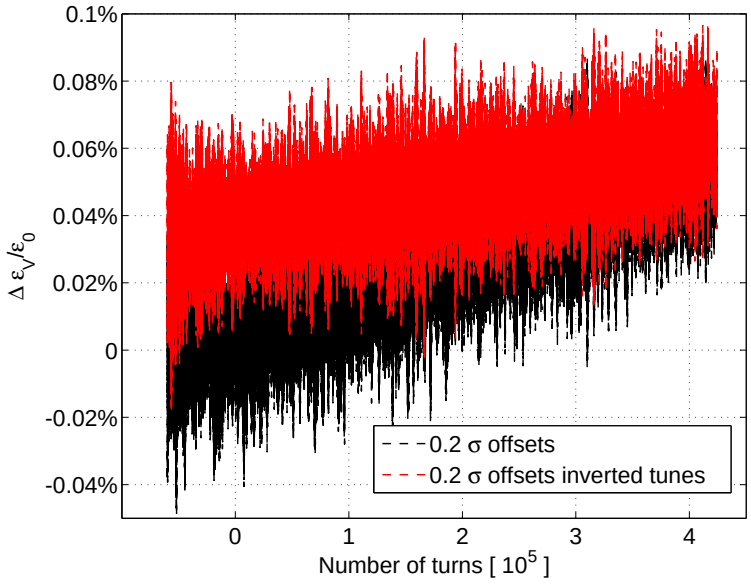

Figure 6.16: Vertical emittance growth as a function of time for different amplitudes of the vertical static offsets applied in a HV crossing in IP1 and IP5.

the absolute amplitude of the growth. We strongly believe that this is related to the fact that the Q_V value is very close to the third order resonance which for sure enhances the effect. This consideration is made on the observation that the same growth rate does not appear for the horizontal emittance since for this plane the betatron frequency 63.31 is further away from the third order resonance.

Further studies should be performed to investigate the tune effects on the growth rate in order to define safer constrains on the machine working point. This is crucial when deciding for new machine working points since offsets at the collision points are unavoidable due to the parasitic encounters and therefore an emittance increase as demonstrated in the previous section is expected. During operation to optimize the machine performances and to keep background levels at the experimental areas under control, the search for better betatron frequencies should be done by looking at the above considerations.

6.6 Summary

In this section we have demonstrated how offsets in collision can lead to emittance growth. Emittance growth in general should be minimized at any time during the collider operation since they can represent a dangerous source of beam losses in the accelerator and will increase the background levels at the experiment locations.

Although the emittance growth for a nominal LHC case with beam parameters as defined in Table 4.1 is very slow, the effect can easily be enhanced and become important by changes on either the beam parameters (beam sizes, intensities) or on the accelerator optical properties (betatron tunes) due to a threshold effect as shown in the dependency

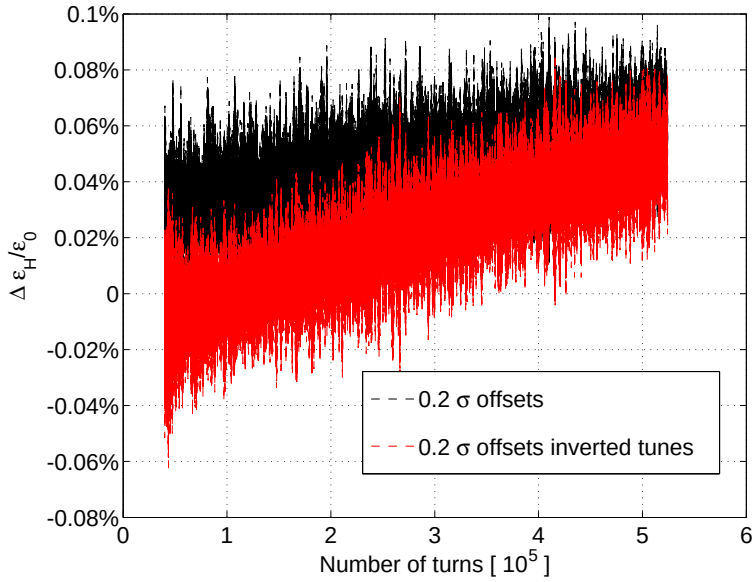

Figure 6.17: Horizontal emittance growth as a function of time for different amplitudes of the vertical static offsets applied in a HV crossing in IP1 and IP5.

on the beam sizes and intensities. The effect on the emittance had been confirmed by independent models. The parametric dependences on beam and collider properties is a further confirmation of the beam-beam effect. The structure of the emittance relative variation as a function of the offset had triggered a look for a possible physical picture to describe the particle interaction. With a very simple model for the non-linear beam-beam force and the beam amplitude distribution we have qualitatively understood the physical picture behind the emittance growth behavior as a function of the beam relative distance in collision. From the study we can say that the double peak picture obtained in Figure 6.13 and Figure 6.14 with independent simulations can be explained as a consequence of the effect of non-linear terms of one beam on the particle amplitude distribution of the opposite. This is clearly demonstrated in Figure 6.15 where the convolution of particle amplitude distribution and the non-linearities is plotted as a function of the beam offset at collision.
Simulations of the emittance behavior as a function of time are very time consuming since the particle samples should be taken on the order of 10^6 to avoid numerical noise on the results. This had been proved for both, HFMM and the Gaussian approximation for the force calculations. Results found with the Gaussian approximation although not quantitatively correct follow the same structure as results from the HFMM. This represents an important result since it allows faster calculations as needed for multiple interactions otherwise almost impossible.

Chapter 7

Coherent beam-beam effect at RHIC

An important point for developing a fully self consistent treatment of the beam-beam interaction for multiple bunches is not only for academic studies but especially to reproduce measurements of the effects in operating accelerators. In the LHC the complex layout of the many beam-beam interactions mixed with the large number of bunches colliding in a non symmetric configuration will lead to strong bunch to bunch differences.
The LHC will have a redundant diagnostic system based on a single bunch measurements (i.e. position, transverse beam size) when required. For interpreting the diagnostic outcome, a reliable and consistent model of the effect should be available. Considerable insight and understanding of the beam behavior may result if sufficient diagnostics are built into the computer code. This simulated diagnostics and instrumentation involves evaluating as a function of time all relevant beam parameters. In this frame different diagnostics devices can be simulated in the model. The instrumentation devices can be allocated along the accelerator as in the real collider in order to allow direct comparison with measurements. The diagnostic devices implemented in the COMBI code are:

- Beam position monitors,
- Beam profile monitors,
- Beam Transfer Functions devices,
- AC Dipole excitation and/or PLL system.

To test the predictive power of the code a benchmark with real measurements was performed at the Relativistic Heavy Ion Collider (RHIC) facility at the Brookhaven National Laboratory [55]. The goal of the study was to interpret the passive Beam Transfer Function (BTF) measurements [57] used during normal machine operation to monitor the beams behavior during the physics run. The BTF measurements are routinely done during operation to keep track of the betatron tunes during the whole store. The measurement is not destructive and therefore represents a very important and useful diagnostic system while the beams are colliding. The study was performed analyzing RHIC 2006 proton-proton physics run data.

7.1 The Relativistic Heavy Ion Collider

The RHIC facility enables studies of nuclear phenomena in collisions of light and heavy ions, as well as polarized protons. The collider was constructed in an existing 3.834 km long circular tunnel, and is in operation since 2000. The main beam parameters of the 2006 proton-proton run, during which the measurements discussed in the following were carried out, are listed in Table 7.1.

Parameter	Unit	Value
Beam energy E	GeV	100
Number of collision points	...	2
Number of bunches N	...	111
Bunch intensity N_b	10^{11}	1.35
RMS emittance $\epsilon_{x,y}$, initial	mm·mrad	2.8
Transverse beam size σ	μm	168
Envelope function at IP β^*	m	1.0
Peak luminosity $\mathcal{L}$	$10^{30}\mathrm{cm}^{-2}\mathrm{s}^{-1}$	35
Average luminosity $\mathcal{L}$	$10^{30}\mathrm{cm}^{-2}\mathrm{s}^{-1}$	20
Beam-beam parameter ξ/IP	...	0.006

Table 7.1: Maximum achieved beam parameters during the 2006 polarized proton run.

The RHIC follows a six fold symmetry structure. The two opposing beams are referred to as Blue (clock-wise) and Yellow (counter clock-wise) beams. Each beam is bunched and travel in two separate rings along the arcs. At the six crossing points symmetrically distributed they share a common beam pipe. The layout is sketched in Figure 7.1. The crossing locations are named IP2, IP4, IP6, IP8, IP10 and IP12. Only at IP6 and IP8, locations of the two experiments STAR and Phenix respectively, the two beams are brought into collision. The collision of the bunches are made at a zero crossing angle while at the other IPs the two beams just cross each other with a vertical separation of 10 mm in order to exchange from the inner to the outer beam pipe in the arcs and vice versa. In the accelerator there are 360 available longitudinal buckets where only one out of every three is filled with a bunch. For physics run in 2006, 111 buckets were filled over 331 possible leaving an abort gap of 29 empty buckets defined by the rise time of the kicker magnet.

7.2 Modeling the collider

In our modeling of the RHIC accelerator we define the machine as made by 120 possible bunch locations. In this simplified scheme the two beams are defined as follows:

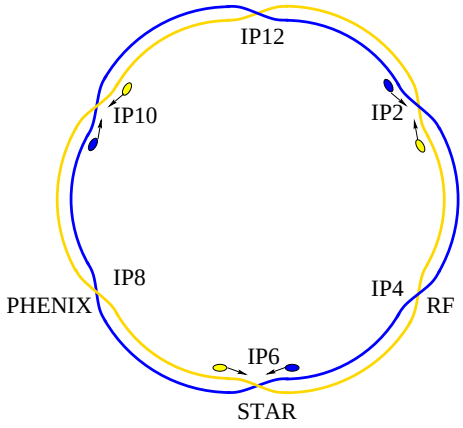

Figure 7.1: RHIC 6-fold symmetry schematic layout. Head-on beam-beam interaction couples bunches in Blue to bunches in Yellow through collisions in IP6 and IP8. There are no long-range beam-beam interactions.

```
# Yellow Beam #                    # Blue Beam #
# Number of groups #               # Number of groups #
2                                  2
 111 1   9 0                        111 1   9 0
```

As a consequence for the collision scheme we have then 240 possible slots where an interaction can occur. The RHIC collision path can then be defined as follows:

```
# RHIC nominal collision scheme #
  1   9    0   0   0   0
 21   3    4.7825   4.78083    4.9475   4.94917
 61   3    4.7825   4.78083    4.9475   4.94917
101   3    4.7825   4.78083    4.9475   4.94917
121   2    0   0   0   0
141   3    4.2825   4.28083    4.4475   4.44917
161   2    0   0   0   0
181   3    4.7825   4.78083    4.9475   4.94917
201   8    0   0   0   0
221   3    4.7825   4.78083    4.9475   4.94917
```

Due to the 6 fold-symmetry configuration therefore we assume that the phase advance in the six arcs is the same and equal to one sixth of the one turn tune of the machine. We therefore define action code 3 at 6 symmetrical locations defined at slot 21, 61, 101, 141, 181 and 221 as shown in the collision scheme above.
The machine nominal working point (Q_x, Q_y) for polarized proton beams in the RHIC during the 2006 run was constrained between 2/3 and 7/10. Additionally, the two beams were set at two different working points to avoid coherent beam-beam effects [15] because

the differences in the tunes break the symmetry and disturb the collective motion of the beam particles, as explained in detail in Chapter 4. In RHIC this is accomplished by "mirroring" the tunes at the $Q_x = Q_y$ diagonal in the tune diagram. For the 2006 proton-proton run the horizontal and vertical design tunes were fixed for the Blue beam at approximately $Q_x = 28.695$ and $Q_y = 29.685$ while for the Yellow beam at $Q_x = 28.685$ and $Q_y = 29.695$. This provides in the ideal case a tune split of approximately $\Delta Q_{x,y} = 0.01$.
In our modeling of the accelerator the two interaction points corresponding to PHENIX and STAR experiment are located at the slots 161 and 121, respectively. At this locations the beams collide head-on. At slot 1 the excitation coming from the BTF system is introduced. At this location the bunch particles receive a time modulated kick. A pick-up is located at slot 201 and will store the amplitude response of the beams. No parasitic long-range interactions are present at RHIC since the longitudinal bunch to bunch distance is larger than the length spent in a common beam pipe before being separated in the arcs in this operational scenario.
To analyze the whole picture we make use of all the tools available and developed for this purpose. For simulations we used the COMBI code with the three (ALM, RBM and MPM) different models for the beam-beam interaction calculations. The MPM was used in parallel mode to afford the number of bunches to simulate.

7.3 Coherent beam-beam modes

We start by analyzing the overall tune spectra without any BTF excitation in simplified cases. Where needed we used parameters to enhance the beam-beam effects. The effect of the BTF excitation will then appear more clearly. In the case of a fully symmetric machine without any abort gap and operating at same tunes of $Q_x = 28.685$ and $Q_y = 29.695$ we expect 2 possible eigenfrequencies: the unperturbed machine tune and the π mode. The spacing between the frequencies is simply given by $N_{HO} \cdot Y \cdot \xi$ where Y is the Yokoya factor for Gaussian bunches and ξ is the beam-beam parameter. The N_{HO} factor is the number of head-on collisions. The maximum tune shift is simply given by summing up the contribution over the head-on collisions. However, as already seen in the previous chapters the number of eigenfrequencies of the coupled system will depend on the machine and filling scheme symmetries.

7.3.1 Effect of asymmetric location of the interaction points

Assumed that the beams can collide head-on at all IPs foreseen in Figure 7.1, the tune spectrum will appear different depending on which IPs are used for the collisions. To distinguish the effects due to symmetric and non-symmetric collision schemes we assume in this section that the two beams have equal tunes in both horizontal and vertical planes.
For a single head-on collision in IP6 we have a horizontal and vertical tune spectrum as the one shown in Figure 7.2 left and right picture, respectively. The tune spectra are obtained with MPM calculations and the results show the characteristic σ and π mode frequencies with the incoherent spectrum in between.

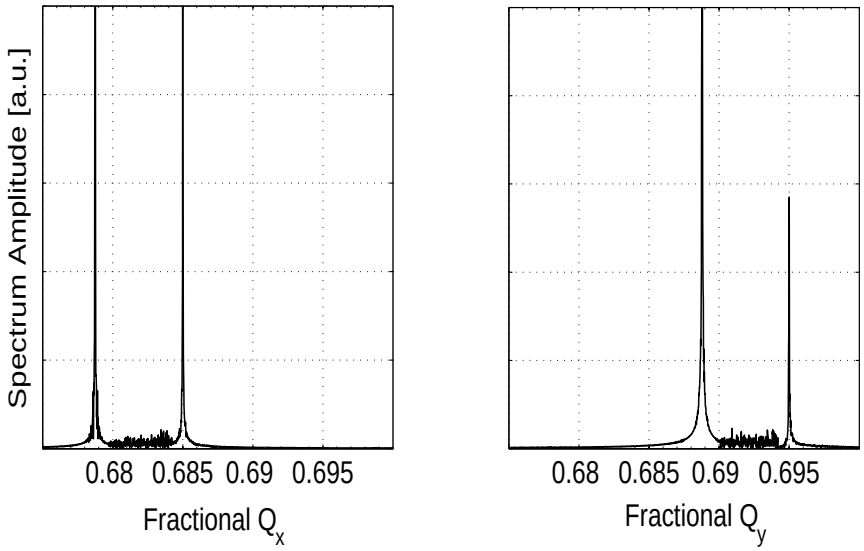

Figure 7.2: MPM simulations of the RHIC horizontal (left) and vertical (right) tune spectra for one head-on collision in IP6.

If we allow two head-on collisions in IP6 and IP12 of Figure 7.1 opposite in azimuth we have the same number of peaks in the tune spectrum but with a tune shift doubled for the π-mode seen in Figure 7.3. For both cases of a single and two head-on collisions the unperturbed tunes of $Q_x = 28.685$ for the horizontal plane and $Q_y = 29.695$ for the vertical were used in the calculations together with a beam-beam parameter $\xi \approx 0.0046$.

The picture changes if the location of the IPs is not symmetric. In Figure 7.4 we show the different eigenfrequencies expected for four different collision schemes in the accelerator, as calculated with the ALM for beams with equal tunes. The different collision schemes are defined by the sequence of the IP names at which a head-on collision occurs. From top to bottom we have 1 head-on collision at IP6 with only 2 eigenfrequencies the well known σ and π modes. The second shows the four spectral lines expected in the realistic RHIC operational case where collisions happen at two non symmetric IPs, IP6 and IP8. The third is the case when the symmetry of collisions is restored, collisions in IP4, IP8 and IP12, and a reduction of the possible eigenfrequencies of our coupled system is reduced to three. The last represents the case when four collisions take place at IP4, IP6, IP8 and IP12 and for this the spectral lines one should expect are four.

For the RHIC accelerator case of equal working points for the two beams one should expect the appearance of two intermediate oscillating frequencies between the σ and π frequencies. This is due to the non symmetric IPs chosen for the physics operation. All eigenfrequencies are visible when we simulate the operational conditions with the ALM as shown in Figure 7.4.

If we simulate the same system with the MPS model not all peaks are visible. Those

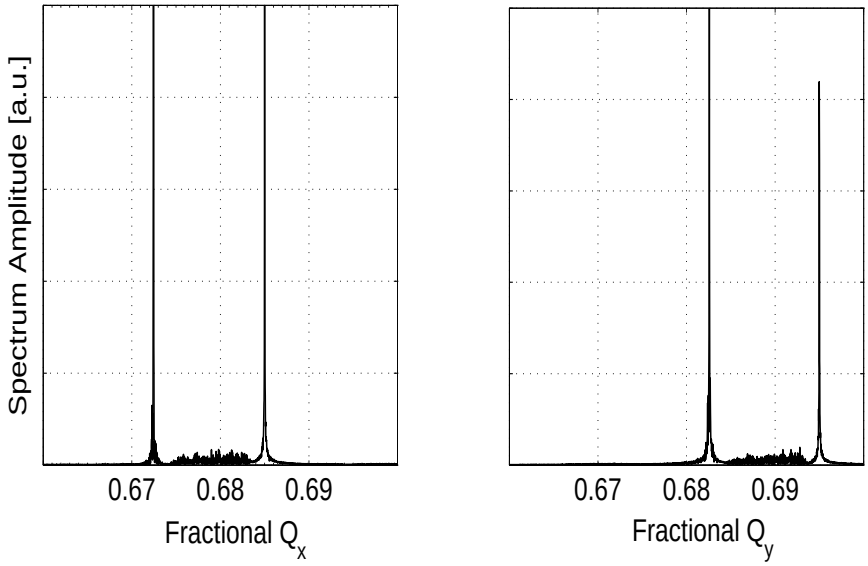

Figure 7.3: MPM simulations of the RHIC horizontal (left) and vertical (right) tune spectra for two head-on collisions in IP6 and IP12 opposite in azimuthal.

with frequency inside the incoherent continuum tune spread are damped due to Landau damping. This is visible in Figure 7.5 where the calculated horizontal (left) and vertical (right) tune spectra obtained with the MPM are plotted. The intermediate modes lay at the limit of the incoherent range of frequencies and therefore not completely damped in this example.

Within their approximations, the ALM and the MPM give a good understanding of the modes behavior of the coupled system of bunches representative of the RHIC accelerator. It is important to observe coherent modes frequencies with the ALM which are otherwise suppressed due to damping mechanism as observed from the MPM evaluations.

7.3.2 Effect of the different working points

If the beams are operated at different working points it is clear from Chapter 4 that the system of coupled bunches tries to keep the organized and collective motion for small values of the tune split. In the tune spectra this is visible since the spectral lines move to new equilibrium values. This is visible for $\Delta Q \ll \xi_{bb}$.

In the RHIC, 4 eigenfrequencies are present due to the asymmetric collision scheme, as demonstrated with the ALM results in Figure 7.4. For different betatron frequencies of the two beams the coherent motion is still effective due to the model (see Figure 7.6). In Figure 7.6 the horizontal (top) and vertical (bottom) tune spectra calculated with the ALM are plotted for the case of a fully symmetric beam filling scheme (12 bunches per beam, no abort gap). The only effect due to the different working points of the beams is the location of the eigenfrequencies which are visibly moved. The two beams found in the horizontal and in the vertical plane a new equilibrium value for the eigenfrequencies depending on the coupling strength. For the examples shown in Figure 7.6 we have applied a $\Delta Q_y \approx 0.009$ and $\Delta Q_x \approx 0.0035$ as measured during a real store of the RHIC

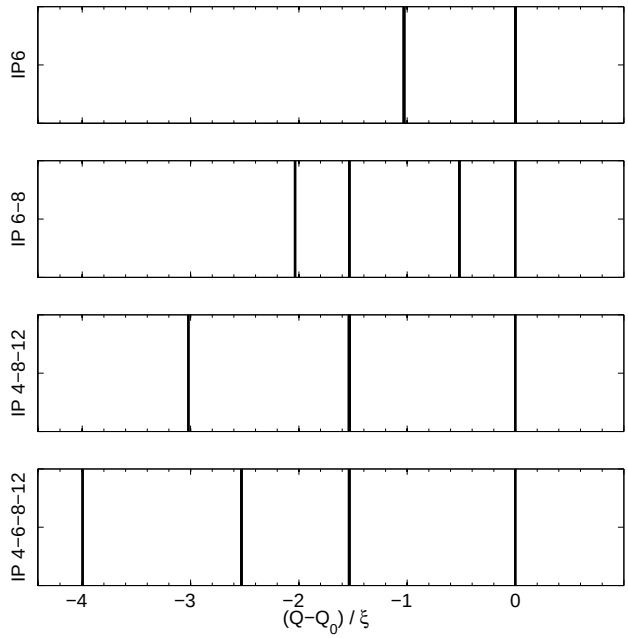

Figure 7.4: Horizontal eigenvalues of the system of coupled bunches for different locations of the interaction points. From top to bottom eigenfrequencies for one head-on collision at IP6, two head-on collisions at IP6 and IP8, 3 collisions at IP4, IP8 and IP12 and 4 collisions at IP4, IP6, Ip8 and IP12. The results are obtained with the ALM.

accelerator as shown in Figure 7.12. In Figure 7.12, the Yellow (top) and Blue (bottom) beam horizontal and vertical tune spectra are plotted before bringing the beams into collision which we assume as our unperturbed tunes. We choose these values for the tunes to have a direct comparison with measured data. The beam-beam parameter used for the following two cases are $\xi = 0.008$ and $\xi \approx 0.004$ per collision for the ALM and the MPM calculation, respectively. A higher ξ was chosen for ALM to enhance the effects.

One can also observe the different effect in the two planes in Figure 7.6. The horizontal intermediate modes (top picture) are more centered with respect to those in the vertical plane (bottom picture). This is due to the different values of ΔQ and how this relates to the beam-beam coupling strength. For the horizontal case we have $\Delta Q_x = 0.003 \ll 2 \cdot \xi$. Therefore, the system is still in a coupled mode as shown with MPM results in Figure 7.7 (left picture) where the horizontal tune spectrum is plotted. In the vertical plane the situation changes since $\Delta Q_y = 0.01 \geq 2 \cdot \xi$. The vertical plane does not display any coherent motion due to the symmetry breaking of the tunes. This is visible in Figure 7.7 (right picture) where the vertical tune spectrum evaluated with MPM is shown, no coherent motion is visible.

In the case of a symmetrical filling scheme (120 bunches longitudinally equispaced in the ring) the RHIC horizontal and vertical tune spectra should appear as those reproduced in Figure 7.7. The coherent motion is almost suppressed due to the tune differences between the beams. In the horizontal plane (Figure 7.7, left picture) a weak coherent motion can be distinguished but there is no evidence of the four peaks since they are at frequencies

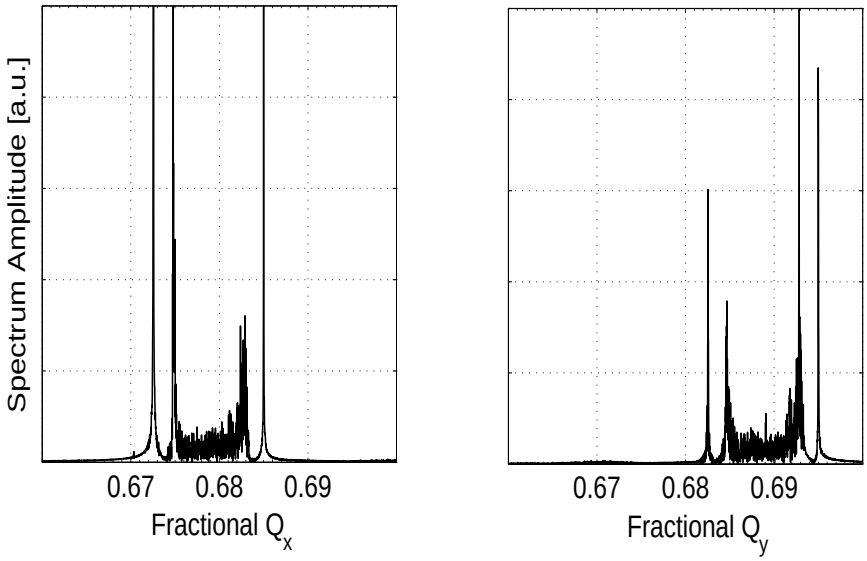

Figure 7.5: MPM simulations of the RHIC horizontal (left picture) and vertical (right picture) tune spectra in the case of beams with equal tunes and with two asymmetric head-on collision in IP6 and IP8.

inside the incoherent continuum and therefore Landau damped. Moreover, the simulation assumes that the bunches have the same intensity which may not be the case in the real collider. Intensity fluctuations are present and represent an additional source of symmetry breaking.

7.3.3 Effects of Asymmetric beams

Another effect which influences the bunch coupling in a collider is the beam symmetry. Asymmetric beams are those where the bunches are not longitudinally equidistant. In the RHIC a longitudinal empty gap is needed to allow for the dump kicker magnet to extract the beam before it can damage the accelerator. This gap is called abort gap and for the RHIC it consists of 27 empty buckets (out of 360) at the end of the 111 bunches. As already discussed, asymmetries in the beam filling schemes as well as in the collision patterns lead to the creation of different sub-families of bunches. In RHIC nominal bunches are those which undergo two head-on collisions per turn in IP6 and IP8 while Superpacman bunches collide only once per turn in IP6 due to the injection symmetry. Different families of bunches lead to different coherent modes. Therefore, in terms of tune spectra one should expect more coherent peaks. Simulations performed with the ALM are shown in Figure 7.8 and Figure 7.9 where the horizontal (top) and vertical (bottom) spectral lines of nominal and superpacman bunches are plotted. The difference between the two figures is the beam-beam parameter used for calculations. In Figure 7.8 we have used $\xi = 0.008$ per IP to show how the frequencies move apart. While in Figure 7.9 we have applied $\xi \approx 0.0041$ per IP which is the RHIC beam-beam parameter as calculated from luminosity measurements of the store of Figure 7.12. It is not possible to distinguish which frequency belongs to the two different bunch families. The intermediate lines in Figure 7.8, most visible in the horizontal plane (smaller tune difference), is the signature

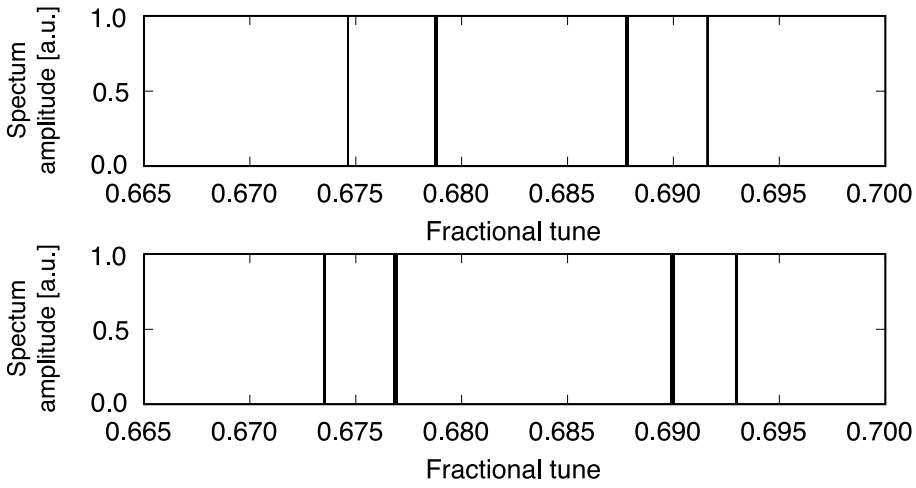

Figure 7.6: Horizontal (top picture) and vertical (bottom picture) eigenvalues of the system of 120 equidistant bunches colliding head-on (with $\xi = 0.008$) at IP6 and IP8 with two different working points for the two beams.

of a single head-on collision of the superpacman bunches. The spectral lines move further apart when the tune difference becomes more significant with respect to the beam-beam strength as visible in Figure 7.9 (right).

In addition one can notice from Figure 7.9 that coupling for the horizontal plane is present but for the vertical plane the spectral lines just follow the two almost independent frequencies. Thus the tune differences can overcome and break the coherent motion of the bunches.

To distinguish between the spectrum of a nominal and a superpacman bunch we made use of the RBM. This still provides all frequency peaks since damping mechanisms are not included. In Figure 7.10 the horizontal (top) and vertical (bottom) tune spectra are plotted for a nominal (black line) and a superpacman (red line) bunch. Here one can identify the superpacman frequency spectrum. As already anticipated the intermediate spectral line in the horizontal plane (top) just below $Q_x = 0.685$ is a signature of a bunch colliding only at IP6.

The same tune spectra were reproduced with the MPM (Figure 7.11). The coherent motion is completely suppressed in the vertical plane (Figure 7.11 bottom) while one can still see them in the horizontal plane (Figure 7.11 top). In the vertical plane the two beams are decoupled because the beam-beam strength is $\xi_{tot} \ll \Delta Q_y$ for both nominal and superpacman bunches [79]. Therefore we only expect two peaks at their independent tunes. In the horizontal plane the beam-beam coupling strength is always larger or equal, for superpacman bunches, to ΔQ_x. Therefore, we have a coupled system of harmonic oscillators, oscillating at two frequencies with the intermediate modes being suppressed due to Landau damping [103].

From our studies coherent modes develop in the RHIC nominal configurations and one should expect bunch to bunch differences due to asymmetries of the operational mode.

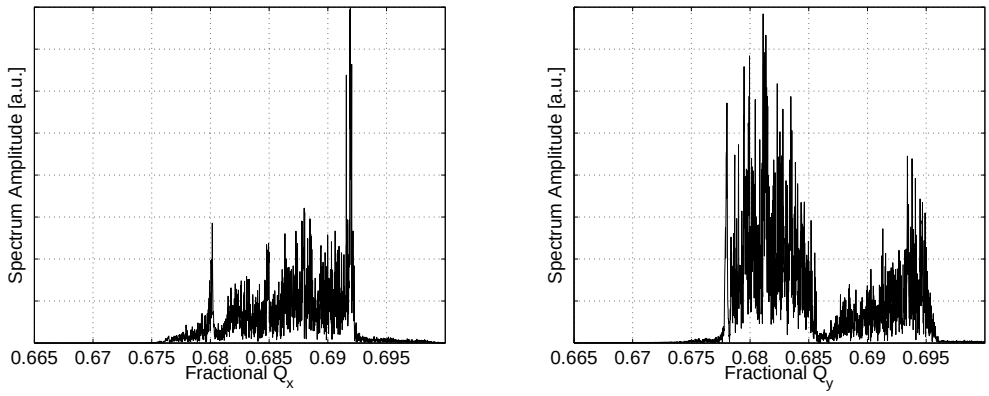

Figure 7.7: Horizontal (left) and vertical (right) tune spectra evaluated with the MPM of the system of 120 equidistant bunches colliding head-on (with $\xi = 0.004$) at IP6 and IP8 with two different working points for the two beams. The horizontal and vertical fractional betatron tunes are for Yellow beam [0.692, 0.688] and Blue beam [0.695, 0.698], respectively.

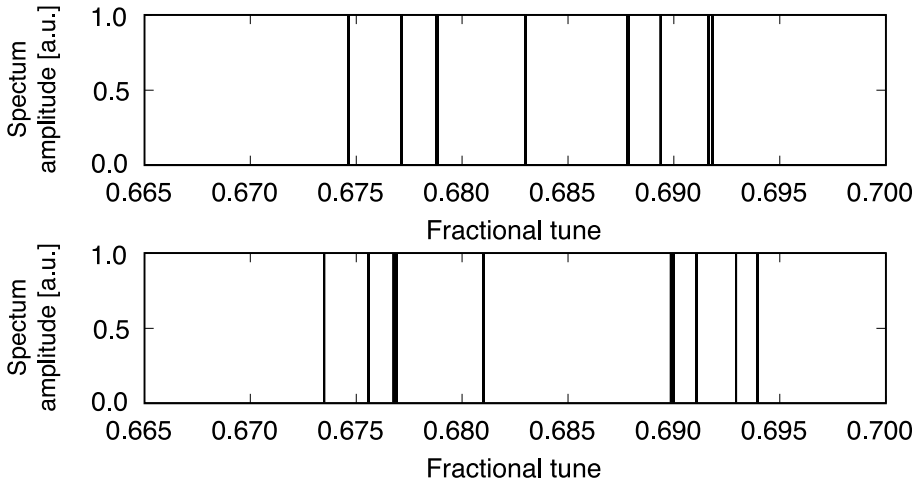

Figure 7.8: Horizontal(top) and vertical (bottom) spectral lines for asymmetric beams and $\xi = 0.008$ to enhance the effects.

However, even if the strategy of different tunes for the two beams breaks the symmetry of the collective motion, sometimes the tune differences applied are not big enough to completely decouple the bunches. In this case coherent modes develop. However, only extreme spectral lines will be visible since intermediate modes are Landau damped.

7.4 Beam-beam transfer function measurements

In practical accelerator operations, it is useful to measure the beam response to a controlled or external sinusoidal driving force. This response can be described in terms of a quantity called Beam Transfer Function (BTF). The interest in the BTF is based on the fact that it contains a wealth of information about the beam and the accelerator lattice. The examination of the BTF constitutes a valuable diagnostic technique to understand the dynamics of the beams in particular during a physics run. In a BTF measurement,

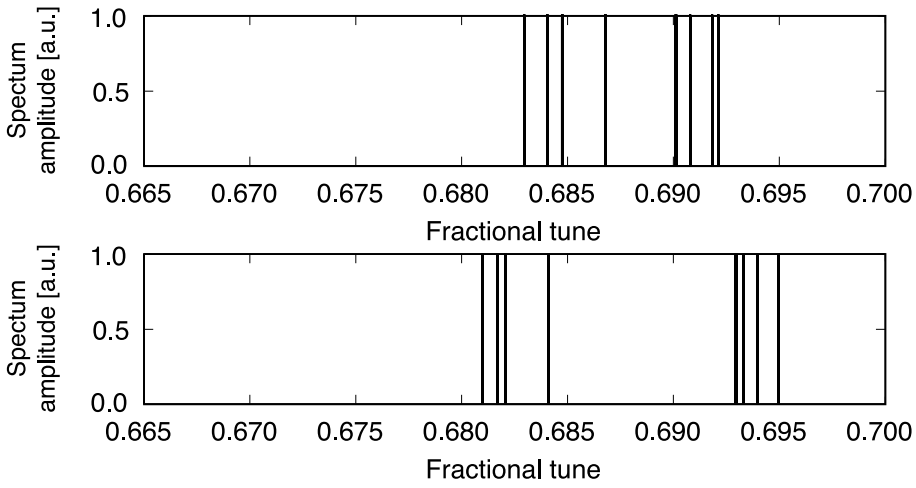

Figure 7.9: RHIC horizontal (top) and vertical (bottom) spectral lines calculated with ALM for the case of a beam filling scheme with missing bunches due the an abort gap for $\xi \approx 0.0041$.

the beam response $\langle x(t) \rangle$ is measured as a function of the external excitation frequency Ω. If particles with a transverse tune distribution $\rho(\omega)$ are excited by an external sinusoidal force of frequency Ω the beam response after transient effects is given by [57]:

$$\langle x(t) \rangle = \frac{A}{2\omega_x} e^{-i\Omega t} [\text{P.V.} \int d\omega \frac{\rho(\omega)}{\omega - \Omega} + i\pi\rho(\Omega)] = \frac{A}{2\omega_x} e^{-i\Omega t} [f(u) + ig(u)]$$

$$\langle x(t) \rangle = \frac{A}{2\omega_x} [\cos(\Omega t + \phi) \text{P.V.} \int d\omega \frac{\rho(\omega)}{\omega - \Omega} + \pi\rho(\Omega) \sin(\Omega t + \phi)].$$

By scanning the frequency Ω the distribution $\rho(\omega)$ can be obtained from the second term in the brackets, which is out of phase with respect to the driving force. We have taken such BTF measurements of colliding proton beams during the RHIC Run-6 in 2006, and compare the measured amplitude response of the beam $\langle x(t) \rangle$ as a function of the exiting frequency Ω with calculated ones. The tune distributions of colliding proton beams in RHIC are dominated by the beam-beam interaction.

7.5 Measurements and simulations of BTF

The BTF measurements are routinely made during the course of a physics store. A typical measurement involves sweeping the kicker frequency across the tune spectrum in steps of approximately 1×10^{-4} tune units and simultaneously recording the amplitude response from the downstream strip-line pickups. A BTF measurement just before collisions at 100 GeV is shown in Figure 7.12.

For reproducing BTF measurements, the *COMBI* code was modified with a specific *action code*. This function gives a frequency dependent kick to the bunches of the two beams at a defined location of the ring, while the amplitude response of the beams is

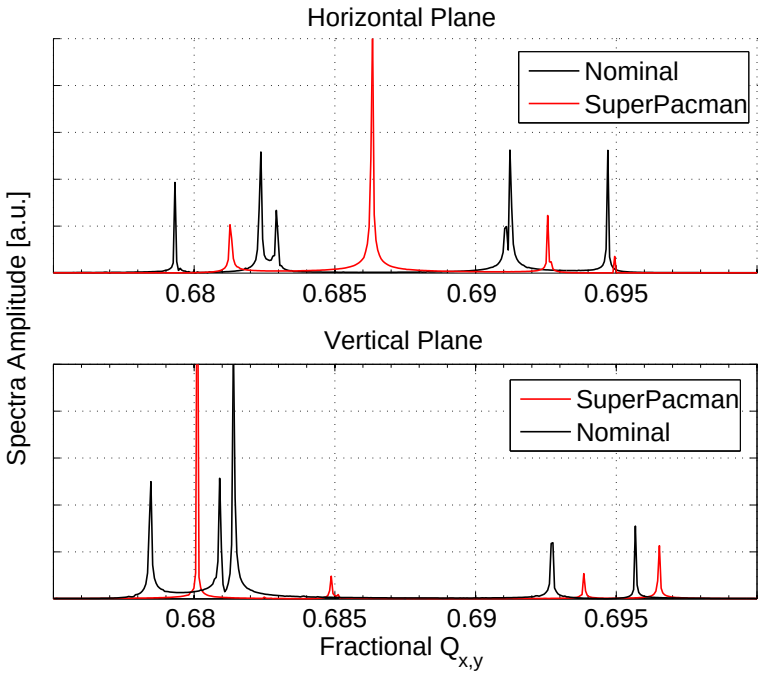

Figure 7.10: Horizontal (top) and vertical (bottom) tune spectra reproduced with the RBM for nominal (black lines) and Superpacman bunches (red lines).

measured at the pickup location. A Fourier analysis of the amplitude response for the different excitation frequencies (made in steps of 2×10^{-4} tune units) gives the amplitude and phase of the response. For the model inputs all measured parameters of the specific run and tunes of the two beams were taken from a BTF measurement. Figure 7.12 shows a BTF measurement result recorded just before the beams were brought in collision. The beam amplitude response is maximum at the the horizontal and vertical betatron frequencies. The peak locations of the spectrum yield the tunes of the beam Yellow (top) and Blue (bottom), respectively.

The measured tune distributions are compared to simulations of nominal and superpacman bunches as shown for the Yellow beam in Figure 7.13 and Figure 7.14. Exciting the beams with varying frequencies in the range of [0.67, 0.7] resonances start to appear with the underlying coherent modes absent in Figure 7.11. In the horizontal plane, for a nominal bunch (Figure 7.13 top), only the two extreme σ and π modes appear. The other two eigenfrequencies are too close to be distinguishable.

For the superpacman bunch (Figure 7.14, top), the intermediate mode, suppressed by Landau damping appears when excited with BTF. In this case the BTF tune distribution is closer to the superpacman bunch than for a nominal bunch. This is perhaps due to the fact that the measurement device is operated on a intensity threshold and is only able to measure the highest intensity bunches, i.e. bunches experiencing fewer number of collisions.

This argument is supported by single bunch intensity measurements as a function of the time in store performed during the same physics run and shown in Figure 7.16 bottom. In the figure an important intensity difference between the two families of bunches is visible.

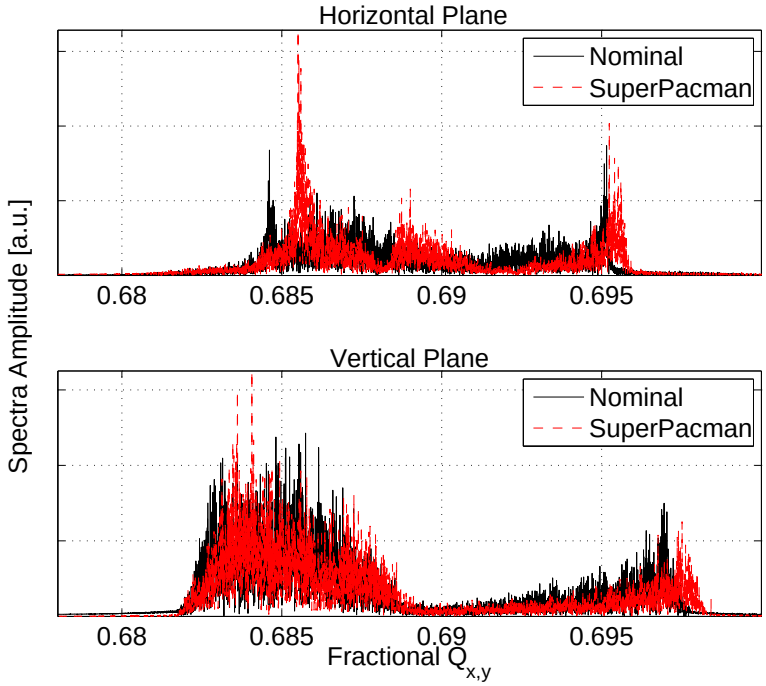

Figure 7.11: Horizontal (top) and vertical (bottom) tune spectra reproduced with the MPM for nominal (black lines) and Superpacman bunches (green and blue lines).

A part of the total intensity differences between the Yellow and Blue beams (Figure 7.16 top) for both beams bunches which undergo only one head-on collision (yellow and light blue lines in Figure 7.16 bottom) have higher intensity respect to those colliding twice at IP6 and IP8 (red and blue lines in Figure 7.16 bottom). Intensity variations between the two colliding beams (Figure 7.16, top) were not taken into account for this simulations. In the vertical plane, Figure 7.13 and Figure 7.14 (bottom), the tune distributions from measurements and simulations agree for both nominal and superpacman bunches. However, the superpacman bunches show a shift of the centroid distribution to higher tunes as in the case of the measurements Figure 7.14. The model and measured tune distributions from the Blue ring are plotted in Figure 7.15 for comparison which is a further confirmation of excitation of coherent modes in the vertical plane.

To study the intensity dependence, the BTF measurements were compared to simulations at the end of the physics run, of approximately 7 hours, for both beams. The bunch intensity decreased from 1.32×10^{11} to 1.06×10^{11} protons per bunch. Simulations and measurements show a good qualitative agreement in the location of the peaks for both beams. Figure 7.17 shows the amplitude response of beam Yellow while Figure 7.18 the response of beam Blue for the horizontal (top plots) and vertical (bottom plots) plane. One should notice for both horizontal and vertical planes the reduced tune spread due to the reduced beam intensities and therefore beam-beam strength ξ. Comparing the tune distributions at the beginning of the store and at the end we observe a reduction of the horizontal tune spreads from $\Delta Q_{x,initial} \approx 0.009$ to $\Delta Q_{x,final} \approx 0.006$. For the vertical plane we have the same effect and the reduction is from $\Delta_{y,initial} \approx 0.017$ to a final spread of $\Delta Q_{y,final} \approx 0.014$. This reduced tune spread is well modeled by the simulation results.

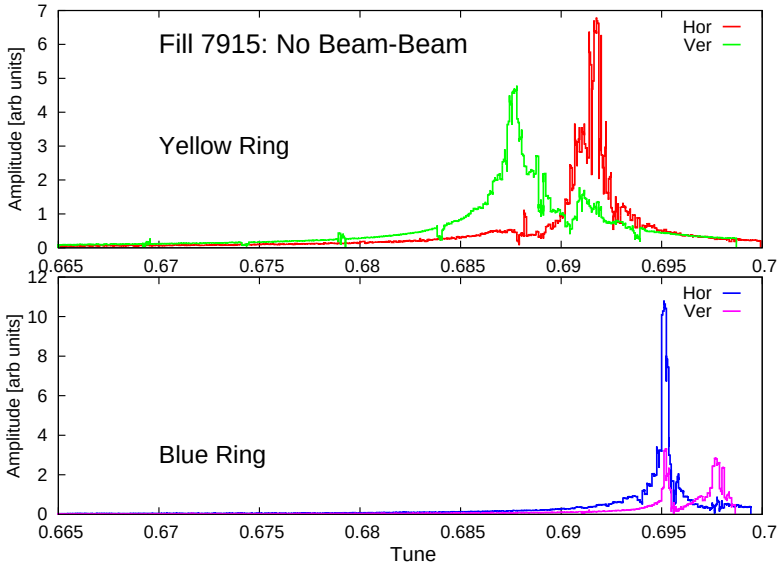

Figure 7.12: Measured amplitude response of the Yellow (top picture) and Blue (bottom picture) beam for RHIC fill 07915. The BTF measurements were taken at the beginning of the store without collisions (no beam-beam). Different colors are used to distinguish between horizontal and vertical components.

Also the locations of the resonant frequencies are reproduced by the model calculations. However, some features of the measurements are not explained such as the width of the peaks which could be strongly related to the bunch to bunch intensity and/or transverse size fluctuations.

One should always look at the results of both beams and both transverse planes to understand the dynamics behind it. One can in fact observe the linear coupling between the two transverse planes as well as the two beam coupling. Due to the transverse plane and two beam coupling the location of the eigenfrequencies could be swapped between the two planes and between the two beams, respectively. This is visible when comparing Figure 7.17 and Figure 7.18. For the horizontal-vertical coupling we should observe that the simulation results for the horizontal tune distribution of the Yellow beam (light blue line Figure 7.17 top) show a peak at a frequency of $Q \approx 0.698$ which is in reality the vertical tune as visible in the bottom picture (magenta line). While for the Yellow-Blue beam coupling one should notice that what is predicted with the model (red line of Figure 7.17 bottom) for the vertical tune distribution of Yellow beam is visible in measurements for the Blue beam (magenta line in Figure 7.18 bottom). For the model we have used a simple linear rotation in phase space along the arcs. The effects of the accelerator non linear imperfections are not taken into account in this study.

7.6 Summary

RHIC is a collider similar to the LHC from the point of view of the beam-beam interactions. It collides equally charged beams with similar parameters to those of the LHC and therefore, represents an interesting test bench for self consistent beam-beam studies. Although, the collision scheme is much simpler due to the reduced number of head-on col-

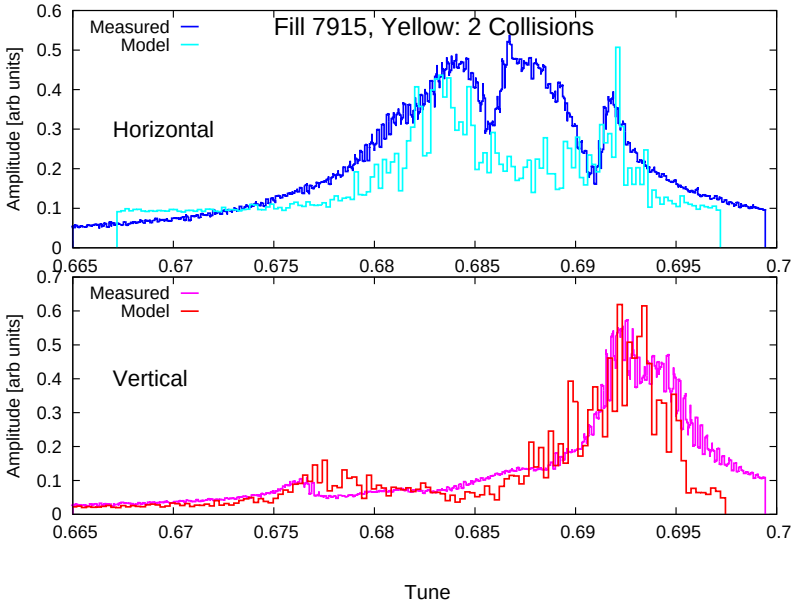

Figure 7.13: Measured and calculated with the MPM amplitude response of a nominal bunch in the Yellow ring for fill 07915. The BTF measurements were taken at the beginning of the store with the beams in collision.

lisions (just two instead of 4) and to the absence of any parasitic encounters, interesting features are still present which can help understanding the more complex LHC scheme later on during its operation.

Coherent effects have been studied and a bench mark of simulation with experimental data was possible. We have given a clear picture of the RHIC coherent beam-beam effects using all the tools available focusing on the superpacman bunches effects. With this study it was possible to explain features appearing during BTF measurements at store which could be calculated. Several BTF measurements had been reproduced and the agreement between model and measurements was good. The physical meaning and the dynamics behind are also understood. Some differences detected can be due to linear coupling between the two transverse planes or a transmission from beam to beam. However, to have a more realistic physical picture a study of chromatic effects should be included to have a quantitative estimate. One should expect an enlarging width of the peaks since it represents a mixing mechanism which can broaden the coherent mode.

A crucial result from the BTF measurements is a clear sign of differences between individual bunches undergoing different number of collisions, i.e. for colliders with pacman and for the case of RHIC with superpacman bunches. Due to non regular filling schemes and asymmetric collision patters, different bunches will show different tune distributions. To interpret the measurement it is essential to predict and understand the differences in order to evaluate measurements outputs.

An interesting proof is the excitation of coherent modes normally damped. Usually, coherent modes lying inside the incoherent tune spread do not appear in the tune spectra due to Landau damping mechanisms. However, when an exciting element is used they can resonantly be excited and develop even if inside the incoherent continuum. This is the case for BTF measurements as demonstrated which allows to study all coherent modes

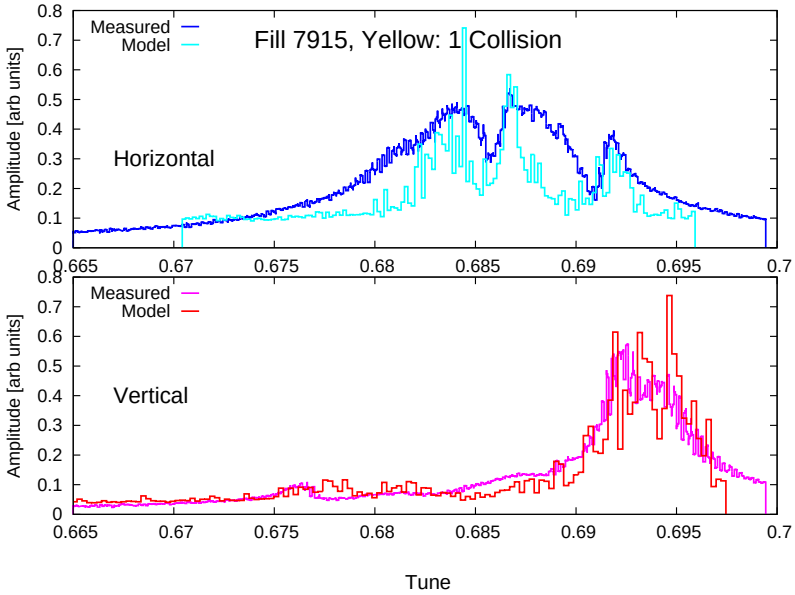

Figure 7.14: Measured and MPM amplitude response of a Superpacman bunch in the Yellow ring for fill 07915. The BTF measurements were taken at the beginning of the store.

otherwise damped. BTF measurements will enhance not only the unperturbed tunes of the machine but also all coherent modes due to the beam-beam coupling mechanism. Measurements can be understood with numerical simulations but only where they allow a multi-bunch beam structure and multiple interaction to reproduce intermediate modes rising from symmetry breaking.

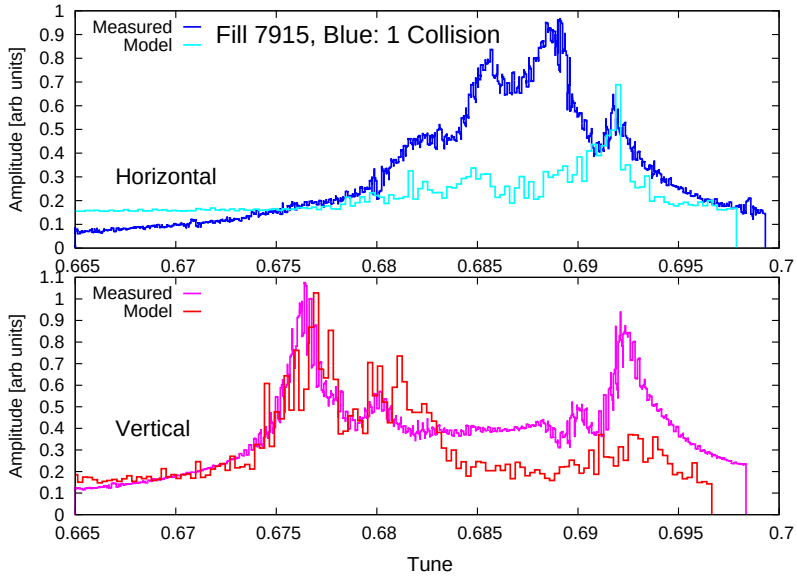

Figure 7.15: Measured and MPM results of the amplitude response of a Superpacman bunch in the Blue ring during fill 07915. The BTF measurements were taken at the beginning of the store.

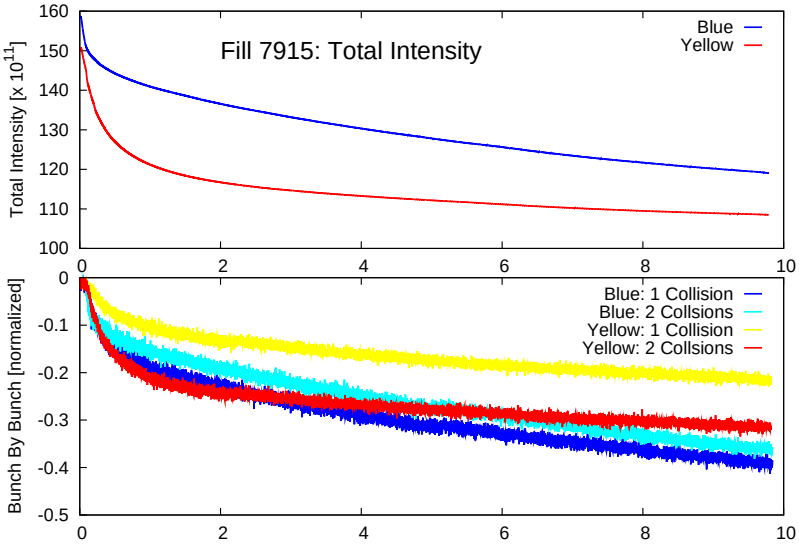

Figure 7.16: Total (top) and single bunch normalized (bottom) intensity as a function of time during Fill 7915. Top picture shows the evolution of intensity during collisions for the Yellow (red line) and Blue (blue line) beam. Bottom picture shows the bunch by bunch normalized intensity as a function of the time in store, nominal (2 collisions lines) and superpacman (1 collision lines) bunches are shown.

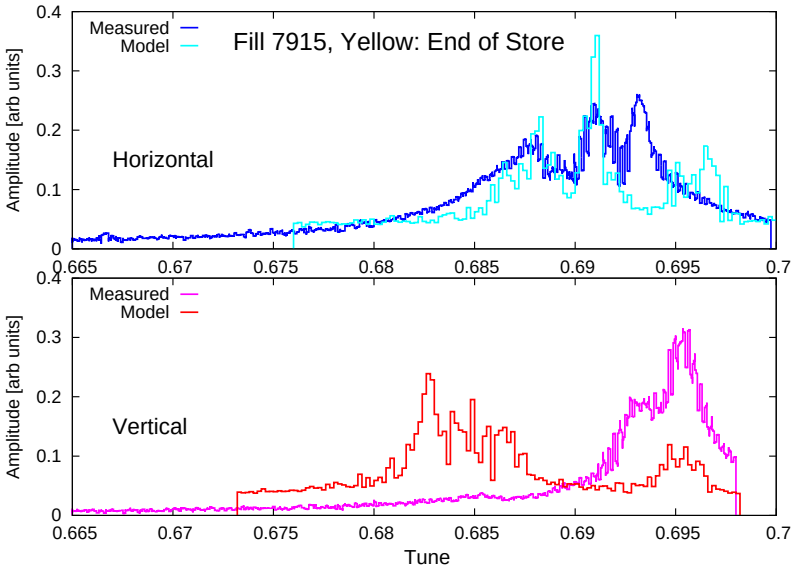

Figure 7.17: Measured and model amplitude response of a Superpacman bunch in the Yellow ring for fill 07915. The BTF measurements were taken at the end of the store.

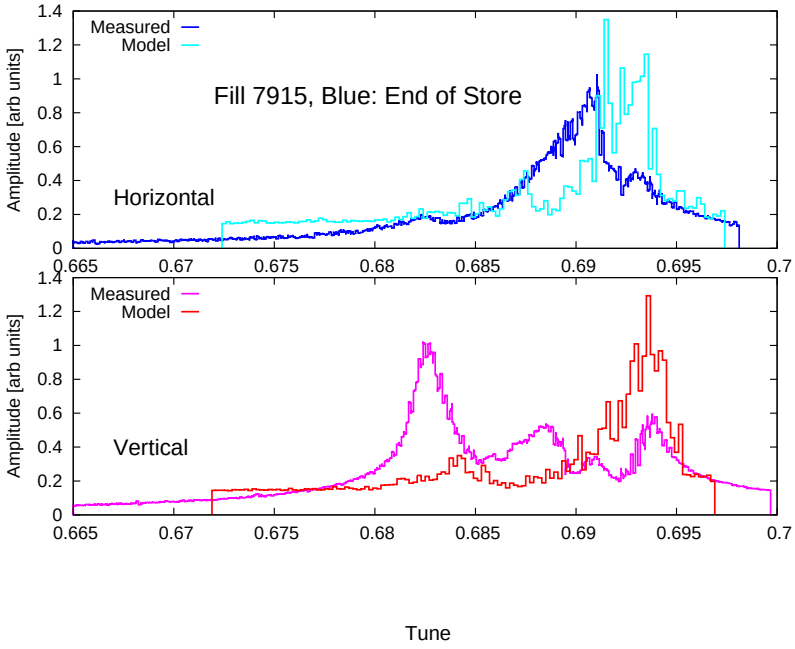

Figure 7.18: Measured and model amplitude response of a Superpacman bunch in the Blue ring for fill 07915. The BTF measurements were taken at the end of the store.

Chapter 8

Conclusions

We have investigated the feasibility of modeling and predicting multiple bunch beam behavior undergoing many beam-beam interactions as for the case of hadron colliders. The argument had been assessed from detailed modeling, numerical studies and experimental validations. We can divide the studies into four main parts:

Beam-beam Models

Three different and complementary models were developed with the goal to reproduce and understand different beam-beam effects for the case of multiple head-on and long range beam-beam interactions for beams with many bunches.

The Analytical Linear Model (ALM) describes the bunches as point like harmonic oscillators coupled through a linearized beam-beam interaction. Solutions of the eigenvalue problem of the one turn matrix give information on the eigenfrequencies of the coupled system and the eigenvectors represent possible oscillating patterns of the bunches. The eigenfrequencies locate the number and frequencies at which coherent modes can occur, the eigenvectors give information on the oscillating pattern. With a one turn matrix method we can define tune spectra and single bunch contributions to the multiple bunch coupling.

The Rigid Bunch Model (RBM) simulates bunches as point like objects but with variable centroid positions and the beam-beam interaction is assumed as analytically found for Gaussian distributions. The bunch centroid motion gives information on the coherent oscillation of each single bunch. Due to the rigid description of the beams it is possible to define the whole spectrum of a bunch since no damping mechanisms are present. For the ALM and the RBM this is a deliberate feature.

The Multi Particle Model (MPM) simulates the beams as a distribution of macro-particles. The field calculation uses two different algorithms the "Soft Gaussian" approximation which assumes a Gaussian distribution for the particles and the Hybrid Fast Multiple Method for any arbitrary distribution of particles. With the MPM we can riproduce the bunch tune spectra in a correct quantitative approach since all non-linearities as well as the bunch properties evolve in a fully self-consistent treatment. In addition to the study of coherent effects it also allows to investigate incoherent beam-beam effects (i.e. emittances evolution). The MPM parallel version allows to extend all studies to the case of beams with a vary large number of bunches and with many beam-beam interactions.

Coherent Effects

With the three complementary models we have shown how to interpret coherent modes

developed for a generic hadron collider with variable filling schemes as well as collision patterns. Due to asymmetric collisions the oscillating spectra became complex and the appearance of Pacman (bunches missing a long range BBI) as well as Superpacman (bunches missing a head-on collision) bunches show differences in the tune spectrum. We have demonstrated how to predict the degeneracy of coherent modes by using the ALM eigenvectors for various scenarios. The damping of intermediate modes inside the incoherent continuum had been shown to apply for all cases. However, due to the symmetry of the collision scheme from head-on collisions, some modes may be outside the damping region and therefore one should expect the presence of intermediate spectral lines. We have also shown how the Landau damping mechanisms does not apply equally to head-on and long range interactions since in the last case the modes are developed by the bunches tails and therefore a smaller number of particles are available to extract energy from the mode.

The Large Hadron Collider (LHC)
For the LHC case which had triggered these studies we have looked at incoherent as well as coherent effects. For the incoherent effects we have studied the beam transverse emittance behavior when a small static offset is present at the collision point. This occurs due to long range interactions. An emittance growth had been found. This growth for the nominal LHC case does not represent a detrimental effect. However, the growth increase for smaller beam r.m.s. size and higher intensity bunches. These results should be considered when the accelerator performances will be pushed for higher luminosity. The betatron frequency was found to be the most crucial parameter. A betatron frequency closer to the third integer resonance affects strongly the growth rate. For the LHC this is the case for the vertical tune. The physical mechanism of the growth was characterized and understood. The dependency of the growth on the offset amplitude shows a characteristic trend which had been explained as due to the effect of the beam-beam non-linearities weighted over the particle amplitude distribution. For the coherent modes we have simulated a representative LHC case with up to 36 bunches per beam. We have studied the effect of the phase advance symmetries on the spectra for the case of head-on only and for the case when few long range interactions are added. We demonstrated that a fully symmetrical phase advance between the interaction points will lead to a reduction of the intermediate frequencies. However, one should expect a part of the extreme σ and π modes a non damped between the end of the incoherent continuum of frequencies and the coherent π mode frequency.

The Relativistic Heavy Ion Collider (RHIC) Coherent Modes
The numerical and analytical models developed had been used to study RHIC at Brookhaven National Laboratory. Coherent modes at RHIC had been described by using the tools developed. The aim was to explain observations obtained with Beam-beam Transfer Function (BTF) measurements. Measurements had been reproduced and numerical results and experimental data show a good agreement in the amplitude response of the beam to an external excitation. We have demonstrated the resonant appearance of coherent modes, normally Landau damped, when excited by an excitation as during BTF measurements. The loss of Landau damping had been defined when an excitation is applied. In addition we have demonstrated the particular effect of Superpacman bunches on the measurement result. Different bunch families show different amplitude responses. We have demon-

strated that the measurement device was actually measuring a Superpacman bunch and not a nominal one as thought. For this reason a gating of the measurement system to the bunch number had been suggested in order to obtain the nominal operational scenario.

In summary, we developed and tested new tools which improve the predictive power of beam-beam calculations for the case of multi bunch beams. Furthermore, these tools allow to understand better the experimental and numerical results in terms of the underlying physics phenomena and will be of help to understand and improve the performance of the LHC.

Bibliography

[1] LHC Beam-Beam Studies; *http://cern.ch/lhc-beam-beam.*

[2] W. Herr; *Dynamic behaviour of nominal and PACMAN bunches for diffarent LHC crossing schemes*, LHC Project Note 856, CERN (2005).

[3] W. Herr, D. Kaltchev, E. McIntosh and F. Schmidt; *Large scale beam-beam simulations for the CERN LHC using distributed computing resources*, LHC Project Report 927, CERN(2006) and Proc. EPAC'06, Edinburgh, UK, June 26-30, 2006.

[4] Y. Luo and F. Schmidt, *Weak-Strong Beam-Beam Tracking for LHC V6.0*, Proc. Workshop on Beam-Beam Effects, Fermilab, June 2001.

[5] MADX Webpage: http://mad.web.cern.ch/mad/.

[6] Courtesy of W. Herr and D. Kaltchev

[7] W. Herr; *Tune shifts and spreads due to short and long range beam-beam interactions in the LHC*, CERN-SL-90-06-AP ; LHC-NOTE-119, 1990.

[8] S.Y. Zhang and V. Ptitsyn; *Proton Beam Emittance Growth at RHIC*, Proceedings of PAC07, Albuquerque, New Mexico, USA, 2007.

[9] W. Herr, Private communication, 2008.

[10] Y. Alexahin; *A study of the coherent beam-beam effect in the framework of the Vlasov perturbation theory*, Nucl. Inst. and Meth. in Phys. Res. A **380** (2002) 253.

[11] K. Yokoya and H. Koiso; *Tune shift of coherent beam-beam oscillations*, Part. Acc. Vol.**27** (1990) 181.

[12] R.W. Hockney and J.W. Eastwood; *Computer Simulation Using Particles*, Institute of Physics Publishing Bristol and Philadelphia, 1988.

[13] P. Collier; *New base line proton filling scheme*, Minutes of the 2nd LHC Technical Committee, 19.2.2003 (2003).

[14] M. Ferro-Luzzi, W. Herr and T. Pieloni; *LHC bunch filling schemes for commissioning and initial luminosity optimization*, CERN-LHC-Project-Note-415, 2008.

[15] W. Fischer; Private communication.

[16] W. Herr, B. Goddard, E. Keil, M. Lamont, M. Meddahi and E. Peschardt; *Experience with bunch trains in LEP* CERN-SL-97-035-AP, Geneva, (1998).

[17] K. Ohmi et al.; *Beam-Beam Effect with an External Noise in LHC*, Proceedings of PAC07, Albuquerque, New Mexico, USA, 2007.

[18] S.Y. Zhang and V. Ptitsyn; *Proton Beam Emittance Growth at the Relativistic Heavy Ion Collider*, Phys. Rev. ST Accel. Beams **11**, 051001, (2008).

[19] R. Littauer, *Proposal for Multi-Bunch Operation of CESR*, IEEE Trans. Nucl. Sci., NS-32, **5**, p. 1610-1613, 1985.

[20] J.D. Jackson;*Classical Electrodynamics*, John Wiley & Sons, New York, NY, 1962.

[21] A. Chao; *The beam-beam instability*, SLAC-PUB-3179 (1983).

[22] L. Evans; *The beam-beam interaction*, CAS Course on proton-antiproton colliders, in CERN 84-15 (1984).

[23] E. Keil; *Beam-beam dynamics*, CERN Accelerator School, Rhodes 1993, CERN 95-06 (1995).

[24] W. Herr; *Beam-beam Interactions*, Lecture at CAS, Zeuthen (2003).

[25] K. Schindl; *Space Charge*, Lecture at CAS, Zeuthen (2003).

[26] A.G. Webster; *Partial Differential Equations of Mathematical Physics*, New York, Hafner Publishing Company, (1950).

[27] I. Bronstein et al.; *Taschenbuch der Mathematik*, Verlag Harri Deutsch, (2001).

[28] O.D. Kellog; *Foundations of Potential Theory*, Dover, New York, U.S.A. (1953).

[29] M. Basetti and G.A. Erskine; *Closed expression for the electrical field of a 2-dimensional Gaussian charge*, CERN-ISR-TH/80-06 (1980).

[30] S. Kheifets; PETRA-Kurzmitteilung 119 (DESY 1976).

[31] A. Chao; *Lie Algebra techniques for Nonlinear Dynamics*, SLAC-PUB-9574 (2002).

[32] J. E. Campbell; *Proc. London Math. Soc.*, 29, 14 (1898)

[33] W. Herr; *Concept of Luminosity*, Lecture at CAS, Zeuthen 2003.

[34] H. Grote, F. Schmidt and L.H.A. Leunissen; *LHC Dynamic Aperture at Collision*, LHC Project Note 197, Geneva, August 1999.

[35] B. Richter; Proc. Int. Sym. Electron and Positron Storage Rings, Savlay,1966, page I-1-1.

[36] A. Piwinski; *Observation of beam-beam effects in PETRA*, IEEE Trans. Nucl. Sc., **NS-26**, 4268 (1979).

[37] R.E. Meller and R.H. Siemann; IEEE Trans. Nucl. Sc., **NS-28**, 2431 (1981).

[38] Y. Alexahin; *On the Landau damping and decoherence of transverse dipole oscillations in colliding beams*, Part. Acc. **59**, 43 (1996).

[39] K. Hirata;*Coherent betatron oscillation modes due to beam-beam interactions*, Nucl. Inst. and Meth. in Phys. Res. A **269** (1988) 7.

[40] W. Herr and M.P. Zorzano; *Coherent dipole modes for multiple interaction regions*, CERN LHC Project Report 462 (2001).

[41] E. Keil; *Coherent beam-beam effect in machines with unequal betatron phase advances between crossing points*, LEP Note 226, unpublished, (1980).

[42] W. Herr; *Consequences of Periodicity and Symmetry for the Beam-Beam Effects in the LHC*, LHC Project Report 49 (1996).

[43] W. Herr; *Effect of missing head-on collisions on beam-beam effects in the LHC*, LHC Project Note 321 (2003).

[44] W. Herr; *Effects of PACMAN bunches in the LHC*, LHC Project Report 39 (1996).

[45] H. Grote; *Self-consistent orbits with beam-beam effects in the LHC*, Proc. of EPAC 2000, Vienna, 26. - 30. 6. 2000, (2000), 1202.

[46] H. Grote and W. Herr; *Self-consistent orbits with beam-beam effects in the LHC*, Proc. of the 2001 workshop on beam-beam effects, FNAL, 25.6.-27.6.2001, (2001).

[47] EPFL MIZAR Cluster webpage; *http://mizar.epfl.ch*.

[48] EPFL BlueGene Cluster webpage; *http://bg1.epfl.ch*.

[49] W. Herr; *Coherent Beam-Beam Effects in the LHC*, LHC-Project-Report-469 ; CERN-LHC-Project-Report-469, Geneva,CH (2001).

[50] W. Herr; *Computer simulation of the coherent beam-beam effect in the LHC*, Proceedings of the 1991 Part. Acc. Conf., San Francisco, U.S.A, May 6-9, 1991, p. 1068 (1991).

[51] W. Herr; *Coherent dipole oscillations and orbit effects induced by long range beam-beam interactions in the LHC*, CERN SL/91-34 (AP) and LHC Note 165 (1991).

[52] W. Herr; *Spectra of multiple bunches coupled by head-on and long range beam-beam interactions*, LHC Note 356 (2004).

[53] W. Herr and T. Pieloni; *Coherent beam-beam modes in the CERN Large Hadron Collider for multiple bunches, different collision schemes and machine symmetries*, Proc. First CARE-HHH-APD Workshop on Beam Dynamics in Future Hadron Colliders and Rapidly Cycling High-Intensity Synchrotrons, CERN, Geneva 8-10 November 2004, also CERN 2005-006 Yellow Book.

[54] W. Herr, M.P. Zorzano, and F. Jones; *A hybrid fast multipole method applied to beam-beam collisions in the strong-strong regime*, Workshop on Beam-beam Effects Beam-beam Effects , Fermilab, Batavia, IL, USA , 25 - 28 Jun 2001.

[55] In collaboration with W. Fischer and R. Calaga at Brookhaven National Laboratory.

[56] G. Arduini, W. Herr, E. Metral and T. Pieloni; *Alternative bunch filling schemes for the LHC*,CERN-LHC-Project-note-401, 2007.

[57] W. A. Chao; *Physics of Collective Beam Instabilities in High Energy Accelerators*, Ch.5, John Wiley & Sons Inc, 1993.

[58] J. Borer, G. Guignard, A. Hofmann et al.; *Information from beam response to longitudinal and transverse excitation* IEEE Transaction on Nuclear Science, Vol. NS-26, No. 3, June 1979.

[59] M.P. Zorzano and F. Zimmermann; *Simulations of coherent beam-beam modes at the Large Hadron Collider*, Phys. Rev. ST Accel. Beams 3, 044401 (2000).

[60] L. Evans and J. Gareyte; *Beam-beam effects*, CERN Accelerator School, Oxford 1985, CERN 87-03 (1987).

[61] A. Zholents; *Beam-beam effects in electron-positron storage rings*, Joint US-CERN School on Particle Accelerators, in Springer, Lecture Notes in Physics, **Vol.400** (1992).

[62] M. Meddahi; *Effets faisceau-faisceau dans le collisionneur proton-antiproton du SPS*, PhD Thesis, Universite de Paris VII (1991).

[63] B. Goddard, W. Herr, E. Keil, M. Lamont, M. Meddahi and E. Peschardt; *Bunch trains for LEP*, Particle Accelerators **57**, 237 (1998).

[64] J.T. Seeman; *Observations of the beam-beam interaction*, Lecture Notes in Physics, **Vol. 247**, Springer, (1986).

[65] S. Myers; IEEE Trans. Nucl. Sc., **NS-28**, 2503 (1981).

[66] S. Myers; *Review of beam-beam simulations*, Lecture Notes in Physics, **Vol. 247**, Springer, (1986).

[67] D. Brandt et al.; *Is LEP beam-beam limited at its highest energy ?*, Proceedings of the Particle Accelerator Conference 1999, New York, (1999) p. 3005.

[68] T. Sen et al.; *Effect of the beam-beam interactions on the dynamic aperture and amplitude growth in the LHC*,Proceedings of the workshop on beam-beam effects in large hadron colliders, LHC99, Geneva, 12-17 April, 1999, CERN-SL-99-039 (AP) (1999) p. 85.

[69] Y. Papaphilippou and F. Zimmermann; *Weak-strong beam-beam simulations for the LHC*, Proceedings of the workshop on beam-beam effects in large hadron colliders, LHC99, Geneva, 12-17 April, 1999, CERN-SL-99-039 (AP) (1999) p. 95.

[70] Y. Luo and F. Schmidt; *Dynamic aperture studies for LHC optics version 6.2 at collision*, CERN LHC Project Note 310 (2003).

[71] W. Herr; *Features and implications of different LHC crossing schemes*, LHC Project Report 628 (2003).

[72] J. Wenninger, private communication.

[73] J.P. Koutchouk; *ISR Performance Report - A numerical estimate of the coherent beam-beam effect in the ISR*, CERN ISR-OP/JPK-bm (1982).

[74] K. Hirata; Nucl. Instr. and Meth. **A 269**, 7 (1988).

[75] A. Hofmann and S. Myers; CERN LEP Note 604 (1988).

[76] W. Herr, *Computational Methods for beam-beam interactions, coherent effects*, Lecture at CERN Accelerator School, Sevilla (2001), at http://cern.ch/lhc-beam-beam/talks/comp2.ps.

[77] A. Hofmann; *Landau damping*, Lecture at CAS, Zeuthen (2003).

[78] Y. Alexahin, H. Grote, W. Herr and M.P. Zorzano; *Coherent beam-beam effects in the LHC*, Presented at HEACC 2001, Tsukuba, Japan, CERN LHC Project Report 466 (2001).

[79] A. Hofmann; *Beam-beam modes for two beams with unequal tunes*, Proceedings of the workshop on beam-beam effects in large hadron colliders, LHC99, Geneva, 12-17 April, 1999, CERN-SL-99-039 (AP) (1999) p. 56.

[80] Y. Alexahin and M.P. Zorzano; *Excitation of coherent beam-beam resonances for beams with unequal tunes in the LHC*, CERN LHC Project Note 226 (2000).

[81] E. Keil and K. Hirata; *Linear beam-beam resonances due to coherent dipole motion*, Part. Acc. **56**, 13 (1996).

[82] W. Herr; *Computational Methods for beam-beam interactions, incoherent effects*, Lecture at CERN Accelerator School, Sevilla (2001), at http://cern.ch/lhc-beam-beam/talks/comp1.ps.

[83] W. Herr and R. Paparella; *Landau damping of coherent modes by overlap with synchrotron sidebands*, CERN LHC Project Note 304 (2002).

[84] V.D. Shiltsev et al.; *Compensation of beam-beam effects in the Tevatron Collider with electron beams*, In Proceedings of the Particle Accelerator Conference 1999, New York, (1999), p. 3728.

[85] V.D. Shiltsev et al.; *Considerations on compensation of beam-beam effects in the Tevatron with electron beams*, Phys. Rev. ST Accel. Beams **2**, 071001 (1999).

[86] J.P. Koutchouk et al.; *Correction of the Long-Range Beam-Beam Effect in LHC using Electro-Magnetic Lenses*, In Proceedings of the Particle Accelerator Conference 1999, New York, (1999) (1999) p. 1681.

[87] R. Talman; *A proposed Möbius accelerator*, Phys. Rev. Lett. **74**, 1590 (1995).

[88] S. Henderson et al.; *Investigation of the Möbius accelerator at CESR*, CBN 99-5 (1999).

[89] A. Chao, P. Bambade and W. Weng; *Non-linear beam-beam resonances*, Lecture Notes in Physics, **Vol. 247**, Springer, (1986).

[90] K. Hirata and E. Keil; *Barycentre motion of beams due to beam-beam interactions in asymmetric ring colliders*, Nucl. Inst. and Meth. in Phys. Res. A **292** (1990) 156.

[91] W. Herr; *Particle tracking with MAD-X including LHC beam-beam interactions*, to be published (2004).

[92] W. Herr, M.P. Zorzano and F. Jones; *A hybrid fast multipole method applied to beam-beam collisions in the strong-strong regime*, Phys. Rev. ST Accel. Beams **4**, 054402 (2001).

[93] R. Garoby; *Base line proton filling scheme with 72 bunches*, Minutes of the 59th LHC Parameters and Layout Committee, 12.4.2000. (2000).

[94] M. Bassetti and G. A. Erskine; CERN-ISR-TH/80-06, 1980.

[95] A. Hofmann; *Beam-Beam Modes for two beams with unequal Tunes* CERN-ISR-TH/80-06, 1980.

[96] LHC Design Report; CERN-2004-003, (2004).

[97] W. Herr; *Beam-Beam Effects in the LHC*, Particle Accelerators, **50**,69-81 (1995) and CERN SL/94-92 (AP) (1994).

[98] O. Brüning, W. Herr and R. Ostojic; *A beam separation and collision scheme for IP1 and IP5 at the LHC for optics version 6.0*, LHC Project Report 315 CERN, (1999).

[99] O. Brüning, W. Herr and R. Ostojic; *A beam separation and collision scheme for IP2 and IP8 at the LHC for optics version 6.0*, LHC Project Report 367 CERN, (1999).

[100] W. Fischer et al.; *Observation of coherent beam-beam modes in RHIC*, Proceedings of Particle Accelerator Conference 2003, Portland, Oregon, U.S.A. (2003) and BNL C-AD/AP/75 (2002).

[101] K. Yokoya; *Limitation of the Gaussian approximation in beam-beam simulations*. Phys. Rev. ST-Accel. Beams, Vol. **3**, 124401 (2000).

[102] S. Krishnagopal and R. Siemann; *Coherent beam-beam interactions in electron-positron colliders*. Phys. Rev. Lett., Vol. **67**, 2461 (1991).

[103] W. Herr and T. Pieloni; *Spectra of multiple bunches coupled by head-on and long range beam-beam interactions*, Proceedings of Particle Accelerator Conference 2005, Knoxville, Tennessee, U.S.A. (2005).

[104] J. Qiang et al.; *Terascale beam-beam simulations for Tevatron, RHIC and LHC*, Proc. PAC 2005, Knoxville, U.S.A. (2005).

[105] J. Qiang et al.; *Strong-strong beam-beam simulation using a Green function approach*, Phys. Rev. ST-Accel. Beams, **5**, 104402, (2002).

[106] J. Qiang et al.; *A parallel particle-in-cell model for beam?beam interaction in high energy ring colliders*, J. Comput. Phys. Vol. **198**, 278 (2004).

[107] L. Greengard; *The rapid evaluation of potential field in particle systems*. Thesis, Yale (1987), Cambridge, Mass. MIT Press, 1988.

[108] L. Greengard and V. Rokhlin; *A fast algorithm for particle simulations*. J. Comput. Phys. Vol. **73**, (1987).

[109] B. Muratori, CERN; *Study of offset collisions and beam adjustment in the LHC using a strong-strong simulation model*, LHC Project Report 593 *and* Proc. EPAC 2002, Paris 2002 (2002).

[110] W. Herr and F. Jones; *Parallel computation of beam-beam interactions including longitudinal motion*, Proceedings of Particle Accelerator Conference 2003, Portland 12.- 16. May 2003 (2003), CERN-AB-2003-019-ABP (2003).

[111] W. Herr and T. Pieloni; *Models to study multi bunch coupling through head-on and long-range beam-beam interactions*, CERN LHC Project Note 937 (2006).

[112] W. Herr and T. Pieloni; *Coherent Beam-Beam Modes in the CERN Large Hadron Collider (LHC) for Multiple Bunches, Different Collisions Schemes and Machine Symmetries*, Proceedings of Particle Accelerator Conference 2005, Knoxville, Tennessee, U.S.A. (2005).

[113] T. Pieloni; *Strong-strong beam-beam simulations*, Proceedings of ICAP 2006, Chamonix, France (2006).

[114] W. Fischer; Private comunication.

[115] T. Pieloni and W. Herr; *Models to study multi bunch coupling through head-on and long-range beam-beam interactions*, CERN LHC Project Report 937 and Proceedings of EPAC06, Edinburgh, United Kindom, 2006.

[116] F. Jones, W. Herr and T. Pieloni; *Parallel Beam-Beam Simulation Incorporating Multiple Bunches and Multiple Interaction Regions*, CERN-LHC-PROJECT-Report-1038 and Proceedings of Particle Accelerator Conference 2007, Albuquerque, New Mexico, USA (2007).

[117] W. Fischer, M. Blaskiewicz, R. Calaga, P. Cameron, Y. Luo and T. Pieloni; *Transverse Beam Transfer Functions of Colliding Beams in RHIC*, Proceedings of PAC07, Albuquerque, New Mexico, USA (2007).

[118] M.P. Zorzano and T. Sen; *Emittance Growth of the LHC Beam due to the effect of Head-on Beam-Beam Interaction and Ground Motion*, Proceedings of EPAC 2000, Vienna, Austria (2000).

[119] F. Zimmermann et al.; *Accelerator Physics Code Web Repository*, 10th European Particle Accelerator Conference (EPAC06), June 26-30, Edinburgh, United Kingdom, (2006) also as CERN-LHC-Project-Report-943.

CURRICULUM VITAE

Tatiana Pieloni

PERSONAL DATA

Nationality:	Italian	*Address:*	31, Rue des Bains
Date of birth:	25 April 1975		1205 Geneva
Place of birth:	Cernusco Naviglio (MI), Italy		Switzerland
S*ex:*	Female	*Phone:*	0041 76 460 8031
Civil status:	Single	*E-mail:Tatiana.Pieloni@cern.ch*	

EDUCATION

2008	Foreseen PhD in Physics at the **Ecole Polytechnique Federale de Lausanne (EPFL), CH,** joint between the Laboratory for High Energy Physics (LPHE) and the Laboratory for Particle Accelerator Physics (LPAP), *A study of beam-beam effects in hadron colliders with a large number of bunches.*
July 2004	Master Degree (Laurea) in Physics at the **Università degli Studi di Milano**, Italy. *An empirical scaling law for the sextupole and decapole snap-back compensation in the Large Hadron Collider (LHC)*

SPECIALIZATION COURSES

Sept 2005	*Cern Accelerator School (CAS), Accelerator Physics Intermediate level,* with final examination passed for EPFL PhD credit validation.
June 2005	*Elementary particles I and II,* by Prof. A Bay, EPFL post graduate course.
Oct 2004	*Cern Accelerator School (CAS), Accelerator Physics Basic level.*
Jan 2003	*Joint Universities Accelerator School (JUAS), Accelerator Physics course.*

LANGUAGES

Italian	Mother tongue.		
English	Reading: Very good.	Speaking: Very good.	Writing: Very good.
French	Reading: Fair.	Speaking: Fair.	Writing: Fair

SOFTWARE KNOWLEDGE

Systems	*Linux, Windows* and Mac OS X.
Languages	*Fortran77, C-C++ languages, Matlab-based programming, HTML, MPI protocol and LabView.*

Tools	*Microsoft Office, Matlab, Mathematica, Gnuplot, LaTex and Emacs.*
Beam dynamics:	*MADX, co-author of COMBI the COherent Multi-bunch Beam-beam Interaction code and SIXTRACK for beam-beam studies.*

WORK EXPERIENCES

Since 07/2004 **European Organization for Nuclear Research (CERN)**, Geneva (Switzerland): Doctoral Student in the AB-ABP-RLC section. Supervisors: Dr. **W. Herr** (CERN), Prof. **A. Bay** (EPFL) and Prof. **L. Rivkin** (EPFL).

01/2003-06/2004 **European Organization for Nuclear Research (CERN)**, Geneva (Switzerland): Technical Student in AT-MTM-AS section. Supervisors: Dr. **L. Bottura** (CERN), and Prof. **L. Rossi** (INFN-LASA Milan).

06/2002-12/2002 **INFN LASA,** Milan (Italy) and **CERN**: *Stagier* in AT-MTM-AS section. Supervisors: Dr. **L. Bottura** (CERN) and Prof. **G. Bellomo** (LASA).

OTHER EXPERIENCE AND COLLABORATIONS

- **EPFL-TRIUMF-CERN collaboration for beam-beam studies.**

Contact: Dr. F. Jones (TRIUMF) and Prof. A. Bay (EPFL)
Date: since May 2006
Parallel processing studies and code migration to EPFL multiple processor clusters (MIZAR and IBM BlueGene) for multiple bunches beam-beam simulations.

- **CERN Neutrino beam to Gran Sasso project (CNGS)**.

Contact: Dr. M. Meddahi
Date: Summer 2006
Optics studies for the CNGS beam line (orthogonal steering on target). Analysis of beam size and position measurements and comparison to theoretical for commissioning.

- **CERN-FERMILAB collaboration for snapback compensation.**

Contact: Dr. P. Bauer
Date: 2003/2004
Analysis of dynamic effects in the TEVATRON superconducting magnets and comparison with respect to the LHC main dipole magnets.

- **EPFL Accelerator Physics Course .**

Contact: P. Bryant
Date: Fall Academic year 2006 and 2007
Professor Assistant for the accelerator physics course.

- **Joint University Accelerator School**

Contact: P. Bryant
Date: Since year 2007
Lecturing "Accelerator Design" course.

- **Brookhaven National Laboratory**

Contact: W. Fischer
Date: May 2007
Beam transfer measurements analysis and modeling.

LIST OF PUBLICATIONS

Collective effects and Beam dynamics:

- M. Ferro-Luzzi, W. Herr and T. Pieloni; *LHC bunch filling schemes for commissioning and initial luminosity optimization*, CERN-LHC-Project-Note-415, 2008.

- G. Arduini, W. Herr, E. Metral and T. Pieloni; *Alternative bunch filling schemes for the LHC*, CERN-LHC-Project-note-401, 2007.

- F .Jones, W, Herr and T. Pieloni; *Parallel Beam-Beam Simulation Incorporating Multiple Bunches and Multiple Interaction Regions*, CERN-LHC-PROJECT-Report-1038 and Proceedings of PAC07, Albuquerque, New Mexico, USA, 2007

- W. Fischer, M. Blaskiewicz, R. Calaga, P. Cameron, Y. Luo and T. Pieloni; *Transverse Beam Transfer Functions of Colliding Beams in RHIC*, Proceedings of PAC07, Albuquerque, New Mexico, USA, 2007.

- T. Pieloni; *Strong-strong beam-beam simulations*, Proceedings of ICAP 2006, Chamonix, France (2006).

- T.Pieloni and W.Herr; *Models to study multi bunch coupling through head-on and long-range beam-beam interactions*, CERN-LHC-Project-Report-937 and Proceedings of EPAC06, Edinburgh, United Kindom, 2006.

- W. Herr and T. Pieloni; *Models to study multi bunch coupling through head-on and long-range beam-beam interactions*, CERN LHC~Project Note~937 (2006).

- F. Zimmermann et al.; *Accelerator Physics Code Web Repository*, 10th European Particle Accelerator Conference (EPAC06), June 26-30, Edinburgh, United Kingdom, (2006) also as CERN-LHC-Project-Report-943.

- W. Herr and T. Pieloni; *Spectra of multiple bunches coupled by head-on and long range beam-beam interactions*, Proceedings of Particle Accelerator Conference 2005, Knoxville, Tennessee, U.S.A. (2005).

- W.Herr and T. Pieloni; *Coherent Beam-Beam Modes in the CERN Large Hadron Collider (LHC) for Multiple Bunches, Different Collisions Schemes and Machine Symmetries*, Proceedings of Particle Accelerator Conference 2005, Knoxville, Tennessee, U.S.A. (2005).

- W. Herr and T. Pieloni; *Coherent beam-beam modes in the CERN Large Hadron Collider for multiple bunches, different collision schemes and machine symmetries*, Proc. First CARE-HHH-APD Workshop on Beam Dynamics in Future Hadron Colliders and Rapidly Cycling High-Intensity Synchrotrons, CERN, Geneva 8-10 November 2004, also CERN 2005-006 Yellow Book.

Cern Neitrino beam to Gran Sasso project:.

- T. Pieloni; and E. Meier; *Orthogonal Steering of the CNGS Beam on Target*, LHC-ABP-Note, to be published.

- T. Pieloni and R. Calaga; *Optics model expectation versus BTVs and BPMs beam sizes and positions along the CNGS beam line during commissioning*, LHC-ABP-Note, to be published.

Superconducting magnets.

- N. Sammut, L. Bottura, P. Bauer, T. Pieloni, J. Micallef; *Mathematical formulation to predict the harmonics of the superconducting Large Hadron Collider magnets; 2, Dynamic field changes and scaling laws*, Physic. Rev. Spec. Top. Accel. Beams 10, (2007).

- N. Sammut et al.; *A Hall Plate Based Instrument to Measure the Snapback in the LHC Superconducting Dipole Magnets*, IEEE Instrumentation and Measurement Technology Conference, April 24-27, Sorrento, Italy (2006).

- L. Bottura, T. Pieloni, and N. Sammut; *Scaling Laws for the Field Quality at Injection in the LHC Dipoles*, CERN-LHC-Project-Note-361, (2004).

- G. Ambrosio, P. Bauer, L. Bottura, M. Haverkamp, T, Pieloni, S. Sanfilippo, G. Velev; *A scaling Law for the Snapback in Superconducting Accelerator Magnets*, IEEE Trans. Appl. Supercond.: 15 (2005) no.2, pp1217-1220.

- T. Pieloni, L. Bottura, S. Sanfilippo, G. Ambrosio, P. Bauer, M. Haverkamp; *A Scaling Law for Predicting Snap-Back in Superconducting Accelerator Magnets*, 9th European Particle Accelerator Conference (EPAC04), July 5-9, Luzern, Switzerland, (2004).

- T. Pieloni et al.; *Field Decay and Snap-back Measurements Using a Fast Hall Probe Sensor*, IEEE Trans. Appl. Supercond.: 14 (2004) no.2, pp1822-1825 and also as CERN-LHC-Project-Report-716, (2004).

- L. Bottura et al.; *Warm Cold Magnetic Field Correlation in the LHC Main Dipoles*, LHC-Project-Note-326, (2003).